SAN ONOFRE
NUCLEAR GENERATING STATION
UNITS 2 & 3

RESPONSES TO NRC QUESTIONS
361.37 THROUGH 361.62

SOUTHERN CALIFORNIA EDISON COMPANY
SAN DIEGO GAS & ELECTRIC COMPANY

QUESTION 361.37

GEOSCIENCES BRANCH

Throughout the Woodward-Clyde (WC) report the Offshore Zone of Deformation (OZD) is characterized as being segmented into the Newport-Inglewood Zone of Deformation (NIZD), South Coast Offshore Zone of Deformation (SCOZD), and Rose Canyon Zone of Deformation (RCZD) segments. On page 8 in Section 2.2, the report states "the hypothesized OZD is not a through going fault." In order to more clearly understand the bases for the tectonic model proposed in the report, provide:

a. the evidence for the postulated discontinuity in the fault between the NIZD and SCOZD, and between the SCOZD and RCZD in the Horizon C level of the Western Geophysical Company subsurface maps.

b. Any other evidence that demonstrates physical discontinuities between these fault segments.

RESPONSE 361.37

Although the Applicants' believe the OZD is discontinuous, WCC's evaluation of ground motion from maximum earthquakes was, nevertheless, based on consideration of the OZD "as a whole" (WCC, 1979, p. 2, lines 18-21) with no attempt to diminish its length. The purpose of referring to various parts or "segments" of the OZD was to facilitate description of the structural characteristics and of the data base which vary along the zone (WCC, 1979, p. 7, lines 22-30, p. 12, lines 12-31).

The Atomic Safety and Licensing Board indicated that discussion of discontinuity among elements of the OZD is moot, being the result of an honest difference of opinion. (Atomic Safety and Licensing Board, Initial Decision Docket Nos. 50-361 & 50-362, October 15, 1973, p. 50-52). Even though there "may be a small preponderance of evidence in (the applicants') favor," according to the Board, applicants have agreed to accept for seismic design purposes the model adopted by the USGS and the NRC staff, which holds that segments of the OZD cannot be disassociated (see Safety Evaluation Report, 1972, p. C-14).

There was no intent in the WCC report to address the subject of discontinuity between the NIZD and other parts of the OZD.

QUESTION 361.38

Why was this new methodology chosen to estimate the maximum earthquake instead of other more conventional methods? Any new methods must be compared to the results of conventional methods. For the Offshore Zone of Deformation compare the results of this new methodology (magnitude 6.5) with the results from conventional methods-for example, fault length versus maximum magnitude relationships, or maximum magnitude based on ranking of faults. Also consider comparison of probabilistic risk on the OZD with the San Andreas and San Jacinto fault zones in southern California. For example, consider the return period of magnitudes 6.5, 7.0, and 7.5 on the OZD. Compare the return periods of these magnitudes on the OZD to the return period design earthquakes on major faults in southern California.

RESPONSE 361.38

Several methodologies were considered in evaluating the maximum earthquake applicable to the hypothesized OZD. The specific approach of the WCC June 1979 report uses both a qualitative comparison of features, such as maximum historic earthquake, fault rupture length, total displacement, and degree of deformation, as well as a quantitative comparison of slip rate on faults as a means of differentiating and ranking faults and evaluating the earthquake potential of the hypthesized OZD. The applicants also evaluated rupture-length versus magnitude, and displacement-per-event versus magnitude relationships, however, use of either of those methodologies alone is not appropriate based upon the uncertainties in the data base available for the hypothesized OZD. The degree-of-fault-activity approach as presented in June 1979 and as supplemented in responses 361.38 and 361.45(e) is neither a new nor unconventional methodology and is neither independent of, nor is it meant to replace other methods of estimating maximum magnitude. The approach extends existing knowledge and provides a viable alternative to other methods when absence or sparsity of data limits the usefulness of other methods, especially for en echelon systems.

Section 361.38(a) includes additional information concerning the basis for selection of degree-of-fault-activity methodology and the applicability of other methodologies to the hypothesized OZD. In addition, 361.38(a) places in perspective the role of the slip rate-maximum magnitude relationship in comparison with other fault parameter relationships used in the degree-of-fault-activity methodology.

In response to the NRC's request for comparison of the results of the applicants' methodology with the results from conventional methods it is worthy of note that the Construction Permit stage assessment of the hypothesized OZD was partially based on ranking of faults (Atomic Safety and Licensing Board Initial Decision in the matter of San Onofre Nuclear Generating Station Units 2 and 3, Construction Permit Stage, Docket Nos. 50-361 and 50-362, October 15, 1973, pp 75-81). As noted in 361.38(a) and the June 1979 WCC report, ranking of faults is the bases for the subject methodology. The fact that the site design parameters determined at the PSAR stage are consistent with the results of the current fault ranking approach (degree-of-faults-activity approach) provides a measure of comparison between the two studies. A comparison between magnitudes predicted using the degree-of-fault-activity approach and magnitudes assigned to other faults based on the fault length-magnitude methodology is provided in Section 361.38 (b).

Section 361.38(c) provides a comparison of probabilistic risk on the hypothesized OZD with the San Andreas and San Jacinto fault zones and provides further demonstration of the conservatism of the applicants' assessment of the hypothesized OZD. Section 361.38(d) compares the expected geologic effects for several hypothetical maximum magnitudes with the observed geologic evidence along the hypothesized OZD.

Applicants consider magnitude 6.5 is a conservative maximum magnitude based on consideration of degree-of-fault-activity, maximum realistic rupture length, fault ordering and historic seismicity. However, the applicants recognize that some of those responsible for review of the project geology/seismology would value presentation of assessment of the site geoseismic setting in terms of a magnitude 7 event on the hypothesized Offshore Zone of Deformation. Accordingly, where possible, applicants have included in the response and several other responses through NRC question 361.62, assessments relative to both magnitude 6.5 and 7 events. This is to facilitate project geology/seismology review.

361.38 (a) Degree of Fault Activity Methodology

The general approach used in the WCC June 1979 report for the assessment of the maximum earthquake is to consider a fault-ranking in terms of degree-of-activity of the hypothesized OZD relative to other faults in the southern California tectonic province and in similar tectonic settings throughout the world. Generally, a degree-of-activity approach considers: relative behavior of faults, particularly in terms of strain or slip rates; the size, periodicity, and energy release of seismic events; the mechanical and compositional properties of the faults; and the tectonic setting. This approach for a specific fault considers evidence of fault behavior in the following steps:

1) the tectonic setting and style of the fault is defined;

2) fault activity parameters are compiled for faults within the tectonic province, including the fault of interest. For this purpose, all faults which have experienced displacement during the currently active tectonic stress regime should be considered "active." The fault activity factors most accessible and germane to characterize the differences in degree of fault activity include: slip rate, stress drop, recurrence for large slip events, slip per event, fault rupture length, and tectonic setting; and,

3) the degree-of-activity parameters are compared so that the fault of interest is placed in context relative to other faults. From this context, a limit for the maximum magnitude can be estimated for each fault.

Techniques such as using fault-length versus magnitude or amount-of-surface-displacement versus magnitude incorporate the range of values for active faults in estimating a maximum earthquake. Typically, however, only one or two aspects of fault behavior are considered in these conventional methods. Such singular approaches fail to describe the complexities of fault behavior; for example, the effect of differing rates of slip on the maximum earthquake associated with faults of similar length is not taken into consideration. Therefore, the degree-of-fault-activity methodology evaluates characteristics of the hypothesized OZD and presents an approach comparing those characteristics to other faults.

The specific approach of the WCC June 1979 report uses both a qualitative comparison of features, such as maximum historic earthquake, fault rupture length, total displacement, and degree of deformation, as well as a quantitative comparison of slip rate on faults as a means of differentiating and ranking faults and evaluating the earthquake potential of the OZD. The type of tectonic regime considered is limited to a strike slip environment (see response 361.47). The result of this analysis is shown in Figure 7 of the WCC June 1979 report and indicates that the maximum historic earthquake of magnitude M_S 6.3 is very close to the maximum earthquake possible for the NIZD. Further refinements and additional data points have been incorporated in the data base originally used for Figure 7, and a revised slip-rate versus magnitude graph has been prepared as discussed in response 361.45(e).

The method used in this approach is an extension of existing techniques in the seismic hazards literature. Slemmons (1977) has described interrelationships among fault-slip rates, recurrence intervals, and earthquake magnitude. Matsuda (1975, 1977) uses geologic slip rates to classify faults and to evaluate recurrence intervals of large-magnitude earthquakes. Cluff (1978) and Packer and Cluff (1977) have described differences in relative degree of activity in terms of slip rate, recurrence interval, and slip per event. Brune (1968) has used seismic moments of earthquakes to obtain average rates of slip on major fault zones. Anderson (1979) extends this analysis to estimate recurrence using geologic slip rate. Molnar (1979) relates these seismic slip rates to geologic and geodetic slip rates and establishes a procedure for estimating return periods for earthquakes with certain moment values. Smith (1976) uses the geologic slip rate to obtain the average rate of seismic activity and to limit the maximum earthquake that can be expected to occur along the fault. In reviewing known methods of estimating maximum magnitude, Chinnery (1978) suggests that the use of slip rate in the context of Smith (1976) is one of the most reasonable. Each of these authors utilizes relationships among various measures of fault activity in a manner similar to that used in the WCC June 1979 report.

Various methods for evaluating maximum magnitude are employed in the state-of-the-practice of seismic hazards analyses (Slemmons, 1977). These methods include several empirical relationships such as historic rupture length versus magnitude, maximum displacement during a single historic event versus magnitude, and maximum magnitude estimates based on tectonic setting and simple ranking of faults. These "conventional" techniques and their applicability to estimating maximum earthquakes are discussed in subsections 361.38 (a)-1 through 3. Subsection 361.38 (a)-4 discusses the application of these methods to the OZD.

361.38 (a)-1 Rupture Length Versus Magnitude Correlation

The rupture-length versus magnitude method consists of correlating the empirical relationship between the fault rupture lengths for various historical earthquakes and the magnitudes of these events. The length is measured either by the observed surface rupture length or (in some analyses) by the aftershock zone. Attempts to refine the method have included adding more rupture-length data to the data set. These additional data are interpreted from 1) rupture lengths calculated from tsunami generation, (Abe, 1973; Acharya, 1979), 2) geodetic data, and 3) the rupture area of the fault surface based on assumed depth and length of an aftershock zone.

Although considerable effort has been put into refining the data base, several difficulties persist. First, the regression lines used to estimate earthquake magnitudes for a given rupture length are averages based on least-squares regressions, so about half of the data points lie below the regression line and half above (Mark, 1977). The conservatism in the analysis is usually introduced by combining as many fault segments as possible to provide a maximum length for the analysis, as in the case of long en echelon fault systems. This is often arbitrary and leads to arbitrary results. Second, the fault-length versus magnitude relationship varies significantly with tectonic province (Acharya, 1979) and style of faulting (Bonilla and Buchanon, 1970; Slemmons, 1977) (Figure 361.38-1); yet no attempt has been made to account for combinations of these variations in general applications of the rupture-length magnitude technique. Third, there is always a major uncertainty in estimating the maximum potential rupture length of a fault being investigated, as will now be discussed.

Most conventional rupture-length magnitude applications assume that half the total mapped fault-length is a conservative rupture length for estimation of maximum earthquakes. This half-length approach was proposed many years ago by Albee and Smith (1966) and Wentworth and others (1969), who argue that rupture of half the length of a fault, or less, is more likely than rupture of the entire fault; this belief is based on historic surface ruptures in southern

California. However, in North America historic ruptures have broken from 2% to more than 75% of the total fault length (Wentworth and others, 1969). In addition, some Japanese earthquakes appear to have been accompanied by rupture of the entire mapped fault lengths and, in one case (Tottori earthquake, Japan, 1943) the rupture was longer than the mapped fault (Bonilla, 1979). Thus, a uniform application of half-length (or one-third-length, or any other fault length) fails to account for the wide range in fault behavior.

Although advances have been made in the understanding of fault behavior since the formulation of the rupture-length method, it is still difficult to estimate the maximum rupture length that can be reasonably expected on a fault. Despite these difficulties and without other information, the choice of half or a third the fault length is still, in practice, presumed to be a reasonable and conservative method for estimating a maximum earthquake.

When using a half-length, third-length, or any other length-defined method of estimating maximum magnitude, it is often difficult to estimate the full length of the fault to which the method is applied. The details of fault rupture processes are not sufficiently understood to assess how readily fault systems with relatively short, discontinuous surface traces can produce lengthy ruptures and large-magnitude earthquakes; and it is not known how effective en echelon breaks in fault zones are in creating barriers to propagation of fault ruptures. For example, several major en echelon fault segments comprise the San Jacinto fault zone, which has ruptured essentially over its entire length in historic time, although the individual historic earthquakes have not approached rupturing half or even one third the entire length. In fact, one of the segments, the Coyote Creek fault, appears to rupture as an independent segment with frequent lower-magnitude earthquakes rather than as a part of the entire zone during one large earthquake (Slemmons, 1977). This type of behavior for en echelon systems may be very typical for other en echelon faults in California, such as in the hypothesized OZD.

361.38 (a)-2 Displacement-per-Event Versus Magnitude Correlation

The displacement/magnitude relationship method compares the empirical correlation of maximum observed surface displacement for a single earthquake to the corresponding earthquake magnitude. To apply this technique to a given fault, either observations of displacements during historic events or geologic data on pre-historic events are required for the fault in question. Typically, this requires data from numerous locations along the fault because amounts of surface displacement during earthquakes are often highly variable along the fault trace. Such data are available for only a few faults.

Several difficulties exist in applying the displacement versus magnitude relationship. First, ideal geologic conditions must exist to preserve displacement per event occurrences. Second, the maximum surface displacement measured for any particular earthquake may not be the characteristic displacement, or may represent an exaggeration of net tectonic displacement. Examples include: 1) the 1976 Guatemala earthquake, with an average surface displacement of 1.1 m, but with a maximum displacement in one location of about 3.4 m (Buckman and others, 1978); and

2) the 1954 Dixie Valley earthquake where the maximum surface displacement was approximately 20% greater than the maximum tectonic displacement because of graben formation and deformation of the downthrown block (Slemmons, 1957). Because definitive data on displacement per event cannot be obtained for the hypothesized OZD, this approach is not directly applicable to estimate a maximum magnitude for the zone.

361.38 (a)-3 Ranking of Faults

Ranking of faults covers a broad range of possible systems for differentiating faults. Among conventional ranking systems are: 1) relative geomorphic expression of the faults being ranked, 2) the relative importance of a fault in its structural-tectonic setting, and 3) relative rates of deformation. Typically, such techniques do not provide a unique maximum earthquake magnitude but often provide ranges of probable earthquake magnitudes for different categories or rankings of faults. Such ranking, however, serves to help evaluate maximum earthquake estimates from the length and displacement methods. In general, ranking of faults is a comprehensive approach which does not rely on a single characteristic of a fault for evaluation of earthquake potential.

One method of ranking faults is by geologic slip rate; this method is particularly useful because it describes quantitatively the relative degree of activity of faults in their present tectonic setting, and it incorporates properties of the mechanics and behavior of faults, including strain accumulation, strain release in earthquakes, and recurrence intervals of earthquakes. And, because geologic slip-rates average fault displacements during a relatively long time interval, the behavior of faults in the past can be evaluated and projected into the future.

361.38 (a)-4 Applicability of Methodologies to the OZD

The nature of the OZD is reviewed below to evaluate the application of the fault-length methodology to the Zone. The Newport-Inglewood zone of deformation, South Coast Offshore zone of deformation, and the Rose Canyon fault zone are collectively known as the hypothesized Offshore Zone of Deformation, (OZD), which is collectively about 200 km in length extending from the Santa Monica Mountains to offshore near the international border. It is best described as a zone of deformation because it is characterized onshore and offshore by a series of en echelon faults and folds, rather than by a continuous zone of faulting. Greene (1980) states that a through-going fault has not been defined and continuity of the en echelon traces is not demonstrated; this is similar to many other California faults composed of short, en echelon faults. The longest single, uninterrupted faults in the OZD extend no more than 40 km (Greene, 1980). The en echelon nature of the hypothesized OZD raises valid questions regarding the ability of the rupture to propagate from fault trace to fault trace. The difficulty in interpreting a magnitude based on fault-length methodologies for the hypothesized OZD is the uncertainty of the maximum length of potential rupture during a maximum earthquake on the zone. Therefore, the length methodology cannot rationally be applied to the hypothesized OZD. However, the reasonableness of the maximum magnitude for the hypothesized OZD can be evaluated by comparing rupture length associated with that magnitude with the physical characteristics of the OZD as discussed in Section 361.38(d).

The displacement-per-event versus maximum-magnitude relationship cannot be applied to the hypothesized OZD because surface traces of the fault are poorly developed along most of the onshore portions of the zone and estimates of past displacements are unavailable. Furthermore, the lack of continuous dramatic surface expression can be used to imply that large displacements, and accompanying large earthquakes, either do not occur on or have not occurred recently on the NIZD and RCFZ.

Because of the difficulties in applying the fault length and displacement correlation methods to evaluating the maximum earthquake on the hypothesized OZD, the applicants evaluated the earthquake potential by using a quantitative fault-ranking criterion, slip rate. The slip-rate ranking method uses maximum, rather than average, values to estimate magnitude. Furthermore, it deals more directly with the earthquake process than other methods by relating and analyzing measures of strain accumulation and release. This method provides an alternative to the length and displacement methods when available data limit or prevent their use.

361.38 (b) Slip Rate Compared to Half-Length Method

The slip-rate versus maximum-magnitude method of the degree-of-activity approach has been specifically applied to a comparison of strike-slip faults in Southern California. The empirical relationship between slip rate and magnitude defined by Southern California faults appears to hold for strike-slip faults in similar tectonic environments in other parts of the world. Some variations appear to occur when different tectonic environments are considered (see response 361.47): As a test of the slip-rate versus maximum-magnitude relationship, the results of the slip-rate method are compared to the half-length maximum-magnitude method in the following paragraphs. The result is a synthesis plot of slip-rate versus maximum-magnitude based on half lengths using the Slemmons (1977) rupture-length versus magnitude correlation (Figure 361.38-1) for strike-slip faults. The synthesis is based on half-length rupture because half the total fault length is often considered to be a conservative estimate (for that portion of the fault that may rupture during the largest earthquake a fault can generate) when applying the rupture-length/magnitude relationship. This synthesis plot is closely comparable to the empirical bounding limit shown in Figure 7 of the WCC June 1979 report, as discussed below.

The slip-rate approach to estimating magnitude can be compared to the half-length method if a relationship between slip rate and half-length can be established. Menard (1962) and Ranalli (1977) have shown that a positive correlation exists between total displacement on a fault and its total length. Since slip rate is related to displacement by time (Rs = D/T), a possible correlation between slip rate and length is suggested.

To investigate this possibility, a log-log plot of selected slip-rate versus length (in this case, half-length), has been constructed (Figure 361.38-2). A least squares regression analysis of half length as a function of slip rate (both expressed as logarithms) was calculated to produce a "best fit" line through the data and to evaluate the correlation of the variables. For the 31 pairs of data, for which both slip rate and length are relatively well known, a correlation coefficient of .730 was calculated. Thus, the data suggest a positive correlation between slip rate and fault length.

Slemmons (1977) used the same regression technique to establish a widely accepted relationship between rupture length and magnitude. The correlation coefficient for slip-rate versus half-fault-length is comparable to the .775 correlation coefficient resulting from the Slemmons (1977) plot of rupture-length versus magnitude for strike-slip faults (Figure 361.38-1). It seems reasonable to synthesize the slip-rate/length relationship and the rupture-length/magnitude relationship of Slemmons (1977) in order to develop a slip-rate/magnitude comparison for strike-slip faults.

Slemmons' (1977) relationship can be expressed:

$$M = 4.651 + .587 \ln L_R$$

where M = magnitude

L_R = rupture length

The relationship of half length to slip rate shown of Figure 361.38-2 can be expressed:

$$L/_2 = 48.1\, R_S{}^{.620}$$

where $L/_2$ = half length

R_S = slip rate

If half length of the fault is taken as the potential rupture length then $L_{1/2} = L_R$.

Combining the two relations,

$$M = 4.651 + .587 \ln (48.1\, R_S{}^{.620})$$

This line represents a slip-rate/maximum-magnitude curve synthesized through consideration of the half-length method.

The line is shown as the SEL (Synthetic Earthquake Line) in Figure 361.38-3.

The degree-of-fault-activity approach, as described in Section 361.38(a), is an alternative method for evaluating maximum magnitude using available slip-rate data to derive an estimated upper bound limit for possible earthquakes on the hypothesized OZD consistent with behavior on other faults. As discussed in the WCC June 1979 report, these data support a maximum magnitude of 6.5. The approach shown in 1979 represents one interpretation of the data set in order to derive a conservative estimate of maximum magnitude. Since preparation of the WCC June 1979 report, the Applicants have continued the data review and have augmented the data base, as described in response 361.45e. The most representative slip-rate values and their associated maximum historical earthquake magnitudes for selected faults are plotted in Figure 361.38-4. Also shown are several faults with no large historical earthquakes. The selection criteria for these data are discussed in response 361.45(e).

A line can be drawn bounding these empirical observations as shown in Figure 361.45-3 and defined as the maximum Historic Earthquake Limit (HEL). This line suggests that there is a consistent limit to the size of an earthquake associated with the geologic slip rate of a strike-slip fault. This assumes that some of the strike-slip faults in the world have had maximum or close-to-maximum earthquakes and that when their maximum data points are enveloped they form a maximum earthquake limit related to slip rate.

The empirical data line (HEL) is compared to the line derived from half-length ruptures related to slip rate (SEL, Fig.

361.38-4). The synthesis line based on half length ruptures has a slightly steeper slope than the empirical line and indicates that slightly larger magnitudes may occur in the lower slip-rate range. However, the lines are generally compatible and their comparison suggests that the empirical plot is reasonably conservative when compared to the results of half length.

The conservatism of the slip rate versus magnitude data set is further investigated by considering the ranges of slip rate and magnitude data obtained from published and unpublished sources. These data, presented in response to question 361.45 e, provide for assessment of uncertainty in the data interpretation.

Based on the evaluation of uncertainty of slip rate and magnitude data as described in 361.45(e) a maximum earthquake line (MEL) was obtained (Fig. 361.45-4). In order to demonstrate the consistency of the results of fault length-magnitude methodology with degree-of-fault-activity results, Figure 361.38-4 compares these three lines, the SEL, MEL and HEL.

361.38 (c) Earthquake Recurrence

In a collective sense, seismic activity on a group of faults is well described by the magnitude-frequency relationships

$$\text{Log } N = a - bM$$

where N is the number of earthquakes of magnitude M and larger occurring within a defined time interval for the group of faults or portion of the earth's surface containing a group of faults. Using this relationship leads directly to numerical estimates for return period as a function of magnitude for the zone.

Significant uncertainties exist in how this relationship should be applied to a single fault. Detailed geologic evidence for earthquake recurrence has only recently been developed for a few faults: for example, Sieh (1978) suggests that, for the central San Andreas fault, episodes of major displacement occur about every 160-240 years. The actual magnitudes of earthquakes producing these episodes are not known. Historical seismicity data appear to be generally inadequate and unreliable in constraining the parameters of the magnitude-frequency relationship for large magnitude earthquakes on a single fault. The frequency of occurrence of earthquakes of a specific magnitude on a fault appears to be highly variable and may be related to cyclic periods of activity and inactivity lasting many tens to hundreds of years. Thus, the geologic and historical data available in California for the past 50 to 180 years primarily provide evidence for consistency with a recurrence model, but do not provide the basis for constructing the model.

An alternative approach to estimating earthquake recurrence is to assume a form of the magnitude-frequency relationship and to distribute the total amount of seismic moment on the fault within the range of possible earthquakes. The assumptions made for this analysis are the following:

1. The total moment rate on a fault is given by the product of the length of the fault or fault zone and the geologic

slip rate. The lengths and moment rates for several Southern California faults are listed in Table 361.51-1.

2. All of the displacement is considered to occur seismically.

3. The magnitude-frequency relationship is considered to be linear with an assumed slope of - 0.85 up to the maximum magnitude assigned to the fault. This slope is selected to be typical for the Southern California tectonic setting and seismicity.

4. Several possible values for maximum magnitude are considered and are shown in Table 361.38-1.

Using these assumptions, the recurrence intervals (return periods) for possible earthquakes on the San Andreas fault, San Jacinto fault, and the hypothesized OZD are calculated and listed in Table 361.38-1. The method of Anderson (1979) was used to calculate the 'a' values. Using the 'a' and 'b' values, the numbers of earthquakes expected annually in the adjoining magnitude ranges 6.25 to 6.75, 6.75 to 7.25, and 7.25 to 7.75, are calculated. The inverses of these numbers are the recurrence intervals of earthquakes within the respective magnitude ranges. For simplicity, the ranges are denoted by their mean values (6.5, 7.0, and 7.5) in the table.

Several observations can be made about the consistency of the recurrence values in Table 361.38-1 with the geologic and historical data:

1. The value of maximum magnitude used in each calculation has an important impact on the recurrence. As illus-

trated in Figure 361.38-5, increasing the maximum magnitude by 0.5 magnitude units reduces the 'a' value by a factor of more than 2.0, assuming constant 'b' value. This effect is produced by the constant slip rate producing a constant average rate of release of seismic moment. Allowing the occurrence of larger earthquakes with large slip reduces the frequency of occurrence of all earthquakes on the fault.

2. The maximum value of 8.0 for the central San Andreas fault gives a recurrence time (200 years) that is reasonably consistent with the geologic data discussed above. The calculated recurrences of large earthquakes (M_S 6.0 to 7.5) are not reflected in the historical data, suggesting that the magnitude-frequency relationship for the San Andreas may not be correct in its parameters or functional form over the magnitude range 6 to 8.

3. For the San Jacinto fault, the predicted recurrence intervals using a maximum earthquake value of 7.5 are more consistent with the seismicity of the past 100 to 180 years than the longer recurrence times produced by maximum earthquakes in the range 8.0 to 8.3.

4. The occurrence of the 1933 earthquake (and possibly the 1800 and 1812 earthquakes) on the hypothesized OZD is consistent with recurrence intervals calculated for the maximum magnitude of 6.5. The low instrumental and historical seismicity of the offshore portions of the hypothesized OZD suggest that the slip-rate value applied to these portions is possibly too high.

5. If the maximum magnitude for the OZD is hypothesized to be M_S 7.5, the recurrence times for smaller earthquakes are longer than the historical data would suggest. The lack of Holocene geologic evidence along the OZD for such large earthquakes is not consistent with the recurrence intervals tabulated for a hypothesized M_S 7 1/2 earthquake in Table 361.38-1.

In summary, the recurrence calculations presented above are consistent with maximum magnitude values less than the MEL values obtained from Figure 361.45-4 and listed in Table 361.38-1.

361.38 (d) Evaluation of Physical Conservatism of the Maximum Earthquake

This section evaluates the physical conservatism of hypothetical maximum earthquake magnitudes of M_S 6.5, M_S 7.0, and M_S 7.5 for the hypothesized OZD by considering how consistent the occurrence of such earthquakes is on the zone with the geologic, geophysical, and seismological environment of the zone. This examination uses the qualitative and quantitative factors included within the more general evaluation of degree of fault activity. For reference purposes the table summarizing fault ranking of the San Andreas, San Jacinto, and Whittier-Elsinore faults, and the hypothesized OZD presented in the September 13, 1979 meeting, is included in Table 361.38-2. More detailed information on the hypothesized OZD from north to south is summarized in Table 361.38-3.

If a large enough shallow earthquake is generated on a fault, it will be accompanied by surface rupture and other ground deformation. These surface disturbances may be ephemeral or may be preserved in the topography depending on the size and periodicity of surface rupture events. In all but the most active geomorphic environments, large earthquakes on faults express their occurrence in the geomorphic features along those faults. Thus, evaluation of the geomorphic features allows the reconstruction of earthquake histories and the estimation of earthquake magnitudes based on the degree of surface disturbance during individual events. This method can be an important tool in the evaluation of maximum earthquakes.

If a fault generates small displacements during earthquakes, those earthquakes are probably not large in magnitude. If geomorphic expression of past displacements are poorly preserved along a fault, then the fault probably has not produced large earthquakes since the landscape formed. In California, most earthquakes with M_S 6 or greater are accompanied by surface rupture (Tocher, 1958), and smaller earthquakes are sometimes accompanied by surface faulting. Thus, the geomorphic expression of a fault can be used to check the size of earthquakes that have occurred in the past.

A lack of dramatic surface morphologic expression of faulting is noted along the hypothesized OZD where late Pleistocene deposits overlie the fault along much of the NIZD. Locally, evidence of Quaternary surface faulting exists, but neither continuous, large scarps nor abundant offset geomorphic features are present. The low degree of geomorphic expression is more apparent within the morphology of the hypothesized OZD is compared to the Elsinore, San Jacinto, or San Andreas faults to the east. The geomorphic processes in southern California have been sufficiently slow to preserve evidence of late Pleistocene displacements on these other faults. The lack of well-developed surface expression along the hypothesized OZD suggests that very large earthquakes have not occurred on the fault at least since Pleistocene.

In the following paragraphs, the geomorphic expression and geologic relationships of the hypothesized OZD are used to test how reasonable is the occurrence of earthquakes of various magnitudes on the zone. Mark (1977) points out that the regression lines of Slemmons (1977) can be used to estimate magnitude from displacement or rupture length, but new equations must be used for the reverse process. For the following analyses, new regressions of rupture length versus magnitude and displacement versus magnitude based on Slemmons (1977) data on historic strike-slip faulting, are used in order to apply the correct statistical procedure. Those regressions are plotted on Figures 361.38-7 and 361.38-8.

According to the empirical relationships of length and displacement, a magnitude 6.5 earthquake should result in approximately 30 kilometers of surface rupture and about .95 meter of surface displacement. Of the entire 70 km length of the Newport-Inglewood portion of the hypothesized OZD, the largest potentially connected fault segments (based on subsurface oil field and ground water interpretation (Yeats, 1973) extend about 36 km from Newport Beach to Signal Hill and have a maximum single segment length of about 18 km. Considering that the rupture associated with the 1933 Long Beach earthquake (M_S 6.3) extended to about 30 km in length along this portion of the NIZD (based on aftershock zone data in the WCC June 1979 report), it appears reasonable that a full rupture of the 36 km zone (Newport Beach to Signal Hill) would be consistent with an earthquake of about M_S 6-1/2. No surface rupture due to faulting was documented in 1933, although much ground disturbance was attributed to liquefaction. The magnitude 6.3 was below, but possibly near, the threshold of causing surface rupture of the NIZD portion of the OZD.

If M_S 7 is considered, the corresponding surface rupture length and surface displacement should approximate 50 km of surface rupture and 1.7 meters of displacement. No surface ruptures are evident along the zone in the geomorphology for this great a distance. In fact, the longest single faults within the zone do not exceed 40 km (Greene, 1980), and a 50 km rupture must, therefore, involve two or more en echelon segments. The 1.7 meters displacement should be observable in the geomorphology along the zone if a 7 magnitude earthquake were typical of the zone. Considering that the recurrence of a 7 magnitude is about 900 years [see response 361.38 (c)] on the hypothesized OZD as a whole, or approximately 3,600 years at a particular point, such as the NIZD, we should see approximately 5 meters of surface displacement in Holocene age sediments and approximately 47 meters of surface displacement in the Pleistocene marine terrace deposits. Certainly, those magnitude displacements should be preserved in the uplifted marine terraces along the NIZD if 7 magnitude earthquakes are the maximum events. The geomorphic evidence does not support such large earthquakes and suggests something smaller.

If a hypothetical M_S 7.5 is considered for the NIZD and for the hypothesized OZD, individual events of that magnitude would be expected to result in about 83 kilometers of surface rupture and about 3.2 meters of surface displacement. These figures are again unreasonably large compared to the geomorphic evidence along the hypothesized OZD. The nature of the hypothesized OZD and the faulting along it indicate that no large surface ruptures have occurred. This is supported by the fact that the faults both onshore and offshore become shorter and less continuous from deeper horizons to shallower horizons. This relationship is clearly indicated for the faults directly offshore from San Onofre where interpretation of the geophysical data shows the individual faults to be most continuous on the acoustic basement (horizon C) and less continuous and shorter in the younger rocks, such as those represented by Horizon B (probably upper Miocene in age).

If the continuity at depth is incomplete, becoming less upward in section, then the surface ruptures cannot be long. In other words the surface ruptures cannot be longer than the faults at these relatively shallow depths. This limitation suggests that large earthquakes equal to M_S 7 or larger have not occurred offshore from San Onofre.

REFERENCES

Abe, K., 1973, Tsunami and mechanism of great earthquakes: Physics of the Earth and Planetary Interiors, v. 7, p. 143-153.

Acharya, H. K., 1979, Regional variations in the rupture-length magntiude relationships and their dynamical significance: Seismological Society of America Bulletin, v. 69, no. 6, p. 2063-2084.

Albee, A. L., and Smith, J. L., 1966, Earthquake characteristics and fault activity in southern California, in Lung, R., and Proctor, R., eds., Engineering Geology in Southern California: Association of Engineering Geologists, Glendale, California, p. 9-33.

Anderson, J. G., 1979, Estimating the seismicity from geologic structure for seismic-risk studies: Seismological Society of America Bulletin, v. 69, no. 1, p. 135-158.

Bonilla, M. G., 1979, Historic surface faulting--map patterns, relation of subsurface faulting, and relation to pre-existing faults: U. S. Geological Survey Open-File Report 79-1239, p. 36-65.

Bonilla, M. G., and Buchanan, J. M., 1970, Interim report on worldwide historic surface faulting: U. S. Geological Survey Open-File Report.

Brune, J. N., 1968, Seismic moment, seismicity and rate of slip along major fault zones: Journal of Geophysical Research, v. 73, no. 2, p. 777-784.

Chinnery, M., 1978, Investigations of the seismological input to the safety design of nuclear power reactors in New England: U. S. Nuclear Regulatory Commission, NUREG/CR-0563.

Cluff, L. S., 1968, Geologic considerations for seismic microzonation: Second International Conference on Microzonation, San Francisco, November 26 to December 1, 1978, Proceedings, v. 1., p. 135-152.

Greene, H. G., 1980, Quaternary tectonics, offshore Los Angeles-San Diego area: U. S. Geological Survey, National Earthquake Hazards Reduction Program, Summaries of Technical Reports, v. 9, p. 11-12.

Mark, R. K., 1977, Application of linear statistical models of earthquake magnitude versus fault length in estimating maximum expectable earthquakes: Geology, v. 5, p. 464-466.

Matsuda, T., 1975, Magnitude and recurrence interval of earthquakes from a fault (in Japaneses): Earthquake, Series 2, v. 28, p. 269-283.

Matsuda, T., 1977, Estimation of future destructive earthquakes from active faults on land in Japan: Journal of Geophysics of the Earth, v. 25, supplement, p. S251-S260.

Menard, H. W., 1962, Correlation between length and offset on very large wrench faults: Journal of Geophysical Research, v. 67, no. 10, p. 4096-4098.

Molnar, P., 1979, Earthquake recurrence intervals and plate tectonics: Seismological Society of America Bulletin, v. 69, no. 1, p. 115-133.

Packer, D. R., and Cluff, L. S., 1978, Comparison of activity of late Cenozoic faults in the western Sierra foothills, California, with other active faults (abs.): Earthquake Notes, v. 49, no. 1, p. 89-90.

Ranali, G., 1977, Correlation between length and offset in strike-slip faults: Tectonophysics, v. 37, p. T1-T7.

Richter, C. F., 1958, Elementary Seismology: W. H. Freeman and Company, San Francisco.

Sieh, K. E., 1978, Prehistoric large earthquakes produced by slip on the San Andreas fault at Pallett Creek, California: Journal of Geophysical Research, v. 83, no. B8, p. 3907-3939.

Shimazaki, D., and Somerville, P., 1979, Static and Dynamic Parameters of the Izu-Oshima, Japan Earthquake of January 14, 1978: Seismological Society of America Bulletin, v. 69 p. 1343-1378.

Slemmons, D. B., 1957, Geological effects of the Dixie Valley-Fairview Peak, Nevada, earthquakes of December 16, 1954: Seismological Society of America Bulletin, v. 47, no. 4, p. 353-375.

Slemmons, D. B., 1977, State-of-the-art for assessing earthquake hazards in the United States--Report 6, Faults and Earthquake Magnitude: U. S. Corps of Army Engineers, Waterways Experiment Station, Soils and Pavements Laboratory, Miscellaneous Papers S-73-1, 129 p.

Smith, W. S., 1976, Determination of maximum earthquake magnitude: Geophysical Research Letters, v. 3, p. 351-354.

Toucher, D., 1958, Earthquake energy and ground breakage: Seismological Society of America Bulletin, v. 48, no. 2, p. 147-153.

Wentworth, C. M., Bonilla, M. G., and Buchanan, J. M., 1969, Burro Flats site seismic environment of the Ventura, California: U. S. Geological Survey Open-File Report 1973.

Woodward-Clyde Consultants, 1979, Report of the evaluation of maximum earthquake and site ground motion parameters associated with the offshore zone of deformation, San Onofre nuclear generating station: report for Southern California Edison Company, June, 241 p.

Wyss, M., 1979, Estimating maximum expectable magnitude of earthquakes from fault dimensions: Geology, v. 7, p. 336-340.

Yeats, R. S., 1973, Newport-Inglewood fault zone, Los Angeles basin, California: American Association of Petroleum Geologists Bulletin, v. 57, no. 1, p. 117-135.

Personal Communications

Schwartz, D., 1979, Woodward-Clyde Consultants, San Francisco.

Table 361.38-1

Recurrence Intervals of Earthquake on
Southern California Faults Calculated from Moment Rates

FAULT**	MAXIMUM† MAGNITUDE	RECURRENCE INTERVAL* (Years) 6.0	6.5	7.0	7.5	8.0
San Andreas	8.0	5	13	30	80	200
(central segment)	8.5 (MEL)	11	30	70	180	450
San Jacinto	7.5	16	40	100	260	
	8.0 (HEL)	36	90	230	570	1440
	8.3 (MEL)	60	150	370	930	2340
OZD	6.5 (DEL)	60	150			
	7.0 (MEL)	130	340	840		
	7.5 (hypothesized)	270	720	1910	5060	

† Used only for calculation of 'a' value assuming b = 0.85; MEL and HEL defined on Figure 361.38-4, and Figures 361.45-3 and 361.45-4, DEL defined on Figure 7 of WCC June 1979 report.

* For events within 0.25 units of the magnitude value listed.

** Fault parameters are listed in Table 361.51-1.

TABLE 361.38-2
SOUTHERN CALIFORNIA STRIKE-SLIP FAULT ZONES
CHARACTERISTICS AND RANKING CRITERIA

FAULT ZONE CHARACTERISTICS	SAN ANDREAS	SAN JACINTO	WHITTIER-ELSINORE-LAGUNA SALADA	HYPOTHESIZED OZD
Dimensions and Segmentation	Total length - 1300 km Imperial-Cerro Prieto segment - 180 km (Imperial Valley to Gulf of California) Southern segment - 225 km (Cajon Pass to Imperial Valley) Central segment - 330 km (Parkfield to Cajon Pass) Creep segment - 135 km (Hollister to Parkfield) Northern segment - 435 km (Cape Mendocino to Hollister)	Total length - 260 km Loma Linda-Claremont - 97 km Casa Loma-Clark - 126 km Coyote Creek - 60 km Superstition Mountain - 50 km Superstition Hills - 53 km	Total length - 339 km Whittier - 42 km Chino - 32 km Eagle-Glen Ivy - 43 km Wildomar-Elsinore - 160 km Laguna Salada 80 km	Total length - 200 km NIZD - 70 km Segment lengths - 6.5-36 km SCOZD - 75 + km Segment lengths - 8-27 km (Horizon B) RCFZ - 65 + km Segment lengths - 20-48 km
Total Displacement	300 km (Miocene-Cretaceous)	24 km (Pliocene)	8-13 km (Tertiary)	3 km (Upper Miocene-NIZD)
Distance from San Andreas Fault (Plate Boundary)	0 km	0-48 km	40-80 km	62-150 km
Historic Rupture Length	435 km (Northern Segment)	33 km (Coyote Creek)	N/A	30 km (Aftershock Zone - NIZD)
Historic Displacement	6.1 m	.38 m (Coyote Creek)	N/A	31 - .46 m (Seismic Moment - NIZD)
Continuity and Geomorphic Features	Great Continuity Long linear surface scarps, numerous traces; traces suggest great continuity; sag pods, offset streams and topography	En echelon Segments Strong linear trends in young alluvium, water barriers; sag depressions, offset streams and topography, linearity and continuity not as pronounced as San Andreas	En enchelon Segments Linear scarps, offset alluvial fans and streams but fault trace vanishes frequently in younger sediments sag depressions	Discontinuous en echelon Segments En enchelon large folds at north end with smaller and more gentle folding to the south. Occasional linear fault scarps at north end with no persistant scarps to the south.
Historic Seismicity	Very High	Very High	Moderate	High in the north, low in central and southern areas
Maximum Historic Magnitude, M_S	8.2 (1857)	6.7 (1968 Coyote Creek) 7.1 (1940 Imperial)	5.5-6 (1910)	6.3 (1933 - NIZD)
Geologic Slip Rate	37 mm/yr	8 mm/yr	2.3 mm/yr (Elsinore) 1.2 mm/yr (Whittier)	0.5 mm/yr (NIZD)

TABLE 361.38-3
COMPARISON OF ZONE CHARACTERISTICS NORTH TO SOUTH ALONG
THE HYPOTHESIZED OFFSHORE ZONE OF DEFORMATION

	NORTH	CENTRAL	SOUTH
FAULT RELATED CHARACTERISTICS	NEWPORT-INGLEWOOD ZONE OF DEFORMATION	SOUTH COAST OFFSHORE ZONE OF DEFORMATION	ROSE CANYON FAULT ZONE
Total Length	70 km	75 $\pm$ km	65 $\pm$ km
Maximum Segment Length	18 km (36 km combined)	48 $\pm$ km (Horizon "B")	35 $\pm$ km (offshore)
Structural Features	Large en echelon folds, En echelon faults, North trending branch faults near basement	Smaller en echelon folds, folds, En echelon faults, North trending branch faults near basement	Gentle folds on opposite sides of fault zone, En echelon faults
Continuity of Geomorphic features	Low en echelon folds, short fault scarps	Little to none Fault scarps up to 1/2 meter	Main fault segments tend to follow Rose Canyon, No persistent fault scarps
Distance from San Andreas Fault (Plate Boundary)	62 - 80 km	85 - 130 km	110 - 150 km
Historic Seismicity	High	Very Low	Low
Maximum Historic Earthquake - M_S	6.3 (1933)	4.5 (1969)	3.7 (1958)
Historic Rupture Length	30 km (Aftershock Zone)	U.K.	U.K.
Geologic Slip Rate	0.5 mm/yr	U.K.	Indeterminant, see Responses to Question 361.44 k)

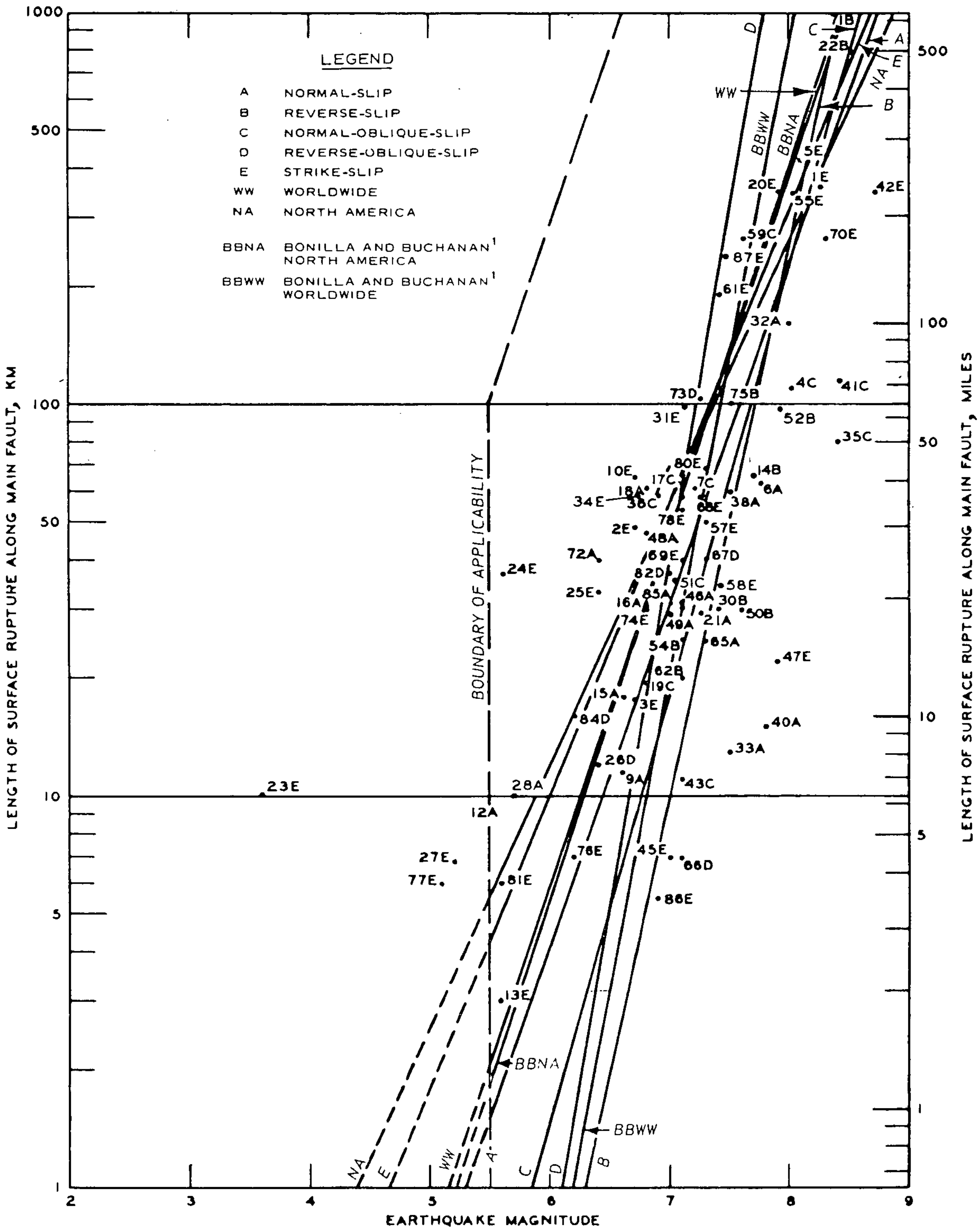

Reprinted from Slemmons, 1977.

[1]Bonilla and Buchanan, 1970.

Figure 361.38 - 1 Relation of earthquake magnitude to length of zone of surface rupture along the main fault zone

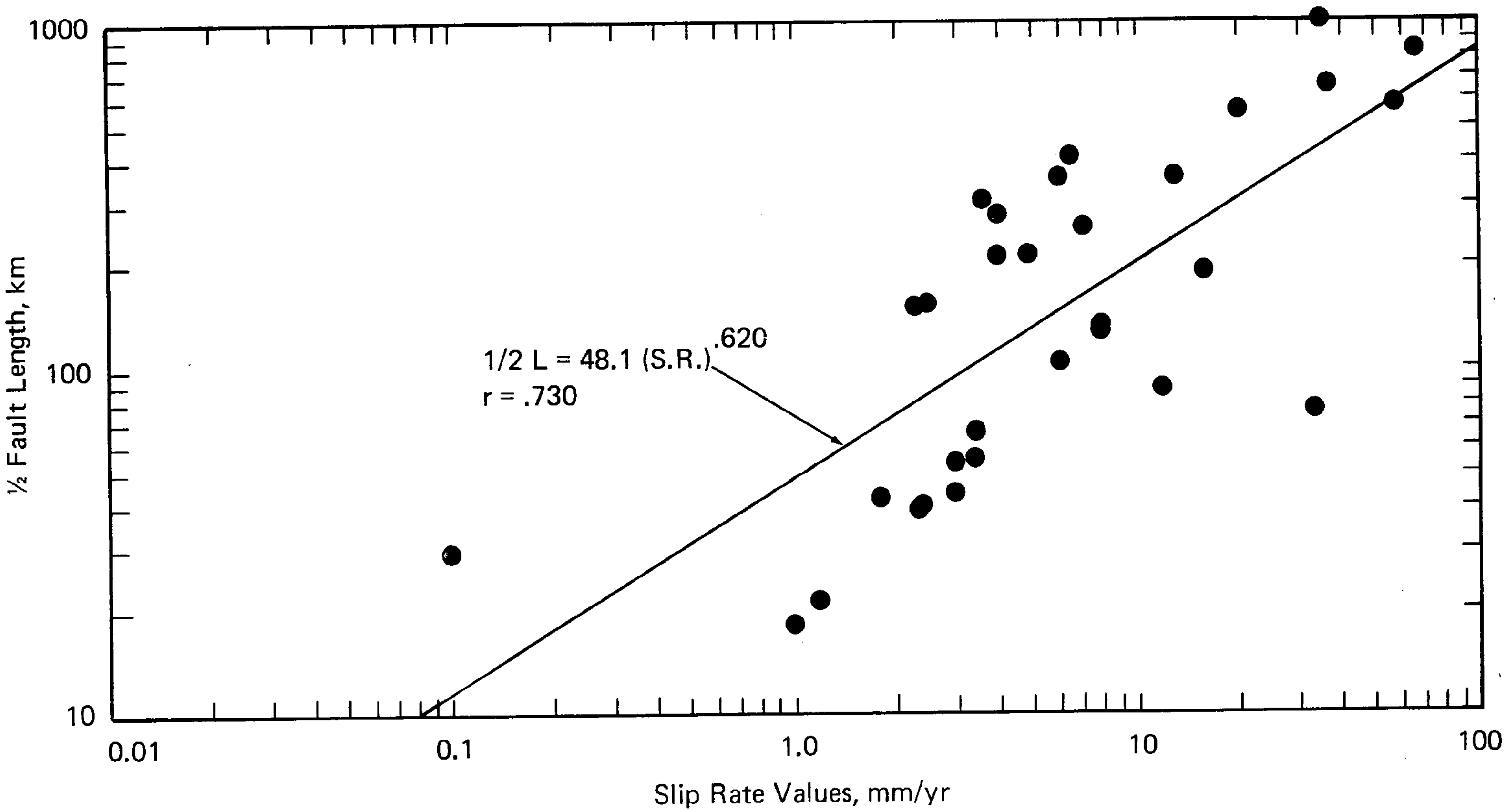

Note: For Data Base See Table 361.51 - 1

Figure 361.38 - 2 Least Squares Linear Regression, 1/2 Fault Length as a Function of Selected Slip Rate

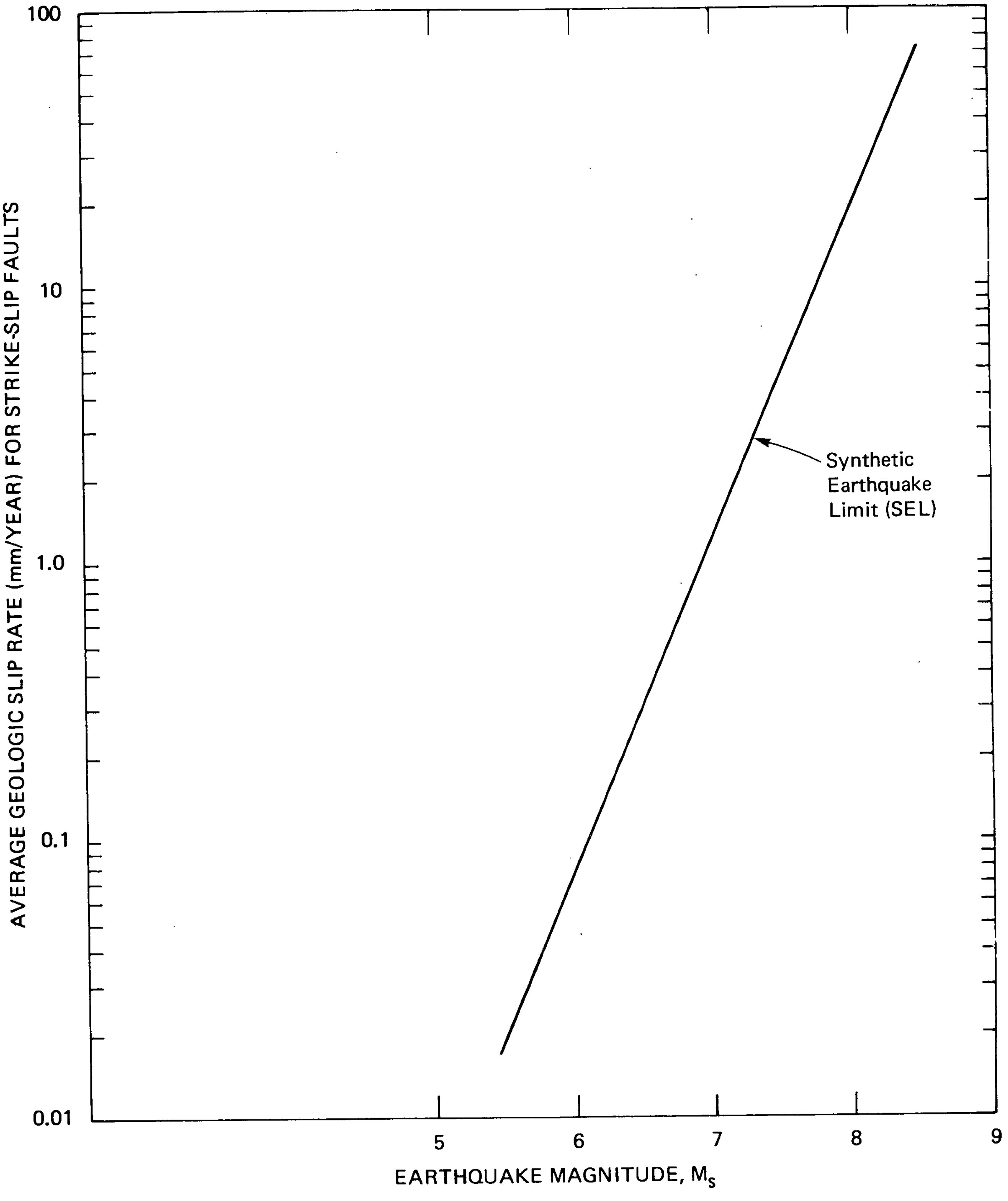

Figure 361.38 - 3 Synthetic Plot Based on Slip Rate vs ½ Fault Length and Slemmons (1977), Rupture Length vs Magnitude for Strike-Slip Faults

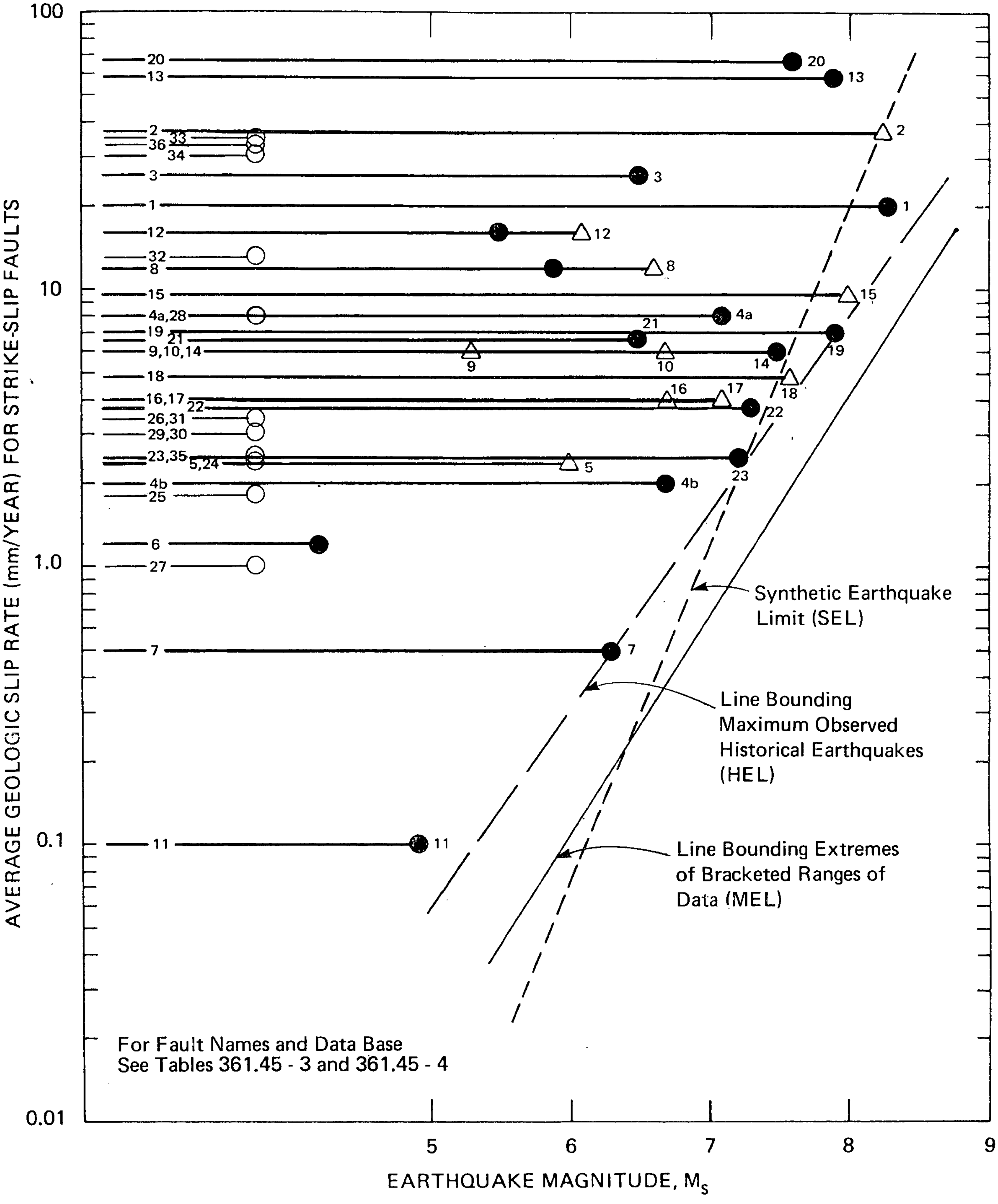

EXPLANATION

- ● Maximum instrumental recording
- △ Maximum pre-instrumental estimates
- — Range over which smaller earthquakes occur
- ○ No maximum magnitude from instrumental or pre-instrumental data.

Figure 361.38 - 4 SEL, MEL, HEL Comparison Geologic Slip Rate VS Historical Magnitude for Strike–Slip Faults

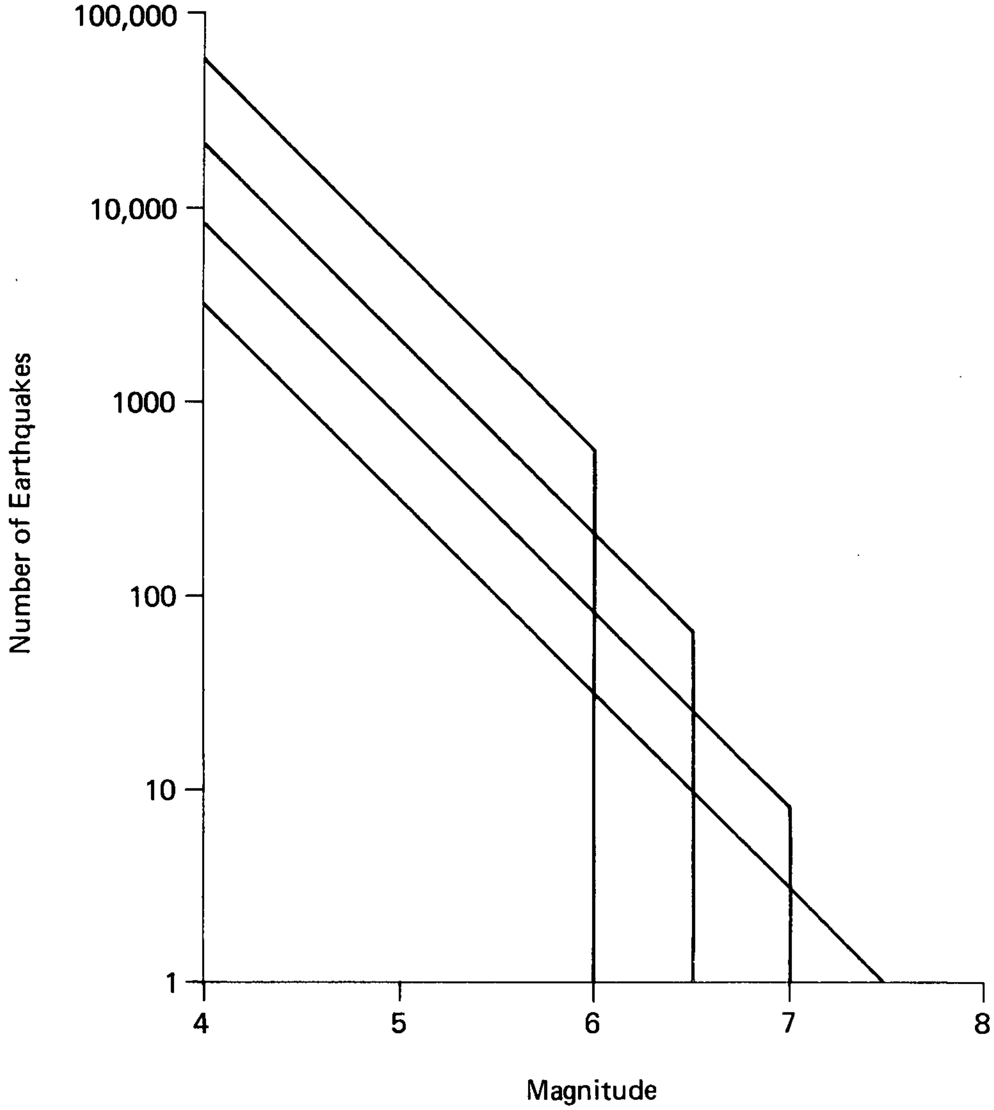

b = 0.85
Constant Slip Rate (Moment Rate)

Figure 361.38 - 5 Effect of Maximum Magnitude on Recurrence

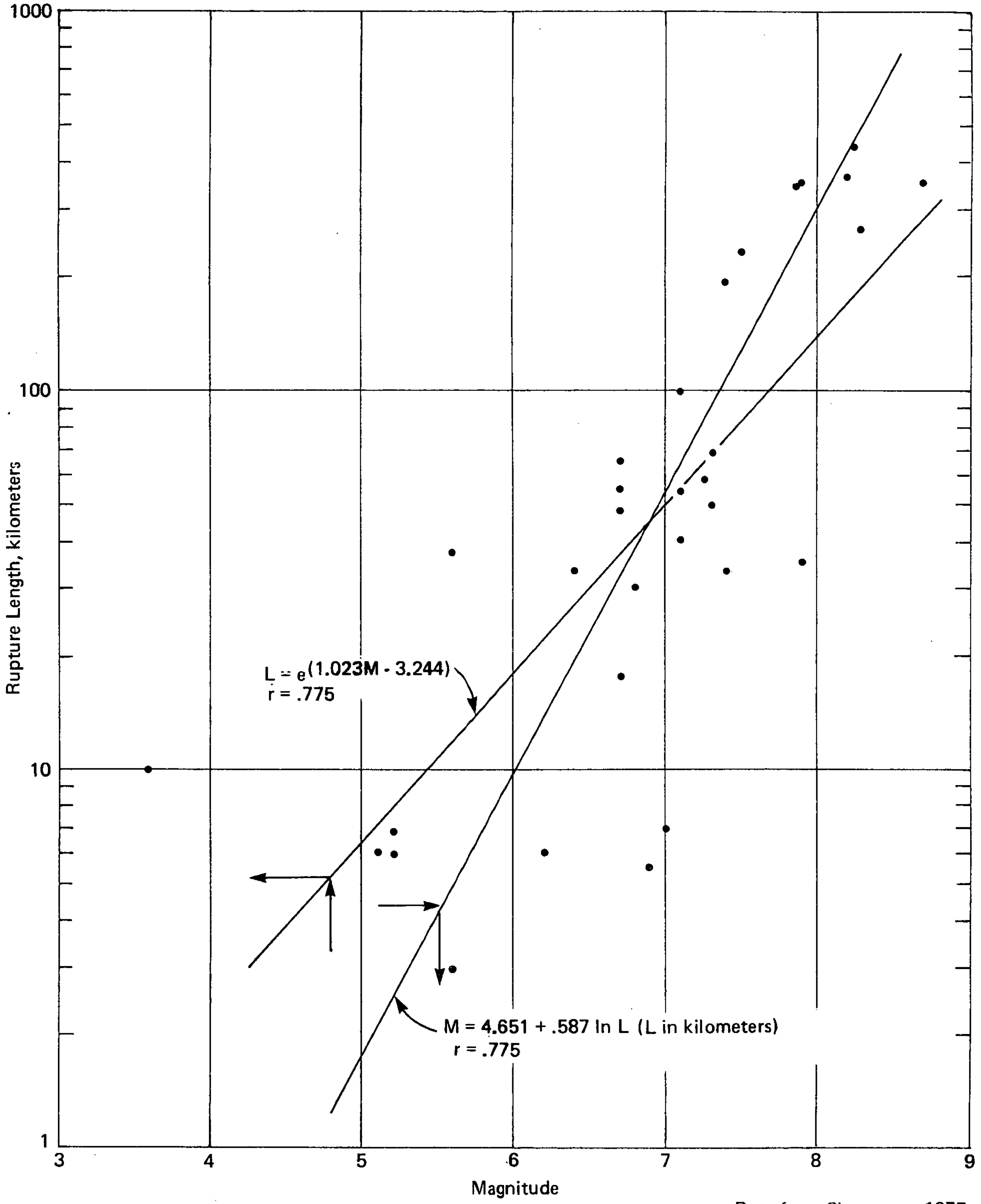

Data from Slemmons, 1977.

Figure 361.38 - 6 Least Squares Linear Regression, Strike-Slip Faults Rupture Length vs. Magnitude

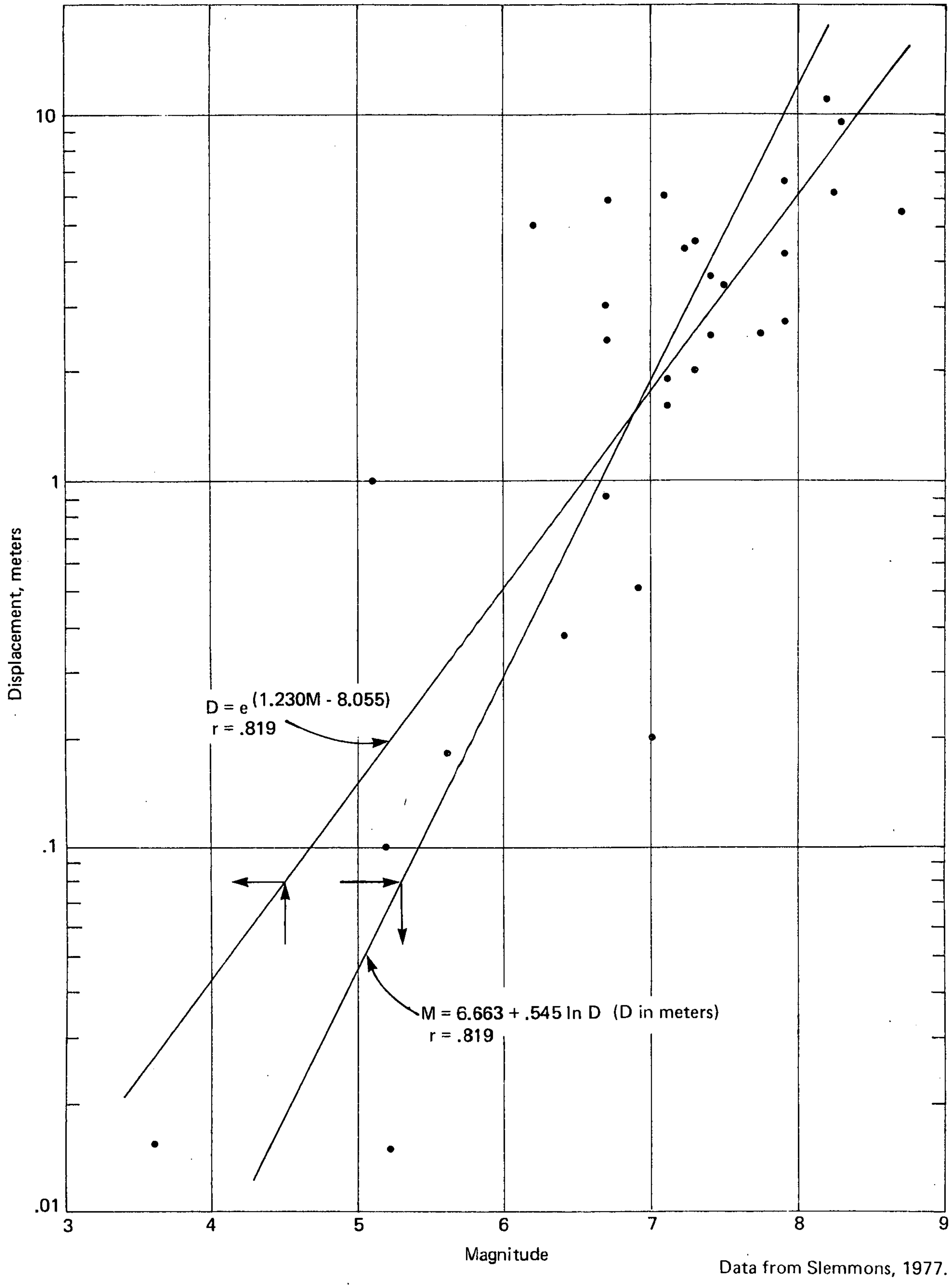

Figure 361.38 - 7 Least Squares Linear Regression, Strike-Slip Faults Displacement vs. Magnitude

QUESTION 361.39

Has the December 8, 1812 Earthquake (M6.5) been considered as being associated with a local structural source in the analysis of the safe shutdown earthquake? If such is the case, how does this conclusion affect the determination (CDMG Open File Report 79-6 SAC)?

RESPONSE 361.39

Two earthquakes reported during the historical period in Southern California have been located by Toppozada and others (1979) in proximity to the OZD: 1) the 22 November 1800 earthquake which caused damage in San Juan Capistrano and cracked buildings in San Diego (maximum intensity VII--MM), and 2) the earthquake of 8 December 1812 which destroyed the San Juan Capistrano Mission (maximum intensity VIII--MM).

The locations of these events have been fixed near San Diego and near San Juan Capistrano by Toppozada and others (1979) on the basis of the felt reports. Magnitude 6 1/2 was estimated for each earthquake based on the maximum reported intensity and estimated isoseismal areas (Toppozoda and others, 1979). Population density and historical record-keeping were so limited at the times of these earthquakes that reports are available from only a few missions along the Southern California coast. Thus, there is limited north-south control on the locations of the events and very little, if any, east-west control.

In order to assess further the location control for these events, comparisons of these early earthquakes were made with the isoseismal distributions of the 1933 Long Beach and

1968 Borrego Mountain earthquakes, both near magnitude 6 1/2. These two strike-slip earthquakes had areas of intensity VII (intensity likely to cause damage) of dimensions approximately 40 km along the strike of the fault and 10 to 20 km on either side of the fault that ruptured (Oakeshott, 1973; Cloud and Scott, 1970). Applying these dimensions to the locations proposed by Toppozada and others (1979) suggests that for each event there are known or possible earthquake sources consistent with the intensity VII isoseismal dimensions that lie between the Elsinore fault to the east and the Palos Verdes and San Clemente faults to the west, bracketing the OZD. Review of the data sources as reported by Toppozada and others (1979), Agnew and others (1979), and Townley and Allen (1939) suggests that it is not possible to establish a specific geologic association for the two earthquakes.

The comparison of the isoseismal felt areas of the 1933 and 1968 earthquakes with the 1800 and 1812 earthquakes suggests that, if the locations near the OZD proposed by Toppozada and others (1979) are correct, then the estimated magnitude values are probably high. Additional felt reports should have been noted for other missions in the area, particularly near the Los Angeles basin. Such reports were noted for another large earthquake that occurred near Santa Barbara on 22 December 1812.

It is possible that the 8 December 1812 and 22 November 1800 events could have been associated with the OZD, but there is no impact on the maximum earthquake evaluation if they were in fact associated with the OZD. With the worst interpretation they could be about comparable to the 1933 Long Beach earthquake in size and intensity. Ground motions for such events are well within the project design basis.

REFERENCES

Agnew, D. C., Legg, M., and Strand, C., 1979, Earthquake history of San Diego, in Abbott, P. L., and Elliott, W. J., eds., Earthquakes and Other Perils, San Diego region: San Diego Association of Geologists for Geological Society of America, Field Trip Guidebook, p. 83-100.

Cloud, W. K, and Scott, N. H., 1970, Intensity distribution and field effects, in The Borrego Mountain Earthquake of April 9, 1968: U. S. Geological Survey Professional Paper 787, p. 142-153.

Oakeshott, G. B., 1973, Forty years ago...the Long Beach-Compton Earthquake of March 10, 1933: California Geology, v. 26, no. 3, p. 55-59.

Toppozada, T. P., Real, C. R., Bezore, S. P., and Parke, D. L., 1979, Compilation of Pre 1900 California Earthquake History--Annual Technical Report Fiscal Year 1978-79: California Division of Mines and Geology Open-File Report OFR79-6SAC, 271 p.

Townley, D., and Allen, M. W., 1939, Description catalog of earthquakes of the Pacific Coast of the United States 1769 to 1928: Seismological Society of America Bulletin, 297 p.

QUESTION 361.40

Why hasn't the Coronado Banks-Palos Verdes fault been considered in the earthquake analysis? The fault has in excess of 50 ft of sea floor offset and shows youthful and long, continuous fault features (Unpublished report, "Final Technical Report, USGS, Office of Earthquake Studies, Contract No. 14-08-0001-17699, Kennedy et al."). The slip rate on this fault may contradict WC's view that all faults west of the San Andres fault have lower slip rates with increasing westerly distance.

RESPONSE 361.40

The Coronado Banks and Palos Verdes faults were not considered in this or in earlier earthquake analyses for SONGS because of their greater distance (35 km) from the site than the hypothesized OZD (8 km) as shown on figure 361.40-1. The Applicants' study of slip-rate/maximum-magnitude relationsips used strike-slip faults. The strike-slip nature of these two faults is conjectural, and both faults display abundant evidence of vertical movement.

The rate of strike slip of either the Palos Verdes or Coronado Banks faults is poorly known, and the lack of conclusive evidence for strike slip precluded their consideration in the Applicants' analysis. The intent with respect to decreasing activity west of the San Andreas was to characterize the structures between the San Andreas and the hypothesized OZD in a relative ranking comparison. There was no intent to claim that faults farther west were similarly less active. Indeed, the San Clemente fault zone is one of those that may be more active than the hypothesized OZD.

QUESTION 361.41

Your seismotectonic model for southern California is based on an apparent decrease in activity to the west of the San Andreas fault zone. The figures shown in the report suggest this relation, but the data shown for the 200-mile radius about the site as given in the FSAR, the surface faulting and earthquake activity to the southeast on the same structural trends as the OZD do not necessarily support this model. The discussion of the seismotectonic setting should include an analysis of the relation of the OZD to faults and earthquake activity to the south in Baja California and into the offshore borderland to the west of Baja California. The discussion should include the apparent increase in level of activity toward the San Miguel and Agua Blanca fault zones, to the southeast along the strike of the OZD. The analysis should include discussions of the possible structural continuity, either at the surface or at depth, with the Vallecitos, Tres Hermanos, San Miguel, Agua Blanca fault zone. The discussion should include where appropriate, the general relationships of conjugate faulting, earthquake mechanism, recurrence relations or other relevant data. In addition to the above features the following should be discussed:

a. Does the post-1975 earthquake activity within a 200-mile radius of San Onofre show any new patterns of activity for the greater than 3, greater than 4, and greater than 5 earthquake magnitude ranges, that is indicated by the San Onofre 2 & 3 FSAR Figures 2.5-15, 16, 17, and 18?

b. Describe the OZD in relation to major geomorphic, structural and topographic zones of Baja California and its adjoining offshore areas.

RESPONSE 361.41

The response to this question has been separated into three sections 361.41 a through c. Section 361.41 a responds to part "a" of the question regarding post-1975 earthquake activity within a a 200-mile radius of San Onofre. Section 361.41 b responds to part "b" of the question regarding the relationship between the OZD and major structural and topographic zones of Baja California. The last section 361.41 c addresses several points commented on in the question relating to the seismicity of Baja. Specifically it discusses the stated apparent increase in activity toward the San Miguel and Agua Blanca fault zones, the seismicity of northern Baja, and microseismicity in northern Baja.

361.41 a Post-1975 Earthquake Activity Within a 200-Mile Radius

In this response the post-1975 earthquake activity (January 1975 through September 1979) of magnitude greater than 3.0 is summarized and compared to the preceding reports of activity in the 200-mile region around the site. No significant change in the activity pattern is noted. Data were obtained from the unpublished data file of the California Institute of Technology; these data are in the same form as those reported by Hileman and others (1973). Although the instrumentation coverage within the California Institute of Technology network is sufficient to provide locations of earthquakes of about magnitude 3 and larger within the onshore U. S. portion study area, detection and locations for activity for offshore and in Mexico as provided by the Caltech array is not necessarily complete and locations are probably less accurate. No better locations are known to be available for this time period, however, so the seismicity of Mexico is described in terms of the Caltech data. The magnitudes reported by the Caltech network are in M_L (local magnitude).

No earthquakes with $M_L \geq 6.0$ occurred during the post-1975 time period. Eight earthquakes occurred with $M_L \geq 5.0$ (see Figure 361.41-1) (4 of these were in Mexico and 4 in southern California) in regions of known historic activity (Hileman and others, 1973; FSAR Figure 2.5-16). None are closer than 70 miles from the site. In July 1975 one earthquake occurred between the San Miguel and Sierra Juarez fault zones with $M_L = 5.0$. This event is located near the 1974 Pino Solo earthquake ($M = 5.0$) (A. Nava, in preparation, Doctoral Dissertation, UCSD, referenced in Brune and others, 1979).

The seismicity with $M_L \geq 4$ is dispersed throughout southern California and Mexico (see Figure 361.41-2). The spatial distribution is generally similar to the 1932-1975 distribution of $M_L \geq 5$ earthquakes (FSAR Figure 2.5-16), suggesting stability of seismic source regions for small earthquakes in time and space. The number of events for the 4 year period ($M_L \geq 4$) is roughly equivalent to the number $M \geq 5$ for the 43 year period, which is consistent with a frequency of $M \geq 4$ about 10 times greater than $M \geq 5$, as expected from the frequency-magnitude relationship $\text{Log } N = a - bM$ (Richter, 1958). The closest earthquake lies about 45 miles SW from the site. In Mexico, the distribution of earthquakes $M \geq 4$ is oriented SW-NE, or perpendicular to the general trend of mapped faults. One earthquake, the 19 August 1978 Canon de la Presa event, has been relocated in a special study by Brune and others (1979). On the basis of that study the true location is north of the Caltech location shown here; i.e., between the NE terminus of the San Miguel fault zone (as shown on the base map) and the City of Tijuana. The Caltech magnitude is

M_L 4.1; Brune and others (1979) assign M_L 3.5. At the magnitude 4 level, no activity is associated with the Newport-Inglewood, OZD, or Rose Canyon fault zones in southern California. Two events occurred along the Whittier-Elsinore, and 4 events along the San Jacinto fault zones.

A low level of seismicity again prevails but is not entirely absent for earthquakes with $M_L \geq 3.0$ within 50 miles of the site (see Figure 361.41-3). The closest earthquake is about 9 miles NW of the site; a second is about 25 miles south. Activity occurs along the Newport-Inglewood fault zone (30-60 miles NW of the site) in the region of the aftershock zone of the 1933 Long Beach earthquake (Richter, 1958). Scattered activity is observed SE and SSE of the site but is not easily associated with known faults. Modest activity (7 events) is observed within about 25 miles of San Diego, but no earthquake is closer than 10 miles from the Rose Canyon fault. Substantial activity occurs between the southern half of the San Miguel and Sierra Juarez fault zones, between 50 and 100 miles SE of Tijuana.

In summary, the seismicity between January 1, 1975, and October 1, 1979, within 200 miles of the site is similar to the long term pattern from 1932 to 1975 and no distinctive, new patterns of activity are evident. Seismic activity suggests an apparent decrease westward between the San Andreas and San Jacinto faults and the hypothesized OZD. The offshore region is somewhat more active than the hypothesized OZD for the post-1975 period.

361.41 b Relationship Between the Hypothesized OZD and Other Major Topographic Features in Baja California

The following discusses the structural relationship of the major fault systems of Baja California and the possible structural and geomorphic continuity of these faults to the OZD. The geographic area to be described consists of the region of Baja California north of the Agua Blanca fault to the U.S./Mexico Border and the region west of the Sierra Juarez to the Pacific Coast. Specific attention will be paid to the geologic and regional tectonic setting, the San Miguel fault zones, the Vallecitos fault zone, the Agua Blanca fault, and the possible connections between the San Miguel fault zone, the Vallecitos fault zone, and the hypothesized OZD.

Geologic Setting

The northwestern corner of Baja California can be divided into three physiographic and geologic provinces (see Figure 361.41-4): (1) a narrow coastal margin characterized by Tertiary marine and nonmarine sedimentary rocks and Tertiary-to-Holocene volcanic and volcanic-derived rocks; (2) the gently seaward sloping foothills between the Pacific Coast and the central high peninsular ranges underlain by pre-batholithic eugeoclinal accumulations of volcanic and sedimentary rocks which were subsequently metamorphosed to varying degrees by intrusion of the batholith; and (3) the Peninsular Range of northeastern Baja California comprised of middle Cretaceous plutonic rocks of the southern California batholith.

Regional Tectonic Setting

Structurally, the western two-thirds of the northern part of Baja California consists of an uplifted and westwardly tilted fault block. The high eastern edge of the block is formed by the mountain ranges of the Sierra Juarez to the north and the Sierra San Pedro Martir to the south. Uplift of the eastern edge began about 10 million years ago (Gastil and others, 1975). The eastern escarpment was created by a series of east-dipping normal faults that downstep antithetic fault blocks towards the Gulf of California depression (Gastil and others, 1979).

The main structural block has been cut by three major fault zones: the Agua Blanca fault zone, the San Miguel fault zone, and the Vallecitos fault zone. The Agua Blanca fault zone trends westerly from its eastern limit in the Sierra Juarez to the Pacific coast south of Ensenada. Movement along the Agua Blanca system began during late Cretaceous time (Gastil and others, 1975).

The major northwest-trending faults of this region (the San Miguel and Vallecitos fault zones) and the adjacent continental borderland faults are believed to have been formed later in Middle Miocene time (Moore, 1969).

Generally, the principal fault systems of the northwest peninsula region are considered to be primarily strike-slip but many show evidence of dip-slip displacement as well. However, they do not appear to connect with the major dip-slip faults of the Sierra Juarez and Sierra San Pedro Martir.

The Agua Blanca fault zone is characterized by a relatively continuous main trace while the San Miguel and Vallecitos fault zones are characterized by en echelon fault segments and associated shorter subparallel faults. Much shorter conjugate set of left-lateral faults trend northeast across the region. Features along the two major northwest-trending fault zones suggest Quaternary activity. The major northwest and west trending faults are discussed separately below.

San Miguel Fault Zone

The San Miguel fault zone consists of two segments. In 1956, a 20-km length of the southern segment broke along a series of short en echelon ruptures (Shor and Roberts, 1958). Measured fault displacements ranged from 0 to 31 inches horizontally to 0 to 36 inches vertically; the sense of offset was uniformly right-lateral and down to the southwest. The southern segment is mapped as a principally dip-slip fault that dies out in the Sierra Juarez and does not connect with either the Agua Blanca fault or the dip-slip faults of the eastern escarpment (Gastil and others, 1975). There is no evidence that this fault offsets this escarpment or connects with faults in the Gulf of California.

The northwest end of the 1956 break lies en echelon to the northern segment. The northern segment can be traced on air photos to the area northeast of Valle San Rafael where offset streams and dikes show right-lateral separation; the most clearly expressed fault trace appears to separate Mesozoic dikes only 100 m (Gastil, 1975, 1979).

Vallecitos Fault Zone

The Vallecitos fault zone is en echelon to the northern segment of the San Miguel fault zone, but separate from it by a distance of 6 to 10 km. The Vallecitos fault has a nearly continuous trace that extends from the western edge of the Sierra Juarez 65 km to the west end of the Valle de las Palmas (about 29 km southeast of Tijuana). As noted by Gastil and others (1979) the main trace of the fault is marked by erosional topographic features, and there is no evidence that the Vallecitos offsets anything younger than the crystalline basement rocks. An unpublished map by a former Stanford graduate student shows only 3 km of right-lateral separation of a Cretaceous pluton boundary (cited in Gastil and others, 1979).

Calabasas Fault

The Calabasas fault is mapped about 5 km east of the Vallecitos fault zone and trends parallel to it for about 30 km in a northwest-southeast direction. In the Valle de las Palmas area, recent movement may be indicated by small sags and saddles, breaks in uplifted alluvial deposits, and relatively uneroded scarplets (Gastil and others, 1975, 1979).

Tres Hermanos Fault

The Tres Hermanos fault zone is located midway between the San Miguel and Agua Blanca fault zones and essentially parallels the San Miguel fault zone. The trace, approximately 45 km long, begins in the batholithic rocks and dies out east of Ensenada. The fault is indicated by pronounced topographic expression and is apparent on high altitude photos, yet recency of movement and sense of displacement are unknown (Gastil and others, 1979).

Agua Blanca Fault Zone

The Agua Blanca fault zone extends about 129 km across the western two-thirds of the Baja California peninsula. The Santo Tomas fault branches off the western portion of the Agua Blanca fault. These faults are distinctive for their west-northwest trend that is more westerly than the strike-slip faults to the north. The trace of the Agua Blanca fault is indicated by abundant geomorphic evidence (Allen and others, 1960; Hamilton, 1971). Typical features are distinct scarps, offset streams, shutteridges, fault sags and saddles, and fault-controlled valleys. Quaternary fan gravels in the Valle de Agua Blanca are offset about 4.8 km in a right-lateral sense; between 11.3 km and 22.6 km of similar separation may be indicated by discontinuous igneous contacts across the fault trace (Allen and others, 1960). Detailed field mapping (Allen and others, 1960; Gastil and others, 1975) indicates that the east end of the Agua Blanca fault dies out in the Sierra San Pedro Martir and does not intersect the dip-slip faults of the eastern escarpment.

The offshore extension of the Agua Blanca fault west of the landward traces of the Agua Blanca and Santo Tomas faults is characterized by complex submarine topography (Krause, 1965). Recent investigations show that the offshore-onshore fault relationship is not present as a continuous through-going feature. Legg and Kennedy (1979) recognized the offshore portion of the Agua Blanca fault as a series of subparallel en echelon segments. A component of vertical movement is indicated locally by Quaternary seafloor scarps with several hundred meters of relief (Krause, 1965; Legg and Kennedy, 1979). Near the Todos Santos Islands northwest of Punta Banda, the fault zone makes a northwest bend and continues north in the form of relatively short en echelon segments trending toward either the San Clemente or the

Coronado Banks fault zones. A more detailed and complete discussion of the offshore borderland faults is presented in response 361.40.

Tectonic Implications

Evidence for the amount of total displacement on faults within the San Miguel and Vallecitos fault zones is limited. The suggested amount of lateral offset, where indicated, is poorly defined and ranges from 100 m to 3 km. North of the Agua Blanca fault zone, the region west of the Sierra Juarez and Sierra San Pedro Matir escarpment has acted as a relatively stable block as indicated by the small amount of overall displacement on the San Miguel fault zone and the Vallecitos fault zone. These two zones are inferred to be relatively young features that, along with similar right-lateral strike-slip faults of the region reflect a change in the relative plate motions from subduction to transform motion along the southern California-Baja California continental margin (Crouch, 1979).

The Agua Blanca fault is an older tectonic element initiated in the late Cretaceous. The east end of the Agua Blanca dies out in the batholithic rocks before reaching the coastal plain of the Gulf. Seismic profiling along the western Gulf margin has shown that the structural elements of the northern Gulf are not continuous with the onshore fault zones in the northern peninsula (Henyey and Bischoff, 1973).

Although some secondary northeast trending faults with scarce indications of left-lateral motion have been mapped in the region, the evidence is generally poor to support the hypothesis of a conjugate fault system. The northwest-trending strike-slip fault systems of the northwestern Baja region appear to be reacting to regional shear influenced by the relative plate motions and are not directly connected with transform features in the Gulf of California.

Possible Connection Between the Rose Canyon and the San Miguel or Vallecitos Fault Zones

Several authors have suggested that an en echelon relationship may exist regionally between the Rose Canyon fault zone and the San Miguel and Vallecitos fault zones (see response 361.60 b for summary and discussion). A possible northwest extension of the presently mapped limits of either the Calabasas or Vallecitos faults has been inferred by these authors largely on the basis of the regional alignment of discontinuous topographic, structural, and geothermal features in the southern San Diego and southeast Tijuana area. However, geologic maps by Kennedy (1975) and Gastil and others (1975) indicate a 55 km distance between the south end of the Rose Canyon fault and the north end of the Vallecitos fault.

Gastil and others (1979) suggest the possibility of a northwest-trending lineament that would continue from the northwesternmost mapped trace of either the Vallecitos or the Calabasas faults, through eastern Tijuana, and across the U.S.-Mexico Border just west of San Ysidro. This suggested lineament crosses an area with an historically quiet seismic record (with the exception of the 1978 Canon de la Presa earthquake.

Features (Gastil and others, 1979) that suggest this lineament are:

(a) the subparallel alignment of the Tijuana River Valley and the Valle de las Palmas, trends of faults in the San Ysidro area, and the alignment of several thermal wells;

(b) the contrast between Eocene stratigraphy north and south of the lineament; and

(c) the mapped traces of northeast-trending dip-slip faults in the southern Tijuana-Rosarito Beach area which do not continue across the lineament.

If the lineament suggested by Gastil and others (1979) is a fault, it would trend northwest from the Valle de las Palmas area, cross the Eocene bedrock exposures, and continue beneath the deeply alluviated Tijuana River Valley possibly into the San Diego Bay area (see response 361.60 a for a discussion of faulting in the San Diego Bay area).

Although this lineament has been suggested by Gastil and others (1979), the lack of faulting in the well-exposed Eocene bedrock, and the lack of fault features recognized on aerial photographs of the area by Gastil suggest that no significant faulting has occurred in this area since Eocene time. Geophysical data by Kennedy (1977) (see Table 361.60-1, in reference to response 361.60a) does not identify significant faulting along the proposed connection of the San Miguel and Vallecitos faults and the Rose Canyon fault in the area south of San Diego Bay and north of the International Border. Therefore, the applicant's position is that the observed evidence is not supportive of a throughgoing fault that could connect the RCFZ with either the Vallecitos or San Miguel fault zones.

The most prominent faulting associated with the southern part of the RCFZ is to the southwest, rather than to the southeast. The south part of the RCFZ is represented by a widening zone of shorter, principally dip-slip faults that are mapped in the offshore area west of San Diego Bay. These faults generally diminish in expression and die out when traced in a southerly direction. This portion of the RCFZ is discussed in detail in the response to question 361.60a.

361.41 c Seismicity of Northern Baja California

Northern Baja California is an area of extremely high seismicity; at least 13 earthquakes of magnitudes greater than 6.0 have occurred since 1900 (Brune and others 1979). Previous epicenters in this region (Hileman and others 1973; FSAR Figure 2.5-16) appear to scatter across the peninsula, suggesting a broad zone of deformation. Recent investigations, including field studies (Reyes et al., 1975; Johnson et al., 1976) and the relocation of epicenters (Leeds, 1979; Brune and others 1979) in the region, indicate that the vast majority of earthquakes are associated with a few active faults.

The San Miguel Fault appears to be the seismically dominant fault in the northern Baja California region. In 1956, four large earthquakes (magnitude 6.1 to 6.8) occurred along the San Miguel fault near the town of San Miguel (Brune and others 1979). In addition, Leeds (1979) has relocated five earthquake epicenters with magnitudes greater than 5.0 to the San Miguel fault zone; one of these was relocated near the northwest end of the San Miguel fault near the Vallecitos fault. Relocation errors as large as 90 km were noted in earlier catalog locations.

Microearthquake activity in the San Miguel fault zone is very high. Reyes and others (1975) operated high-gain portable seismographs at 22 stations in this region with detection level estimated to be less than magnitude 2. Sixteen of these stations reported microearthquake rates greater than 27 events per day. The highest rates, exceeding 100 events per day, were recorded near the southeast end of the San Miguel fault. In a study by Johnson and others (1976), the San Miguel fault was found to be seismically active along its length and responsible for the vast majority of recorded earthquakes in this region. Hypocenters on the San Miguel fault ranged in depths from 0 to 20 kilometers. Composite focal mechanisms from this study indicated a mixture of right-lateral and dip-slip (east side up) movement that was consistent with surface evidence.

No large historic earthquakes are positively correlated with the Agua Blanca fault (Allen and others, 1960; Brune and others, 1979). Magnitude 6.0 and 6.3 earthquakes of 1954, previously located along this fault, have been relocated to the San Miguel fault (Leeds, 1979). Very low rates of microearthquake activity have been recorded on the Agua Blanca fault (Johnson and others 1976).

The activity of the plate boundary to the east of the hypothesized OZD is compared with parallel faults in the June 1979 report and a westward decrease in activity is noted. It is clarified in the response to question 361.40 that areas to the west of the hypothesized OZD do not necessarily maintain that westward decrease in seismicity. In Baja California, the basis for evaluating comparative levels of activity is limited by data availability; however, the seismic activity in Baja during the period 1971 to the present does provide a limited basis for such an evaluation.

In considering all the earthquakes with M_L of 6.0 or greater north of 31.5 degrees latitude, most seismic slip appears to be associated with either the San Miguel fault or with the ridge-transform fault system extending from the Gulf of California to the Salton Sea. These earthquakes are listed in Table 361.41-1 and are taken from Brune and others (1979), Hileman and others (1973), and Caltech (unpublished). The relationship of Thatcher and Hanks (1973) can be used to calculate moment values for these earthquakes. Although the relationship proposed by Thatcher and Hanks was developed for M_s, the use of M_L values will not produce a significant discrepancy and is suitable for comparative purposes. The cumulative moment thus calculated for the San Miguel zone is 2.9×10^{26} dyne-cm and for the plate boundary zone is 12.4×10^{26} dyne-cm. Assuming that the fault zones are of similar depth, the total seismic slip is directly proportional to the moment and varies inversely as the fault length. Since the plate boundary zone is about twice as long as the San Miguel fault zone, the total slip on the plate boundary is about twice the total slip on the San Miguel. Thus, for the Baja California area, there is a decrease in historical seismicity to the west of the plate boundary faults, but the westward activity is dominated by the San Miguel fault.

Various authors have alternately proposed and contested that the hypothesized OZD, NIZD, RCZD, and San Miguel fault zones are connected (Abbott and Elliott, 1979). At the present time "exact relationships between these fault zones have not been established" (Brune and others, 1979). Based on data presented available (Abbott and Elliott, 1979; Hileman and others, 1979; Reyes and others, 1979), large or small earthquakes or microearthquakes do not delineate such a connection. A very small number of small earthquakes have occurred in the San Diego and Tijuana regions and near the hypothesized OZD: however, the pattern is highly diffuse (Hileman and others, 1979). The only tentative pattern in the seismicity is a short EW trend at San Diego which may intersect a weak NW-SE trending zone of activity near the Coronado Banks fault zone (Legg and Kennedy, 1979). This can only be seen in the more accurately located epicenters. One earthquake (M_L = 3.5, Brune and others, 1979; M_L = 4.1, Caltech) has been well located between Tijuana and the mapped trace of the San Miguel fault zone. This event does not consititute evidence of a connection between the San Miguel and Rose Canyon, since events of this size commonly occur in many areas of southern California and Mexico with no proximity to through-going faults (Hileman and others, 1979). An example of a well located event of this kind in Mexico is the Pino Solo earthquake (M = 5.0) of 1974 (Brune and others, 1979).

In summary, (1) the historical seismicity of the northern Baja California area is dominated by the high level of activity of the San Miguel fault, although this level is about one-half as high as that on the plate boundary faults (Cerro Prieto, Imperial, and others) to the east. (2) based on seismological evidence the San Miguel fault does not appear to be mechanically connected to the hypothesized OZD to the north.

REFERENCES

Abbott, P. L., ed., 1979, Geological excursions in the southern California area--prepared for the Geological Society of America Annual Meeting: San Diego State University Department of Geological Sciences, 217 p.

Abbott, P. L., and Elliott, W. J., eds., 1979, Earthquakes and Other Perils, San Diego region: San Diego Association of Geologists for Geological Society of America, Field Trip Guidebook, p. 83-100.

Allen, C. R., Silver, L. T., Stehli, F. G., 1960, Agua Blanca fault--a major transverse structure of northern Baja California, Mexico: Geological Society of America Bulletin, v. 71, p. 457-482.

Brune, J. N., and Simmons, R. S., Rebollar, C., and Reyes, A., 1979, Seismicity and faulting in northern Baja California, in Abbott, P. L., and Elliott, W. J., eds., Earthquakes and Other Perils, San Diego region: San Diego Association of Geologists for Geological Society of America, Field Trip Guidebook, p. 83-100.

Crouch, J. K., 1979, Neogene tectonic evolution of the California continental borderland and western transverse ranges: Geological Society of America Bulletin, part 1, v. 90, p. 338-345.

Crowell, J. C., and Sylvester A. G., eds., 1979, Tectonics of the juncture between the San Andreas fault system and the Salton Trough, southeastern California--A guidebook for the Annual Meeting Geological Society of America: University of California at Santa Barbara, Department of Geological Sciences, 193 p.

Flynn, C. J., 1970, Post-batholithic geology of the La Gloria-Presa Rodriguez area, Baja California, Mexico: Geological Society of America Bulletin, v. 81, p. 1789-1806.

Gastil, R. G., Phillips, R. P., and Allison, E. C., 1975, Reconnaissance geology of the State of Baja California, Mexico: Geological Society of America, Memoir 140, p. 170.

Gastil, R. G., Kies, R., and Melius, D. J., 1979, Active and potentially active faults; San Diego County and northwestern-most Baja California, in Abbott, P. L., and Elliott, W. J., eds., Earthquakes and Other Perils, San Diego region: San Diego Association of Geologists for Geological Society of America, Field Trip Guidebook, p. 47-60.

Hamilton, W., 1971, Recognition on space photographs of structural elements of Baja California: U. S. Geological Survey Professional Paper 718, p. 26.

Henyey, T., and Bischoff, J. L., 1973, Tectonic Elements of the Northern part of the Gulf of California: Geological Society of America Bulletin, v. 84, p. 315-330.

Hileman, J. A., Allen, C. R., and Nordquist, J. M., 1973, Seismicity of the southern California region, 1 January 1932 to 31 December, 1972: California Institute of Technology, Pasadena, 487 p.

Johnson, T. L., Madrid, J., and Koczynski, T., 1976, A study of microsesimicity in northern Baja California, Mexico: Seismological Society of America Bulletin, v. 66, no. 6, p. 1921-1929.

Kennedy, M P., 1975, Geology of the western San Diego metropolitan area in Geology of the San Diego metropolitan area: California Division of Mines and Geology, Bulletin 200, p. 113-39.

Kennedy, M. P., Welday, E. E., Borchard, G., Chase, G. W., and Chapman, R. H., 1977, Studies of surface faulting and liquefaction as potential earthquake hazards in urban San Diego, California: California Division of Mines and Geology final technical report.

Krause, D. C., 1965, Tectonics, Bathymetry, and Geomagnetism of the Southern Continental Borderland West of Baja California Mexico: Geological Society of America Bulletin, v. 76, p. 617-650.

Leeds, A. L., 1979, Relocation of M > 5.0 northern Baja California earthquakes using S-P times: Master's thesis (unpublished) University of California, San Diego.

Legg, M. R., and Kennedy, M. P., 1979, Faulting offshore San Diego and northern Baja California, in Abbott, P. L., and Elliott, W. J., eds., Earthquakes and Other Perils, San Diego region: San Diego Association of Geologists for Geological Society of America, Field Trip Guidebook, p. 29-46.

Moore, D. G., 1969, Reflection profiling studies of the California continental borderland: Structure and Quaternary turbidite basins: Geological Society of America Special paper 107, p. 142.

Reyes, A., Brune, J., Barker, T., et. al., 1975, A microearthquake survey of the San Miguel fault zone, Baja California, Mexico: Geophysical Research Letters, v. 2, no. 2, p. 56-59.

Richter, C. F., 1958, Elementary seismology: W. H. Freeman, San Francisco and London, 768 p.

Shor, G., and Roberts, E. E., 1958, San Miguel, Baja California Norte, earthquakes of February, 1956--A field report: Seismological Society of America Bulletin, v. 48, p. 101-116.

Thatcher, W., and Hanks, T. C., 1973, Source parameters of southern California earthquakes: Journal of Geophysical Research, v. 78, no. 35, p. 8547-8576.

Table 361.41-1

Earthquakes of Magnitude 6.0 and

Greater Along Plate Boundary and in Northern Baja

DATE	MAGNITUDE	FAULT
11-21-15	7.1	Cerro Prieto
12-30-34	6.5	Laguna Salada
12-31-34	7.1	Cerro Prieto
2-24-35	6.0	San Miguel
5-19-40	6.7	Imperial
12-07-40	6.0	Cerro Prieto
10-24-54	6.0	San Miguel
11-12-54	6.3	San Miguel
2-09-56	6.8	San Miguel
2-09-56	6.1	San Miguel
2-14-56	6.3	San Miguel
2-15-56	6.4	San Miguel
8-07-65	6.3	Cerro Prieto
4-09-68	6.5	Borrego
10-15-79	6.6	Imperial

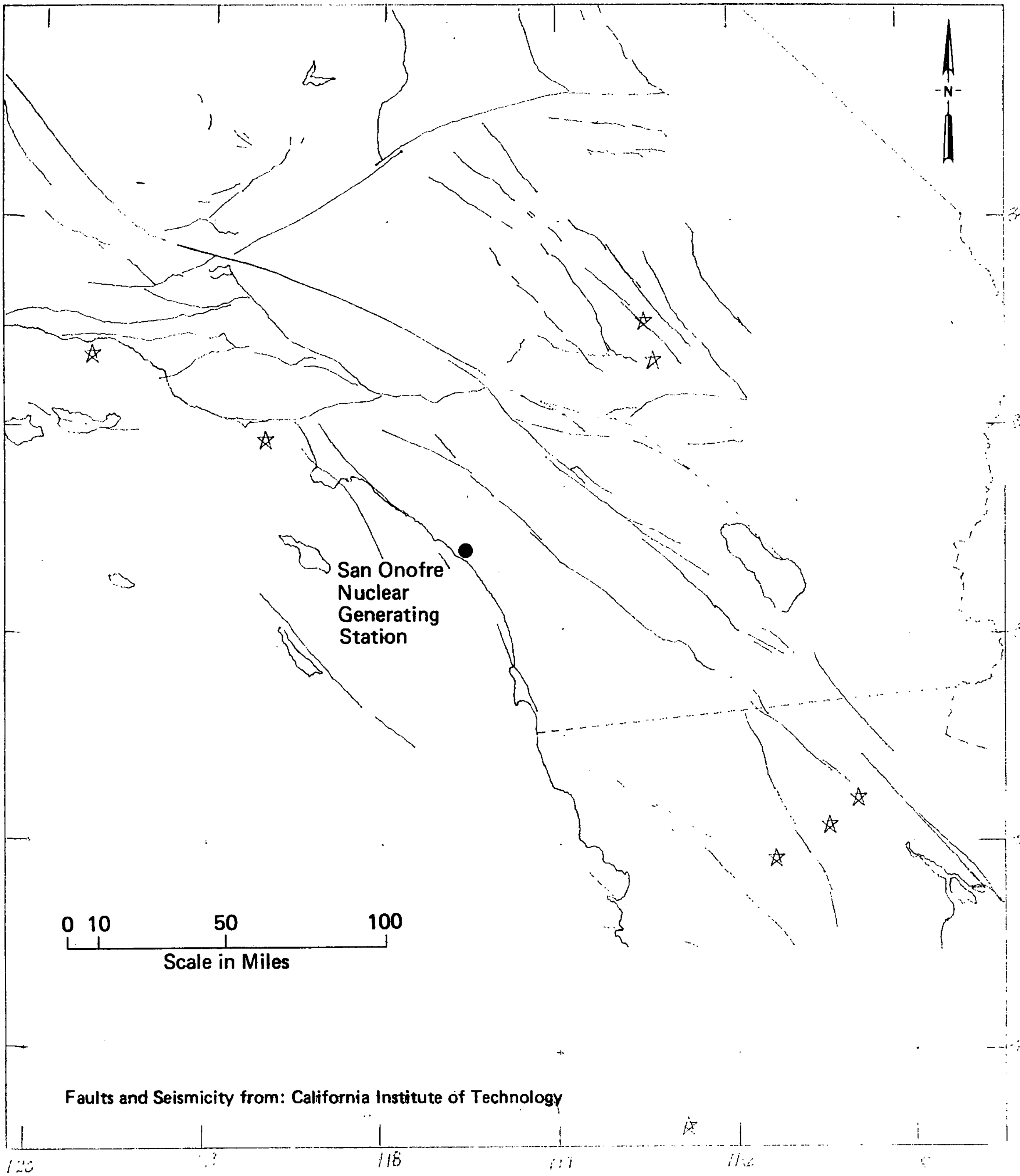

Figure 361.41 - 1 Seismicity Within 200 Miles of the San Onofre Site
January 1975 - September 1979; $M_L \geq 5$

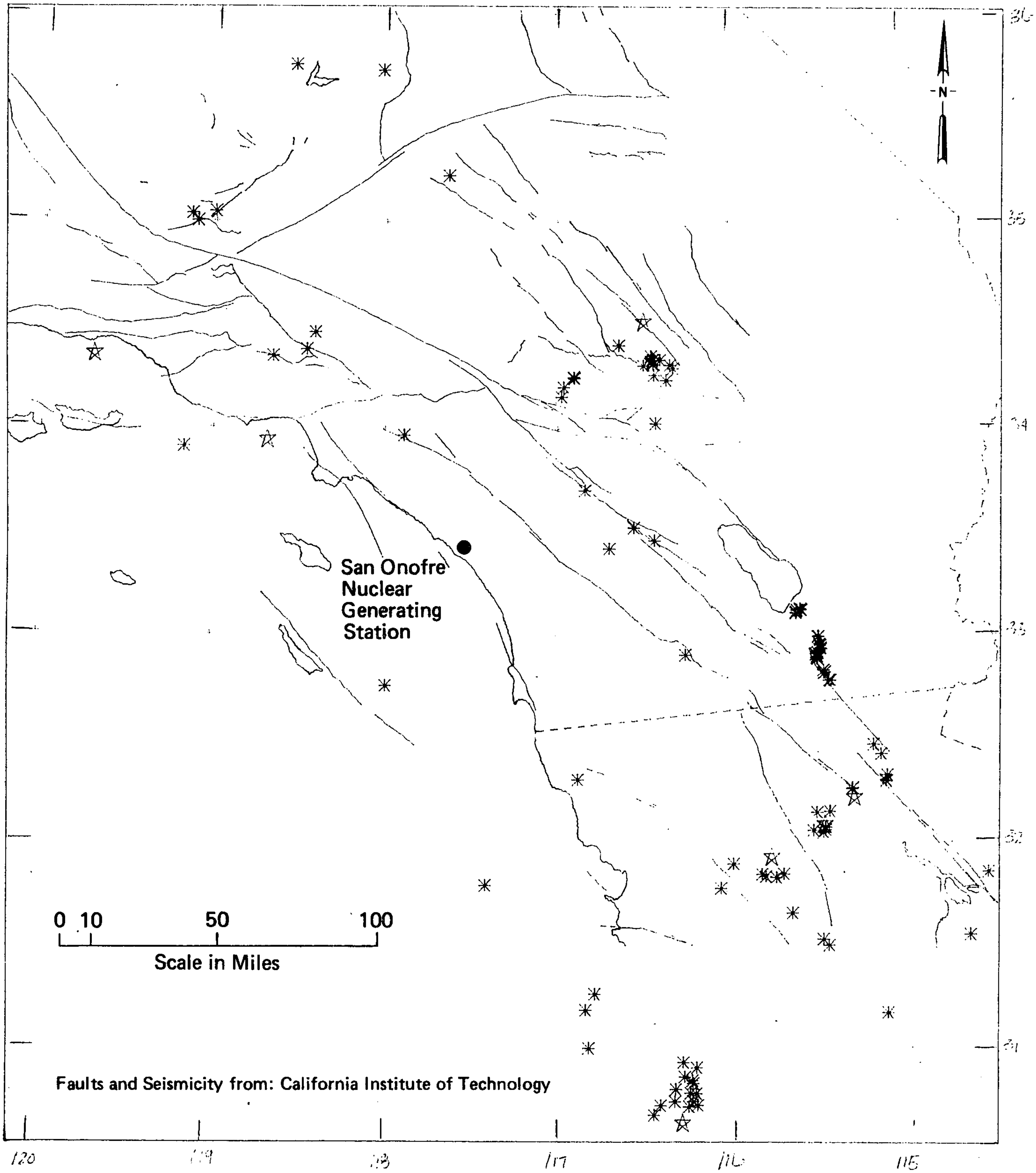

Figure 361.41 - 2 Seismicity Within 200 Miles of the San Onofre Site
January 1975 - September 1979: $M_L \geq 4$

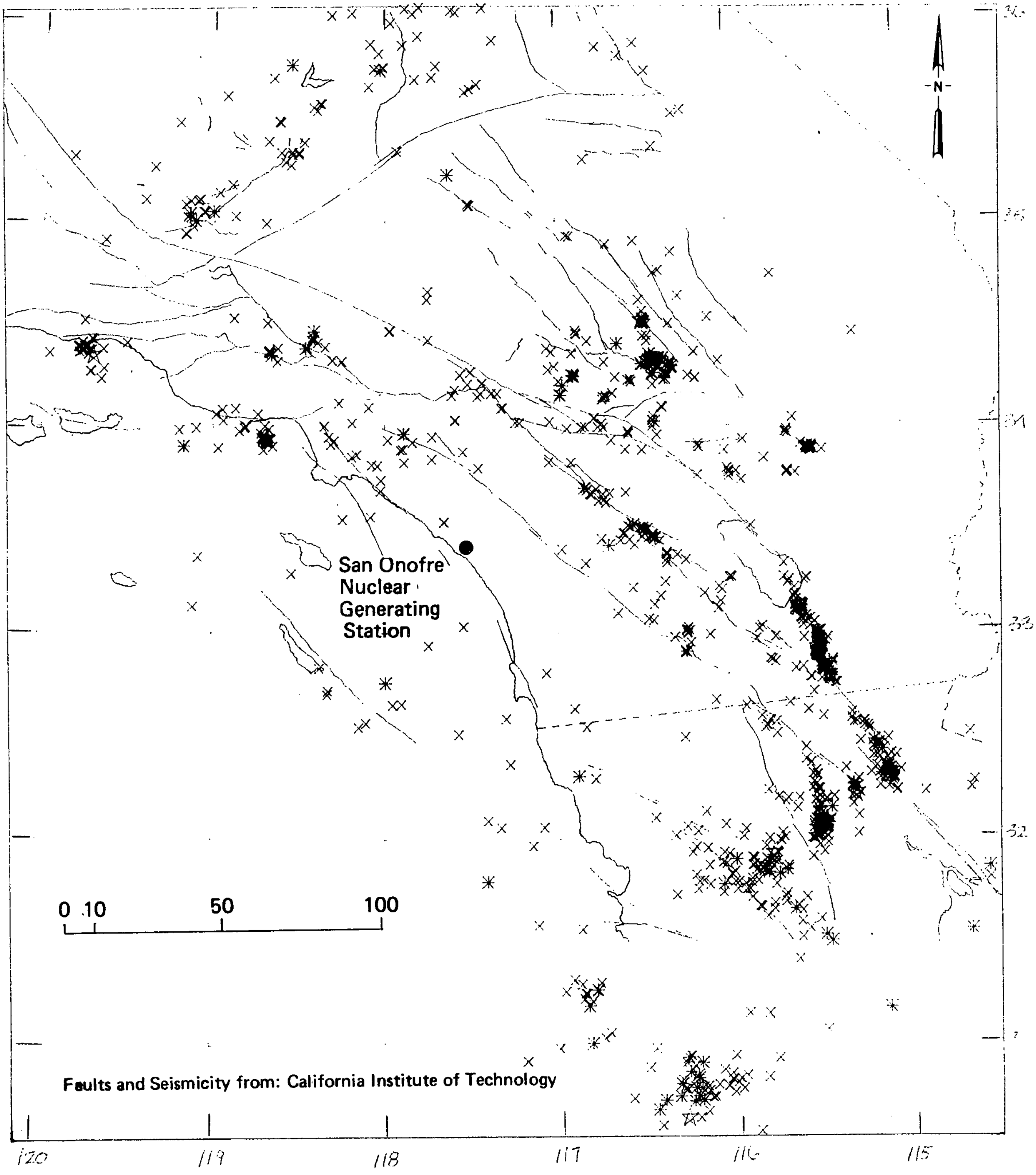

Figure 361.41 - 3 Seismicity Within 200 Miles of the San Onofre Site
January 1975 - September 1979; $M_l \geq 3$

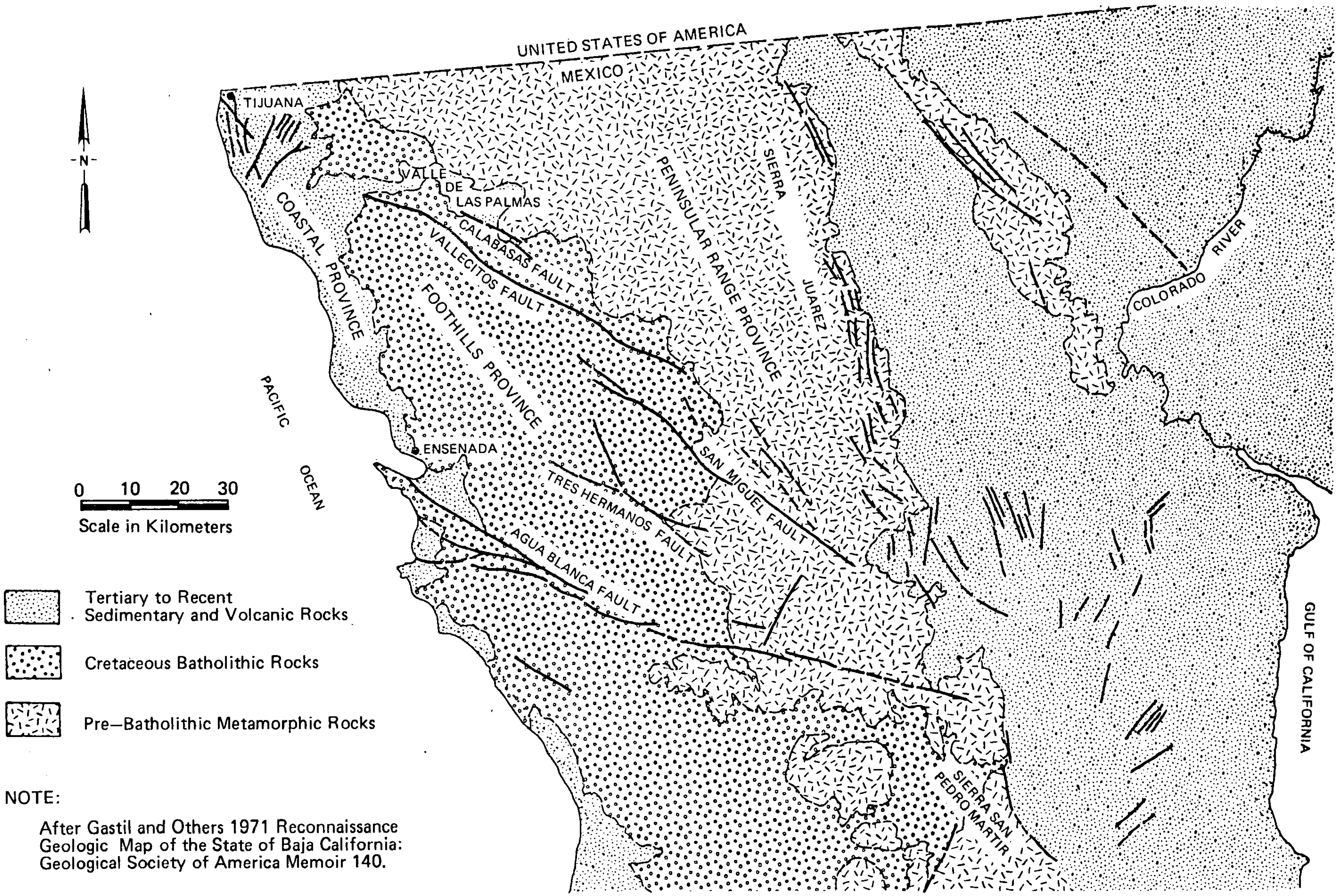

Figure 361.41 - 4 Generalized Map of Northern Baja California Physiographic Provinces and Distinct Geologic Terrane.

QUESTION 361.42

There were many new reports presented at the November 1979 Geological Society of America meeting at San Diego. These reports include new onshore and offshore data on the major tectonic structures of the region west of California and Baja California. Those reports which are pertinent to the Woodward-Clyde Consultants study should be considered in your responses to these questions. Provide copies of the pertinent reports, including, as a minimum, the following:

Crowell, J. C., and Sylvester, A. G. (editors), November 1979, Tectonics of the juncture between the San Andreas fault system and the Salton Trough, southeastern California: Dept. Geol. Sci., Univ. Calif., Santa Barbara, 193 p.

Abbott, P. L., November 1979, Geological excursions in the Southern California area: Dept. Geol. Sci., San Diego State University, 217 p.

Abbott, P. L., and Elliott, W. J., November 1979, earthquakes and other perils, San Diego region: San Diego Association of Geologists, 227 p.

RESPONSE 361.42

In accordance with the provisions of Table 1.8 of the FSAR, seven copies of each of the requested reports are being provided in response to this question.

QUESTION 361.43

On page 16 you state "gravity data in the Los Angeles Basin exhibits a Bouguer anomaly coincident with the NIZD basement discontinuity. This Bouguer anomaly does not continue south to coincide with the SCOZD; however, a similar Bouguer anomaly exists 16 kilometers (10 miles) to the west of the SCOZD."

a) Provide the evidence for the existence of the anomaly as described.

b) discuss the significance of the anomaly which exists 16 kilometers west of the SONGS site and its possible correlation with the Coronado Banks fault.

c) Discuss the significance of this correlation.

RESPONSE 361.43

361.43 a and b

The data on which the question concerning the existence of the anomaly was based are presented in the Bouguer gravity map accompanying the Western Geophysical Report to SCE (PSAR, Appendix 2E). This map was based on data reported by Harrison and others (1966) and by McCulloh (1957, 1960). Some of these early data are now known to be somewhat inaccurate (Biehler, personal communication, 1980). However, the reevaluation has not changed the significance or location of the hypothesized OZD. The general trend of the isogals is essentially the same as previous interpretations indicated it was, although the large gravity closure over the San Joaquin Hills is diminished in magnitude and becomes part of a positive north-south trending gravity ridge that extends offshore of San Onofre across the OZD trend. The extension of the gravity high is represented by the anomaly shown some 20 kilometers west of the site; the center of this anomaly coincides directly with the minimum in reflection time mapped on Horizon C (Effective Acoustic Basement) (PSAR, Appendix 2E). The minimum reflection time correlates directly with the offshore gravity maximum.

361.43 c

The Offshore north-south trending gravity ridge is not correlated in any way to the Coronado Banks fault. The gravity structure does not change the applicants' geologic model of the hypothesized OZD nor does it influence seismic criteria used at San Onofre.

REFERENCES

Harrison, J. C., Von Huene, R. E., and Corbato, C. E., 1966, Bouguer Gravity anomalies off the coast of southern California: Journal of Geophysical Research, v. 71, p. 4921-4941.

McCulloh, T. H., 1957, Simple Bouguer gravity and generalized geologic map of the northwestern part of the Los Angeles basin, California: U. S. Geological Survey Geophysical Investigatins Map GP149.

McCulloh, T. H., 1960, Gravity variations and the geology of the Los Angeles basin of California: U. S. Geological Survey Professional Paper 400-B.

Personal Communication

Beihler, S., 1980, University of California at Riverside.

QUESTION 361.44

Review of the data suggests possible corrections or additions to the data base used for the Woodward-Clyde Consultants report of June 1979. The following list includes those that have been noted during review of the report.

a. Ben-Menahem (1976) cites Girdler (1958) for a 10 mm/year slip rate on the Jordan-Red Sea Fault Zone; this figure couldn't be found in this reference. The 6.5 and 7.5 mm/year rates appear to be sound. The pre-instrumental earthquakes have suggestions of magnitudes of 6 to 7 (M_s); see p.46.

b. The data of Dewey and the Woodward-Clyde Consultants study of the late 1960's suggests a mainly strike-slip mechanism on the Bocono Fault (Venezuela). More discussion of the style of faulting as a matter of debate is needed. The Woodward-Clyde Consultants study suggests 320 ft/10,000 years or 9.9 mm/year, a similar value to the values of 7, 10, and 8-10 obtained by other workers. The macroseismic data suggests the 1812 earthquake had a magnitude of 8 $\pm$ 0.25. The data for this point appears to be as good as that of many of the other points used for the Figures 6 and 7.

c. The data for 5 to 6 mm/year slip rates and the 8.0 $\pm$ 0.25 magnitude for the Wairarapa Fault (New Zealand) appear to be fairly good values for plotting the data on Figure 6 and 7. There should be a discussion of why this data point should be rejected. The magnitude is listed by Slemmons (1977) and is estimated in several New Zealand publications, including Clark and others (1965), who show much larger isoseismal areas than the

1929 earthquake of $M_s = 7.6$. The guidebook by Lensen (1973) shows two rates for the fault slip, with a preferred estimate of 9.4 mm/year for the Waiohine terraces. The linearity of the fault shows a nearly vertical fault plane. The many well studied terraces of this area should permit a rather accurate appraisal of the error bands.

d. The paper of Schwartz et al (1979) appears to support a slip rate of 1.5 to 6 mm/year, rather than the 6-10 mm/year rate cited for the Montagua fault zone.

e. The data for the Tanna fault in Japan shows for Matsuda's (1976) Figure 1, a 1 km displacement for 0.5 my. This suggests a rate of about 2 mm/year, rather than the 3.2 mm/year rate of WCC's Table G-1.

f. Kopet-Dagh should show $M_s = 7.3$ according to Gutenberg and Richter (1954). The best value for slip rate appears to be the 3.6 mm/year for the irrigation systems. This appears to be a boundary zone event.

g. Calaveras fault should show Herd (1978) as 12 to 15 mm/year rate. The source data for this should be checked. The NRC values for maximum design earthquake should be 7.0 to 7.5.

h. The San Jacinto should use new data from Sharp, if possible. May be possible to open file the data.

i. The San Andreas fault (Cholame to Cajon Pass sector) should recheck the data of Seih (1979) who now gives a $M_s = 8.25+$ for this zone, 37 mm/year slip rate is a reasonable value.

j. The northern San Andreas does not have any satisfactory values for the average slip rate, although the figure 20 mm/year is widely cited.

k. CDMG special report 123 shows a slip rate of 1-2 mm/year on the Rose Canyon fault.

RESPONSE 361.44

<u>361.44 a</u>

Ben-Menahem and others (1976, p. 21) state: "The estimates of the average rate of slip vary from 0.65 cm/year (Freund et al., 1970) to 1.0 cm/year for the past 3-4 m.y. (Girdler, 1958)." Neither the 1.0-cm/year rate nor any other rate of slip can be found in Girdler (1958). It appears that the citation of Girdler (1958) by Ben-Menahem and others is either incorrect or unfounded, or that the authors are inferring something from Girdler's paper that is not inherently obvious to the reader. The 1.0-cm/year rate is not substantiated by the available data. The 0.65-cm/year rate of slip for the Jordan-Dead Sea fault can be found in Freund and others (1979).

For the empirical plot of slip rate versus magnitude (WCC, June 1979, Figures 6 and 7), the selected slip rate value was chosen as 7.5 mm/year; this value was based on Quaternary displacements along the Jordan-Dead Sea fault (Zak and Freund, 1966). In 1970, Freund and others (1970) presented a range of slip rate values from 3.5 mm/year to 6.0 mm/year for the 40 to 45-km displacements during the past 7 to 12 million years. In the same paper, the Quaternary rate of 6.5 mm/year is given, revising the age given in the Zak and Freund (1966) paper. This range of 3.5 to 6.5 mm/year from Freund and others (1970) is the selected data range and is used in the revised slip-rate/maximum-magnitude data base documented in response 361.45 e. The range of values provided by Ben-Menahem and others (1976) is not considered because confirmation of the higher rate of slip cited in the paper is lacking.

The pre-instrumental earthquakes associated with the Jordan-Dead Sea fault are listed by Ben-Menahem and others (1976, p. 46). During a 2000-year time span from 117 B.C. to 1956 A.D., 40 earthquakes occurred in the estimated range of 5 to 7 magnitude. Of those earthquakes only the ones which occurred in 1546 and 1927 have specific magnitude assignments. The 1927 earthquake was assigned magnitude 6.2 (Ben-Menahem and others, 1976, Table III, p. 8); the 1546 earthquake was assigned magnitude 6.5 on the basis of a comparison of it with the 1927 earthquake. Because the event of 1546 and other early events occurred so long ago, assignment of Richter magnitude is purely speculative and the confidence in these data is low enough to exclude them from comparison with more readily verifiable earthquake magnitudes on other faults of the world. Therefore, to maintain the quality and integrity of the data being used in the slip-rate/maximum-magnitude data base, magnitude estimates of the early events on the Jordan-Dead Sea fault have not been included. The 1927 magnitude 6.2 earthquake on the Jordan-Dead Sea fault is included in the data base, as documented in response 361.45 e.

<u>361.44 b</u>

The Bocono fault was first discussed in the literature by Rod (1956), who recognized it as one of the most important structural features of the Venezuelan Andes and the only major Venezuelan strike-slip fault for which the relative horizontal displacement could be directly measured. Mencher

(1963) has suggested that the Bocono fault may have originated as a series of normal faults that later coalesced into a right-lateral system. Dewey (1972) has suggested that the Bocono fault represents a portion of the plate boundary between the Carribean plate and the South American plate and that, because of the northeast-trend of the fault, the net slip on the fault could be right-reverse oblique slip. However, displaced Pleistocene glacial moraines in the Paramo de Muchuchies clearly show that the dominant displacement over the past 10,000 years has been right-slip (Rod, 1956; Schubert and Sifontes, 1970; Woodward-Clyde and Associates, 1969). A review of the data presented by these authors indicates a slip rate of 8 to 10 mm/year for the past 10,000 years, with an estimate of 9.75 mm/year based on a measured displacement of glacial moraine of 320 ft (97.5 m).

Woodward-Clyde and Associates (1969) also provide an estimate of the magnitude of the 1812 earthquake, which they believe is the largest event on the Bocono fault in historical time. They estimate a Richter magnitude of from 7 3/4 to 8 1/4 and use 8 as an average. This estimate has been used in conjunction with the estimated slip rate to provide an additional data point for the slip-rate maximum-magnitude data base as documented in response 361.45 e. However, the magnitude is only an estimate of an event that occurred approximately 168 years ago and is therefore speculative.

361.44 c

The West Wairarapa fault in New Zealand has been added to the slip-rate/maximum-magnitude data base, as documented in response 361.45 e and discussed below.

The slip rate for the West Wairarapa fault was developed from the cumulative displacements of the offset Waiohine River Terrace Sequence. The faulting of these terrace sequences has been discussed by Lensen (1973) and by Lensen and Vella (1971) and is summarized in Figures 14 and 21 of Lensen's Guidebook (1973). The units of measure for the displacements listed in Figure 14 of Lensen's Guidebook (1973) are not clearly labeled. However, a close comparison of the units used for displacement of the Waiohine Terraces in Figure 11, in the graph of Figure 21, and in the text of the guidebook reveals that the values listed for cumulative displacements in Figure 14 are in feet. The range of total cumulative displacements reported by Lensen (1973) for the Waiohine River Terraces is 329 to 389 feet (100 m to 118 m). This wide range results from uncertainties in the amount of the initial displacement of the oldest displaced terrace (the Waiohine surface).

The age of Waiohine surface has not been definitely established. The problems in the age estimates result from uncertainties in the correlation of the Waiohine surface either with an earlier glacial advance in the Otira Glacial stage (35000 years B.P.) or with the latest principal glacial advance in the Otira Glacial stage (20,000 years B.P.). The ages of these glacial advances are supported by radiocarbon dates obtained in other regions of New Zealand (Lensen, 1973; Suggate, 1963; Vella, 1963).

Calculated slip rates from the data in Table 14 of Lensen's Guidebook (1973) range from 2.9 to 6 mm/year. The slip-rate range was extended to 6.6 mm/year because Suggate and Lensen (1973) have suggested 18,000 years B.P. may be the youngest age for the latest principal glacial advance in the Otira Glacial stage in New Zealand. An average slip rate of 4.8 mm/year is considered the best selected value. However, the processes of lateral erosion during the time of formation of the Waiohine River terraces most likely resulted in apparent terrace displacements smaller than the displacement values that actually occurred; thus, the displacement values and the calculated slip rates should be considered as minimum values.

The largest earthquake known to have occurred on the West Wairarapa fault was in 1855. Slemmons (1977) estimated a magnitude 8 for this earthquake; however, there is no direct evidence available for establishing a magnitude. No New Zealand literature publishes a magnitude estimate for this earthquake. Although surface rupture of the West Wairarapa fault was reported, no measurements of the amount of displacement that occurred during the earthquake were obtained. The comparison of isoseismals of the 1855 event and the 1929 event is made in Figure 361.44-1 as suggested in question 361.44 c. Clark and others (1965) provided estimated isoseismal contours, using both Modified Mercalli and Rossi-Forel scales, for the 1855 earthquake (Figure 361.44-1). Modified Mercalli isoseismals contours were also presented by Clark and others (1965) for the 1929 West Nelson (magnitude 7.6) earthquake, the first large instrument-recorded earthquake in New Zealand (Richter, 1958). However, caution must be exercised when comparing equivalent Modified Mercalli isoseismals of these two earthquakes because 1) the delineation of intensity isoseismal contours is based on subjective judgments and 2) the earthquakes occurred in two separate regions of New Zealand on two different faults.

A comparison of areas covered by the Modified Mercalli isoseismals presented by Clark and others (1965) for the 1855 earthquake and the 1929 earthquake shows they are very similar. It should be noted here that the Rossi-Forel scale isoseismals for the 1855 earthquake are much larger than the Modified Mercalli isoseismals and that different scales should not be compared to one another. Thus a reasonable assessment of Clark's data would be that the 1855 earthquake was similar in size to the 1929 earthquake (magnitude 7.6). For this reason a value of M_s 7.6 was used in the slip rate-maximum magnitude data base as documented in response 361.45 e.

361.44 d

Subsequent to the publication of Schwartz and others (1979), new field data (Schwartz, personal communication, 1979) suggest that the low slip-rate value of 1.5 mm/year presented in the publication is not valid, and it is therefore not presented in the slip-rate versus maximum-magnitude analysis. Thus, the 6 mm/year rate on the Motagua fault is the only value presented to represent the fault. The 10 mm/year rate presented in the June 1979 report was based on preliminary data and is not supported by recent data.

361.44 e

The 3.2 mm/year value of slip rate on the Tanna fault reported in the WCC June 1979 report was subsequently revised to 1.5 to 2.5 mm/year on the basis of a review of Matsuda (1977) and a recent personal communication with Matsuda (December, 1979). Though this revised data point is accomodated by the slip-rate maximum-magnitude relationship shown in Figure 361.38-7, the Japanese data have been deleted from the data base as discussed in responses 361.46 b, 361.47, and 361.50.

361.44 f

The Kopet-Dagh fault zone is included in the slip-rate maximum-magnitude data base as documented in response 361.45 e. Data provided by Trifonov (1971 and 1978), and Krymus and Lykov (1969) indicate a possible range of slip-rate values for the Kopet-Dagh fault zone between 3.6 mm/year and 8 mm/year. The Quaternary data were reviewed for slip-rate values and, on the basis of the criteria in response 361.45 e, the 3.6 mm/year value has been selected as a representative slip rate (Trifonov, 1978).

The 1948 Ashkhabad earthquake is attributed to the Kopet-Dagh fault. Various station estimates of magnitude for the earthquake range from 6.5 to 7.5 (Louderback, 1949). Gutenberg and Richter (1954) cited a magnitude of 7.3. In general, most magnitudes are in the 7.0 to 7.3 range. The 7.3 magnitude is an average of several stations and is thus representative.

361.44 g

Herd (1978) estimates that the present slip rate on the Calaveras-Paicines fault (the southern section of the Calaveras fault, south of the junction with the Hayward fault) is from 12 to 15 mm/year based on the difference in apparent long-term slip rate on the San Andreas fault north and south of the Calaveras branch. This rate appears to be consistent with modern-day creep but is not based on direct geologic data. Prowell (1974) estimates a rate of 5 mm/year from mid-Pliocene to the present based on tentative correlations of volcanic rock terranes. Thus, a range from 5 mm/year to 15 mm/year seems reasonable for this southern segment of the fault. Herd states that the slip rate is at least 12 mm/year.

To the north, the slip of 12 to 15 mm/year is apportioned between the Hayward and Calaveras-Sunol faults. Herd (1978) suggests that this apportionment should be about equally divided considering the similar creep measurements of 6 mm/year on both faults. These slip rates, though not based on geologic correlations, appear reasonable. Prowell (1974) calculates a slip rate for the Calaveras-Sunol fault from displaced volcanic rocks of approximately 8 mm/year. Based on similar volcanic rock displacements, he calculates a slip rate of 5 to 5.5 mm/year for the Hayward fault. Both sets of data are considered together and are included in the slip-rate maximum-magnitude data base, as documented in response 361.45 e.

<u>361.44 h</u>

New data on possible slip rates along the San Jacinto fault have been discussed with Robert V. Sharp (December, 1979) and are presented in the most recent U.S.G.S. volume of Summaries of Technical Reports (Sharp, 1980). Sharp gives estimates of strike-slip displacements of strata and possible slip rates for three areas along the fault, one on the main trace or Casa Loma-Clark segment and two on the Coyote Creek segment. This recent work is summarized below.

Sharp (1980) reports minimum horizontal offsets of Pleistocene gravels of between 5.7 and 8.6 km on the Casa Loma-Clark segment. He states that these units have been offset since 730,000 years B.P. and calculates a slip rate of 8-12 mm/year. This is a slight increase from the minimum rate of 7.1 mm/year quoted earlier by Sharp (1978).

Sharp presents two estimates of Holocene displacements based on trenching studies of stratigraphic offsets on the Coyote Creek fault. For one of these estimates, Sharp (1980) uses data from Clark and others (1972) to develop a horizontal slip of 1.7 m; this value is based on measured vertical offsets and on a vertical to horizontal offset ratio derived from measurements taken following the 1968 Borrego Mountain earthquake. Sharp (1980) uses this estimate of displacement for the "youngest sediment" of Lake Cahuilla since its deposition 283 to 478 years B.P. The corresponding slip rate is between 3 and 5 mm/year but is suspect because it is not based on actual measurement of strike-slip offset.

At another trench site on the Coyote Creek fault, Sharp (1980) cites 10.9 m of right-slip of a buried stream channel older than 5,000 years B.P. but younger than 6,800 years B.P. He states that using an intermediate time period of 5,400± to 6,000± years B.P. gives an estimated slip rate of 1 to 2 mm/year (however, calculations based on the quoted numbers actually give 1.8 to 2.0mm/year).

Sharp (1980) goes on to conclude that the average rates of slip for these three time intervals indicate a major relatively quiescent period for the San Jacinto fault zone from about 4,000 B.C. to about 1,600 A.D. The applicants find this conclusion hard to support because Sharp's analysis looks at only two segments of the fault zone. The variations in slip rates due to low rates for the Coyote Creek fault could well be explained by apportionment of the total zone slip to adjacent known and suspected segments of the San Jacinto fault zone, whereas Sharp's data presented above for the Casa Loma-Clark fault appear to represent movement on a major segment of the zone and have been considered as representative of the total fault zone potential. The lower slip rate, calculated for the Coyote Creek fault segment alone, has been used in conjunction with the magnitude 6.7 Borrego Mountain earthquake of 1968 in preparing the slip-rate maximum-magnitude relationship.

Both of these data sets are included in the slip-rate maximum-magnitude data base, as documented in response 361.45 e.

361.44 i

The central section of the San Andreas fault from Cholame to Cajon Pass has been considered separately for the slip-rate maximum-magnitude comparison; this separate consideration was considered appropriate because abundant data are available to estimate the late Holocene slip rate and maximum historical earthquake. Sieh's (1978) data are reasonable and are the best avaiable (i.e., a slip rate of 34 to 41 mm/year with the best estimate being 37 mm/year and M_s approximately equal to 8.25 for the 1857, Fort Tejon earthquake). These figures are used in the slip-rate maximum-magnitude data base documented in response 361.45 e.

361.44 j

The northern section of the San Andreas fault from Hollister to Cape Mendocino has also been considered separately for comparison purposes. The most recent and perhaps best summary of the slip rate on this section of the fault is presented by Herd (1978) in which he selects 20 mm/year as the most reasonable rate. This figure has been used in the slip-rate maximum-magnitude data base, as documented in response 361.45 e.

The strike-slip displacement and resulting slip rate reported for the Rose Canyon fault in CDMG Special Report 123 are based on the distribution of the San Diego Formation along the fault and on the Z-shaped bend in the coastline where the fault crosses it at La Jolla Bay. The observational data needed to evaluate the validity of these proposed offsets are not provided in Special Report 123, but they have been published by Kennedy (1975) in CDMG Bulletin 200 and by Moore and Kennedy (1975) in the U.S.G.S. Journal of Research (v. 3, p. 589-595). In addition, Kern (1977) has published data on the displacement and slip rate of the Rose Canyon fault based on his correlation and projection of Late Pleistocene marine terraces in the La Jolla area.

Each of the proposed offsets and resulting slip rates is discussed below and is shown to be based on speculative assumptions which are either incorrect or unsupportable. Although the available data provide no unique geologic line which can be used as piercing points for the precise determination of net slip along the Rose Canyon fault, geologic relationships discussed below indicate that the displacement is dominantly dip-slip with little or no strike-slip displacement.

Data pertaining to the published displacements and slip rates cited are discussed in order from the largest to the smallest proposed displacements. Figure 361.44-2 is a generalized geologic map of San Diego area and the Rose Canyon fault showing the published displacements.

1. Moore and Kennedy (1975, p. 593) state that: "The north edge of the San Diego basin has been offset 6 km right laterally as marked by the Eocene-

Pliocene unconformity at Mission Bay" (Kennedy and Moore, 1971), Figure 361.44-2. Referring to the same feature Kennedy (1975, p. 36) states that: "The distribution of the San Diego Formation along the Rose Canyon fault zone between Pacific Beach and Tecolote Canyon is interpreted as resulting from 4 km of right-lateral strike-slip motion on the Rose Canyon fault."

The above proposed offsets of 6 and 4 km are based on the assumption that the line formed by the pinching out of the Late Pliocene San Diego Formation beneath the Pleistocene Lindavista Formation was originally east-west trending and that the pinch-out line on Mount Soledad west of the fault originated opposite the pinch-out line located east of the fault, near the San Diego River, Figure 361.44-2 (Kennedy and Moore, 1971). The cited offsets have different magnitudes because Moore and Kennedy (1975) obtained theirs from a generalized geologic map which shows the San Diego Formation as pinching out on the south side of the San Diego River, whereas Kennedy (1975) based his offset on an occurrence of the San Diego Formation on the ridge along the north side of the San Diego River.

Both of the proposed offsets have questionable validity because the basic premise of an east-west pinch-out line on each side of the fault is incorrect. As mapped by Kennedy (1975), the San Diego Formation pinches out toward the east and thickens toward the west in the vicinity of the San Diego River east of the Rose Canyon fault and pinches out toward the north and thickens toward the south on Mt. Soledad, west of the fault. If on the east side of the fault, a straight line were extended from the pinch-out point south of the river through the pinch-out line north of the river, the line would project about N25W, that is, subparallel to the Rose Canyon fault, thus nullifying its use as a piercing point for offset determination. The actual pinch-out line probably followed a curved path which crossed the Rose Canyon fault near the mouth of the Rose Canyon fault and lapped onto Mount Soledad (see Figure 361.44-2). The observed relationship can be explained without any lateral displacement on the Rose Canyon fault as pointed out by Threet (1979).

The offset correlation is also questioned because the San Diego Formation rests on different formations at the presumed "match points" for the pinch-out line on opposite sides of the fault. West of the fault on Mount Soledad it overlies the Eocene Ardath Shale, whereas east of the fault at the "match points" it overlies the Eocene Scripps Formation on the ridge north of the San Diego River and the Eocene Mission Valley Formation on the ridge south of the river; thus the correlation cannot be reconciled.

Therefore, the published right-lateral displacements of 6 and 4 km are invalid and do not represent a reasonable interpretation of the available data.

2. Moore and Kennedy (1975, p. 593) state that: "The 200-m depth contour has been offset about 4 km right laterally where the fault zone passes out to sea near Point La Jolla."

This refers to the fact that the continental shelf offshore from La Jolla is broader and extends farther seaward west of the Rose Canyon fault than east of the fault. Differential vertical uplift provides a more logical explanation for the observed relationship than does right slip on the Rose Canyon fault.

The west side of the Rose Canyon fault has been uplifted relative to the east side as demonstrated by the exposure of Late Cretaceous formations on Mount Soledad and along the coast west of the fault, whereas the oldest formations exposed east of the fault are of Eocene age. The amount of uplift west of the fault increases in a westward direction as shown by the eastward dip of Cretaceous strata exposed along the coast. Thus, the broad continental shelf west of the fault was probably formed by the combined effects of tectonic uplift and marine planation during low stands of sea level. To explain it by strike-slip displacement on the Rose Canyon fault is an unreasonable interpretation of available data, as pointed out by Threet (1979).

3. "The coast on opposite sides of the fault zone where it passes out to sea near Point La Jolla has rocks of similar resistance to erosion and a similar structural elevation of the Lindavista Formation. The southwestward coast has been moved seaward right laterally 1 km to form the point." (Moore and Kennedy, 1975, p. 593).

This statement and a similar but less explicit statement by Kennedy and others (1975, p. 8) are based on the same reasoning as the one dealing with the 200-m subsea contour. In essence, Moore and Kennedy (1975) believe that the coast juts out along the south side of La Jolla Bay because of right slip on the Rose Canyon fault. It is more reasonable to explain the bend in the coast by greater uplift on the south side of the bay. This uplift is indicated by exposures of Cretaceous strata there, whereas only Eocene strata are exposed on the north side of the bay.

Moore and Kennedy (1975) seem to rule out vertical uplift by inferring that the base of the Pleistocene Lindavista Formation is at the same altitude on either side of the fault in this area. Although the base of the Lindavista Formation east of the fault is broadly planar and nearly horizontal, it is not so on Mt. Soledad. On Mt. Soledad the base occurs instead as a series of wave cut terraces, and, consequently, it is not a reliable reference for measuring deformation.

4. In reference to relationships across the projection of the Rose Canyon fault in the vicinity of La Jolla Bay, Kern (1977, p. 1,563) interprets the Nestor terrace shoreline angle to be offset approximately 150 m right laterally and 55 m vertically (with the east side up) within the past 120,000 years. This yields an average displacement rate of 1.25 mm/year right slip and 0.46 mm/year vertical slip.

The vertical component of the above offset depends upon correlation of the same shoreline angle on opposite sides of the fault. The lateral component not only depends on the proper correlation of shoreline angles but also requires the proper projection of the shoreline angle to the fault trace.

There is a gap of about 2 km on the east side of the fault where the shoreline angle is concealed. A field examination of exposures in this area suggests that Kern (1977) has erred in his correlation of terraces. As mapped and correlated by Kern (1977, Figures 2, 5, and 7), the shoreline angles of the Bird Rock and Nestor terraces rise in altitude as they approach the Rose Canyon fault from the south. An examination of exposures in this area leads to the alternate conclusion that the terraces do not experience significant uplift as they approach the Rose Canyon fault. Instead, there appear to be several discrete wave cut benches arranged in stairstep fashion.

Along the coast extending eastward from Point La Jolla, the lowest benches have been removed by subsequent erosional undercutting along the present beach. Extending for a distance of several kilometers southward from Point La Jolla, there are numerous remnants of a wave cut bench at an elevation of about 10 m above sea level. Kern correlates this bench with the Bird Rock terrace along the southern part of the coast, but he maps the Bird Rock terrace as rising along the northern part of the coast. However, exposures are poor in this area because the ground is covered by roads and buildings of the La Jolla metropolitan area and by Quaternary sediments concealing the erosion surface at the base of this terrace. In this location, Kern (1977) appears to consider the entire terrace to be underlain by a single wave cut bench of the Nestor terrace; however, a field examination suggests that the terrace includes at least two, and probably more, discrete wave cut benches as suggested by breaks in slopes along the streets within the area and by exposures in the sea cliffs east of Point La Jolla. As interpreted here, the Bird Rock terrace and its shoreline angle extend about 300 m east from Point La Jolla but have been removed by coastal erosion farther to the east. Furthermore, a terrace exposed on Goldfish Point appears to be the Nestor terrace, not the Bird Rock terrace as mapped by Kern (1977). Its shoreline angle is exposed at an estimated elevation of 15 to 20 m above sea level in the cliff east of Goldfish Point. Farther east is a higher terrace; the shoreline angle of this terrace does not appear to be exposed. It is on this higher terrace that Kern (1977, Figure 2) located a shoreline angle at 60 m above sea level which he correlates with the Nestor terrace.

In the area northeast of the Rose Canyon fault only one terrace is exposed below the elevation of the Lindavista terrace. The shoreline angle of this terrace crops out about 5 m above sea level in the sea cliff, a short distance north of the Scripps Institute pier. The shoreline angle trends southward into the cliff, and the wave cut platform dips westward. The platform has a relatively steep dip adjacent to the shoreline angle where it is armored by sandstone blocks from the adjacent bluff. The dip of the platform flattens and the armor diminishes in exposures toward the south. Kern (1977, Figure 2, p. 1,563) tentatively correlates this terrace with the Nestor terrace but considers that it might instead be the Bird Rock terrace. He projects the shoreline angle inland toward the Rose Canyon fault essentially along the contact between the Pleistocene Bay Point Formation and the Eocene bedrock, as mapped by Kennedy (1975). This forms the basis for his estimate of the amount of displacement on the Rose Canyon fault during the past 120,000 years (the age of the Nestor terrace). However, Kern's correlation of the terraces and his projection of the shoreline angle appear to be incorrect.

In order for the 5-m terrace exposed near the Scripps Institute pier to be the Nestor terrace, it would have to have been downwarped about 15 m along the east side of the Rose Canyon fault; however, there is no evidence for downwarping in either the Eocene bedrock or the base of the Lindavista terrace. The Eocene bedrock dips toward the northeast away from the fault. This suggests uplift near the fault rather than downwarping. The platform at the base of the Lindavista Formation is at an altitude of about 100 m where it is exposed in the bluffs inland from La Jolla Bay to the east of Rose Canyon fault. The base of the Lindavista Formation remains at a nearly constant altitude for at least 14 km northwestward along the coast. This indicates that no significant warping has occurred in this area since the formation of the Lindavista platform. In this area, the Lindavista platform is at essentially the same elevation as at Point Loma where terrace relationships are well-known and where the Nestor shoreline angle is at 20 m and the Bird Rock shoreline angle is at 8 m. Consequently, the 5-m terrace at Scripps Institute is more likely to correlate with the Bird Rock terrace; however, there is no compelling reason to correlate it with either the Bird Rock or Nestor terraces.

The 5-m terrace at Scripps Institute has a different origin that most of the terraces elsewhere along the coast. It was formed in a coastal embayment, the La Jolla embayment, rather than along a straight coastline. The embayment appears to result from the erosion of a canyon along the north side of the Mount Soledad uplift and is probably a landward extension of the La Jolla submarine canyon. It may have been eroded in a submarine environment during early or middle Pleistocene by sluicing of sand banked against the Mt. Soledad headland, or it may be a product of normal stream erosion. In either case, its configuration suggests that it was formed by processes other than wave erosion. It has an analogous origin to estuaries which occur elsewhere along the present coast. During early stages of submergence associated with a rise in sea level, the shoreline would conform to an altitude contour along the side of the partially submerged canyon without regard to the shape of the contours. With time, longshore drift would build a smoothly curving bar across the mouth of the canyon and leave a lagoon behind the bar. Carter (1957, p. 217-254) presents evidence documenting such an origin for the La Jolla embayment. Kern (1977) seems to assume implicitly that the embayment was cut exclusively by wave erosion simultaneous with a gradual offsetting of the coastline by right slip along the Rose Canyon fault. Kern's projection of the 5-m shoreline angle is at best an indication of the degree to which the coast was embayed during its formation. It is not a measure of fault offset.

In summary, there is no compelling evidence for strike-slip displacement on the Rose Canyon fault. None of the published data on the magnitude and rate of horizontal displacement are valid. Efforts to establish valid measures of slip have been frustrated by the inability to locate points at which unique geologic lines cross the fault. It is clear that dip-slip displacement has occurred along the fault with the amount varying along the trace because formations east of the fault are essentially horizontal whereas those to the west are folded. Accordingly, the slip rate developed in CDMG 123 has not been included in the slip-rate/maximum-magnitude analysis.

REFERENCES

Ben-Menahem, A., Nur, A., and Vered, M., 1976, Tectonics, seismicity and structure of the Afro-Eurasian juction--The breaking of an incoherent plate: Physics of the Earth and Planetary Interiors, v. 12, p. 1-50.

Carter, G. F., 1957, Pleistocene Man at San Diego: Baltimore, John Hopkins Press, 400 p.

Clark, M. M., Grantz, A., and Rubin, M., 1972, Holocene activity of the Coyote Creek fault as recorded in sediments of Lake Cahuilla, in The Borrego Mountain Earthquake of April 9, 1968: U. S. Geological Survey Professional Paper 787, p. 112-130.

Clark, R. H., Dibble, R. R., Fyfe, H. E., Lensen, G. J., and Suggate, R. P., 1965, Tectonic and earthquake risk zoning: Royal Society of New Zealand, Transactions, general, v. 1, no. 10, p. 113-126.

Dewey, J. W., 1972, Seismicity and tectonics of Western Venezula: Seismological Society of America Bulletin, v. 62, no. 6, p. 1711-1751.

Euge, K. M., and Miller, D. S., 1973, Evidence for a possible onshore extension of the Rose Canyon fault in the vicinity of Oceanside, California: Geological Society of America, Abstracts with Programs, v. 5, no. 1, 39 p.

Freund, R., Garfunkel, Z., Zak, I., Goldberg, M., Weissbrod, T., and Derin, B., 1970, The shear along the Dead Sea rift: Philosophical Transactions, Royal Society of London, Series A, v. 267, p. 107-130.

Gastil, R. G., Phillips, R. P., and Allison, E. C., 1975, Reconnaissance geology of the state of Baja California: Geological Society of America Memoir 140, 170 p.

Gastil, R. G., Kies, R., and Melins, D. J., 1979, Active and potentially active faults--San Diego County and northernmost Baja California in Abbott, P. L., and Elliott, W. J., eds., Earthquakes and other perils, San Diego region, p. 47-60.

Girdler, R. W., 1958, The relationship of the Red Sea to the East Africa rift system: Quarterly Journal of the Geological Society of London, v. 114, p. 79-115.

Gutenberg, B., and Richter, C. F., 1954, Seismicity of the Earth and Associated Phenomena: Hafner Publishing Company, New York and London, reprinted 1965, 310 p.

Herd, D. G., 1978, Neotectonic framework of central coastal California and its implications to microzonation of the San Francisco Bay region, in Second International Conference on Microzonation for Safer Construction--Research and Application, Proceedings, v. 1, p. 231-240.

Kennedy, M. P., 1975, Del Mar, La Jolla and Point Loma Quadrangles, western San Diego metropolitan area, California: California Division of Mines and Geology Bulletin 200A, p. 9-39.

Kennedy, M. P., Bailey, K. A., Greene, H. G., and Clark, S. H., 1978, Recency and character of faulting offshore from metropolitan San Diego, California: California Division of Mines and Geology Final Technical report.

Kennedy, M. P., and Moore, G. W., 1971, Stratigraphic relationship of upper Cretaceous Eocene formations, San Diego coastal area, California: American Association of Petroleum Geologists Bulletin, v. 55, no. 5, p. 709-722.

Kennedy, M. P., Tan, S. S., Chapman, R. H., and Chase, G. W., 1975, Character and recency of faulting, San Diego metropolitan area, California: California Division of Mines and Geology Special Report 123.

Kern, J. P., 1977, Origin and history of upper Pleistocene marine terraces, San Diego, California: Geological Society of America Bulletin, v. 88, p. 1553-1566.

Kyrmus, V. N., and Lykov, V. I., 1969, The character of the junction of the Epi-Hercynian platform and the Alpine folded belt, south Turkmenia: Geotectonics, Academy of Science, U. S. S. R., translated by the American Geophysical Union, v. 6, p. 391-396.

Legg, M. R., and Kennedy, M. P., 1979, Faulting offshore San Diego and northern Baja California, in Abbott, P. L., and Elliott, W. J., eds., Earthquakes and Other Perils, San Diego region: San Diego Association of Geologists for Geological Society of America, Field Trip Guidebook, p. 29-46.

Lensen, G. J., 1970, Elastic and non-elastic surface deformation in New Zealand: New Zealand Society of Earthquake Engineering Bulletin, v. 3, no. 4, p. 131-142.

Lensen, G. J., 1973, Guidebook for excursion A-10, Tour Guide for International Association of Quaternary Research Conference, Christchurch, New Zealand, 76 p.

Lensen, G. J., and Vella, P., 1971, The Waiohine faulted terrace sequence--recent crustal movements: Royal Society of New Zealand, Bulletin 9, p. 117-119.

Louderback, C. D., ed., 1949, Seismological notes: Seismological Society of America Bulletin v. 39, no. 1, p. 61.

Matsuta, T., 1976, Empirical rules on sense and rate of recent crustal movement: Journal of Geodetic Society of Japan, v. 22, no. 4, p. 252-263.

Mencher, E., 1963, Tectonic history of Venezuela in Backbone of the Americas: American Association of Petroleum Geologists Memior 2, p. 73-89.

Moore, G. W., 1972, Offshore extension of the Rose Canyon fault, San Diego, California: U. S. Geological Survey Professional Paper 800-C, p. 113-116.

Moore, G. W., and Kennedy, M. P., 1975, Quaternary faults at San Diego Bay, California: Journal of Research of the U. S. Geological Survey, v. 3, no. 5, p. 589-595.

Prowell, D. C., 1974, Geology of selected Tertiary volcanics in the central coast range mountains of California and their bearing on the Calaveras and Hayward fault problems: University of California Santa Cruz, unpublished Ph.D. thesis, 182 p.

Richter, C. F., 1958, Elementary seismology: W. H. Freeman, San Francisco and London, 768 p.

Rod, E., 1956, Strike-slip faults of northern Venezuela: American Association of Petroleum Geologists, v. 40, no. 3, p. 457-476.

Schubert, C., and Sifontes, R. S., 1970, Bocono fault, Venezuelan Andes, evidence of postglacial movement: Science, v. 170, p. 66-69.

Schwartz, D., Cluff, L. S., and Donnelly, T., 1979, Quaternary faulting along the Caribbean and North American plate boundary: Tectonophysics, v. 52 (in press).

Sharp, R. V., 1978, Salton trough tectonics: U. S. Geological Survey, National Earthquake Hazards Reduction, Summaries of Technical Reports, v. 7, p. 34-35.

Sharp, R. V., 1980, Salton trough tectonics: U. S. Geological Survey, National Earthquake Hazards Reduction Program, Summaries of Technical Reports, v. 9, Open-File Report 80-6.

Sieh, K. E., 1978, Prehistoric large earthquakes produced by slip on the San Andreas fault at Pallett Creek, California: Journal of Geophysical Research, v. 83, no. B8, p. 3907-3939.

Sieh, K. E., 1979, Late Holocene behavior of the San Andreas fault--U. S. Geological Survey Contract No. 14-08-0001-16774: U. S. Geological Survey, National Earthquake Hazard Reduction Program, Summaries of Technical Reports, v. 8, June, p. 50.

Slemmons, D. B., 1977, State-of-the-art for assessing earthquake hazards in the United States--Report 6, Faults and Earthquake Magnitude: U. S. Army Corps of Engineers, Waterways Experiment Station, Soils and pavements Laboratory,Miscellaneous Paper S-73-1, 129 p.

Suggate, R. P., 1963, The Alpine fault: Transactions of the Royal Society of New Zealand, v. 2., no. 7, p. 105-129.

Suggate, R. P., and Lensen, G. J., 1973, Rate of horizontal fault displacement in New Zealand: Nature, v. 242, p. 815.

Threet, R. L., 1979, Rose Canyon fault--An alternative interpretation, in Abbott, P. L., and Elliott, W. J., eds., Earthquakes and Other Perils, San Diego region: Geological Society of America, Field Trip Guidebook, November, p. 61-71.

Trifonov, V. G., 1971, The pulse-like character of tectonic movements in regions of most recent mountain-building (Kopec Dagh and southeast Caucasus): Geotectonics, U. S. S. R., Academy of Sciences, Geological Institute, no. 1, p. 234-235.

Trifonov, V. G., 1978, Late Quaternary tectonic movements of western and central Asia: Geological Society of America Bulletin, v. 89, no. 7, p. 1059-1072.

Vella, P., 1963, Upper Pleistocene succession in the inland part of Wairarapa Valley, New Zealand: Royal Society of New Zealand (Geology) Transactions, v. 2, no. 4, p. 63-78.

Woodward, Clyde and Associates, 1969, Seismicity and seismic geology of northwestern Venezuela: Report to Shell Oil Company of Venezuela, v. 2, 77 p.

Woodward-Clyde Consultants, 1979, Report of the evaluation of maximum earthquake and site ground motion parameters associated with the offshore zone of deformation, San Onofre nuclear generating station: Report for Southern California Edison Company, June, 241 p.

Zak, I., and Freund, R., 1966, Recent strike slip movements along the Dead Sea rift: Israel Journal of Earth Sciences, v. 15, p. 33-37.

Ziony, J. I., 1973, Recency of faulting in the greater San Diego area, California, in Ross, A., and Dowlen, R. J., eds., Studies on the geology and geologic hazards of the greater San Diego area, California: San Diego Association of Geologists and Association of Engineering Geologists, 1973 Guidebook, p. 68-75.

Personal Communications

Matsuda, T., 1979, Earthquake Research Institute, University of Tokyo, Japan.

Schwartz, D., 1979, Woodward-Clyde Consultants, San Francisco.

Sharp, R., 1979, U. S. Geological Survey.

Isoseismal Maps of 1929 and 1855 Earthquakes

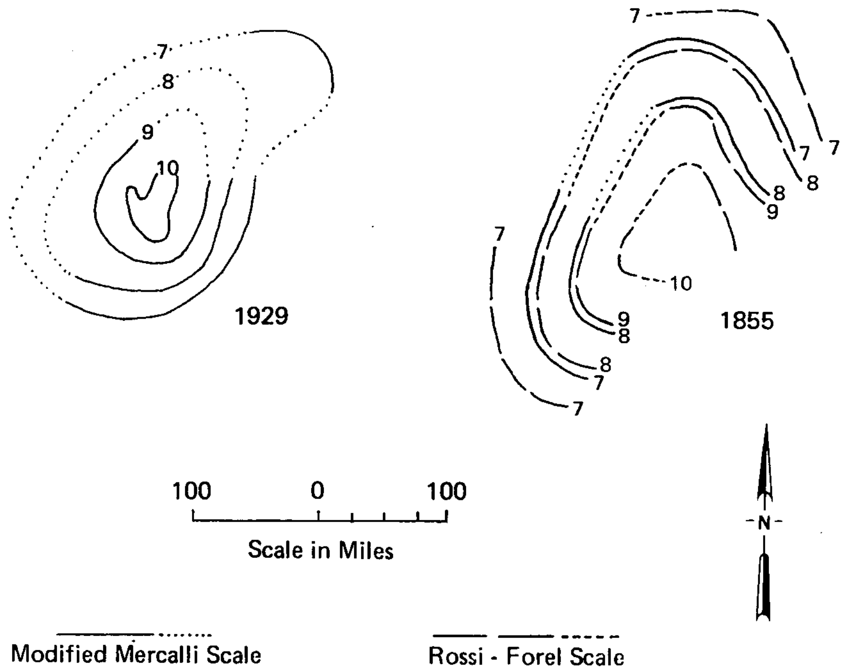

Isoseismal Comparisons

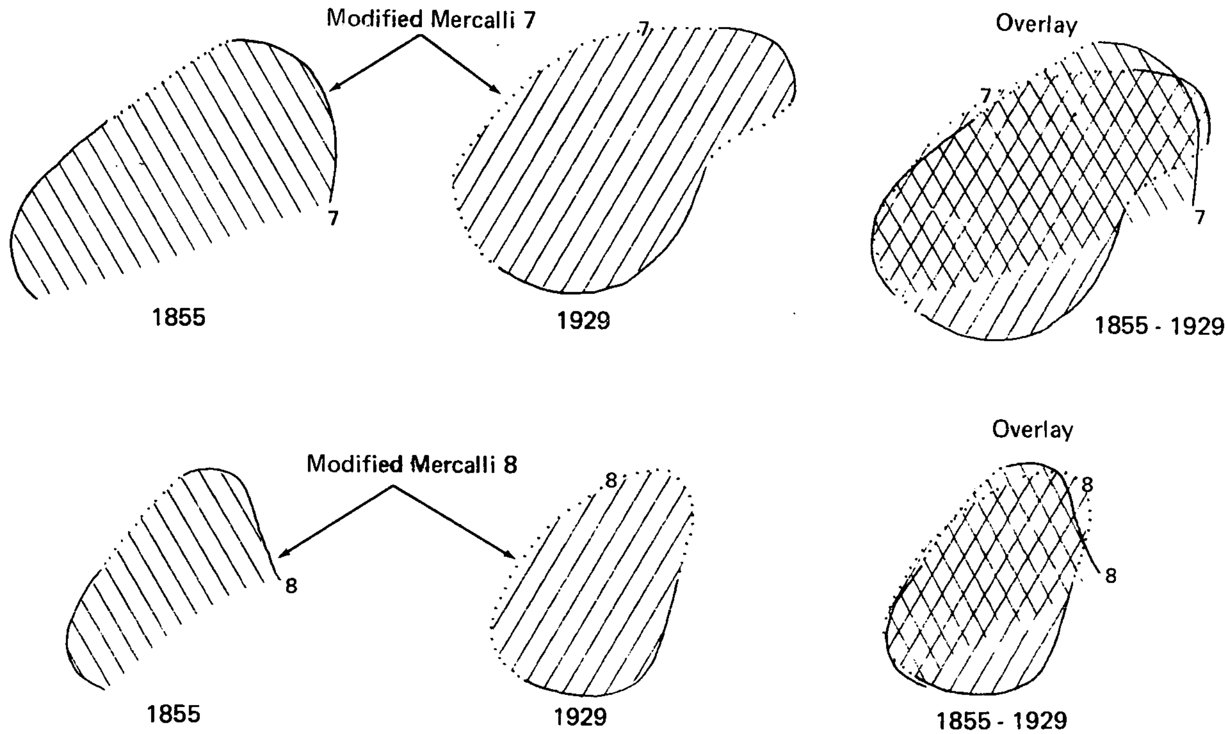

Note: Data from Clark and others, 1965

Figure 361.44 - 1 Comparison of 1855 and 1929 (M 7.6) New Zealand Earthquakes

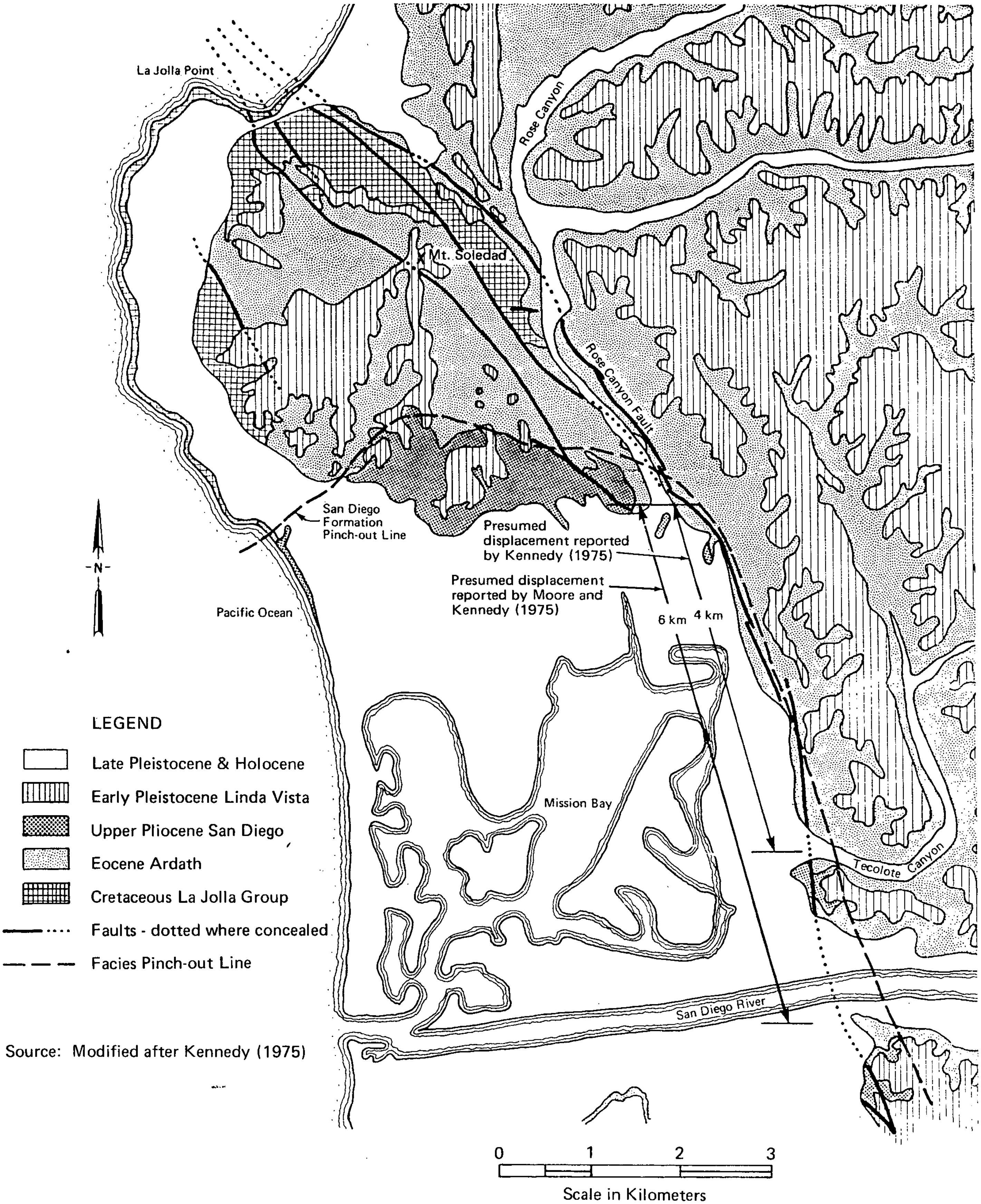

Source: Modified after Kennedy (1975)

Figure 361.44 - 2 Generalized Geologic Map - San Diego
Showing Rose Canyon Fault and Pinch-out Line of San Diego Formation

QUESTION 361.45

The relation of slip rate to maximum earthquake magnitude of Figures 6 and 7 of the WC report suggests that maximum earthquake magnitude to be expected for strike-slip faults may have upper bound limits of some type. Several of the values used require more detailed descriptions of rationale, definitions, and possible basic differences from relations from dip-slip faults. The values selected do not show the error bands or variation in determinations, or detailed descriptions of the methods of selecting or rejecting basic data. The design earthquake limits of Figure 7 do not include possible families of boundaries for such limiting values as maximum probable, maximum credible, maximum possible, or other defined types of boundary values. Some of the alternative types of boundary values include the definition of maximum earthquakes based on full fault length, fault half-length, fault third-length or other methods of establishing limiting values for fault zones. These relationships suggest the need for more complete discussions of the following questions:

a. What will be the effect on the San Onofre design basis, if the boundary of Figure 7 is changed by either refinement in current data points by newer studies, or by possible generation of new earthquakes of higher magnitude on faults of low slip rate?

b. Four faults, the San Andreas, San Jacinto, Hayward, and Calaveras faults, are plotted by x marks for maximum design earthquake. Other values than those shown have been established by the U. S. Geological Survey or in other publications. What methodology should be used for selection or rejection of data points of this type and what results are obtained if other well studied faults also are included in this type of compilation?

c. What effect on the boundary limits is obtained if the limiting maximum design earthquakes are based on maximum probable, maximum possible, maximum credible or on other defined types of maximum design earthquakes?

d. What are the relations to maximum or limiting values? Is the procedure of using fault half-length, or fault third-length or other types of calculated limits used?

e. The data supporting the slip rate versus magnitude points plotted should have a more thorough description of the details of data selection and rejection and the range in possible error, including the M_S determination. Describe any steps taken in this process that lead to results that provide conservatism in the results of the analysis. The range in slip rate rather than single values should be plotted.

f. The sparse nature of the data for faults with slip rates of less than about 3 mm/year average slip rate may, in part, be due to a poor data base for faults with slow strain rates. Statistically, what effect does this factor have in the validity of the data base and on the results of the analysis?

g. The geologic time scale that was used should be tabulated for reference and the assumed age, where general terms are used in the primary literature, e.g. Holocene, lower Pleistocene, etc., show the methods used in assigning an absolute age and show the error bands in the result that develop from the assumptions.

RESPONSE 361.45

361.45 a

The data base for Figure 7 of the WCC June 1979 report, which was used in part to establish the maximum earthquake for the hypothesized OZD, has been reviewed and revised as discussed in response 361.45 e. The results of these studies are incorporated in response 361.38. The historical earthquake limit (HEL) shown in Figure 361.45-3 was modified from Figure 7. The maximum earthquake limit (MEL) defined in response to question 361.45 e is shown in Figure 361.45-4. The maximum magnitude estimates for the hypothesized OZD are based on various lines of evidence which are summarized in section 361.38. These values are conservative with respect to the limit of the historic data as shown in Figures 361.38-4 and 361.45-4. Because of this conservative interpretation, the Applicants do not consider it credible to have higher magnitudes on low slip-rate strike-slip faults (in southern California or in similar tectonic environments) that would fall to the right of the MEL (Figures 361.38-4 and 361.45-4.). There would thus be no effect on the San Onofre design basis earthquake.

REFERENCES

Woodward-Clyde Consultants, 1979, Report of the evaluation of maximum earthquake and site ground motion parameters associated with the offshore zone of deformation, San Onofre nuclear generating station: Report for Southern California Edison Company, June, 241 p.

361.45 b

The predicted maximum earthquakes, marked by x's in Figures 6 and 7 were presented for comparison and as a reference framework, but, are not used in the derivation of the maximum earthquake line discussed in response 361.45 e. The maximum magnitude values for the San Andreas, San Jacinto, Hayward, and Calaveras faults, as shown in Figure 7 of the WCC June 1979 report, were taken from or based upon the rupture-length versus magnitude relationship discussed by Slemmons (1977). However, on the basis of a review of numerous professional publications and consulting reports, a wide variation was found to exist in the approaches used for various earthquake hazard investigations to establish conservative maximum earthquake values. For example, Table 361.45-1 lists the range of maximum earthquake values that have been used for several more intensively studied faults. These values were generally based upon half-fault-length/ magnitude relationships coupled with judged levels of conservatism. The wide range in values reflect the many different bases of evaluation used.

In many cases, the maximum magnitude estimates for other purposes were based on a limited investigation or were based on very conservative assumptions. The conditions leading to the use of high maximum values include the following:

1) the fault for which the maximum magnitude was selected may have been at sufficient distance from the project under investigation to render the project design insensitive to highly conservative maximum magnitude estimates for the fault;

2) the type of structure or development may not have been sensitive to large earthquake motions; and

3) the time required to investigate the fault more fully may have been of greater impact to the project than the cost of additional conservatism in design and construction.

For the above reasons and because of the differences in the scale and scope of work among the many investigators, inconsistencies should be expected among reports on maximum magnitude for a given fault.

In order to circumvent these variations, the data base for the selection of a maximum magnitude for the hypothesized OZD has been expanded from that of the WCC June 1979 report and ranges of both magnitude and slip rate data have been addressed. This is discussed in response 361.38. The degree-of-fault-activity approach, incorporating slip rate in conjunction with all other geologic data, is a comprehensive procedure for the selection of maximum magnitude on the hypothesized OZD. Uncertainties in the data base for the slip-rate/maximum-magnitude relationship and analysis of the physical constraints on earthquake magnitude provide the basis for constraining the maximum magnitude earthquake for the hypothesized OZD.

REFERENCES

Slemmons, D. B., 1977, State-of-the-art for assessing earthquake hazards in the United States, Report 6, Faults and Earthquake Magnitude: U. S. Army Corps of Engineers Waterways Experiment Station, Soils and Pavement Laboratory, Miscellaneous Paper S-73-1, 129 p.

Woodward-Clyde Consultants, 1979, Report of the evaluation of maximum earthquake and site ground motion parameters associated with the offshore zone of deformation, San Onofre nuclear generating station: Report for Southern California Edison Company, June, 241 p.

Table 361.45-1

Reported Maximum Earthquake Values

Fault	Magnitude Range	Number of Reports Cited*
San Andreas	8+ - 8.5	49
Hayward	6.7 - 8.4	16
Calaveras	7.0 - 8.4	16
San Jacinto	7.25 - 8.25	28

* Many different reports may use the same sources for maximum earthquake values.

361.45 c

The definitions set forth by the California Division of Mines and Geology (CDMG, 1977) for Maximum Credible and Maximum Probable earthquakes are:

> Maximum Credible Earthquake - The maximum credible earthquake is the maximum earthquake that appears capable of occurring under the presently known tectonic framework.
>
> Maximum Probable Earthquake - The maximum probable earthquake is the maximum earthquake that is likely to occur during a 100-year interval.

Though the limit line (MEL, Figure 361.38-5) has not been established according to these specific definitions, it is most compatible with that of the Maximum Credible Earthquake. That is, for the OZD, it represents the largest earthquake that is physically realizable as constrained by the level of fault activity and by the other specific physical characteristics of the OZD (response 361.38-d). For the maximum probable earthquake, a consistent criterion with the above definition is a 50% chance of occurrence in a period of 100 years. This is consistent with an average recurrence interval of about 130 to 150 years (Mortgat and others, 1977). Using the recurrence results tabulated in Table 361.38-1, a recurrence interval of 130 to 150 years corresponds to a maximum on the order of M_S 6.0+ for the hypothesized OZD. Therefore, for the hypothesized OZD, the Maximum Probable Earthquake as defined above would lie on or to the left of the historical earthquake limit (HEL).

The Maximum Possible Earthquake has not been explicitly defined and, therefore, has not been addressed in this response.

361.45 d

The relationship of maximum or limiting values to fault half-length, fault third-length, or other types of calculated limits was evaluated and compared to the geologic slip-rate/maximum-magnitude relationship. These comparisons and relationships are discussed in response 361.38 and 361.45 e.

361.45 e

Data Selection Process

Table G-1 was presented by the Applicants in the WCC June 1979 report as a data base representing the displacement and slip-rate data from as many authors as possible for strike-slip faults; according to the criteria set forth on pages G-1 and G-2. The table presents the possible range of data and the possible interpretations of slip rates for faults described in the literature, but it includes no attempt to appraise the quality or validity of the data. The twenty-four faults shown in Table G-1 are those that provided any slip rate data identified during a review of approximately 100 strike-slip faults identified in various literature sources. In preparation of Figures 6 and 7, the data in Table G-1 were not used directly but were subjected to a discriminating evaluation of the quality of the data. The most reliable data were selected in preparation of Table H-1 and in subsequent preparation of Figures 6 and 7.

In response to the NRC request, and to clarify this selection process, a more detailed description of data used or rejected in the construction of Figures 6 and 7 is given and all of the data presented in Table G-1 of the WCC June 1979 report have been reviewed and tabulated on a revised Table G-1 (Table 361.45-2). The revised table also contains additional data obtained since the publication of the WCC June 1979 report; thus, several modifications to the slip rates presented in Table G-1 are presented and several faults have been added. The new table is reorganized to clarify better which data are from literature sources and which are based on the assumptions or interpretations, if any, made by the Applicants. Data determined to be extraneous and unverifiable which were included in June 1979 have been eliminated in the revised table. The following screening criteria apply to the fault data presented in Table 361.45-2.

1) Only faults with tectonic settings and styles of faulting similar to the Southern California strike-slip faults are presented. For example, more detailed examination of the tectonic setting in Japan indicates that the strike-slip faults there cannot be equated to the California faults and they have thus been excluded from the slip-rate comparison. See response to NRC questions 361.46 b, 361.47, and 361.50 for further discussion.

2) Geologic data are used for estimating rates of slip. Total plate motion, geodetic slip, and fault creep are not necessarily representative of long term geologic slip. Generally, these data are not considered unless supported by geologic data.

3) Quaternary offsets are preferred for slip-rate calculations because they probably most accurately reflect the present tectonic setting and current rate of slip. However, when Quaternary offsets are not available, longer term offsets are accepted when they are believed to reflect the present day tectonic setting. Generally these longer term offsets are not greater than 10 to 15 million years.

4) Strike-slip faults with large dip-slip components are eliminated in order to keep the data set as similar as possible to the strike-slip style of the Southern California faulting. In general, the cut-off is approximately five to one (horizontal to vertical ratio).

5) The data range encompasses the data that are based on sound geologic fact as judged in the literature or through personal communications. Rough estimates of ages or of offsets are excluded so that unsubstantiated estimates of data are not equated to more detailed, factual data.

Table 361.45-3 summarizes the data presented in Table 361.45-2 providing the slip-rate range as well as a selected slip-rate value, which best represents the fault. The following criteria were used to select those values for each fault plotted on the revised slip-rate versus magnitude graphs (Figures 361.45-1 and 361.45-2). One of the three categories of selection criteria were used for each fault.

1) The selected ranges are primarily based on the value cited by most workers and are from the current and most credible workers' data. For example, Kerry Sieh's work on the San Andreas fault is most widely accepted, and Robert Sharp is accepted on the primary authority of Quaternary slip-rate values along the San Jacinto fault. Preference is always given to the slip-rate values based on Quaternary data because they best represent the current tectonic environment and activity of the faults. The selected value is based on the referenced author's preferred slip-rate value.

2) For some faults that have no slip rate assignments, but for which data are presented and can be used to calculate slip-rate values, the Applicants have selected the range and single values based on the most precise age and displacement data. Quaternary data are selected whenever possible.

3) If a range of values is cited in the literature, or if several slip-rate values can be calculated from the data presented and no single value is explicity presented, the Applicants have selected the mean value of the range of values to represent a particular fault.

The range of data and the selected slip-rate values for each fault along with the rationale and appropriate criteria used to choose each selected value are presented in Table 361.45-3. The data from Table 361.45-3 and historical earthquake magnitudes are plotted on the revised slip-rate versus magnitude graphs (Figures 361.45-1 and 361.45-2).

Magnitudes of earthquakes are presented as surface wave magnitudes (M_s). The values of earthquakes shown in Table 361.45-3 are taken from the various publications which discuss the seismology or geology of the faults. Pre-instrumental estimates are also taken from the various literature sources. The applicant has made no detailed efforts to determine independent M_s values from instrumental recordings or from pre-instrumental data. Generally, M_s values or their equivalent are available in the literature (for example, Gutenberg and Richter, 1954).

The surface wave magnitude for the 1933 Long Beach earthquake is of particular interest. It was reported by Gutenberg and Richter (1949a) as M_s 6.25; review of the unpublished worksheets prepared by Gutenberg and Richter (1949b) shows that 17 station readings were used and that the computed average is 6.2 $\pm$ .2 with a mode of 6.3. Thus, the M_s 6.3 value is a conservatively accurate value.

Application of Conservatism

Selection of the slip rate value which best represent the fault was based on data presented by the various researchers and authors and assumes no specific conservatism other than to best represent the faults degree of activity. The degree of conservatism in the selected values depends on each author's interpretation of this data. In order to further evaluate these data a line can be drawn bounding these empirical observations as shown in Figure 361.45-3. This line suggests that there is a consistent limit to the size of an earthquake associated with the geologic slip rate of a strike-slip fault. This assumes that some of the strike-slip faults in the world have had maximum or close-to-maximum earthquakes and that when these maximum data points are enveloped they form a maximum historic earthquake limit (HEL) related to slip rate. Several procedures are used to assess the conservatism and the significance of this observational limit.

The conservatism of the slip rate versus magnitude data set is evaluated by considering the ranges of slip rate and magnitude data obtained from published and unpublished sources. The data presented in Tables 361.45-3 and 361.45-4 provide for this assessment of uncertainty in the data interpretation.

To account for possible uncertainty in earthquake magnitude values and to provide another degree of conservatism, a magnitude range is assigned to each earthquake. The earliest surface wave magnitude estimates were considered to be dependable to one quarter of a unit (Richter, 1958, p. 347). Modern estimates, based on a larger and better distributed set of stations, are dependable to one tenth of a unit at a confidence level of 95% (e.g., Shimazaki and

Somerville, 1979, p. 1373-1374). The Applicants therefore conclude that a value of two tenths of a unit plus or minus is a conservative estimate of the uncertainty associated with surface wave magnitude estimates.

Another method of adding conservatism is to extend the possible ranges of slip rates for each of the faults. The ranges shown in Figure 361.45 (e) have been extended to the widest reasonable extent as discussed in available literature. Confidence in these ranges, presented in the literature, varies widely and is dependent upon how current and detailed the particular study us.

The widest reasonable ranges can be used in conjunction with the magnitude ranges to establish a maximum earthquake limit line (MEL) (Figure 361.45-4). The MEL is interpreted most conservatively by enveloping the lowest slip-rate ranges and the maximum-magnitude ranges of all the data points. The most conservative use of the line is to estimate a maximum earthquake by reading the MEL value based on the maximum slip-rate value provided for each fault. The Applicants believe that the MEL line represents an outer bound for maximum magnitude which will not be exceeded by future earthquakes on these faults. This line does not mean that each of these faults is capable of the MEL earthquake, but only that this line will not be exceeded by future earthquakes.

On the basis of the most conservative interpretation of the MEL line, the maximum magnitude for the NIZD associated with the highest slip rate of 0.68 mm/year results in M_S 7.0. The physical conservatism of both the M_S 6.5 and M_S 7.0 as maximum values are discussed in sections 361.38 (c) and (d).

REFERENCES

Addicott, W. O., 1968, Mid-Tertiary zoogeographic and paleogeographic discontinuities across the San Andreas fault, California: Conference on Geologic Problems of San Andreas Fault System, Stanford University, September 14-16, 1967, Proceedings, Stanford University Publications, v. 11, p. 144-165.

Arpat, E. and Saroglu, F., 1975, Some recent tectonic events in Turkey: Geological Society of Turkey Bulletin, v. 18, p. 91-101 (in Turkish).

Barrows, A. G., Beeby, D. J., and Kahle, J. E., 1979, Earthquake hazards geologic mapping of the San Andreas fault zone, Los Angeles County, California, near Valyermo, Lake Hughes, Three Points and Quail Lake: U. S. Geological Survey, National Earthquake Hazards Reduction Program, Summaries of Technical Reports, v. VIII, June.

Ben-Menahem, A., Nur, A., and Vered, M., 1976, Tectonics, seismicity and structure of the Afro-Eurasian junction--The breaking of an incoherent plate: Physics of the Earth and Planetary Interiors, v. 12, p. 1-50.

Burke, D. B., and Helley, E. J., 1973, Map showing evidence for recent fault activity in the vicinity of Antioch, Contra Costa County, California: U. S. Geological Survey Miscellaneous Field Studies Map MF-533, scale 1:24,000.

Canitez, N., 1976, Dynamics of the North Anatolian fault: Cento Seminar on Earthquake Hazard Minimization, Teheran, Proceedings, p. 353-366.

Castle, R. O., and Yerkes, R. F., 1976, Recent surface movements in the Baldwin Hills, Los Angeles County, California: U. S. Geological Survey Professional Paper 882, 125 p.

Clark, M. M., Grantz, A., and Rubin, M., 1972, Holocene activity of the Coyote Creek fault as recorded in sediments of Lake Cahuilla, in The Borrego Mountain Earthquake of April 9, 1968: U. S. Geological Survey Professional Paper 787, p. 112-130.

Clark, S. H., Jr., and Nilsen, T. H., 1973, Displacement of Eocene strata and implications for the history of offset along the San Andreas fault, central and northern California: Conference on Tectonic Problems of the San Andreas fault system, Stanford University, June 20-23, 1973, Proceedings, Stanford University Publications, v. 13, p. 358-367.

Clayton, L., 1966, Tectonic depressions along the Hope fault, a transcurrent fault in North Canterbury, New Zealand: New Zealand Journal of Geology and Geophysics, v. 9, p. 95-104.

Crittenden, M. D., Jr., 1951, Geology of the San Jose-Mount Hamilton area, California: California Division of Mines and Geology Bulletin 157, 74 p.

Crowell, J. C., 1973, Problems concerning the San Andreas fault system in southern California: Conference on Tectonic Problems of the San Andreas Fault System, Stanford University, June 20-23, 1973, Proceedings, Stanford University Publications, v. 13, p. 125-135.

Cummings, J. C., 1968, The Santa Clara formation and possible post-Pliocene slip on the San Andreas fault in central California: Conference on Geologic Problems of San Andreas Fault System, Stanford University, September 14-16, 1967, Proceedings, Stanford University Publications, v. 11, p. 191-207.

Dewey, J. W., 1972, Seismicity and tectonics of Western Venezula: Seismological Society of America Bulletin, v. 62, no. 6, p. 1711-1751.

Dudley, P. H., 1954, Geology of the Long Beach oil field, Los Angeles County: California Division of Mines and Geology Bulletin 170, Map Sheet 34.

Durham, D. L., and Yerkes, R. F., 1964, Geology and oil resources of the eastern Puente Hills area, southern California: U. S. Geological Survey Professional Paper 420-B, 62 p.

Ehlig, P. L., Ehlert, K. W., and Crowe, B. M., 1975, Offset of the upper Miocene Caliente and Mint Canyon formations along the San Gabriel and San Andreas faults, in San Andreas fault in southern California: California Division of Mines and Geology Special Report 118, p. 83-92.

Freund, R., 1971, The Hope fault: A strike-slip fault in New Zealand: New Zealand Geological Survey Bulletin, n. 5, 86, 49 p.

Freund, R., Garfunkel, Z., Zak, I., Goldberg, M., Weissbrod, T., and Derin, B., 1970, The shear along the Dead Sea rift: Philosophical Transactions, Royal Society of London, Series A, v. 267, p. 107-130.

Girdler, R. W., 1958, The relationship of the Red Sea to the East Africa rift system: Quarterly Journal of the Geological Society of London, v. 114, p. 79-115.

Graham, S. A., and Dickinson, W. R., 1977, Apparent offsets of on-land geologic features across the San Gregorio-Hosgri fault trend: Geological Society of America Abstracts with Programs, 73rd annual meeting, v. 9, no. 4, p. 424.

Greene, H. G., 1977, Slivering of the Salinian block along the Palo Colorado-San Gregorio and associated fault zones: Geological Society of America Abstracts with Programs, 73rd annual meeting, v. 9, no. 4, p. 425.

Gutenberg, B., and Richter, C. F., 1949a, Seismicity of the earth and associated phenommena: Princeton University Press, Princeton, 273 p.

Gutenberg, B., and Richter, C., F., 1949b, Unpublished work-sheets for Seismicity of the Earth: California Institute of Technology, Milikan Library Archives, Pasadena.

Gutenberg, B., and Richter, C. F., 1954, Seismicity of the earth and associated phenomena: Hafna Publishing Company, New York, 310 p.

Hamilton, D. H., and Willingham, C. R., 1978, Evidence for a maximum of 20 km of Neogene right slip along the San Gregorio fault zone of central California: EOS Transactions, American Geophysical Union, v. 59, no. 12, p. 1210.

Heath, E. G., 1954, Geology along the Whittier fault north of Horseshoe Bend, Santa Ana Canyon, California: Master's thesis, Claremont Graduate School, 84 p.

Herd, D. G., 1978, Neotectonic framework of central coastal California and its implications to microzonation of the San Francisco Bay region, in Second Internation Conference on Microzonation for Safer Construction - research and application, Proceedings, v. 1, p. 231-240.

Hill, L., 1971, Newport-Inglewood zone and Mesozoic subduction, California: Geological Society of America Bulletin, v. 82, p. 2957-2962.

Huffman, O. F., 1972, Lateral displacement of upper Miocene rocks and the Neogene history of offset along the San Andreas fault in central California: Geological Society of America Bulletin, v. 83, n. 10, p. 2913-2946.

Huffman, O. F., Turner, D. L., and Jack, R. N., 1973, Offset of late Oliogocene-early Miocene volcanic rocks along the San Andreas fault in central California: Conference on Tectonic Problems of the San Andreas fault system, Stanford University, June 20-23, 1973, Proceedings, Stanford University Publications, v. 13, p. 368-373.

Kanamori, H., Jennings, P. C., 1978, Determination of local magnitude, M_L, from strong-motion accelerograms: Seismlogical Society of America Bulletin, v. 68, no. 2, p. 471-485.

Kennedy, M. P., 1977, Recency and character of faulting along the Elsinore fault zone in southern Riverside County, California: California Division of Mines and Geology Special Report 131, 12 p.

Knuepfer, P. L., 1977, Geomorphic investigations of the Vaca and Antioch fault systems, Solano and Contra Costa Counties, California: Master's thesis, Stanford University, 53 p.

Krymus, V. N., and Lykov, V. I., 1969, The character of the junction of the Epi-Hercynian platform and the Alpine folded belt, south Turkmenia: Geotectonics, Academy of Science, U. S. S. R., translated by the American Geophysical Union, v. 6, p. 391-396.

Lamar, D. L., Merifield, P. M., and Proctor, R. J., 1973, Earthquake recurrence intervals on major faults in southern California, in Moran, D. E., Slosson, J. E., Stone, R. O., and Yelverton, C. A., eds., Geology, Seismicity, and Environmental Impact: Association of Engineering Geologists Special Publication, p. 265-276.

Lensen, G. J., 1958, The Wellington fault from Cook Strait to Manawatu Gorge: New Zealand Journal of Geology and Geophysics, v. 1, no. 1, p. 364-374.

Lensen, G. J., 1973, Guidebook for excursion A-10, Tour Guide for International Association of Quaternary Research Christchurch, New Zealand, 76 p.

Lensen, G. J., 1975, Earth-deformation studies in New Zealand: Tectonophysics, v. 29, p. 541-551.

Lensen, G. J., and Vella, P., 1971, The Waiohine faulted terrace sequence--recent crustal movements: Royal Society of New Zealand, Bulletin 9, p. 117-119.

Morton, D. M., 1979, Earthquake hazard studies, upper Santa Ana Valley and adjacent areas: U. S. Geological Survey National Earthquake Hazards Reduction Program, Summaries of Technical Reports, v. 8, June.

Nardin, T. R., and Henyey, T. L., 1978, Pliocene-Pleistocene diastrophism of Santa Monica and San Pedro shelves, California continental borderland: American Assocation of Petroleum Geologists Bulletin, v. 62, n. 2, p. 247-272.

Neev, D., and Emery, K. O., 1967, The Dead Sea, depositional processes and environments of evaporites: Geological Survey of Israel Bulletin, v. 41, p. 147.

Norris, R. M., Keller, E. A., and Meyer, G. L., 1979, Geomorphology of the Salton Basin, selected observations in Abbott, P. L., ed., Geologic Excursions in the Southern California Area: Department of Geological Science, San Diego State Univesity, p. 19-46.

Page, R. A., 1969, Late Cenozoic movement on the Fairweather fault in southeastern Alaska: Geological Society of America Bulletin, v. 80, p. 1873-1877.

Peterson, M. S., 1975, Geology of the Coachella fanglomerate, in San Andreas fault in southern California: California Division of Mines and Geology Special Report 118, p. 119-126.

Plafker, G., Hudson, T., and Bruns, T., 1978, Late Quaternary offsets along the Fairweather fault and crustal plate interactions in southern Alaska: Canadian Journal of Earth Science, v. 15, p. 805-816.

Posavec, M., Taylor, D., Van Leeuwen, T., and Spector, A., 1973, Tectonic controls of volcanism and complex movements along the Sumatran fault system: Geological Society of Malaysia Bulletin, no. 6, p. 43-60.

Prowell, D. C., 1974, Geology of selected Tertiary volcanics in the central coast range mountains of California and their bearing on the Calaveras and Hayward fault problems: University of California Santa Cruz, unpublished Ph.D. thesis, 182 p.

Quennell, A. M., 1958, The structure and geomorphic evolution of the Dea Sea rift: Quarterly Journal of the Geological Society of London, v. 114, pt. 1, p. 1-24.

Richter, C. F., 1958, Elementary Seismology: W. B. Freeman and Company, San Francisco.

Rod, E., 1956, Strike-slip faults of northern Venezuela: American Association of Petroleum Geologists, v. 40, no. 3, p. 457-476.

Sage, O., 1973, Paleocene geography of the Los Angeles region, in Kovach, R. L., and Nur, A., eds., Conference on Tectonic Problems of the San Andreas fault system, Proceedings: Stanford University Publication in Geological Sciences, v. 13, p. 348-357.

Sengor, A. M. C., 1979, North Anatolian transform fault-its age, offset and tectonic significance: Journal of the Geological Society of London, v. 136, p. 269-282.

Scholz, C. H., Rynn, J. M., Weed, R. W., Frohlich, C., 1973, Detailed seismicity of the Alpine fault zone and Fiordland region, New Zealand: Geological Society of America Bulletin, v. 84, no. 10, p. 3279-3316.

Schubert, C., and Sifontes, R. S, 1970, Bocona fault, Venezuelan Andes, evidence of postglacial movement: Science, v. 170, p. 66-69.

Schwartz, D., Cluff, L. S., and Donnelly T., 1979, Quaternary faulting along the Caribbean and North American plate boundary: Tectonophysics, v. 52 (in press).

Sharp, R. V., 1967, San Jacinto fault zone in the Peninsular Ranges of southern California: Geological Society of America Bulletin, v. 78, no. 6, p. 705-730.

Sharp, R. V., 1978, Salton Trough tectonics: U. S. Geological Society, National Earthquake Hazards Reduction Program, Summaries of Technical Reports, v. 7, p. 34-35.

Sharp, R. V., 1980, Salton Trough tectonics: U. S. Geological Society, National Earthquake Hazards Reduction Program, Summaries of Technical Reports, Open-File Report 80-6, v. 9.

Shimazaki, D., and Somerville, P., 1979, Static and Dynamic Parameters of the Izu-Oshima, Japan Earthquake of January 14, 1978: Seismological Society of America Bulletin, v. 69 p. 1343-1378.

Shor, G. G., 1955, Deep reflections from southern California blasts: Transactions of the American Geophysical Union, v. 36, p. 133-138.

Sieh, K. E., 1977, A study of Holocene displacement history along the south-central reach of the San Andreas fault: Ph.D. thesis, Stanford University, 219 p.

Sieh, K. E., 1978, Prehistoric large earthquakes produced by slip on the San Andreas fault at Pallett Creek, California: Journal of Geophysical Research, v. 83, no. B8, p. 3907-3939.

Silver, E., 1977, Are the San Gregorio and Hosgri fault zones a single fault system?: Geological Society of America, Abstracts with Programs, 73rd annual meeting, v. 9, no 4, p. 500.

Suggate, R. P., 1960, The interpretation of progresssive fault displacement of flights of terraces: New Zealand Journal of Geology and Geophysics, v. 3.

Suggate, R. P., and Lensen, G. J., 1973, Rate of horizontal fault displacement in New Zealand: Nature, v. 242, p. 518.

Tchalenko, J. S., and Berberian, M., 1975, Dasht-e Bayaz fault, Iran-Earthquake and earlier related structures in bedrock: Geological Society of America Bulletin, v. 86, no. 5, p. 703-709.

Tjia, H. D., 1970, Rates of diastrophic movement during the Quaternary in Indonesia: Geologie en Mijnouw (Journal of the Royal Geological and Mining Society of the Netherlands), v. 49, no. 4, p. 335-338.

Trifonov, V. G., 1971, The pulse-like character of tectonic movements in regions of most recent mountain-building (Kopet Dagh and southeast Caucasus): Geotectonics, U. S. S. R. Academy of Sciences, Geological Institute, no. 1, p. 234-235.

Trifonov, V. G., 1978, Late Quaternary tectonic movements of western and central Asia: Geological Society of America Bulletin, v. 89, no. 7, p. 1059-1072.

Van Eysinga, F. W. B., 1975, Geologic Time Scale: Elsevier Scientific Publishing Company, Amsterdam, 3rd Edition, 1 sheet.

Vedder, J. G., 1975, Juxtaposed Teritary strata along the San Andreas fault in the Temblor and Caliente Ranges, California, in San Andreas fault in southern California: California Division of Mines and Geology Special Report 118, p. 234-240.

Weber, G. E., and La Joie, K. R., 1979, Late Pleistocene rates of movement along the San Gregorio fault zone determined from offset marine terrace shoreline angles in Weber and others, eds., Coastal Tectonics and Hazards in Santa Cruz and San Mateo Counties, California: Field Trip Guide, Cordilleran section of the Geological Society of America, 75th annual meeting.

Weber, F. H., Jr., 1977a, Total right lateral offset along the Elsinore fault zone, southern California: Geological Society of America Abstracts with Programs, v. 9, no. 4, p. 523-524.

Weber, F. H., Jr., 1977b, Seismic hazards related to geologic factors, Elsinore and Chino fault zones, northwestern Riverside County, California: California Division of Mines and Geology Open-File Report 77-4LA.

Wellman, H. W., 1969, Wrench (transcurrent) fault systems: American Geophysical Union Monograph 13.

Woodward, Clyde and Associates, 1969, Seismicity and seismic geology of northwestern Venezuela: Report to Shell Oil Company of Venezuela, v. 2, 77 p.

Woodward-Clyde Consultants, 1979, Report of the evaluation of maximum earthquake and site ground motion parameters associated with the offshore zone of deformation, San Onofre nuclear generating station: Report for Southern California Edison Company, June 241 p.

Wright, T. L., Parker, S., Erickson, R. C., 1973, Stratigraphic evidence for the timing and nature of late Cenozoic deformation in the Los Angeles basin: Paper presented at National American Association of Petroleum Geologists convention, Anaheim, California, May, 1973.

Yerkes, R. F., 1972, Geology and oil resources of the western Puente Hills area, southern California: U. S. Geological Survey Professional Paper 420-C, 63 p.

Yerkes, R. F., McCulloh, T. H., Schoellhamer, J. E., and Vedder, J. G., 1965, Geology of the Los Angeles basin--an introduction: U. S. Geological Survey Professional Paper 420-A, 57 p.

Zak, I., and Freund, R., 1966, Recent strike slip movements along the Dead Sea rift: Israel Journal of Earth Sciences, v. 15, p. 33-37.

Personal Communications

Knuefer, P. L., 1979, Woodward-Clyde Consultants. San Francisco, California.

Seih, K., 1979, California Institute of Technology, Pasadena, California.

Schwartz, D., 1979, Woodward-Clyde Consultants, San Francisco, California.

Welden, R., 1979, California Institute of Technology, Pasadena, California.

Table 361.45-2
SELECTED GEOLOGIC SLIP RATE INFORMATION FOR STRIKE-SLIP FAULTS
IN CALIFORNIA AND SIMILAR TECTONC REGIONS

Fault Reference Number	Fault Name/ Locality	Reference	Displacement Data from Reference: Offset Feature	Age of Feature	Amount of Offset	Age of Offset	Slip Rate mm/yr	Slip Rate Evaluation: Assumptions	Slip Rate mm/yr	Comments
1	San Andreas (northern section)	Herd, 1978	Rocks	Pliocene	-	1.8-5 m.y.	6-22	-	-	Cites Addicot, 1968. No estimate of time of initiation of faulting given.
			Deposits	1-3 m.y.	-	1-3 m.y.	10-30	-	-	Cites Cummings, 1968. Questionable time constraints.
			-	-	-	-	20	-	-	Generalized rate based on data of Addicot, 1968, and Cummings, 1968, also generally accepted rate in northern California.
		Cummings, 1968	Source of Corte Modera facies	Early Pleistocene 1-3 m.y.	28 km	1-3 m.y.	10-30	Author's offset and range of Early Pleistocene of 0.7 to 1.8 m.y.	15-40	Questionable time constraints; not used.
2	San Andreas (central section)	Huffman, 1972	Source areas of clastic units	Mohnian 8-12 m.y.	224-256 km	-	-	Author's offset; Mohnian at 6-12 m.y.	19-43	Best data for Late Miocene north of Big Bend.
		Clark and Neilson, 1973	Point of Rocks Sandstone and Butano Sandstone; Kreyenhagen Shale-Twobar Shale	Eocene 44-49 m.y. (K-Ar date)	305-330 km	44-49 m.y.	-	-	-	Ages are too old to be representative of present rates. Not used.
		Huffman, and others, 1973	Pinnacles volcanics-Neenach volcanics and associated sedimentary rocks	Oligocene-Miocene boundary 22-23.5 m.y. (K-Ar date)	295 km	22-23.5 m.y.	-	-	-	Ages are too old to be representative of present rates. Not used.
		Vedder, 1975	Source areas of lithologic units	Middle Miocene	300 km	Middle Miocene	-	12-15 m.y. for Middle Miocene; author's offset	20-25	Vedder bases data on previous studies. Time constraints are assumed.
			Source areas of marine mudstones and sandstones	Early Pliocene	80 km	Early Pliocene	-	3.1-5 m.y. for Early Pliocene; author's offset	16-25	Time constraints are assumed.

Table 361.45-2 (continued)

Fault Reference Number	Fault Name/ Locality	Reference	Displacement Data from Reference: Offset Feature	Age of Feature	Amount of Offset	Age of Offset	Slip Rate mm/yr	Slip Rate Evaluation: Assumptions	Slip Rate mm/yr	Comments
	San Andreas (central section) continued	Sieh, 1977	Wallace Creek channel	3430± 160 yr (C^{14} date)	118-138 m	3430±160 yr	34-41	-	-	Sieh indicates 37 mm/yr is most likely. Best data available for this section of the fault.
		Sieh, 1978	Marsh deposits at Pallett Creek	Holocene 500-1857 A.D.	4.5 m/ event	-	30	-	-	Assumes 4.5 meters per major event and 160 year recurrence. Speculative, not used.
		Barrows and others, 1979	Harold Fm.	Post Rancho La Brea 600,000 yrs	15 km	600,000 yr or younger	-	Author's age and offset	25	Rate represents a minimum.
	San Andreas (south and central sections)	Crowell, 1973	Sedimentary units and Pelona-Orocopia Schist	Paleocene to Miocene	260+ km	Late Miocene 8-12 m.y.	22-32	Late Miocene at 6-12 m.y.	22-43	Includes San Gabriel fault in Big Bend area.
		Ehlig and others, 1975	Source of Soledad and Mint Canyon formations	Middle to Late Miocene	297-307 km	12 m.y.	-	Author's age and offset	25-26	Good constraint on amount of offset but not on time of initiation of faulting.
3	San Andreas-(southern section)	Peterson, 1975	Source of Coachella Fanglomerate	Miocene 10±1.2 m.y. (K-Ar Date)	215 km	10±1.2 m.y.	-	Author's age and offset	19-25	-
		Weldon, Ray and Seih, 1979 (personal communication)	Terrace riser	Holocene 9400 - 12500 yr	Approx. 250 m	9400-12500 yr	20-25	-	-	Age based on well constrained extrapolation of sedimentation rates from C^{13}/C^{12} dates. Good estimate for southern section.
		Norris and others, 1979	Pediment-alluvial fan	Late Pleistocene	900 m	17000-70000 yr	10-50 (40-50 preferred)	Author's age and offset	13-53	Ages not well controlled; range too wide for present use.
4	San Jacinto/ Southern California	Sharp, 1967	Source of Bautista gravel beds	Pleistocene	5.2 km	as old as 2 m.y.	2.6	-	-	Age uncertain; superceded by Sharp, 1980. Not used.

Table 361.45-2 (continued)

Fault Reference Number	Fault Name/ Locality	Reference	Displacement Data from Reference: Offset Feature	Age of Feature	Amount of Offset	Age of Offset	Slip Rate mm/yr	Slip Rate Evaluation: Assumptions	Slip Rate mm/yr	Comments
	San Jacinto continued	Sharp, 1967 continued	Basement rocks	Middle to Late Cretaceous	24 km	-	-	Initiation of faulting at opening of Gulf of California, 4-5 m.y.	4.8-6	Offsets differ from later study (Morton, 1979). Rates appear reasonable.
			Sedimentary rocks	Cenozoic	29-32 km	-	-	as above	5.8-8	as above
		Sharp, 1978	Source of Boutista gravel beds	Pleistocene, less than 0.73 m.y.	5.2 km	less than 0.73 m.y.	greater than 7.1	-	-	Date based on chemical correlation of underlying Ash bed with K-Ar dated Bishop Ash elsewhere. Displacement considered minimum; age maximum.
		Morton, 1979	Igneous rocks correlated by K-Ar dates	Cretaceous	22 km	-	-	Initiation of faulting at opening of Gulf of California, 4-5 m.y.	4.4-5.5	Author states Pliocene units offset same amount; sets lower slip rate limit.
		Sharp, 1980	Source of Boutista gravel beds	Pleistocene, less than 0-73 m.y.	5.7-8.6 km	less than 0.73 m.y.	greater than 8-12	-	-	Most recent and best data on one of the main traces of the fault zone, Claremont-Clark segment.
4b	San Jacinto (Coyote Creek segment)/ Southern California	Clark and others, 1972	Lake Cahuilla sediments	Serveral up to 3080+600 yr (C^{14} date)	Up to 1.7 m vertical	Up to 3080±600 yr	1.4-4 (3 preferred)	-	-	Based on vertical to horizontal ratio of 1:2.7 and offset to drag ratios of 0:1 to 2:1 from 1968 Borrego Mtn. earthquake; speculative; not used.
			Lake Cahuilla sediments	200 yr recurrence interval	.3 to .38 m horizontal + drag at 1:1	1968 Borrego Mtn. earthquake	3-3.8	-	-	Recurrence interval based on C^{14} dated offsets up to 3000 yr old; speculative, not used.
		Sharp, 1980	Lake Cahuilla sediments	Holocene 283-478 yr (C^{14} dates)	1.70 m	283-478 yr	3-5	Author's offset and age range	3.5-6	Offset based on vertical data, vertical to horizontal ratio and recurrence intervals after Clark and others, 1972, for Borrego Mtn. earthquake. May not be valid.
			Stream channel	Holocene 5000 yr (C^{14} date)	10.9 m	5400-6000 yr	1-2	Author's age and offset recalculated	1.8-2.0	Lower bound on Coyote Creek segment as timing of fault could be later.

Table 361.45-2 (continued)

Fault Reference Number	Fault Name/ Locality	Reference	Displacement Data from Reference: Offset Feature	Age of Feature	Amount of Offset	Age of Offset	Slip Rate mm/yr	Slip Rate Evaluation: Assumptions	Slip Rate mm/yr	Comments
5	Elsinore/ Southern California	Weber, 1977a, 1977b	Bedford Canyon Fm; pegmatite dikes; contact of basement and Santigo Peak Volcanics	Late Cretaceous	9-11 km	-	-	Initiation of strike-slip faulting at opening of Gulf of California, 4-5 m.y.	1.8-2.75	Faulting style may have changed to strike slip at opening of Gulf.
			Sespe-Vaqueros contact	Late Eocene	10-13 km	-	-	Initiation of strike-slip faulting at opening of Gulf of California, 4-5 m.y.	2-3.25	Faulting style may have changed to strike slip at opening of the Gulf.
		Weber, 1977a	Fault contact	Paleocene	9.5 km	-	-	Initiation of strike-slip faulting at opening of Gulf of California, 4-5 m.y.	1.9-2.4	Faulting style may have changed to strike slip opening of the Gulf.
		Lamar and others, 1973	Sediments	Post Late Miocene	32 km	Post late Miocene	-	-	-	Correlation not well supported. Not used.
		Kennedy, 1977	Facies change	Lower Pleistocene	5 km	-	-	Author's offset and .7 to 1.8 m.y.	2.8-7.1	Age not well constrained; seems to be an upper value.
		Sage, 1973	Paleogeography of similar lithologic terrane	Paleocene rocks	40 km	Post Miocene	-	-	-	Offset and age are speculative. Not used.
6	Whittier/ Southern California	Heath, 1954	Fault contact	Late Miocene units faulted	3.7 km	Late Miocene or Post Miocene	-	Author's offset and 3-6 m.y.	.6-1.2	Age of faulting not well defined; probably yields minimum slip-rate value. Not used.

Table 361.45-2 (continued)

Fault Reference Number	Fault Name/ Locality	Reference	Displacement Data from Reference: Offset Feature	Age of Feature	Amount of Offset	Age of Offset	Slip Rate mm/yr	Slip Rate Evaluation: Assumptions	Slip Rate mm/yr	Comments
	Whittier/ Southern California continued	Heath, 1954	Stream channels	Pleistocene	2.5 km	Pleistocene	-	Author's offset and 1.0-1.8 m.y. age at beginning of Pleistocene	1.4-2.5	Age of stream channels poorly dedefined; probably yields maximum slip-rate value; not used.
		Lamar and others, 1973	Sediments	Upper Miocene and Pliocene	4.7-4.8 km	6 m.y.	0.8	Author's offset and 3-6 m.y.	0.8-1.6	Age of offset poorly defined.
			Stream channels	Pleistocene	2.4 km	Pleistocene	-	Author's offset and assume 1.0-1.8 m.y. at beginning of Pleistocene	1.3-2.4	Age of stream channels poorly defined. Not used.
		Yerkes, 1972, Durham and Yerkes, 1964 and Yerkes and others, 1965	Fault contact	Upper Mohnian	4.6 km	Upper Mohnian	-	Author's offset; Upper Mohnian to Early Pliocene, 4-6 m.y.	0.8-1.2	Offset is based on projection of fault contact. Faulting of contact could be younger
7	Newport-Inglewood Zone of Deformation/ Southern California	Castle and Yerkes, 1976	"Gyroidina" zone; Inglewood oil field	Mid to Late Pliocene	3000 to 4000 ft. (915-1220 m)	-	-	Absolute ages based on Nardin & Henyey (1978), 1.8-3.0 m.y.	0.3-0.68	Generalized displacement and age but gives good overall range. Poor age control.
			Stream channel	Late Quaternary	100 to 150 ft (30-45 m)	-	-	-	-	Stream channel not dated.
		Wright and others, 1973	Anticlinal axis, Inglewood oil field	Latest Pliocene	4000 ft (1220 m)	Post Latest Pliocene	-	Absolute ages based on Nardin and Henyey, (1978), 1.8-2.5 m.y.	0.5-0.68	Good data, may indicate slightly higher rates at north end of NIZD.
		Yerkes and others, 1965	Oil Bearing sediments	Lower Pliocene	3000 to 5000 ft (915-1525 m)	-	-	-	-	Age of offset not stated; poorly defined offset; not used.
		Hill, M. L., 1971	Sediments with E-log correlations	Miocene	10000 ft (3050 m)	-	-	Age of offset 5 to 8 m.y.	0.38-0.61	Age of offset not defined but believed to be good range for maximum reported offset.

Table 361.45-2 (continued)

Fault Reference Number	Fault Name/ Locality	Reference	Displacement Data from Reference: Offset Feature	Age of Feature	Amount of Offset	Age of Offset	Slip Rate mm/yr	Slip Rate Evaluation: Assumptions	Slip Rate mm/yr	Comments
	Newport-Inglewood continued	Dudley, 1954	Top of brown zone structure Long Beach field	Lower Plio-cene	3000 ft (915 m)	-	-	-	-	Poor age and displacement control.
		Woodward-Clyde Con-sultants 1979	Sediments with E-log correlations, Huntington Beach oil field	Late Mio-cene	12000 ft (3660 m)	Late Mio-cene	0.52 (ave.)	-	-	Detailed offset and age data pre-sented in Appendix B of referenced report.
			Sediments with E-log correlations, Seal Beach oil field	Pliocene	4000 to 8000 ft (1220-2440 m)	Pliocene	0.49 (ave.)	-	-	Detailed offset and age data pre-sented in Appendix B of referenced report.
			Sediments with E-log correla-tions, Long Beach oil field	Late Miocene and Pliocene	2000 to 10000 ft (610-3050 m)	Late Mio-cene to Pliocene	0.5 (ave.)	-	-	Detailed offset and age data pre-sented in Appendix B of referenced report.
8	Calaveras-Paicines (South of Hayward branch)/ Central California	Prowell, 1974	Quien Sabe-Coyote Lake volcanics	Pliocene 3.5 m.y. (K.-Ar date)	11-27 km	3.5 m.y.	5 mm/yr	-	-	Author gives two correlations and an average slip rate of 5 mm/yr.
			San Filipe-Coyote Lake volcanics	Pliocene 3.5 m.y. (K-Ar date)	7-21 km	3.5 m.y.	as above	-	-	as above
		Herd, 1978	Anderson-Coyote Lake volcanic rocks	Pliocene	unstated	Pliocene	1.4-7.1	-	-	Considered as a minimum rate by Herd.
			-	-	-	-	12-15	-	-	Based on difference in apparent slip rate on the San Andreas north and south of the Calaveras-Pacicines fault. Limited geologic data. Consistent with creep rates.

Table 361.45-2 (continued)

Fault Reference Number	Fault Name/ Locality	Reference	Displacement Data from Reference: Offset Feature	Age of Feature	Amount of Offset	Age of Offset	Slip Rate mm/yr	Slip Rate Evaluation: Assumptions	Slip Rate mm/yr	Comments
9	Calaveras-Sunol (North of Hayward Branch)/ Central California	Crittenden, 1951	Tularcitos syncline	Plio-Miocene (Blancan)	3 mi (4.8 km)	-	-	-	-	Long term geologic rate without control of recency of offset; not used.
		Prowell, 1974	Quien Sabe area - Mt. Hamilton volcanics	Late Miocene 8.2 m.y. (K-Ar date)	66-73 km	8.2 m.y.	8	-	-	Probably upper bound for slip rate
		Herd, 1978	-	-	-	-	6-7.5	-	-	Author apportions 50% of Calaveras-Paicines slip rate to the Calaveras-Sunol branch. Indirect geologic data.
10	Hayward/ Central California	Prowell, 1974	Grisley Peak volcanics	Late Miocene 8.2 m.y. (K-AR dating)	42-45 km	8.2 m.y.	-	Author's age and offset	5-5.5	Only known correlation across the Hayward fault.
		Herd, 1978	-	-	-	-	6-7.5	-	-	Author apportions 50% of Calaveras-Paicines slip rate to the Hayward fault. Indirect geologic data.
11	Antioch-Vaca and Davis/ Central California	Burke and Halley, 1973	Nortonville Shale	Eocene	1.2 km (map)	-	-	-	-	Horizontal separation could be affected by vertical offset of shallowly dipping beds. Not used.
			Ciebro Sandstone	Upper Miocene	.18 km (map)	-	-	Post Middle Miocene initiation 4-8 m.y.	.022-.045	At base of unit across Antioch fault.
			Ciebro Sandstone	Upper Miocene	.38 km (map)	-	-	Post Middle Miocene initiation, 4-8 m.y.	.047-.095	At base of unit across Davis fault.
			Ciebro Sandstone	Upper Miocene	.56 km (map)	-	-	Post Middle Miocene initiation 4-8 m.y.	.07-.14	At base of unit across Antioch-Davis zone.
		Knuepfer, 1977	Volcanic tuff	Middle Miocene	.18 to .66 km	-	-	Middle Miocene from 8 m.y.; initiation of faulting may be 4 m.y.	.022-.16	Tuff is near base of unit across Antioch fault.

Table 361.45-2 (continued)

Fault Reference Number	Fault Name/ Locality	Reference	Displacement Data from Reference: Offset Feature	Age of Feature	Amount of Offset	Age of Offset	Slip Rate mm/yr	Slip Rate Evaluation: Assumptions	Slip Rate mm/yr	Comments
	Antioch-Vaca and Davis/ Central California	Knuepfer, 1979 (personal communication)	Streams in alluvium	Streams same age as Quaternary alluvium	35 m	Since 120,000 to 500,000 yr	-	Author's age range	.07-.29	On Vaca fault (continuation of Antioch fault to north).
12	San Gregorio/ Central California	Silver, 1977	unstated	Miocene	100 km	80-90% in Miocene	-	-	-	Applies to the Miocene and not present tectonics.
				Post Miocene	10-20 km	Post Miocene	-	Maximum of 5 m.y.	2-4	Offset cited from Hamilton and Willingham, 1978; data not well defined. Not used.
		Graham, and Dickinson, 1977	Lithologic units	Post Early Miocene and probably post Late Miocene	115 km	-	-	5-15 m.y. for post Early through Late Miocene	7.7-23	Age not well defined. Not used.
	San Gregorio continued	Greene, 1977	Pioneer and Ascension faults	Middle Miocene 20 m.y.	110 km	20 m.y.	none	Author's offset and age	5.5	Correlation and age seem speculative. Not used.
		Weber and La Joie, 1979	Shoreline angles	Late Pleistocene (amino acid dates; unspecified)	unstated	Late Pleistocene	16 (ave.)	From author's graph; minimum and average values	9-16	Authors present slip rate graphs across 3 faults within zone.
13	Fairweather/ Alaska	Page, 1969	Vertical offset of ground surface	1000 yr	6 m vertical (36 - 42 m horizontal)	1000 yr	40	-	-	Page assumes 6:1 to 7:1 horizontal to vertical ratios to derive horizontal slip rate.
		Plafker, and others 1978	Three streams	940 ± 200 yr (C_{14} date)	55 m	940 ± 200 yr	48-58 (58 preferred)	Author's offset and age	58	Streams post-date the latest glacial advance.

Table 361.45-2 (continued)

Fault Reference Number	Fault Name/ Locality	Reference	Displacement Data from Reference: Offset Feature	Age of Feature	Amount of Offset	Age of Offset	Slip Rate mm/yr	Slip Rate Evaluation: Assumptions	Slip Rate mm/yr	Comments
	Fairweather/ Alaska continued	Plafker, and others 1978	lateral moraine	1300 ± 200 yr (C_{14} date)	50 m	1300 ± 200 yr	-	Author's offset and age	38	-
14	Motagua/ Guatemala	Schwartz and others, 1979	Stream terrace	10000 to 40000 yr	58.3 m	10000 to 40000 yr	1.5-6.0 (6.0 is most representative)	-	-	40000 year age of offset is not valid (Personnel Communication Schwartz 1979)
		Schwartz, 1979 (personal communication)	Stream terrace	10000 yr	58.3 m	10000 yr	6	-	-	Lower terrace yields date of 1300 years, suggests offset terrace is "quite young".
15	Bocono/ South America	Schubert and Sifontes, 1970	Glacial moraines	10,070 yr	66 m	10,070 yrs	6.6	-	-	Not maximum offset of moraines; not used.
		Dewey, 1972	unstated	5 m.y.	50 km	5 m.y.	10	-	-	Suggests plate motions are more E-W than N40°E parallel to the Bocono fault, thus motion may be right-reverse-oblique.
		Rod, 1956	Glacial moraines	Late Pleistocene	80-100 m	Late Pleistocene	-	Faulting continuous since end of Pleistocene 10,000 yr	8-10	-
		Woodward, Clyde and Associates, 1969	Glacial moraines	Late Pleistocene 10,000 yr	320 ft (97.5 m)	10,000 yr	9.75	-	-	Most accurate measurements of offsets; best estimate of rate. Authors measured numerous offsets.
16	Hope/ New Zealand	Scholz and others, 1973	unstated	-	20 km	Since Miocene	-	5 m.y. since Miocene	4	Author quotes Freund, 1971 and Clayton, 1966.

Table 361.45-2 (continued)

Fault Reference Number	Fault Name/ Locality	Reference	Displacement Data from Reference: Offset Feature	Age of Feature	Amount of Offset	Age of Offset	Slip Rate mm/yr	Slip Rate Evaluation: Assumptions	Slip Rate mm/yr	Comments
17	Awatere/ New Zealand	Lensen, 1973	River terraces	35000 to 40000 yr	330-350 ft (100-107m)	-	2.9	-	-	Age based on correlation of glacial deposits with C^{14} age deposits elsewhere. Author's rate from slip rate summary chart.
			River terraces	20,000	220-240 ft (67-73 m)	-	-	Author's age and 18000 yr for age of last glacial after Suggate and Lensen, 1973	3.4-4	Measured offsets may be low because of lateral erosion prior to downcutting. Highest rate estimate appears most reasonable.
18	West Wairarapa/ New Zealand	Lensen, 1973	Waiohine aggradation surface	20000 or 35000 yr	329-390 ft (100-120 m)	20000 or 35000 yr	2.8-3.1	Author's age and offset ranges; extending lower age to 18000 yr Suggate and Lenson, 1978)	2.9-6.6	Question as to which glacial advance created the aggradation surfaces. In cited reference, author prefers lower rate.
19	North Anatolian/ Middle East	Wellman, 1969	Lithologic units	unstated	350 km	Miocene	20	-	-	Offset from Pavoni, 1961, Cretaceous rocks, shown to be incorrect by later studies (Sengor, 1979). Not used.
		Canitez, 1976	Boundary between ancient crustal plates	Middle Miocene	85-95 km	15 m.y.	5-6	-	-	Data and rates from Seyman, 1968, based on reconstruction of depositional and metamorphic environments.
			unstated	unstated	unstated	.5 m.y.	>7	-	-	Data and "minimun rate" from Arpat and Saroglu, 1975
		Sengor, 1979	Pontide-Anatolide Suture	Budigalian	80-90 km	Budigalian to Pliocene	-	Author's offset and 5-15 m.y.	5.3-18	Age is poorly constrained but provides constraint to slip-rate range.
			unstated	unstated	50-100 km	unstated	-	-	-	Insufficient data, not used.

Table 361.45-2 (continued)

Fault Reference Number	Fault Name/ Locality	Reference	Displacement Data from Reference: Offset Feature	Age of Feature	Amount of Offset	Age of Offset	Slip Rate mm/yr	Slip Rate Evaluation: Assumptions	Slip Rate mm/yr	Comments
20	Sumatra/ Indonesia	Posavec and others, 1973	Streams	unstated	1 km	-	-	-	-	Other offsets such as lahars, lake terraces. No age data. Not used.
			Volcanic centers sources	unstated	130 km	-	-	-	-	Age reference is vague and undefined. Data not used.
		Tjia, 1970	unstated	unstated	unstated	4-5 m.y.	5-7	-	-	Substantiation of data is not presented.
		Tjia, 1973	Toba Ignimbrite	Less than 300,000 yrs	20 km	Less than 300,000 yrs	70	Author's age and offset	66.7	Only Quaternary data available.
21	Jordan-Dead Sea/ Middle East	Quennel, 1958	Geologic units dikes, faults	Pre Early Miocene	62 km	During Miocene and early Pliocene	-	-	-	Timing poorly defined; does not relate to present tectonic regime. Not used.
			Lisan "Delta"	Late Pleisto-cene	45 km	Late Pleisto-ocene	-	-	-	Offset delta deposits have been disproven (Zak and Freund, 1966).
		Zak and Freund, 1966	Geologic features	Precam-brian to Upper Cretaceous	100 km	Post-Cretaceous	-	-	-	Data from other authors; time spans older tectonic regime; not used.
			Alluvial fans, Lisan Marl	20000 yr	150 m	20000 yr	-	Author's age and offset	7.5	Age revised in Freund and others, 1970; other offsets in undated alluvium to 600 m. Not used.

Table 361.45-2 (continued)

Fault Reference Number	Fault Name/ Locality	Reference	Displacement Data from Reference: Offset Feature	Age of Feature	Amount of Offset	Age of Offset	Slip Rate mm/yr	Slip Rate Evaluation: Assumptions	Slip Rate mm/yr	Comments
	Jordan-Dead Sea/ Middle East	Freund and others, 1970	Lisan Marl	older than 23,000 yr	150m	older than 23000 yr	6.5	-	-	Absolute age from Neev and Emery, 1967.
	continued		Rock bodies	Miocene, Early Pliocene	40-45 km	7-12 m.y.	3.5-6	-	-	Offset feature not clearly defined; age limits speculative.
		Ben-Menahem and others 1976	-	-	-	-	6.5	-	-	Quotes Freund and others, 1970.
			-	-	-	3-4 m.y.	10	-	-	Quotes Girdler, 1958. No slip rate discussion in that reference.
22	Kopet-Dagh/ Middle East	Krymus and Lykov, 1969	unstated	Middle Pliocene	20 km	Middle to Late Pliocene	-	Author's offset data and 2.5 -4 m.y.	5-8	Older age is probably most appropriate.
				Middle Pleistocene	55-60 m	Middle Pleistocene	-	-	-	Age data are unconstrained. Data not used.
		Trifonov, V. G., 1971	unstated	500 yr recurrence intervals	1.78 m	1948 Ashkhabad earthquake	-	Assume 1.78 m per 500 year recurrence	3.6	Trifonov says the rate derived is comparable to geologic data.
			Kyarizes (water tunnels)	Holocene	3-8 m	1000-2000 yrs	-	1000 to 2000 yrs for largest offset during that time, 8 m.y.	4-8	Lesser offsets are the younger Kyarizes.
			Streams	Holocene	6-10 m	Holocene	-	-	-	Could be any time in Holocene, poor data. Data not used.
			Streams	Middle Pleistocene	55-60 m	Middle Pleistocene	-	-	-	Age data are unconstrained. Data not used.
		Trifonov, 1978	Walls of Palace in Nissa	unstated	0.3 m	-	-	-	-	Age not known. Data not used.

Table 361.45-2 (continued)

Fault Reference Number	Fault Name/ Locality	Reference	Displacement Data from Reference: Offset Feature	Age of Feature	Amount of Offset	Age of Offset	Slip Rate mm/yr	Slip Rate Evaluation: Assumptions	Slip Rate mm/yr	Comments
	Kopet-Dagh continued	Trifonov, 1978 continued	Wall of Chugundor Fortress	Middle ages	2.5 m	-	-	-	-	Age not known. Data not used.
			Kyarizes (water tunnels)	5th Century B.C. (2500 yr)	9 m	2500 yr	-	Author's age and offset	3.6	Appears to be best age and offset control.
			Streams	Holocene	8 m $\pm$	Holocene	-	-	-	Age not known.
			Streams	Holocene Late Pleistocene	55-60 m	Holocene	-	Author's offset; Holocene-Pleistocene boundary, 10000 yr	5.5-6.0	Offset streams may be older than 10000 yr
23	Dasht-e Bayaz	Tchalenko and Berberian, 1975	Black limestone	Cretaceous	4 km	-	-	-	-	Offset unconstrained; initiation of faulting age not known.
			Volcanics	Eocene	400 m	-	-	-	-	Same as above
			Stream channels	Holocene	8-24 m	-	-	Maximum age of Holocene of 10,000 yr; 24 m offset probably oldest	2.4	Rate is minimum based on assumption.

Notes: Absolute ages cited under "Assumptions" are from Van Eysinga, 1975, unless otherwise noted.

TABLE 361.45-3
SUMMARY OF SELECTED GEOLOGIC SLIP RATES AND MAXIMUM EARTHQUAKES FOR STRIKE-SLIP FAULTS

Reference Number	Faults	Maximum Earthquake M_S	Reasonable Data Range Slip Rate mm/yr	References	Selected Values Slip Rate (mm/yr)	Comments on Geologic Slip Rates **
1	San Andreas (Northern)	8.3, 1906	20	Herd, 1978	20	Generally accepted in northern California; selected value from Herd, 1978. Criterion 1.
2	San Andreas (Central)	8.25+, 1857*	34-41	Sieh, 1978	37	Based on C^{14} dates and trenching at Wallace Creek. Criterion 1.
3	San Andreas (Southern)	6.5, 1948	20-25	Walden, 1979 Sieh, 1979	25	Based on C^{14} dates on displaced Holocene deposits, Lost Lake area. Criterion 1.
4	a San Jacinto fault zone	7.1, 1940	4.4-12	Sharp, 1967, 1978, 1980 Morton, 1979	8.0	Based on offsets across main single trace of fault (Casa Loma Clark fault). Criterion 1.
	b Coyote Creek fault segment	6.7, 1968	1.8-5.0	Sharp, 1980	2	Based on offsets of Coyote Creek segment only. Criterion 1.
5	Elsinore	5.5-6, 1910*	1.8-7.1	Weber, 1977 Kennedy, 1977	2.3	Selected value based on the best documented offsets of 9-11 km. Criteria 2 and 3.
6	Whittier	4.2, 1976	.6-1.6	Heath, 1954 Yerkes, 1972 Lamar and others, 1973	1.2	Both offset and age data are not well controlled. Criterion 2.
7	Newport-Inglewood	6.3, 1933	.3-.68	Castle and Yerkes, 1976 Woodward-Clyde, 1979 Hill, 1971	.5	Offset and age data cited in literature, confirmed by WCC Special Investigation (Appendix B). Criterion 3.

TABLE 361.45-3

SUMMARY OF SELECTED GEOLOGIC SLIP RATES AND MAXIMUM EARTHQUAKES FOR STRIKE-SLIP FAULTS

Reference Number	Faults	Maximum Earthquake M_S	Reasonable Data Range Slip Rate mm/yr	References	Selected Values Slip Rate (mm/yr)	Comments on Geologic Slip Rates**
8	Calaveras-Paicines (south of Hayward branch)	5.9, 1979 6.6, 1911*	5-15	Herd, 1978 Prowell, 1974	12	Based on difference in slip rates between north and central portions of San Andreas, and limited geologic data. Criterion 2.
9	Calaveras - Sunol (north of Hayward branch)	5.3, 1861* 5.3, 1864*	6-8	Herd, 1978 Prowell, 1974	6	Herd apportions 50% of Calaveras-Pacines slip rate to Calveras-Sunol and Hayward faults respectively. Criterion 2.
10	Hayward	6.7, 1868*	5-7.5	Herd, 1978 Prowell, 1974	6	Herd apportions 50% of Calaveras-Pacines slip rate to Calaveras-Sunol and Hayward faults respectively. Criterion 2.
11	Antioch (and Vaca)	4.9, 1965	.022-.29	Knuepfer, 1977, 1979 Burke and Helley, 1973	.1	Data gives wide range because of limited data for ages of offsets. Criterion 2.
12	San Gregorio	5.5, 1969 6.1, 1926*	9-16	Weber and LaJoie (1979)	16	Weber and LaJoie state 16 mm/yr is best estimate. Criterion 1.
13	Fairweather	7.9, 1958	38-58	Plafker, and others 1978	58	Of the two rates determined from C^{14} ages, Plafker indicates 58 mm/yr is most accurate value. Criterion 1.
14	Motagua Guatemala	7.5, 1976	6	Schwartz and others, 1979 Schwartz, 1979 (personal communication)	6	Authors state that selected value is only reliable estimate. Criterion 1.

TABLE 361.45-3

SUMMARY OF SELECTED GEOLOGIC SLIP RATES AND MAXIMUM EARTHQUAKES FOR STRIKE-SLIP FAULTS

Reference Number	Faults	Maximum Earthquake M_S	Reasonable Data Range Slip Rate mm/yr	References	Selected Values Slip Rate (mm/yr)	Comments on Geologic Slip Rates**
15	Bocono Venezuela	8, 1812*	8-10	Rod, 1956 Dewey, 1972 Woodward, Clyde and Associates, 1969	9.75	Best data from Cluff and Hansen, 1969. Criterion 1.
16	Hope New Zealand	6.7, 1888*	4	Scholz, and others, 1973	4	Author does not present data to check. Criterion 1.
17	Awatere New Zealand	7.1, 1848*	2.9-4	Lensen, 1964 Lensen, 1958	4	Offset river terraces and aggredation surfaces. Criterion 3.
18	West Wairarapa New Zealand	7.6, 1855*	2.9-6.6	Lensen, 1973	4.8	Offset Waiohine aggredation surface. Criterion 3.
19	North Anatolian Turkey	7.9, 1939	5-18	Canitez, 1977	7	Based on total offset and various times of initiation of faulting. Criterion 1.
20	Sumatra	7.6, 1943	66.7-70	Tjia, 1973	67	Based on dated ignimbrite deposit. Criterion 1.
21	Jordan-Dead Sea	6.5, 1927	3.5-6.5	Ben Menahem and others, 1976	6.5	Selected value is based on dated Quaternary offset. Criterion 1.
22	Kopet-Dagh Iran-USSR	7.3, 1948	3.6-8	Krymus, and Lykov, 1969 Trifonov, 1971 Trifonov, 1978	3.6	Best age and offset data in Quaternary results in 3.6 mm/yr Criterion 2.
23	Dasht-E-Bayaz	7.2, 1968	2.4	Tohalenko and Berberian, 1975	2.4	Minimum rate based on maximum age for Holocene offset. Criterion 3.

* Pre-instrumental earthquake estimates

** Criterion described in Response to Question 361.45-e

Table 361.45-4

Estimated Slip Rates for Strike-Slip Faults
Which do Not Have Estimates for Large Historical Earthquakes

REFERENCE NUMBER	NAME (LOCATION)	GEOLOGIC SLIP RATE RANGE (mm/year)*	SELECTED SLIP RATE VALUE (mm/year)	REFERENCES(S) SELECTION CRITERIA**
24	Big Pine (California)	2.1 - 2.7	2.4	Crowell, 1962; Kahle, 1966. Criterion 3
25	Blue Cut (California)	1 - 2.5	1.8	Hope, 1969, Garfunkel, 1974. Criterion 3
26	Calico (California)	1.8 - 5	3.4	Garfunkel, 1974. Criterion 3
27	Collayami (California)	1	1	Hearn and others, 1976 Criterion 1
28	Garlock (California)	3.4 - 12.9	8	Dibblee, 1967, Carter, 1971 Criterion 1
29	Helendale (California)	2 - 4	3	Garfunkel, 1974. Criterion 3
30	Pinto Mountain (California)	2 - 4	3	Dibblee, 1967a, b, c Criterion 3
31	Sheep Hole - Ludlow (California)	3 - 3.75	3.4	Garfunkel, 1974. Criterion 3
32	Darvaz (Asia)	3.3 - 14	13	Trifonov, 1978 Criteria 1 and 3
33	Denali (Alaska)	11 - 35	35	Richter and Matson, 1971 Criteria 1 and 2
34	Lembang (W. Java)	13 - 83	30	Tjia, 1968, 1970. Criterion 1
35	Talemazar (Asia)	2.5	2.5	Wellman, 1965. Criterion 3
36	Totschunda (Alaska)	5 - 33	33	Richter and Matson, 1971 Criteria 1 and 2

* Includes faults with poor control of displacements and age of displacement but included for statistical analyses.

** Criteria described in response to question 361.45 e.

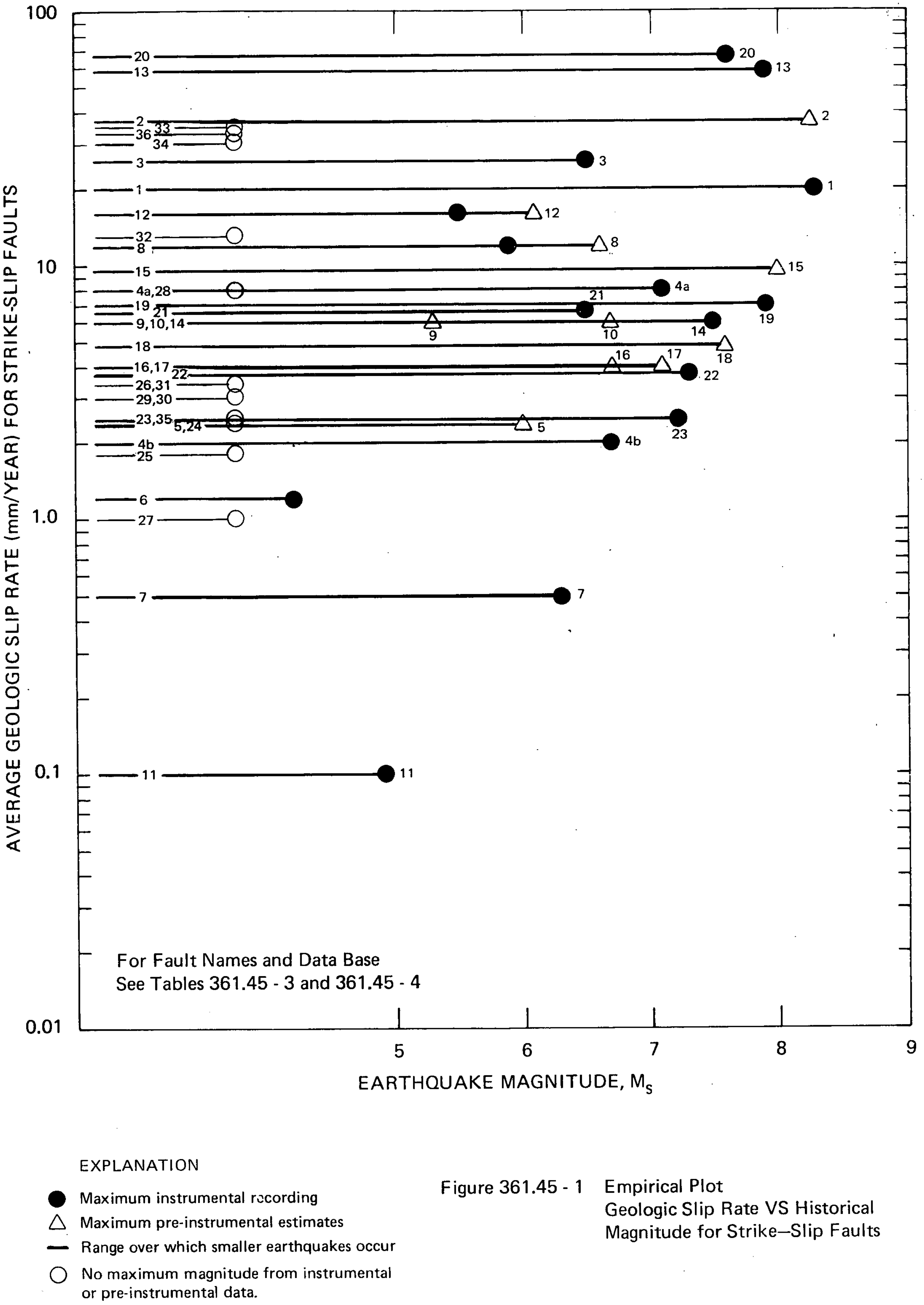

Figure 361.45 - 1 Empirical Plot
Geologic Slip Rate VS Historical
Magnitude for Strike–Slip Faults

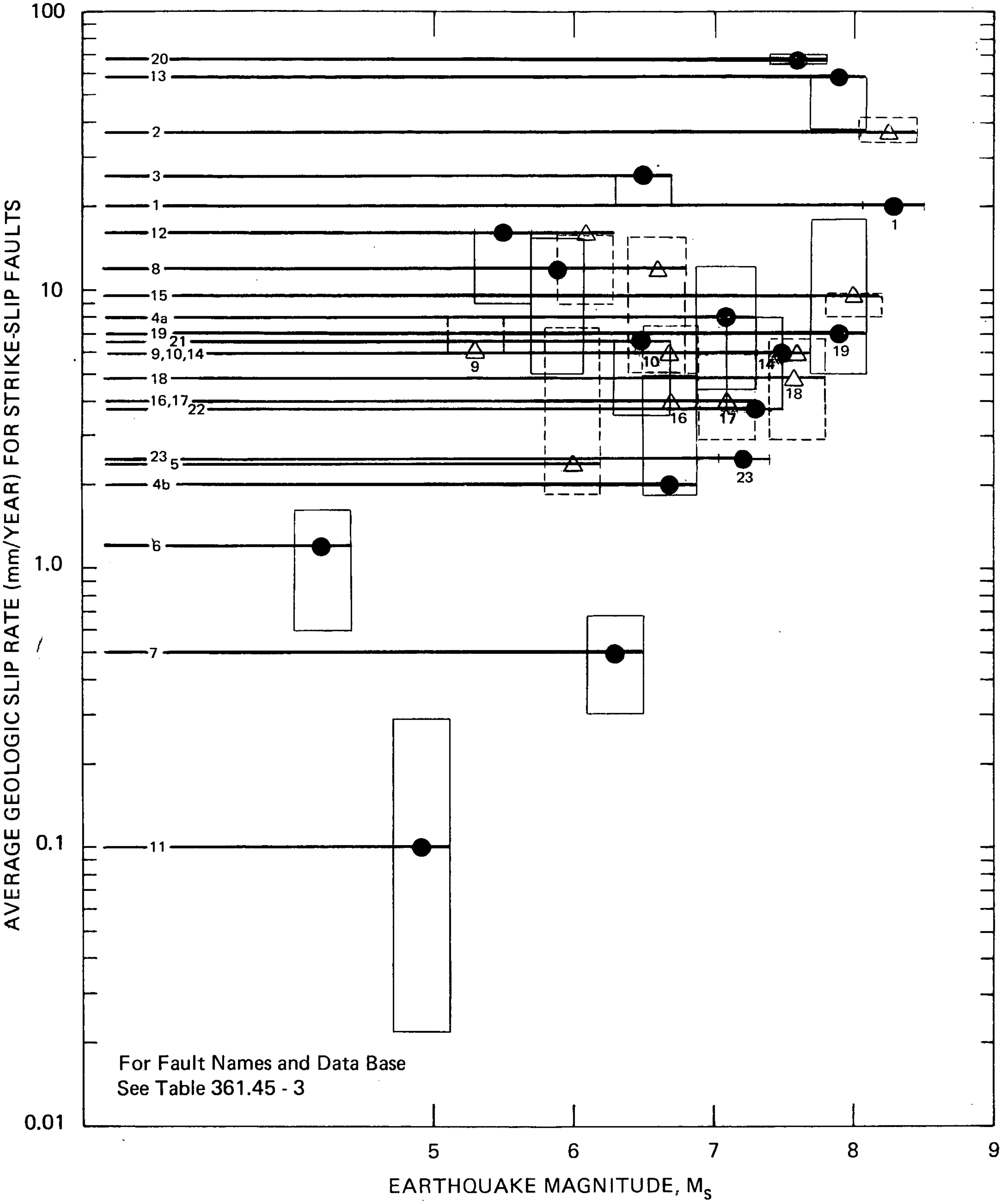

EXPLANATION

- ● Maximum instrumental recording
- △ Maximum pre-instrumental estimate
- — Range over which smaller earthquakes occur
- Box represents most likely range of geologic slip rate data and possible error range of ±0.2 in Magnitude calculation. Dashed box represents uncertainty of pre-instrumental estimates.

Figure 361.45 - 2 Data Range Analysis
Geologic Slip Rate VS Historical
Magnitude for Strike–Slip Faults

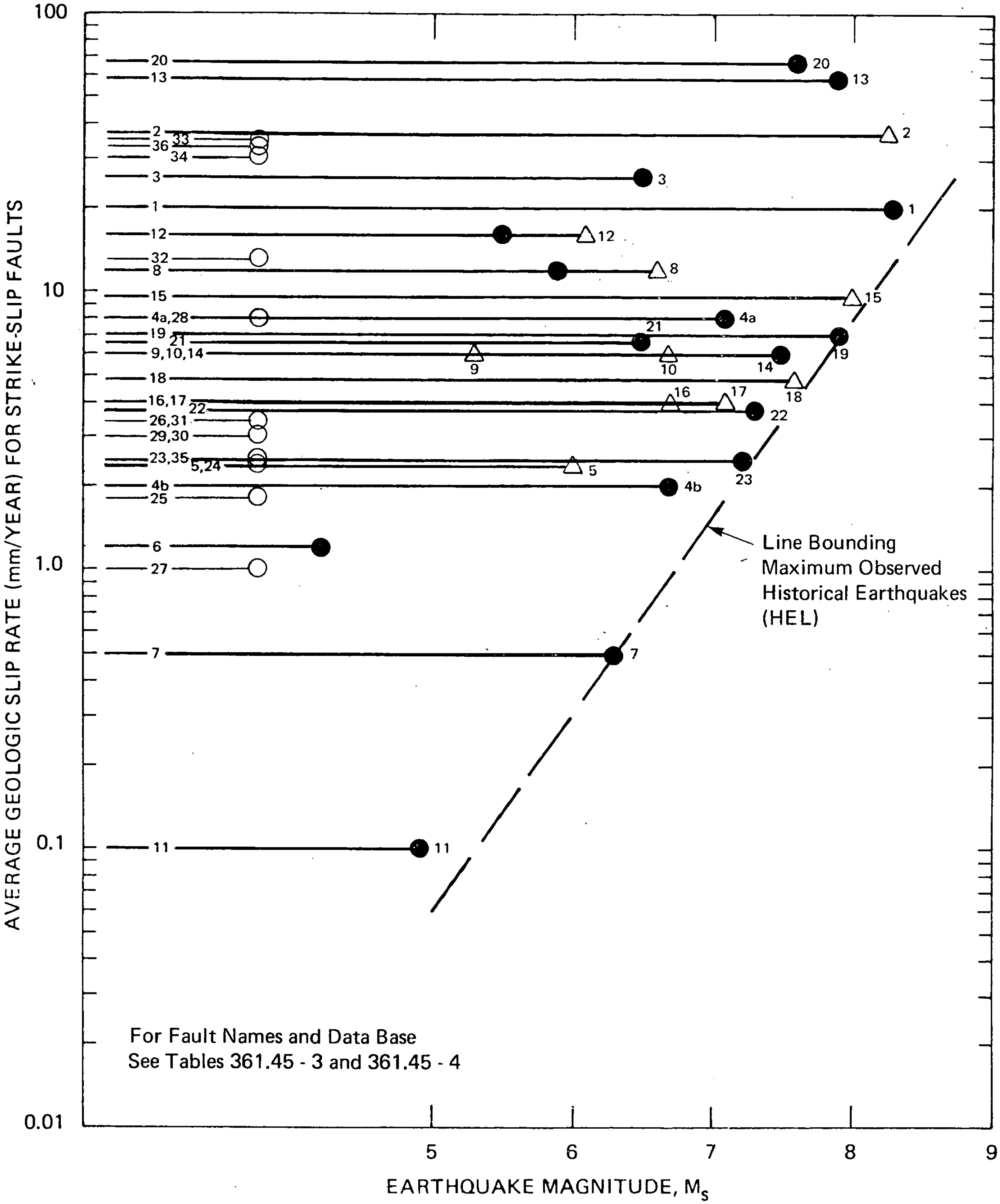

EXPLANATION

- ● Maximum instrumental recording
- △ Maximum pre-instrumental estimates
- — Range over which smaller earthquakes occur
- ○ No maximum magnitude from instrumental or pre-instrumental data.

Figure 361.45 - 3 Historical Earthquake Limit Geologic Slip Rate VS Historical Magnitude for Strike–Slip Faults

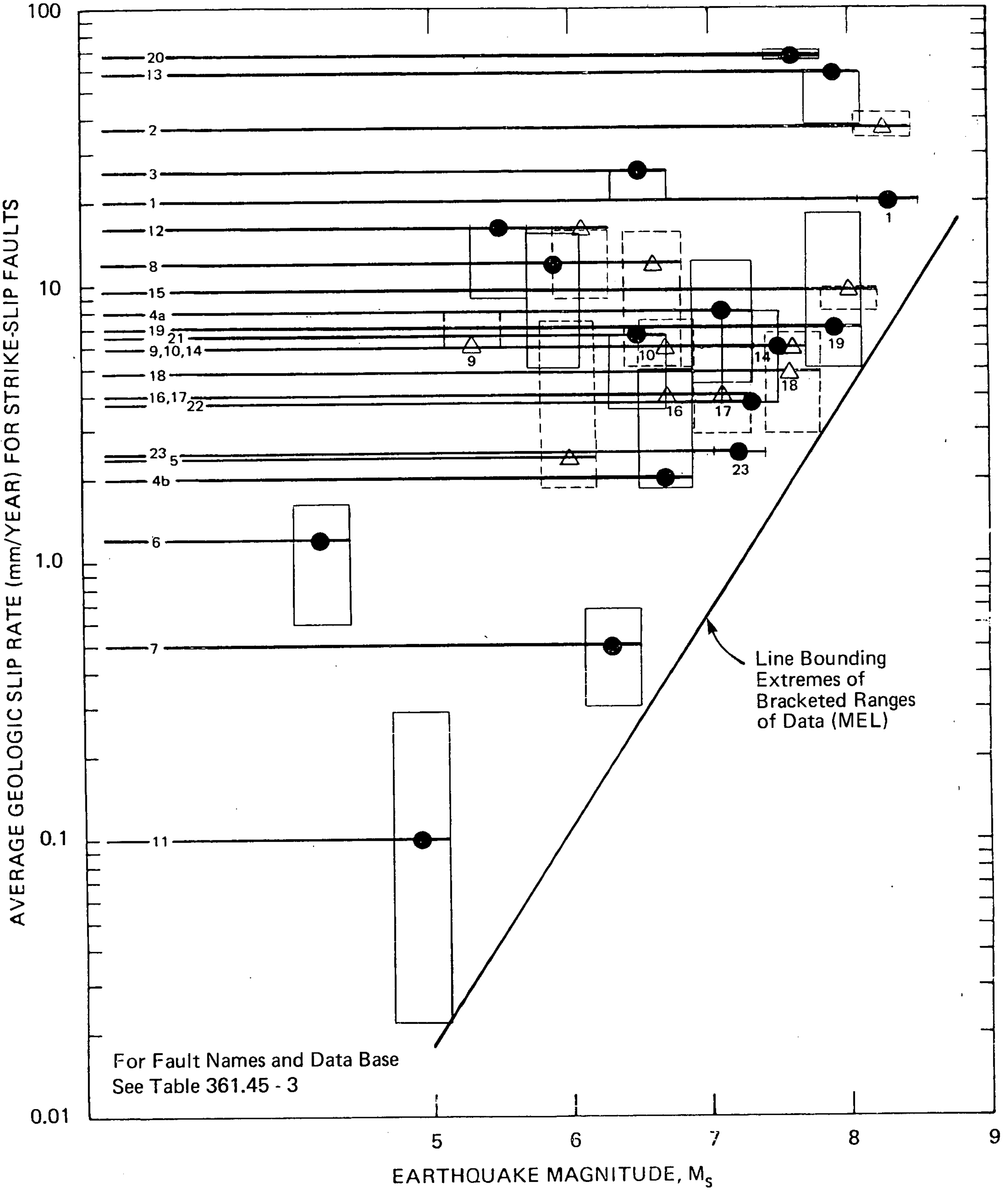

EXPLANATION

- Maximum instrumental recording
- △ Maximum pre-instrumental estimate
- — Range over which smaller earthquakes occur
- Box represents most likely range of geologic slip rate data and possible error range of ±0.2 in Magnitude calculation. Dashed box represents uncertainty of pre-instrumental estimates.

Figure 361.45 - 4 Maximum Earthquake Limit Geologic Slip Rate VS Historical Magnitude for Strike–Slip Faults

361.45 f

It is natural that the best known faults should be those with high slip rates. This leads to a bias towards high slip rates in the distribution of faults whose slip rates are known. For example, in California it is likely that all faults with high slip rates have been included in the data set, while there may be many low slip-rate faults that are not included because the slip rate is unknown or because the fault has not even been identified yet. A search for larger earthquakes, particularly in California, that might be associated with previously excluded strike-slip faults did not result in added data points for Figures 361.38-4. The inclusion of all of the possible low slip-rate faults would clearly increase the confidence in the slip-rate/maximum-magnitude relation at low slip rates; their omission (due to the lack of data) constitutes a conservative bias.

As discussed in response 361.51 and illustrated in Table 361.51-1, the number of faults in the median slip-rate group (3.5 to 17.5 mm/year) is almost identical to the number of faults in the lower slip-rate group (0.7 to 3.5 mm/year). The data base has been expanded, particularly for low slip-rate faults, as discussed in response 361.45 e. These added data provide substantial statistical support to the validity of the data base. The slip rate relation has not been altered by the expanded base, thus confidence in its significance is increased.

361.45 g

Two geologic time scales were used in analysis of published displacements and in preparation of the data base presented in Table G-1 of the WCC (June 1979) Report and in its revision, Table 361.45-2 of Response 361.45 e. For general use on a worldwide basis, geologic ages, periods, and epochs were correlated with absolute geologic time using the Geologic Time Table of Van Eysinga (1975). In the Los Angeles Basin, where detailed stratigraphic analysis of displaced facies relationships along the Newport-Inglewood Zone of Deformation (NIZD) was required, the absolute geologic ages of the Tertiary and Quaternary epochs were estimated from the upper Cenozoic Geologic Time and Stratigraphic Column for the Los Angeles Basin by Nardin and Henyey (1978). Stratigraphic correlations along the NIZD were based on the Summary of Operations volumes of the various oil fields by the California Division of Oil and Gas (referenced in Appendix B of the WCC June 1979 Report) and the Cenozoic Correlation Section Across the Los Angeles Basin, published by the American Association of Petroleum Geologists (Knapp and others, 1962).

In the study of the NIZD, absolute ages were assigned to the particular facies being correlated on the basis of their relative positions within the time-stratigraphic section (e.g., beginning of Upper Pliocene). To accommodate possible errors in this judgmental assignment of absolute ages, a ±10% error factor was added to the estimate and included in Table 1, Appendix B, of the WCC June 1979 Report. This 10% error factor is considered reasonable because: 1) the stratigraphic units and their relative geologic ages are well defined and; 2) the absolute age span of the sediments involved covers a relatively short and well-defined geologic time span. The error and uncertainty factors for each age determination are presented graphically in Figures B-7 and B-8 of Appendix B of the WCC (June 1979) Report, and in Figures 361.61-1 and 361.61-2 given in Response 361.61.

For review of geologic slip rates for strike-slip faults presented in Response 361.45 e, the range of possible ages are given in Table 361.45-2. Those ages and ranges of age are based on historic or radiometric dating techniques wherever reported in the literature. Other offsets are assigned ranges of ages to encompass the ages of offset features or the timing of commencement of faulting according to the literature. The range of possible ages was incorporated in estimating the range of geologic slip rates applicable to any one fault. These ranges are presented in Tables 361.45-2 and 361.45-3 and were used in preparation of the slip-rate/maximum-magnitude relationship graph, Figure 361.45-2 (see Response 361.45 e).

REFERENCES

Knapp, R. R., Traxler, J. D., Newbill, T. J., Laughlin, D. J., Stewart, R. D., Heath, E. G., Stark, H. E., Wissler, S. G., and Holman, W. H., 1962, Cenozoic correlation section across Los Angeles basin from Beverly Hills to Newport, California: American Association of Petroleum Geolgoists, Pacific Section.

Nardin, T. R., and Henyey, T. L., 1978, Pliocene-Pleistocene diastrophism of Santa Monica and San Pedro shelves, California continental borderland: American Association of Petroleum Geologists Bulletin, v. 62, no. 2, p. 247-272.

Van Eysinga, F. W. B., 1975, Geologic Time Table: Elsevier Scientific Publishing Company, Amsterdam, Third Edition, 1 sheet.

Woodward-Clyde Consultants, 1979, Report of the evaluation of maximum earthquake and site ground-motion parameters associated with the offshore zone of deformation, San Onofre nuclear generating station: Report for Southern California Edison Company, June, 241 p.

QUESTION 361.46

The new data of the Woodward-Clyde Consultants report included a thorough search of the conventional literature of major strike-slip faults and their recurrence intervals. Several additional sources of information should be included in order to provide a more accurate and up-to-date record for some of the major faults. These include:

a. Gerald Lensen, R. P. Suggate and H. Wellman for New Zealand and Iranian faults. Their data should be reviewed for the Alpine, Hope, Clarence, Awatere, East Wairarapa and West Wairarapa and possibly the Wellington (partly reverse-slip) faults. Many of these faults have new detailed strip maps of late Quaternary faulting. Some newer data may be available to scale the magnitudes of preinstrumental earthquakes (e.g. Clark and others, 1965, Figure 12); or more recent studies by the staff of the Geophysics Div. DSIR).

b. T. Matsuda, K. Nakamura and A. Sugimura of the University of Tokyo and the Earthquake Research Institute; and N. Ikebe of the Osaka City University. They have conducted a number of detailed studies that may supplement or modify the data provided for Tanna fault, or make it possible to add other strike slip faults of Japan (Atera, Median Tectonic Line, or others).

RESPONSE 361.46

361.46 a

The North and South Islands of New Zealand contains several different provinces of diverse tectonic characteristics, all part of the complex boundary between the Pacific and Indian Ocean lithospheric plates. The deformational styles, characteristics of the different provinces, vary and include: normal faulting, sinistral-oblique slip faulting, dextral-oblique slip faulting, and essentially pure dextral slip faulting. The area of essentially pure dextral deformation is a shear zone containing several late Quaternary faults. The shear zone is approximately 60 miles (97 km) wide, and extends from the northeast portion of the North Island, through Marlborough on the South Island, to the Alpine fault located in the western portion of the South Island, a distance of 400+ miles (644+ km) (Lensen, 1975; Suggate, 1963). The several dextral slip faults within the shear zone help transfer the strain developing along the plate boundary between Hikurangi trough, located east of the North Island, and the Alpine fault - Puysegur trench complex along the west coast of the South Island and offshore southwest of the South Island.

Suggate (1963) has identified four major dextral faults within the shear zone. The names of these faults are listed below; first with their North Island name followed by the name applied to their South Island continuations:

1. East Wairarapa - Hope fault,

2. West Wairarapa - Clarence fault,

3. Wellington - Awatere fault, and

4. Wairau fault - located on the South Island (the North Island continuation of the Wairau fault has not been clearly identified).

The available literature published by Gerald Lensen, R. R. Suggate, and M. Welman, and others (see reference list) has been reviewed for data on the above faults. Summing the maximum and minimum values in the range of slip-rates estimated for each of these faults within the dextral shear zone, based on information available in the literature, a total of 13 to 19 mm/year of dextral slip is being accomodated across the entire shear zone. This manner of accomodating the majority of the dextral strain across a region or zone in the earths crust by movements on individual dextral faults is very similar to what is occurring along the dextral slip faults included in the San Andreas fault system in southern California south of Cajon Pass.

The Awatere fault, West Wairarapa, and Hope faults have been added to the data base as documented in the response to question 361.45 e. The Awatere fault was the generating source for the 1848, estimated M_s 7.1 earthquake (Slemmons, 1977). The range of slip rates estimated from data presented by Lensen (1973, unpublished) are 2.9 to 4 mm/year for the Awatere fault and 3 to 3.7 mm/year for its North Island continuation (the Wellington fault). These slip-rate estimates are based on offset post glacial and late Pleistocene river terrace sequences. The West Wairarapa fault was the generating source of an 1855 earthquake estimated to be M_s 7.6. For a more detailed discussion of the West Wairarapa fault, refer to the response to question 361.44 c. Dextral slip rates for the West Wairarapa fault are estimated in the range of 3 to 6.6 mm/year based on offset river terraces and the Waiohine surface, which has been correlated with late Pleistocene glacial advances (Lensen, 1973).

The Hope fault had a reported 3 m right-lateral surface displacement during the estimated M 6.7 earthquake of 1888 (Scholz and others, 1973; Lensen, 1973). Based on displaced Miocene stratigraphy and structures, the slip rate for the Hope fault is estimated as 4 mm/year (Scholz and others, 1972; and Lensen, 1979 and 1973).

The Wairau fault has an estimated slip-rate range of 3 to 4 mm/year based on displaced post Glacial and late Pleistocene river terraces which cross the fault (Lensen, 1973). The Wairau fault and the Wellington fault have no large historic earthquakes reported and are not used in the data base. Both the Clarence fault, reported to be the South Island continuation of the West Wairarapa fault, and the East Wairarapa fault, reported to be the North Island continuation of the Hope fault, (Suggate, 1963) were not included in the data base because geologic evidence does not exist to evaluate slip rates and no associated major earthquakes are reported in the literature.

The Alpine fault is not included in the data base because it is not considered a pure dextral slip fault. The Alpine fault had predominate dextral slip during late Mesozoic and possibly early Tertiary time. However, during the Quaternary and presently, the Alpine fault has a major thrust component of displacement (Suggate, 1960, 1963; Lensen, 1968; Scholz and others, 1973). In addition, the Alpine fault has no associated major historic earthquakes.

Numerous strike-slip faults in the Middle East (Wellman, 1966 and 1969) have been evaluated for slip-rate values. Two of those faults (Dasht-e Bayez and Kopet Dagh) have had large earthquakes and sufficient data to calculate geologic slip rates (Tchalenko and Berberian, 1975; Trifonov, 1978). Those faults have been included in the slip rate-maximum magnitude data base as documented in the response to question 361.45 e.

REFERENCES

Clark R. H., Dibble, R. R., Fyfe, H. E., Lensen, G. J., and Suggate, R. P., 1965, Tectonic and earthquake risk zoning: Royal Society of New Zealand, General Transactions, v. 1, no. 10, p. 113-126.

Lensen, G. J., 1968, Analysis of progressive fault displacement during downcutting at the Branch River terraces South Island, New Zealand.

Lensen, G. J., 1970, Elastic and non-elastic surface deformation in New Zealand: Bulletin of the New Zealand Society of Earthquake Engineering, v. 3, no. 4, p. 131-142.

Lensen, G. J., 1973, Guidebook for excursion A-10, Tour Guide for International Association of Quaternary Research Christchurch, New Zealand, 76 p.

Lensen, G. J., 1975, Earth-deformation studies in New Zealand: Tectonophysics, v. 29, p. 541-551.

Scholz, C. H., Rynn, J. M., Weed, R. W., Frohlich, C., 1973, Detailed seismicity of the Alpine fault zone and Fiordland region, New Zealand: Geological Society of America Bulletin, v. 84, no. 10, p. 3279-3316.

Slemmons, D. B., 1977, State-of-the-art for assessing earthquake hazards in the United States, Report 6--Faults and earthquake magnitude: U. S. Army Corps of Engineers, Waterways Experiment Station, Soils and Pavement Laboratory,Miscellaneous Paper S-73-1, 129 p.

Suggate, R. P., 1960, The interpretation of progressive fault displacement of flights of terraces: New Zealand Journal of Geology and Geophysics, v. 3, August 1960.

Suggate, R. P., 1963, The Alpine fault: Transactions of the Royal Society of New Zealand, v. 2, no. 7, p. 105-129.

361.46 b

Literature references on faults of Japan have been reviewed by the Applicants. Specific discussions on the Tanna fault and various Japanese earthquakes are presented in responses to questions 361.44 e and 361.50, respectively. Discussion of the accuracy of the slip rate values on various faults is included in section 361.46 b-1 below. The differences in the mechanics of faulting between southern California and Japan has led the Applicants to remove the Tanna fault from the data base together with eliminating all Japanese faults from consideration. A description of the tectonics of Japan is presented in section 361.46 b-2 below. This tectonic description together with the comparisons between Japan and southern California presented in the response to question 361.47 forms the basis for the applicants' position.

361.46 b-1 Accuracy Completeness of Data for Specific Japanese Faults

Although the most recent reference to the Atera fault is the 1965 paper of Sugimura and Matsuda, it is known that a good deal of unpublished work has been done since then by Matsuda and other workers. The best summary of Okada's work on the Median Tectonic Line is given by Shimazaki (1976); this includes some data that Okada himself has not yet published. Okada and his students at Aichi Prefectural University, Nagoya, are still actively engaged in studies of this fault. Other studies of active strike-slip faults in progress at present include work on the Sunzu fault, Shizuoka prefecture by Tsuneishi of the Earthquake Research Institute, Tokyo University, and studies (including trenching) of the Yamaski fault, Hyogo prefecture by Ando of the Disaster Prevention Research Institute, Kyoto University. Three additional faults whose slip rates have been estimated are listed by Matsuda (1977, Table 2).

None of the faults mentioned above has experienced a large earthquake during the past one thousand years, and hence they cannot be used explicitly to define the maximum magnitude relation. Nevertheless, these faults are among the most active strike-slip faults in Japan, and play an important role in considerations of the mechanisms of strain accumulation and release in Japan, as discussed in section 361.46 b-2.

The best estimate of the slip rate of the Tanna fault has been discussed in the answer to question 261.44 e. This fault, together with four others listed in Matsuda (1977), Table 1, and referred to in question 261.50, have all had large earthquakes during the past one hundred years.

Among these five faults, the Tanna and Irozaki faults have slip rates which are based on precise age measurements, and are considered to be accurate within a factor of two or so (Matsuda, personal communication, December 1979). The slip rates of the remaining three faults are based on offsets of topographic features whose ages are not known precisely, or on an approximate ranking system based qualitatively on geomorphic appearance, and are considered to be accurate within an order of magnitude (Matsuda, personal communication, 1979).

361.46 b-2 Tectonics of Japan

Tectonic Setting

The Philippine Sea plate is colliding with the Eurasian plate in south central Honshu, and descending beneath southwest Japan along the Nankai trough (Figure 361.46-1). Active strike-slip faults on land in Japan are confined almost exclusively to southwest Japan, and appear to be associated almost exclusively with this plate interaction.

Thrust faults in southwest Japan tend to bound blocks, and are frequently associated with the margins of mountain ranges. The thrust and strike-slip faults are generally confined to separate regions.

Faulting in northeast Japan, in contrast with that in southwest Japan, consists primarily of thrust faulting parallel to the continental margin, and is interpreted as crustal shortening caused by the subduction of the Pacific plate beneath Japan.

The rate of energy release along the Nankai trough in great interplate thrust earthquakes is at least one order of magnitude greater than that released on land in intraplate earthquakes. The temporal and spatial coupling between interplate and intraplate earthquakes implies that intraplate earthquakes (including strike-slip earthquakes on land) are a secondary phenomenon caused by, but incidental to the primary process of plate covergence.

Recency and Rate of Strike-Slip Motion

Major strike-slip faults on land in Japan began to move in the early Quaternary (about one million years ago) and have continued to move in the same direction with an average rate of a few millimeters per year (Matsuda and Okada, 1968). The total displacements are not greater than 12 km. This small total amount of displacement and the youthfulness of the origin of their recent movement are characteristic of Japanese active faults, and are in contrast with the history of such major faults as the San Andreas fault in California or the Alpine fault in New Zealand (Matsuda, 1976). Vertical motion (as represented in the elevation of mountain ranges), which is presumably associated with thrust faulting, appears to have begun at about the same time and proceeded at the same rate as strike-slip motion.

Sense and Distribution of Faulting

In the focal region of earthquakes, the coseismic displacements are always consistent in sense with late Quaternary geologic crustal movements (Matsuda, 1976). Faults having lower long-term average-slip rates during the late Quaternary are much more numerous than those with higher slip rates (Matsuda, 1977). This is reflected in the fact that destructive earthquakes (M > 6.5) occur less frequently on major faults (i.e. those which are easily recognized and commonly shown on maps) than on minor faults. This means that seismic energy release is broadly distributed on many small faults, rather than being concentrated on a single fault or fault system. Since there is such a high density of active faults, recurrence intervals of earthquakes on a given fault are long, and lie in the range of several hundred to a thousand years (Matsuda, 1967). Japanese strike-slip earthquakes differ from all other strike-slip earthquakes in many ways. The most conspicuous differences are the large displacement relative to rupture length, the shortness of rupture length and overall fault length, the fact that commonly the entire mapped length of the fault breaks in one earthquake and that conjugate pairs of faults often rupture at the same time.

Izu Peninsula Faults

The Izu Peninsula constitutes the northwestern tip of the Philippine Sea plate which is colliding with the Eurasian plate in south central Honshu (Matsuda, 1978). The intraplate deformation of the Izu Peninsula may be understood as resulting from this collision (Somerville, 1978). The intraplate strike-slip faults in the Izu Peninsula have short lengths, lie within a few tens of kilometers of the plate boundary, and are mechanically closely coupled with interplate motions. For example, earthquakes on the Tanna fault occur within a few tens of years after great interplate oblique thrust earthquakes along the Sagami Trough, and may be regarded as releasing stress concentrated by interplate events (Somerville, 1978).

There have been three major strike-slip earthquakes in the Izu Peninsula this century (Table 1): the 1930 Kita-Izu earthquake on the Tanna fault (Abe, 1978); the Izu-Hanto earthquake on the Orozaki fault (Abe, 1978); and the 1978 Izu-Oshima earthquake on the Izu Oshima fault (Shimazaki and Somerville, 1979).

Southwest Japan

Plate subduction along the Nankai trough commenced recently (a few million years ago) and is characterized by frequent great interplate earthquakes (Ando, 1975; Kanamori, 1972a). It has been suggested that the oblique covergence between the Philippine Sea Plate and the Eurasian Plate along the Nankai trough causes a dragging force parallel to the plate boundary on the edge of the continental plate (Fitch, 1972; Shimazaki, 1976a). This should be the case since a component of horizontal shear stress is applied at the plate interface by the oblique covergence. This shear stress applied at the boundary of continental Japan is presumably responsible for the intraplate deformation of southwest Japan.

The primary geological structural lineament in southwest Japan is the Median Tectonic Line - "MTL" (Okada, 1970) which extends the entire length of southwest Japan and lies roughly parallel to the Nankai trough.

The western part of the MTL (on the island of Shikoku) has had a slip rate of between 5-10 mm/year during the late Quaternary (Okada, 1973), and appears to accomodate most of the shear applied at the plate boundary. The absence of earthquake activity in historical time (Shimazaki, 1976a) or fault creep at the present time (Okada, 1970) on this segment of the MTL implies that it is storing a large amount of strain energy (Shimazaki, 1976a).

The eastern part of the MTL is geologically inactive. However, intraplate seismicity has been high on a well-developed mozaic-like conjugate system of strike-slip faults and adjacent thrust faults which lie northwest of the MTL. It has been shown (Shimazaki, 1976b) that this intraplate activity is strongly correlated in time with the occurrence of great interplate earthquakes on the Nankai trough. During the past one hundred years, 24% of all intraplate earthquakes in southwest Japan have preceded great interplate events by less than 5 years; 69% followed great interplate events by less than 10 years. This suggests that the intermittent underthrusting drag exerted by the Philippine Sea Plate controls the intraplate seismicity, which partly accommodates the relative plate motion as internal deformation (Shimazaki, 1976a).

Approximately ten intraplate events with magnitude larger than 6.3 are associated with each great interplate event. This suggests that the adjustment of the continental block to the drag force applied at the trench occurs in an incoherent manner rather than on a single continuous fault (as may be the case on the MTL in Shiloku). This incoherent response is reflected in the short length and high density of faults which form the mozaic-like conjugate system.

The major strike-slip seismicity of the eastern part of southwest Japan during the past one hundred years (Table 361.50-1) includes the 1891 (Nobi) Mino-Owari earthquake on the Neo-Dani fault (Ando and Mikumo, 1974); the 1927 Tango earthquake on the Gomura and Yamada faults (Kanamori, 1973); the 1943 Tottori earthquake (Kanamori, 1972b); the 1948 Fukui earthquake (Kanamori, 1973); the 1963 Wakasa Bay earthquake (Abe, 1974); and the 1969 Gifu earthquake (Mikumo, 1973). The Atera fault has one of the highest slip rates among faults in this region (Sugimura and Matsuda, 1965) but has not ruptured in the past one hundred years.

REFERENCES

Abe, K., 1974, Fault parameters determined by near- and far-field data--The Wakasa Bay earthquake of March 26, 1963: Seismological Society of America Bulletin 64, lp. 1369-1382.

Abe, K., 1978, Dislocations, source and dimensions and stresses associated with earthquakes in the Izu Peninsula, Japan: Journal of the Physics of the Earth, v. 26, p. 253-274.

Ando, M., 1975, Source mechanism and tectonic significance of historical earthquakes along the Nankai trough, Japan: Tectonophysics, v. 27, p. 119-140.

Ando, M., and Mikumo, T., 1974, A fault-origin model of the Mino-Owari earthquake of 1891: Spring Meeting Seismological Society Japan, Proceedings, 1974, p. 25.

Boore, D., and Dunbar, W., 1977, Effect of the free surface on calculated stress drops: Seismological Society of America Bulletin 67, p. 1661-1664.

Fitch, J. J., 1972, Plate convergence, transcurrent faults, and internal deformation adjacent to Southeast Asia and the western Pacific: Journal of Geophysical Research, v. 77, p. 4432-4460.

Kanamori, H., 1971, Faulting of the great Kanto earthquake of 1923 as revealed by seismological data: Earthquake Research Institute Bulletin, Tokyo University, v. 49, p. 13-18.

Kanamori, H., 1972a, Tectonic implications of the 1944 Tonankai and the 1946 Nandaido earthquakes: Physics of the Earth and Planetary Interiors, v. 5, p. 129-139.

Kanamori, H., 1972b, Determination of effective tectonic stress associated with earthquake faulting--the Tottori earthquake of 1943: Phyics of the Earth and Planetory Interiors, v. 5, p. 426-434.

Kanamori, H., 1973, Mode of strain release associated with major earthquakes in Japan in Donath and others, ed., Annual Review of Earthquake and Planetary Sciences, v. 2.

Matsuda, T., 1976, Empirical rules on sense and rate of recent crustal movements: Journal of Geodetic Society Japan, v. 22, p. 252-263.

Matsuda, T., 1977, Estimation of future destructive earthquakes from active faults on land in Japan: Journal of the Physics of the Earth, v. 25, supplement, p. S251-S260.

Matsuda, T., 1978, Collision of the Izu-Bouin arc with central Houshu-Cenozoic tectonics of the Fossa Magna: Journal of the Physics of the Earth, supplement, p. S409-S421.

Matsuda, T., and Okada, A., 1968, Studies of active faults in Japan: Quaternary Research (Daiyonki Kenkyu), v. 7, p. 188-199.

Matsuda, T., Okada, A., and Huzita, K., 1976, Distribution map and catalogue of active faults in Japan: Mem. Geological Society of Japan, v. 12, p. 185-198.

Mikumo, T., 1973, Faulting mechanism of the Gifu earthquake of September 9, 1969, and some related problems: Journal of Physics of the Earth, v. 21, p. 191-212.

Okada, A., 1970, Fault topography and rate of faulting along the Median Tectonic Line in the drainage basin of the river Yoshino, northeastern Shikoku, Japan: Geographical Review of Japan, v. 43, p. 1-21.

Okada, A., 1973, Quaternary faulting of the Median Tectonic Line in the central part of Shikoku: Geographical Review of Japan, v. 46, p. 295-322.

Shimazaki, K., 1976a, Intraplate seismicity gap along the Median Tectonic Line and oblique plate convergence in southwest Japan: Tectonophysics, v. 31, p. 139-156.

Shimazaki, K., 1976b, Intraplate seismicity and interplate earthquakes--historical activity in southwest Japan: Tectonophysics, v. 33, p. 33-42.

Shimazaki, K., and Somerville, P., 1979, Static and dynamic parameters of the Izu-Oshima earthquake of January 14, 1978: Seismological Society of America Bulletin, v. 69, p. 1343-1378.

Somerville, P., 1978, The accommodation of plate collision by deformation in the Izu block, Japan: Earthquake Research Institute Bulletin, Tokyo University, v. 53, p. 629-648.

Sugimura, A., and Matsuda, T., 1965, Atera fault and its displacement vectors: Geological Society of America Bulletin 76, p. 509-522.

TABLE 361.46-1

SLIP RATES AND EARTHQUAKE FAULT PARAMETERS OF STRIKE-SLIP FAULTS IN JAPAN *

FAULT	REGION	SLIP-RATE (1) (mm/yr)	LARGEST EARTHQUAKE Year	M (JMA)	Mo ($x10^{26}$ dyne cm)	D (M)	L (Km)	W (Km)	$\Delta\sigma$ (bars)	REF
Neo-dani	Nobi (Mino-Owari)	1 - 5	1891	7.9	12.5	4	80	13	61	(2)
Gomura & Yamada	Tango	.05 - .1	1927	7.75	4.6	3	35	13	53	(3)
Tanna	Kita-Izu	1.5 - 2.5	1930	7.0	2.0	3	22	12	63	(4)
Shikano & Yoshioka	Tottori	.05 - .1	1943	7.4	3.6	2.5	33	13	44	(5)
--	Fukui	--	1948	7.3	3.3	2.5	30	13	46	(3)
--	Wakasa Bay	--	1963	6.9	0.33	0.6	20	8	17	(6)
--	Gifu	--	1969	6.6	0.35	0.64	18	10	16	(7)
Irozaki	Izu-Hanto	.5 - 1	1974	6.9	0.59	1.2	18	8	36	(4)
Izu-Oshima	Izu-Oshima	--	1978	6.8	1.1	1.85	17	10	50	(8)
Median Tectonic Line	Shikoku	5 - 10	--							
Atera	Gifu	3 - 5	--							

* M = JMA Magnitude, Mo = moment, D = average displacement determined seismologically, L = rupture length, W = depth range of faulting, $\Delta\sigma$ = stress drop, calculated using the results of Boore and Dunbar, 1977, and assuming that the shear modulus is 3 x 10" dyne/cm^2. References: (1) Matsuda, 1977. (2) Ando and Mikumo, 1974. (3) Kanamori, 1973. (4) Abe, 1978. (5) Kanamori, 1972. (6) Abe, 1974. (7) Mikumo, 1973. (8) Shimazaki and Somerville, 1979.

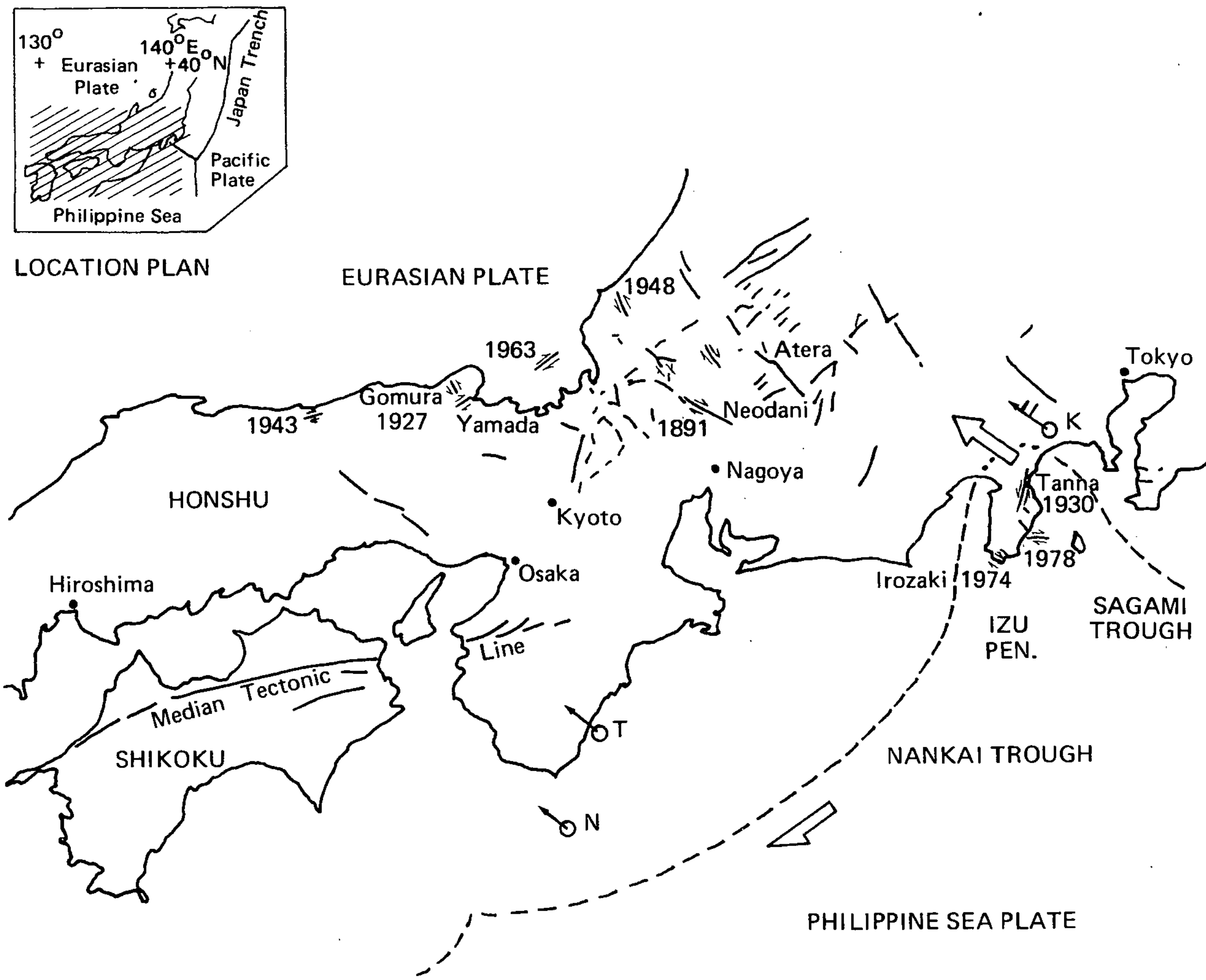

LEGEND

Solid lines indicate active strike-slip faults (Matsuda, Okada and Huzita, 1976). Faults that have experienced large earthquakes in the past 100 years (Table 361.50 - 1) are shown with the year of occurence and sense of slip. Major faults and named faults that have ruptured are labeled. Open circles with arrows show the epicenters and horizontal projection of relative slip of the Philippine Sea plate during the (K) Kanto earthquake of 1944 and the (N) Nankaido earthquake of 1946 (Kanamori, 1972). The Eurasian Plate is suggested (after Shimazaki, 1976a) as pushed at the northern neck of the Izu Peninsula (open arrow) and dragged southwestward along the Nankai trough by the Philippine Sea plate (open half arrow).

Fig. 361.46 - 1 The Tectonic Setting of Japan

QUESTION 361.47

The relations shown by Figures 6 and 7 of the Woodward-Clyde Consultants report may not hold for dip-slip faults. The Pleasant Valley earthquake of 7.7 magnitude as listed by Gutenberg and Richter (1954) has a low normal-slip rate. This may also be true for reverse-slip faults. Provide a model to justify not including dip-slip faults.

RESPONSE 361.47

The relationships shown by Figures 6 and 7 of the Woodward-Clyde Consultants June 1979 report and by Figures 361.38-4 and 361.38-5 of these responses were constructed specifically for strike-slip faults in Southern California and for strike-slip faults in other similar tectonic environments. Criteria for data selection are given in response 361.45e. Analysis was carefully limited to these faults because fundamental differences in fault behavior appear to exist between this group of faults and both dip-slip faults and strike-slip faults in different tectonic environments. The current state of understanding of fault behavior precludes any simple quantitative model encompassing the differences between dip-slip and strike-slip faults. However, lines a conceptual model reflecting differences in tectonic environments is discussed below. Specific examples of these differences are presented, along with a general discussion of some observational and conceptual distinctions between dip-slip and strike-slip faults.

Abundant data are available on normal faults and their tectonic setting in the Basin and Range province of Nevada and surrounding areas (Slemmons, 1967; Smith and Eaton, 1978; Stewart, 1978). Individual faults having the potential of releasing magnitude 7 or greater earthquakes within the Basin and Range province appear to have long term (Pleistocene or longer) slip rates often less than 1 mm/year, although higher rates may characterize faults located at the boundaries of the province (Thompson and Burke, 1973; Slemmons and others, 1979). In the short-term, hundreds to thousands of years, specific faults such as the Pleasant Valley fault and the Dixie Valley fault have experienced a higher rate of seismic activity. Slemmons (1967) suggests that the historical fault rupture pattern in the Basin and Range is not typical of long-term activity, and that the locus of fault activity will likely shift from the present zones to others that now appear less active. Thus, the general mode of fault activity within the Basin and Range province appears to involve long-term cycles of adjustments among the various blocks of the Basin and Range, with the regional extension distributed more evenly across the province than is true of historical activity.

The Basin and Range is largely in isostatic balance, with regional isostatic anomalies averaging no more than 10 mgals (Eaton and others, 1978). The isostatic balance means that a shift of mass by crustal faulting in one location is regionaly accommodated by compensating shifts elsewhere producing cycles of activity and inactivity as suggested by Slemmons (1977). This is consistent with the argument that long-term activity across the Basin and Range is broadly similar in magnitude throughout the province. Thus, faults in the Basin and Range province appear to respond to regionally consistent long-term stress release, resulting in low long-term slip rates but locally high short-term activity.

Extensive data also are available on strike-slip and dip-slip faults in Japan. Many of these data are discussed in

Responses 361.46b and 361.50. These active faults in Japan are numerous, widely distributed, and complex; they represent the horizontal and vertical movements of fault blocks that overlie the subduction zone between the Eurasian plate and the Philippine and Pacific plates (Matsuda and others, 1976).

Recent studies of seismic activity in Japan have suggested that the occurrence of shallow intraplate earthquakes is temporally and spatially coupled to the stress and deformation associated with great subduction zone earthquakes (Shimazaki, 1976b, 1978; Somerville, 1978). The alternate loading and unloading of the interplate boundary during cycles of stress buildup and release in great subduction zone earthquakes is thought to produce regionally varying stresses that cause dependent behavior of short strike-slip and reverse faults. Total displacement and rate of slip on a particular fault appear to be controlled by both the local structural relationships and the subduction loading cycle. Matsuda (1977) notes low slip-rate faults (both strike-slip and dip-slip) with historic earthquakes of magnitude 7+. Thus, intraplate fault activity in Japan appears to have a close spatial and temporal relation to the compressive and shear stress regime of great subduction zone events; stress release during earthquakes on these faults appears to be dependent on the occurrence of major interplate events.

The Basin and Range and the Japanese intraplate tectonic environments are fundamentally different in fault geometry and regional stress from the Southern California tectonic environment described in the Woodward-Clyde Consultants June 1979 report. The behavior of faults in these environments also is fundamentally different, as described above. Thus, the fault behavior in the Basin and Range province and in Japan is not comparable to fault behavior in California and the data from these different areas should not be combined.

Different relationships exist for the observed data on historical rupture-length versus magnitude and displacement versus magnitude for dip-slip and strike-slip faults. Bonilla and Buchanan (1970) and Slemmons (1977) have recognized these differences and have tried to show them by plotting different regression lines for the various kinds of faults. Similarly, different relationships exist for dip-slip and strike-slip faults with respect to slip-rate versus magnitude. Large earthquakes having long recurrence intervals have been observed on several dip-slip faults having relatively low slip rates (including Pleasant Valley). If it were argued that dip-slip and strike-slip faults are indeed comparable, then it follows that at least a few strike-slip faults should have exhibited maximum historic earthquake magnitude values that are comparable to the values for dip-slip faults with similar slip rates. No such strike-slip faults have been observed in tectonic environments similar to California. Thus, the observed data suggest that the behavior of dip-slip and strike-slip faults is different and, therefore, it is inappropriate to combine these data.

The substantial observational differences between dip-slip and strike-slip faults suggest that fundamental mechanical differences exist among the various types of faults. Among others, these differences include: the relative geometric orientations of the plane of faulting, the free surface, and the maximum compressive stress; the mechanics of the fault rupture process; and physical limits to cumulative displacement across a fault. There are substantial differences in the geologic and tectonic regimes as discussed above. The deformation and resulting faults have distinct differences in Japan, Basin and Range, and in Southern California. The data selected in the slip-rate analysis represents faults world-wide that appear to be deforming in a similar manner to strike-slip faults in Southern California.

REFERENCES

Bonilla, M. G., and Buchanan, J. M., Interim Report on Worldwide Historic Surface Faulting: U. S. Geological Survey Open-File Report,

Eaton, G. P., Wahl, R. R., Prostka, H. J., Mabey, D. R., and Kleinkopf, B. D., 1978, Regional gravity and tectonic patterns--their relation to late Cenozoic epeirogeny and lateral spreading in the western Cordillera, in Smith, R. B., and Eaton, G. P., Cenozoic Tectonics and Regional Geophysics of the Western Cordillera: Geological Society of America, Memoir 152, p. 51-92.

Matsuda, T., Okada, A., and Huzita, K., 1976, Distribution map and catalogue of active faults in Japan: Geological Society of Japan, Memoir, v. 12, p. 185-198.

Shimazaki, K., 1976, Intraplate seismicity and interplate earthquakes--historical activity in southwest Japan: Tectonophysics, v. 33, p. 33-42.

Shimazaki, K., 1978, Correlation between intraplate seismicity and interplate earthquakes in Tohoku, northeast Japan: Seismological Society of America Bulletin, v. 68, no. 1, p. 181-192.

Slemmons, D. B., 1967, Pliocene and Quaternary crustal movements of the Basin-and Range Province, U. S. A.: Osaka City University Journal of Geoscience, v. 10, p. 91-103.

Slemmons, D. B., 1977, State-of-the-art for assessing earthquake hazards in the United States, Report 6--Faults and earthquake magntiude: U. S. Army Corps of Engineers Miscellaneous Paper S-73-1, 129 p.

Slemmons, D. B., Van Worme, E. J., Bell, S. L., Silberman, 1979, Recent crustal movements in the Sierra Nevada--Walker Lane region of California-Nevada, Part 1, rate and style of deformation: Tectonophysics, v. 52, p. 561-570.

Smith, R. B., and Eaton, G. P., 1978, Cenozoic Tectonics and Regional Geophysics of Western Cordillera: Geological Society of America Memoir 152, p 388.

Somerville, P., 1978, The accommodation of plate collision by deformation in the Izu block, Japan: Earthquake Reseach Institute Bulletin, Tokyo University, v. 53, p. 629-648.

Woodward-Clyde Consultants, 1979, Report of the evaluation of maximum earthquake and site ground motion parameters associated with the offshore zone of deformation, San Onofre nuclear generating station: Report for Southern California Edison Company, June, 241 p.

QUESTION 361.48

Explain why certain of the data in Table G-1 for seemingly applicable faults, i. e., Bocono, Wairarapa, Magellanes, Kopet-Dagh, Hope, and Dasht-e Bayas, are not included in Figure 7 of the Woodward-Clyde report. Provide the criteria which excluded these faults.

RESPONSE 361.48

Bocono Fault

The Bocono fault was included in Figure 7 of the Woodward-Clyde June 1979 report; however, because low confidence was given to the magnitude estimate of the 1812 earthquake, that earthquake was not plotted in Figure 7. Following a review of the basic data presented in the WCC June 1979 report, however, this estimate was added to the data base in order to see how it might possibly affect the slip-rate/maximum-magnitude relationship. The Bocono fault is discussed in more detail in response 361.44 b.

West Wairarapa Fault

The West Wairarapa fault has been included in the revised slip-rate/maximum-magnitude data base documented in response 361.45 e. A detailed discussion of the West Wairarapa fault and of the 1855 earthquake are presented in response 361.44 c.

Magellanes Fault

Magellanes fault of Tierra del Fuego is described by Winslow (1976) as showing abundant evidence of contemporary displacement, such as 6-meter-high fresh scarps, sag ponds, truncated streams and drainages, and offset moraines and lake terraces. However, the only measured offset is reported to be up to 100 km of left-slip that is perhaps as young as Miocene (Winslow, 1976, and Winslow personal communication, 1978). Since the data available are insufficient to estimate both the age of initiation of faulting and, consequently, the slip rate, the fault could not be included in the analysis.

Kopet-Dagh Fault

The Kopet-Dagh fault zone is now included within the data set used in the revised slip-rate/maximum-magnitude data base documented in response 361.45 e. A detailed discussion of the Kopet-Dagh data is presented in response 361.44 f.

Hope Fault

The Hope fault had a reported 3 m of right-lateral surface displacement during the estimated M 6.7 earthquake of 1888 (Scholz and others, 1973). The slip rate for the Hope fault is about 4 mm/year based on displaced Miocene stratigraphy (Scholz and others, 1973). Although the slip rate is not well constrained, it is included in the revised slip-rate/maximum-magnitude data base documented in response 361.45 e. The Hope fault is also discussed in response 361.46 a.

Dasht-e Bayaz

The Dasht-e Bayaz fault in Iran generated the 7.2 magnitude earthquake of August 31, 1968. The displacements suggest both vertical and horizontal components of slip; however, the structure of the zone is interpreted as a simple shear type of deformation (Tchalenko and Ambraseys, 1970). Data on total cumulative displacement are described as conjectural (Tchalenko and Berberian, 1975) and cannot be used to evaluate slip rate. The Quaternary record, however, does indicate left lateral offsets of streams from 8 to 24 meters. Tchalenko and Berberian (1975) state that the stream offsets occurred during the Holocene Epoch. Assuming that the largest displacement initiated at the beginning of Holocene, a slip rate has been estimated using 10,000 years for 24 meters of offset. The applicant has included the Dasht-e Bayaz fault slip rate of 2.4 mm/year in the revised slip-rate/maximum-magnitude data base documented in response 361.45 e.

Walker Lane

The Walker Lane was presented in Figures 6 and 7 of the WCC June 1979 report without an associated earthquake. The 1932 Cedar Mountain earthquake occurred adjacent to and partly within the northwest-trending Walker Lane but the individual surface ruptures associated with the earthquake trended in a north-northeast direction forming a discontinuous zone 4 to 9 miles wide and 38 miles long, trending north-northwest (Gianella and Callahan, 1934). The en echelon pattern of the ruptures is suggestive of horizontal right-lateral shear (Gianella and Callahan, 1934). Shawe (1965) associated the ruptures from the Cedar Mountain earthquake with an arcuate series of northeasterly historic earthquake ruptures termed the Churchill arc; the arc extends from the Dixie Valley-Fairview Peak and Pleasant Valley areas to the Walker Lane. Along the arc, the style of faulting changes from the typical Basin and Range dip-slip faulting in the northeast to predominantly strike-slip at the Walker Lane. The surface ruptures of the Cedar Mountain earthquake included both dip-slip and strike-slip faulting. A preliminary focal mechanism solution is consistent with normal faulting on a plane striking north-south and dipping steeply to the east but is inconsistent with strike-slip faulting. Because definitive data on Walker Lane are lacking in published literature, with respect to the Cedar Mountain earthquake surface ruptures and the possible association of a dip-slip faulting mechanism, the Cedar Mountain earthquake was not assigned to the Walker Lane in the WCC 1979 report.

Five factors led to the exclusion of the Walker Lane in the data base for Figures 361.45-1 and 361.45-2. First, the slip rate was based on offsets of units which are 22 million years old. No other data point on the slip-rate/magnitude graph is based on times of fault initiation as old as the Walker Lane data. Second, the slip rate during the past 22 million years may not be representative of the Quaternary or Holocene activity on the Walker Lane. And third, Slemmons and others (1979) indicate that current rates of slip have not been established but may be higher than the rate based on the offset cited by Hardyman (1975). Fourth, after discussions with Hardyman (1979) and on the basis of Hardyman (1975), the Walker Lane appears to be associated with strike-slip faulting as well as with dip-slip faulting, and it is strongly complicated by the possible presence of large detachment faults at depth which affect the surface faulting and width of the zone at the surface. Fifth, Hardyman (personal communication, 1979) believes that much larger displacements across the zone exist but that mapping is not yet sufficient to define these larger offsets.

REFERENCES

Clark, R. H., Dibble, R. R., Fyfe, H. E., Lensen, G. J., and Suggate, R. P., 1965, Tectonic and earthquake risk zoning: Royal Society of New Zealand, General Transactions, v. 1, no. 10, p. 113-126.

Richter, C. F., 1958, Elementary Seismology: W. H. Freeman, San Francisco and London, 768 p.

Scholz, C. H., Rynn, J. M., Weed, R. W., Frohlich, C., 1973, Detailed seismicity of the Alpine fault zone and Fiordland region, New Zealand: Geological Society of America Bulletin, v. 84, no. 10, p. 3279-3316.

Shawe, D. R., 1965, Strike-slip control of basin and range structure indicated by historic faults in western Nevada: Geological Society of America Bulletin, v. 76, p. 1361-1378.

Tchalenko, J. S., and Ambraseys, N. N., 1970, Structural analysis of the Dasht-e Bayaz (Iran) earthquake fractures: Geological Society of America Bulletin, v. 81, p. 41-60.

Tchalenko, J. S., and Berberian, M., 1975, Dasht-e Bayaz fault, Iran-Earthquake and earlier related structures in bedrock: Geological Society of America Bulletin, v. 86, no. 5, p. 703-709.

Winslow, M. A., 1976, Active transcurrent shear zones in southern Chile as landward expressions of transform plate boundaries: Geological Society of America, Abstracts with programs, v. 8, no. 6, p. 1173-1174.

Woodward, Clyde and Associates, 1969, Seismicity and seismic geology of northwestern Venezuela: Report to Shell Oil Company of Venezuela, v. 2, 77 p.

Woodward-Clyde Consultants, 1979, Report of the evaluation of maximum earthquake and site ground motion parameters associated with the offshore zone of deformation, San Onofre nuclear generating station: Report for Southern California Edison Company, June, 241 p.

Personal Communication

Hardyman, 1979, Boise State University, Idaho.

Winslow, M. A., 1978, Lamont-Doherty Geological Observatory, Columbia University.

QUESTION 361.49

At the September 13, 1979 Menlo Park meeting between NRC, USGS, CDMG, and SCE, Dr. E. Heath, consultant to SCE, referred to a statistical analysis that computed the number of earthquakes one would have expected to the right of the Design Earthquake Limit Line (DELL) assuming a 8 1/2 maximum magnitude for a) all of the faults plotted in Figure 7 and b) all California faults. Describe this statistical analysis in detail.

RESPONSE 361.49

At the September 13, 1979 Menlo Park meeting, a preliminary analysis was presented of the significance of the absence of earthquakes to the right of the design earthquake limit (DEL) line shown in Figure 7 of the June 1979 report. This analysis consisted of estimating the number of earthquakes that might occur on each of the tabulated faults in the magnitude range between the design earthquake limit for each fault and the magnitude value M_s 8.5. Thus all faults were considered capable of magnitude 8.5 earthquakes, for purposes of this hypothetical analysis.

Because the number of large earthquakes predicted for the historical period will be small (generally less than one) for an individual fault, it is necessary to consider the ensemble behavior of all the faults to achieve maximum resolution from the analysis. For each fault a frequency-magnitude relationship is developed that is characterized by the parameters 'A', 'b', and maximum magnitude in the relation

$$\text{Log } N = A - bM \text{ for } M \leq 8.5$$
$$N = 0 \text{ for } M > 8.5$$

The level of seismic activity for each fault was calculated using the following assumptions and procedures:

1. All slip occurs seismically.

2. In the frequency-magnitude relation, the value of 'b' was assumed to be 0.8, generally consistent with observations in California (Hileman and others, 1973; Bolt and Miller, 1971)

3. The frequency of occurrence of earthquakes was scaled according to the slip rate of each fault. The slip rate of the San Andreas fault was the fundamental unit. The 'A' value for the San Andreas relationship was selected to produce one magnitude 8.0 or greater earthquake every 200 years, and the 'A' values for other faults were determined in direct proportionality to the San Andreas slip rate.

4. The number of earthquakes for each fault during the 200 year time period was calculated using the relationship

$$N = \frac{S_i}{S_{SA}} \left(10^{-8\,(M_i-8.0)} - 10^{-.4}\right)$$

where N = the number of earthquakes occurring between M_i and 8.5

M_i = maximum magnitude value of fault "i"

S_i = slip rate of fault "i"

S_{SA} = slip rate of San Andreas

(after Richter, 1958).

For the data set in Figure 7 of the June 1979 report, the calculations yielded a total of 8.3 earthquake data points that should have been observed to the right of the DEL during the past two centuries on all the faults studied. In fact, no such earthquakes have been observed: thus there is confidence in the hypotheses that the design earthquake limit for the group of faults considered is substantially less than M_s 8.5 and that the data base is extensive enough to indicate a trend of maximum earthquake values. The ensemble behavior of all 25 faults used in the analysis is equivalent to observing the behavior of an average fault for several thousand years.

In the preceeding analysis the model used for large earthquake activity is subject to limitations in several respects. The time interval of 200 years used in assumption 4 above is generally too long. The actual observation periods range from 80 to 206 years and average about 150 years as listed in Table 361.51-1. As a result, the number of events to be expected has been slightly overestimated. When the calculations are repeated using the total of 34 faults and the observation periods listed in Table 361.51-1, a total of 8.0 earthquake data points is expected to be observed to the right of the DEL. Of these 4.7 events are expected for the 19 California faults. As noted before, there were no such events observed during the historical period.

In lieu of assumption 3, it is more realistic to use the assumption that the 'A' value is proportional to the moment rate (defined as the product of slip rate and fault area in the response to question 361.51). Because total fault lengths generally decrease with decreasing slip rate, for the data set noted in Table 361.51-1, the 'A' values and the number of events to be expected were overestimated. The assumption that all faults are capable of magnitude 8.5 earthquakes is also unrealistic in many cases and physically impossible for some faults due to their short length. This assumption produces very long recurrence times for the largest earthquakes and thus an underestimate of the number of earthquakes to be expected in the historic time interval. More realistic maximum values would allow more frequent, smaller earthquakes. These inconsistencies in the analysis assumptions compensate for one another to some extent, but effectively reduce confidence in the specific numerical result. However, the results of the analysis validate the slip rate data base as being sufficient to define a trend of maximum earthquake magnitude values decreasing with decreasing slip rate.

REFERENCES

Bolt, B. A., and Miller, R. D., 1971 , Seismicity of northern and central California, 1965-1969: Seismological Society of America Bulletin, v. 61, no. 6, p. 1831-1847.

Hileman, J. A., Allen, C. R., and Nordquist, J. M., 1973, Seismicity of the southern California region, 1 January 1932 to 31 December, 1972: California Institute of Technology, Pasadena, 487 p.

Richter, C. F., 1958, Elementry seismology: W. H. Freeman, San Francisco and London, 768 p.

QUESTION 361.50

Based on the literature, some strike-slip faults fall well outside the "Design Earthquake Limit" line shown on Figure 7. Matsuda (1977, Table 1) gives slip rates for several strike-slip faults that have had large historic earthquakes, as follows:

Earthquake	Magnitude	Slip Rate, mm/yr
1891 Nobi	7.9 (probably from intensity)	1-5
1927 Tango	7.5	0.05-0.1
1943 Tottori	7.4	0.05-0.1
1974 Izi-Hanto	6.9	0.5-1.0

The slip rate of 20 mm/year used by Woodward-Clyde for the North Anatolian fault has been modified in some recent literature. The 20 mm/year rate is based on Pavoni's interpretation of 300-400 km displacement on the Anatolian fault, but this interpretation is strongly disputed by Ketin (1969) who concludes that the displacement is much less. A later report (Canitez, 1977) says the slip rate in the last 15 m.y. has been 5-6 mm/year and in the last 1/2 m.y. has been "about 7 mm/year" (abstract) or "greater than 7 mm/year" (text).

The 1976 Tan Shan earthquake of magnitude 7.8 was a complex event that was predominantly strike-slip with about 1.5 meters of displacement. The Chinese were aware of the fault in the coal mines, but did not consider it active. Inasmuch as Chinese civilization has been centered near Tan Shan for several thousand years, the geologic slip rate on the fault is very probably less than 1 mm/year.

Kanamori (1973) states that the 1948 Fukui M 7.3 earthquake, predominantly strike-slip, occurred on a fault with a slip rate less than 0.3 mm/year.

Please assess the impact of these comments on the slip-rate technique for estimating earthquake magnitudes.

References

Canitez, Nezihi, 1977, Dynamics of the North Anatolian Fault, in Proceedings of the CENTO seminar on recent advances in earthquake hazard minimization: Iran Tech. Research and Standards Bureau, Plan and Budget Organization, Publication 70, p. 353-366.

Kanamori, H., Mode of strain release associated with major earthquakes in Japan, Annual Review of Earthquake and Planetary Sciences, vol. 2, Donath et al. eds., 1973.

Ketin, Ihsan, 1969, Uber die nordanatolische horizontal-vershiebung: Mineral Res. and Exploration Inst. of Turkey, Bull. (Foreign Ed.), no. 72, p. 1-28.

Matsuda, Tokihiko, 1977, Estimation of future destructive earthquakes from active faults on land in Japan: Journal of Physics of the Earth, v. 25, suppl., p. S251-S260.

RESPONSE 361.50

Japanese Earthquakes

It is well known that Japanese strike-slip faults are different in many respects from California strike-slip faults. This difference is apparent from plots of various fault parameters such as those of Slemmons (1977). The most conspicuous features are the large displacement relative to rupture length, and the fact that commonly the entire mapped length of the fault breaks in one earthquake or that conjugate sets of faults rupture. The precision of the slip rates associated with the four faults listed in the question has been addressed in response 361.46 b. Though the slip rate values are not well founded, there is a trend of apparently low slip rates for some strike-slip faults in Japan that produce large earthquakes. This situation is peculiar to the tectonic setting of Japan as discussed in responses 361.46 b and 361.47. To the extent that strike-slip faults in Japan and California fall into almost mutually exclusive groups when these fault properties are compared, the Applicants conclude that faulting of the kind that occurs in Japan cannot occur in California. Accordingly, it is inappropriate to include faults in Japan in an analysis of fault behavior of strike-slip faults in California.

Kanamori (1973) assigns a strike-slip rate of 0.3 mm/year or less for the fault that ruptured in the M 7.4 Tottori earthquake and presents no direct data on the slip rate for the causative fault of the 1948 Fukui earthquake.

In his conclusions based on Matsuda's (1968) interpretation of topographical features, Kanamori (1973, p. 233) groups together the four intraplate earthquakes that are analyzed and assigns a slip rate of less than 0.3 mm/year to all of them. However, he does not give any references except to the Tottori earthquake faults (as discussed above). One of the faults (Niigata) is offshore. The applicant believes that Kanamori had no geologic or other explicit basis for assigning this slip-rate value to the other faults. It is therefore concluded that the slip rate on the fault associated with the 1948 Fukui earthquake is unknown.

North Anatolian Fault

The 20 mm/year slip rate calculated for the North Anatolian fault in the WCC June 1979 report is based on displacements assigned by Pavoni, (1961). Those displacements (350-400 km) are challenged by several authors because the values are based on incorrect data (Ketin, 1969; Canitez, 1977; and Sengor, 1979). The general consensus of work, since Pavoni, brackets the minimum and maximum total displacement between 50 and 100 km (Sengor, 1979). Thus, the 20 mm/year slip rate is no longer considered valid for the North Anatolian fault.

Canitez (1977), indicates that the average slip rate on the North Anatolian fault has been 5-6 mm/year during the past 15 million years since the initiation of faulting in Miocene. Data from Sengor (1979), supports a range of 5.3 to 18 mm/year since Miocene. Geologic mapping supports a rate of greater than 7 mm/year during the past 0.5 million years of the Quaternary (Cantinez, 1977). The total range of values of slip rate from Miocene and Quaternary data is 5 to 18 mm/year. Because the Quaternary data are probably most representative of the present tectonic behavior of the fault, 7 mm/year is selected to represent the North Anatolian fault with the understanding that the slip rate may be higher. This interpretation is incorporated in the slip-rate/maximum-magnitude data base as documented in response 361.45 e.

Tang Shan Earthquake, China

The Chinese did not expect the large (M_s 7.7) Tang Shan earthquake of 1976; the fault was not considered active until the event occurred (Lucile Jones, personal communication, 1979). Currently, no data are available to estimate the slip rate on the fault which generated the Tang Shan earthquake of 1976. In general, very little data regarding slip rate are available for any faults in China (Deng Qidong, personal communication, 1980). The Chinese historical earthquake catalog lists no earthquakes of comparable magnitude in the Tang Shan area during the 3,000 years of reported earthquakes (although a M 8 earthquake occurred 100 km to the west in 1679). This suggests that the recurrence interval on the Tang Shan fault may be quite long; but data to estimate a slip rate are not available and the approximate 1 mm per year slip rate stated in question 361.50 is unfounded.

The July 27, 1976 Tang Shan earthquake was a complex intraplate earthquake sequence (Butler, Stewart, and Kanamori, 1979). The main shock was primarily a right-lateral strike-slip mechanism shortly followed by two thrust mechanisms and then by an exceptionally large oblique-normal aftershock (M_s 7.2). The preferred fault-plane orientation of this large aftershock is nearly perpendicular to the main shock fault plane. This sequence of earthquakes indicates a complex interplay of several faulting mechanisms, especially of the dominant strike-slip and oblique normal faulting.

The Applicants believe that the Tang Shan earthquake cannot be analyzed by the slip-rate/magnitude methodology because 1) no data are available to calculate slip rates for the fault and any estimates are speculative; 2) the complex nature of the earthquake sequence suggests that the tectonic setting in this part of China is fundamentally different from that in Southern California; and 3) the faults in China are intraplate whereas in Southern California they are interplate. Even though the Chinese did not consider the fault active prior to the earthquake (this opinion is based primarily on the historical record of the area), this does not mean that its activity could not have been anticipated from the Quaternary geologic record. An analogous situation in California occurred in 1952 when the White Wolf fault ruptured in the M_s 7.7 Kern County earthquake. The White Wolf fault was considered inactive prior to the 1952 earthquake because Quaternary geologic data was lacking; but if properly thorough mapping had been done, the fault would clearly have been classified as active.

REFERENCES

Butler, R., Stewart, G. S., and Kanamori, H., 1969, The July 27, 1976, Tang Shan earthquake--a complex sequence of intraplate events: Seismological Society of America Bulletin, v. 69, no. 1, p. 207-220.

Canitez, N., 1977, Dynamics of the North Anatolian fault in CENTO seminar on Recent Advances in Earthquake Hazard Minimization, Proceedings: Iran Technical Research Standards Bureau, Plan and Budget Organization, Publication 70, p. 353-366.

Kanamori, H., 1973, Mode of strain release associated with major earthquakes in Japan, in Donath and others, eds., Annual Review of Earthquakes and Planetary Sciences, v. 2.

Kefin, I., 1969, Uber die Nordanatolische horizontal-vershiebung: Mineral Research and Exploration Institute of Turkey, Bulletin, no. 72, p. 1-28.

Matsuda, T., 1977, Estimation of future destructive earthquakes from active faults on land in Japan: Journal of Physics of the Earth, v. 26, supplement, S409-S421.

Pavoni, N., 1961, Die Nordanatulische horizontal vershiebung: Geologische Rundschau, v. 51, p. 122-139.

Sengor, A. M. C., 1979, The North Anatolian transform fault--its age, offset and tectonic significance: Journal of the Geological Society of London, v. 136, p. 269-282.

Slemmons, D. B., 1977, State-of-the-art for assessing earthquake hazards in the United States, Report 6, faults and earthquake magnitude: U. S. Army Corps of Engineers Waterways Experiment Station, Soils and Pavement Laboratory, Miscellaneous Paper S-73-1, 129 p.

Personal Communications

Jones, Lucile, 1979, Massachusetts Institute of Technology.

Qidong, Deng, 1980, State Seismological Bureau, Beijing, China

QUESTION 361.51

In Woodward-Clyde's empirical search for a correlation between geologic slip rate and maximum magnitude there is a serious sampling bias in the restriction of magnitude data to historic earthquakes, even though there may be no alternative. A fault with a small geologic slip rate will have a smaller rate of seismic activity, on the average. Therefore, the largest earthquake experienced in historic time is less likely to be near the "maximum magnitude" for a fault with a small slip rate. Please explain how this concept impacts the confidence in the placement of the "Design Earthquake Limit" line on Figure 7.

RESPONSE 361.51

The significance of possible recurrence times for low slip-rate faults is evaluated by making use of the equivalence of time and ensemble averages of random stationary stochastic processes. The seismicity in a region is often represented as a random, stationary process as discussed by Gardner and Knopoff (1974). This Poisson model is most valid for the largest events occurring on each fault (Shlein and Toksoz, 1971).

Given this assumption, the statistics of the seismicity of a set of N faults of equal length, each having unit slip rate, may be regarded as equivalent to the statistics of a single fault of the same length having a slip rate of N units. Accordingly, the likelihood of the largest earthquake occurring during some interval of time on any of the faults with unit slip rate being near the maximum magnitude is equivalent to the likelihood for a single fault having a slip rate of N units. To examine this ensemble behavior for the slip-rate data set, the group of faults is divided into three principal ranges of slip rate, each of which spans a factor of five in slip rate. These groups are indicated in Table 361.51-1 and defined as follows:

> Group one consists of seven faults whose slip rates are 20 mm/year or higher.
>
> Group two consists of fourteen faults whose slip rates lie between 3.5 and 17.5 mm/year.
>
> Group three consists of eleven faults whose slip rates lie between 0.7 and 3.5 mm/year. The OZD (with a slip rate of 0.5 mm/year) falls just outside this group, while the Antioch fault lies considerably lower at 0.1 mm/year.

The ensemble sum of moment rates of group 3 (the low slip rate faults) is compared with the ensemble average of group 2 (moderate slip-rate faults.) Moment rate is used as a measure of activity and is equal to the product of slip rate, total fault length, fault width, and the shear modulus. The total moment rate for group 3 is roughly equal to the average rate for group 2 (Table 361.51-1). Therefore, the small faults of group 3, taken together, have seismic potential (as expressed in the moment rate) that is numerically equivalent to the average of the faults of group 2.

According to the equivalence of time and ensemble averages, the statistics of the combined set of group 3 faults should be the same as that of the average group 2 fault. Therefore, the confidence that there are enough faults in group 3 to have produced a maximum event on one of the faults is equivalent to the confidence of having observed a maximum event on the average group 2 fault. Since the latter confidence is quite high, there is a corresponding high confidence that there has been sufficient observation of low slip rate faults for the largest observed event among those to be a maximum magnitude event. As none of the observed events exceeds the HEL it is concluded that the maximum magnitude relation holds for low slip rate faults.

The above conclusion has been reached by studying a quite limited group of low slip rate faults. While most high slip rate faults have been identified and studied, there is a large number of low slip rate faults which have not been identified or where slip rates have not been measured. For example, in California it is likely that all faults with high slip rates have been included in the data set, while there may be many low slip-rate faults that are not included because the slip rate is unknown, or because the fault has not even been identified yet. If all of the low slip rate fault data were available, then the inclusion of a much larger number of low slip rate faults would greatly increase the total moment rate of group 3 faults. This increased moment rate would further increase confidence that the maximum magnitude relation holds for low slip rate faults.

REFERENCES

Gardner, J. K., and Knopoff, L., 1974, Is the sequence of Earthquakes in southern California with aftershocks removed poissonian: Seismological Society of America Bulletin,, v. 64, no. 5, p. 1363-1367.

Shlien, S., and Toksoz, M. N., 1970, A clustering model for earthquake occurrences: Seismological Society of America, Bulletin, v. 60, p. 1765-1787.

TABLE 361.51-1

FAULT AND SEISMICITY PARAMETERS

Fault	Slip Rate (mm/yr)	Maximum Historic Magnitude (m_S)	Historic Observation Period	Total Fault Length	Total Fault Width	Moment Rate (dyne-cm/yr) $\times 10^{23}$	
Sumatra	67.	7.6	81	1650	15	49747.50	
Fairweather	58.	7.9	80	1150	15	30015.00	
Central San Andreas	37.	8.2	200	330	15	5494.50	Group
Denali	35.	*	100	2150	15	33862.50	1
Totschunda	33.	*	100	150	15	2227.50	
South San Andreas	25.	6.5	200	225	15	2531.25	
North San Andreas	20.	8.3	200	435	15	3915.00	
San Gregorio-Hosgri	16.	6.1	138	375	15	2700.00	
Darvaz	13.	*	100	700	15	4095.00	
Calaveras-Paicines	12.	6.6	130	171	15	923.40	
Bocono	9.75	8.0	167	500	15	2193.75	
Garlock	8.	*	200	265	15	954.00	
San Jacinto	8.	7.1	130	260	15	936.00	
Jordan-Dead Sea	6.5	7.5	142	800	15	2340.00	Group
North Anatolia	7.	7.9	200	1180	15	3717.00	2
Hayward-Healdsburg	6.	6.7	200	205	15	553.50	
Motagua	6.	7.5	206	700	15	1890.00	
Clarence-W.Wairarapa	4.8	7.6	141	430	15	928.80	1710
Awatare-Wellington	4.	7.1	141	547	15	984.60	(mean)
Hope-E.Wairarapa	4.	6.7	141	418	15	752.40	
Kopet-Dagh	3.6	7.3	84	600	15	972.00	
Calico	3.4	*	130	129	15	197.37	
Sheep Hole-Ludlow	3.4	*	130	106	15	162.18	
Helendale	3.	*	130	105	15	141.75	
Pinto Mountain	3.	*	130	85	15	114.75	
Talemazar	2.5	*	100	300	15	337.50	
Dasht-e bayas	2.4	7.2	100	80	15	86.40	Group
Big Pine	2.4	*	130	80	15	86.40	3
Elsinore-Laguna Sal.	2.3	6.	130	297	15	307.39	
Blue Cut	1.8	*	130	83	15	67.23	1520
Whittier	1.2	*	130	42	15	22.68	(total)
Collayami	1.	*	130	35	15	15.79	
OZD	.50	6.3	167	200	15	45.00	
Antioch	.10	4.9	130	58	15	2.61	

*Maximum observed magnitude is less than 6.0.

QUESTION 361.52

Why was M_S used in Figure 6, but M_L used in the data collection?

RESPONSE 361.52

For those earthquakes for which both M_L and M_S determinations have been made, and M_S of 6-1/2 typically corresponds to an M_L of approximately 6-1/2. The attenuation relationships developed for SONGS and the recommended mean and 84th percentile instrumental peak accelerations and the response spectra were intended to represent ground motions from a magnitude 6-1/2 earthquake on the hypothesized OZD. The estimated magnitude of 6-1/2 represented the maximum magnitude associated with the hypothesized OZD and was estimated based on an empirical relationship between fault slip rate and surface wave magnitude, M_S. For many earthquakes in the western United States, however, M_S determinations have not been made and only M_L values have been reported.

The data set selected for SONGS consists of 56 accelerograms from seven earthquakes with M_L of approximately 6-1/2. As shown in Table 361.52-1 these data are also representative of M_S of approximately 6-1/2.

As can be observed in Table 361.52-1, the majority of the recordings (48 out of the total of 56 accelerograms) were obtained during earthquakes of M_S = 6.6 to 6.7. Reference to the Table 361.52-2 (expanded form of the table on page J-5 of the June 1979 WCC report) also shows that for the weighted regression analysis, 10 out of 14 weighted data groups had an M_S of 6.6 or 6.7. Therefore, it can be concluded that the ground motion values developed for SONGS should be considered applicable to an M_S of 6.6.

TABLE 361.52-1

SELECTED EARTHQUAKES AND NUMBER OF ACCELEROGRAMS FOR SONGS DATA BASE

EARTHQUAKE	M_L	M_S	NUMBER OF ACCELEROGRAMS
LONG BEACH (33-3-11)	6.3	6.3	2
EUREKA (34-7-6)	6.5	(6.5+)*	2
NORTHWEST CALIF. (41.2-9)	6.4	(6.4+)*	2
NORTHERN CALIF. (41-10-3)	6.4	(6.4+)*	2
EUREKA (54-12-21)	6.5	6.6	4
BORREGO MOUNTAIN (68-4-8)	6.4	6.7	2
SAN FERNANDO (71-2-9)	6.4	6.6	42
			56

*For these earthquakes, M_S determinations have not been made; values within brackets are estimates of the M_S.

TABLE 361.52-2

GROUPING OF DATA FOR WEIGHTED REGRESSION ANALYSIS -- NUMBER OF DATA POINTS FROM VARIOUS EARTHQUAKES IN SELECTED DISTANCE INTERVALS

Distance Range	Number of Weighted Data Groups	Earthquake (M_S, Number of Data Points)
10 - 14 km	0	None
14 - 20 km	2	1954 Eureka (6.6, 2); 1971 San Fernando (6.6, 2)
20 - 28 km	2	1933 Long Beach (6.3, 2); 1971 San Fernando (6.6, 6)
28 - 40 km	1	1971 San Fernando (6.6, 20)
40 - 57 km	3	1941 Northern California (6.4+, 2); 1954 Eureka (6.6, 2); 1971 San Fernando (6.6, 4)
57 - 80 km	1	1971 San Fernando (6.6, 6)
80 - 113 km	2	1941 Northwest California (6.4+, 2); 1971 San Fernando (6.6, 2)
113 - 160 km	3	1934 Eureka (6.5+, 2); 1968 Borrego Mountain (6.7, 2); 1971 San Fernando (6.6, 2)

QUESTION 361.53

During the September 13, 1979 meeting, Ross Sadigh and David Hadley presented arguments for using the regression equation on page 25 and for choosing C equal to 20. Describe this analysis in detail, especially the synthetic seismogram modeling study. Show why the data at greater distances can be extrapolated back to a distance of 10 kilometers (see question 361.62). Show how directivity (focussing) was accounted for in the modeling study and show sample theoretical seismograms that demonstrate directivity.

USGS indicates that there is a problem with the functional form $\propto(R + C)^{\beta}$ used in the regression and with the value adopted for C. There is no physical basis for the form $\propto(R + C)^{\beta}$. Furthermore, C = 20 has not been demonstrated to give a better fit than other values. Furthermore, it needs to be demonstrated not only that C = 20 gives a better fit but also that the better fit is statistically significant. Moreover, site-specific data set should be used to determine C. If C means anything at all, it should be considered a site-dependent property, since a likely mechanism for limiting acceleration is the finite strength of the near-surface materials at the recording site. Consequently please explain the validity of the quantity C = 20.

RESPONSE 361.53

1. <u>Review of Empirical Approach Contained in Appendix I of June 1979 WCC and New Empirical Data</u>

Appendix I of the June 1979 WCC report contains the results of analyses to develop and examine attenuation relationships for peak horizontal acceleration using, as a data base, all available high-quality, digitized and uniformly processed recordings obtained on soil sites from western United States earthquakes with magnitude approximately equal to 6-1/2. One of the main objectives of these analyses was to examine the suitability of attenuation form $a = \alpha(R + C)^{\beta}$ and to provide a basis for selecting an appropriate value for parameter C for magnitude 6-1/2 earthquakes. To accomplish this, a substantially large number of recordings (196 accelerograms from 12 earthquakes recorded on soil sites) covering the distance range of about 10 to 150 kilometers was examined. Peak accelerations for these recordings were plotted versus distance (see the June 1979 WCC report, Figure I-1) and the trend of the data indicated that the attenuation relationship should flatten at closer source-to-site distances. It was noted that this trend would require a non-zero value of C in the regression equation.

To further examine the trend of these data, regression analyses were conducted using values of C ranging from zero to 40. Although the difference in standard error of estimate for different values of C could not be considered statistically significant, the standard error of estimate obtained from these analyses was found to decrease with increasing C. Thus the analysis results supported the general trend shown by visual examination of the data and indicated that a non-zero value of C should be used in the regression equation. The results of regression analysis for C = 20, superimposed on the soil data, was judged to fit the general trend of the data reasonably well.

Since the issuance of the June 1979 WCC report, additional strong motion recordings were obtained during the October 15, 1979 Imperial Valley earthquake (M_s = 6.8). There is particular significance in the large number of recordings obtained within 15 km of the fault rupture surface (for details see the response to questions 361.55 and 361.57). The acceleration data from the Imperial Valley earthquake recordings are plotted versus closest distance from the fault rupture surface in Figure 361.55-1. These data provide more definitive empirical evidence regarding the trend of peak acceleration at near-source distances and emphasize the need for a non-zero value of C. Further discussion of the Imperial Valley data with regard to variation of standard error of estimate corresponding to different values of C is provided in Section 3 of this response.

2. Synthetic Seismogram Modeling Study

2.a - Description of Analysis Procedure

The seismogram recorded by a strong motion accelerograph is the result of the physical interaction of many complex processes. As the rupture front passes a point on the fault, each particle accelerates, reaches some peak velocity and finally slows to a stop. As each particle accelerates, it radiates seismic energy. Before this energy is recorded at the station, it is filtered in several significant ways. The energy is absorbed by anelastic wave propagation and scattered by heterogeneities. Purely elastic propagation through the earth also filters the signal (e.g., Helmberger and Malone, 1975; Heaton and Helmberger, 1978). Finally interaction with the surface of the earth results in further distortions. Each physical process can be reprsented by a filter or operator. The final signal is then the convolution of each operation that transfers energy from each particle on the fault to the station.

Provided the various operators are known in sufficient detail, the generation of synthetic time histories is fairly straightforward.

In a recent study of the 1940 Imperial Valley earthquake, Hartzel (1978) observed that the main-shock seismogram recorded at El Centro could be simulated by the superposition of several of the major aftershocks. Physically, this simulation is very attractive. The record for each aftershock is the cumulative result, for a portion of the fault, of all physical processes described above. To simulate the main shock requires only fairly simple scaling for moment. The lag time for the superposition of each aftershock record is determined by the progression of the rupture front. Kanamori (1978) carried this technique further by using regional records from the $M_s = 6.7$ Borrego Mountain earthquake to simulate rupture along the San Andreas for a magnitude 8 earthquake. Since the Borrego Mountain records were not obtained over the full range of distances and azimuths that would be required to properly simulate ground motion in Los Angeles, some scaling of the observed records was necessary. In particular, as the observed records were primarily surface waves, amplitudes were scaled for distance by $r^{-1/2}$. Finally, the amplitudes were corrected by radiation pattern and the scaled observed records were lagged in time to simulate the rupture process.

The estimation of strong ground motion at near source distances resulting from a large earthquake has also been studied with a simulation technique that relied heavily upon the more extensive data set from smaller earthquakes (Hadley and Helmberger, 1980). These investigators used accelerograms from smaller earthquakes as Green's functions for the elements of a larger fault. The results of that study indicate that the slope of the peak acceleration versus distance curve (Δ = 5 to 25 km, for hard rock sites) flattened as the magnitude increased. The scaling study by Hadley and Helmberger (1980) does not incorporate any non-linear, near surface effects. The flattening of the peak acceleration curve at near source distances with increasing magnitude was primarily related to the physical dimensions of the fault.

2.b Considerations of Directivity

The effects of directivity (focusing) are explicitly incorporated in the simulation study by Hadley and Helmberger (1980). The four rupture geometries investigated in that study are shown in Figure 361.53-1. In that simulation, accelerograms resulting from rupture in each grid element of the fault are added together. Clearly if the fault ruptures towards a station, the time interval over which the seismic pulses arrive at the station is compressed. This effect can significantly increase the amplitude of the accelerogram. Conversely, if the rupture proceeds away from the station, the time interval is expanded and the peak accelerations are reduced. An example of each case is shown in Figure 361.53-2 and 361.53-3. The rupture geometries for these cases are, respectively, 1 and 2, shown in Figure 361.53-1. The distance to the fault trace is 5 km.

Directivity has the largest effect when the radiation pattern, as seen from the recording site, is constant and on a maximum lobe during the entire rupture process. This results in strong constructive interference of a single wave-type, either SH or SV. An example of this condition for strike-slip faults is rupture towards a recording station that is situated directly on the fault. Directivity will not be as significant if the radiation pattern seen by the station is rapidly changing as the rupture proceeds. For example, a station 10 km perpendicular from the end of a long fault initially sees transversely polarized waves.

When the rupture reaches a point about 10 km down the fault, the radiation pattern has rotated such that the maximum energy comes from SV-waves, polarized in a radial direction. Finally, when the rupture reaches the end of the fault, radiation has shifted back to a maximum transversely polarized, SH wave. The rotation of the focal mechanism during the rupture process, as seen from the station, rapidly diminishes the effectiveness of directivity. Indeed, for distances greater than about 5 km from the fault trace, rupture towards the recording site does not in general result in the largest peak accelerations. Bilateral rupture or unilateral rupture past the station (geometries 3 and 4, Figure 361.53-1) systematically results in as large or larger peak accelerations. This results because at any given distance, twice as much energy is released by the fault as compared with geometries 1 or 2, Figure 361.53-1. The strength of each record that is added into the simulation decreases in amplitude approximately as R^{β}. The compression in time of the energy radiated by the fault that ruptures toward the site, when modulated by the radiation pattern of the source, is not as effective in increasing the peak accelerations as is doubling the fault area at each distance.

3. Function Form for Attenuation and Quantification of C

The functional form of the attenuation relationship ($a = \propto(R + C)^{\beta}$) was first discussed by Esteva (1970). The principal guiding philosophy in selecting the functional form of any equation used to describe data has been, and should be, that the function capture the real trends in the data and that it use a minimum number of parameters. An arbitrarily selected form cannot, in general accurately model the phenomenon; Instead, it can only represent mathematically the empirical effects of the phemomenon. The adopted form of attenuation relationship ($a = \alpha(R + C)^{\beta}$) used in the San Onofre study is the most widely used form (Idriss, 1978). As discussed below, both observational data (e.g. data from the 1979 Imperial Valley earthquake) and simulation studies show that this functional form is adequate for establishing values of peak acceleration at close distances from the fault (say 5 to 10 km).

The exponent of the attenuation relationship [$a = \alpha(R + C)^{\beta}$] controls the decay of the curve at distances of $R >> C$. With increasing distances it is commonly observed that seismograms systematically shift to a longer dominant period. In the far-field, the amplitude of the long-period pulse from an earthquake is commonly assumed to scale with moment. Hence, a reasonable and fairly common assumption (e.g., Donovan, 1975; Esteva, 1970) is that the exponent is either independent or only weakly dependent on the magnitude. This assumption is also well supported by a study involving 2900 accelerograms recorded over the distance range 1 to 600 km from nuclear events ranging in yield from 1 to 1200 kilotons (Murphy and Lahoud, 1969).

Simulation studies can extend and supplement observational data. The results from studies of simulating larger earthquakes, briefly described above and described in detail in Hadley and Helmberger (1980), can be used to examine the form of the attenuation relationship. Peak acceleration values computed in each simulation have been used in a regression analysis identical to one performed for the Imperial Valley data. A series of curves were fit to the peak acceleration values of the simulation for $M = 6.5$. The variation of standard error of the resulting regression curves computed for a range values of C (for constant $\beta = -1.75$) is shown in Figure 361.53-4. Further, the simulations provide a means to investigate the dependence of C on magnitude. The best fitting values of C as a function of magnitude (assuming a constant value of β, as described above) derived from the simulation results are:

Magnitude	C
4.5	6
5.5	12
6.5	22
7.0	30

Further support for non-zero and magnitude dependency of the parameter C is provided through empirical attenuation relationships; for example the best fit to the relationships for peak acceleration by Schnabel and Seed (1973) which are applicable to rock sites requires the following values for the parameter C:

Magnitude	C
5.6	14
6.6	22
7.6	34

Accelerograms recorded during the 1979 Imperial Valley earthquake provided significant data on peak acceleration at distances up to 15 km for strike-slip faulting. These data are discussed above, section 1 of this response, and are plotted on Figure 361.55-1. An attenuation relationship that adequately describes these observations clearly requires flattening of the curve for distances close to the fault. These recently obtained data can be used to judge the adequacy of the assumed attenuation relationship. Results of the regression analysis using the Imperial Valley data are shown in Figure 361.53-4; these results are in terms of the standard error of estimate corresponding to values of C ranging from zero to 40 km. These results show that the best fitting form of the attenuation relationship requires a non-zero value of C. This is in agreement with the conclusion derived from the simulation study.

In considering constraints provided by both empirical and computational studies, it is concluded that the assumed functional form of the attenuation relationship is quite adequate for describing the behavior of peak horizontal acceleration. It is further concluded that the trend towards saturation of peak accleration with increasing magnitudes (similar to the saturation of peak response at 1 sec found by Kanamori and Jennings, 1978) requires that C increase with magnitude. As discussed above, the modeling study does not incorporate non-linear near-surface effects. Therefore, the behavior of C derived from the modeling cannot be attributed to near-surface material properties. The only change in modeling the events M = 5.5, 6.5, and 7.0 was the size of the grid used in the simulation. Hence it is concluded that C is related to the physical dimensions of the fault.

Based on the preceding discussion, it is concluded that the assumed value of C = 20 for magnitude 6-1/2, used in the June 1979, WCC report, is consistent with both the constraints and guidelines provided by both empirical and computational studies.

REFERENCES

Donovan, N. C., 1973, A statistical evaluation of strong motion data including the February 9, 1971 San Fernando earthquake: 5th World Conference on Earthquake Engineering, Rome, 1, Proceedings, p. 1252-1261.

Esteva, L., 1974, Geology and predictability in the assessment of seismic risk: 2nd International Conference Association of Engineers and Geologists, Proceedings, Sao Paolo.

Esteva, L., 1970, Seismic risk and seismic design decisions, in, Hansen, R. J., eds., Seismic Design for Nuclear Power Plants, MIT Press, Cambridge, Mass., p. 142-182.

Hadley, D. M., and Helmberger, D. V., 1980, Simulation of strong ground motions: Seismological Society of America Bulletin, v. 70, no. 2.

Hartzell, S. H., 1978, Interpretation of earthquake strong ground motion and implications for earthquake mechanism: Ph.D. dissertation, University of California, San Diego, p. 269.

Heaton, T. H., and Helmberger, D. V., 1978, Predictability of strong ground motion in the Imperial Valley--Modeling the M = 4.9, November 4, 1976 Brawley earthquake: Seismological Society of America Bulletin, v. 68, p. 31-48.

Helmberger, D. V., and Malone, S. D., 1975, Modeling local earthquakes as shear dislocations in a layered half space: Journal of Geophysical Research, v. 80, p. 4881-4888.

Idriss, I. M., 1978, Characteristics of earthquake ground motions: Specialty Conference on Earthquake Engineering and Soil Dynamics, ASCE, Pasadena, CA., 115 p.

Kanamori, H., 1978, Application of earthquake mechanism studies to prediction of long-period ground motion related problems, U. S. Geological Survey Final Technical Report, Contract No. 14-08-0001-16776.

Kanamori, H., and Jennings, P. C., 1978, Determination of local magnitude, M_L, from strong-motion accelerograms: Seismological Society of America, v. 68, p. 471-485.

Murphy, J. R., and Lahoud, J. A., 1969. Analysis of seismic peak amplitudes from underground nuclear explosions: Seismological Society of America, v. 59, p. 2325-2341.

Schnabel, P. B., and Seed, H. B., 1973, Accelerations in Rock for Earthquakes in the Western United States: Seismologial Society of America, v. 63, no. 2., p. 501-516.

RUPTURE GEOMETRY

Fault Length

| ←——— 24 km ———→ |

1\.

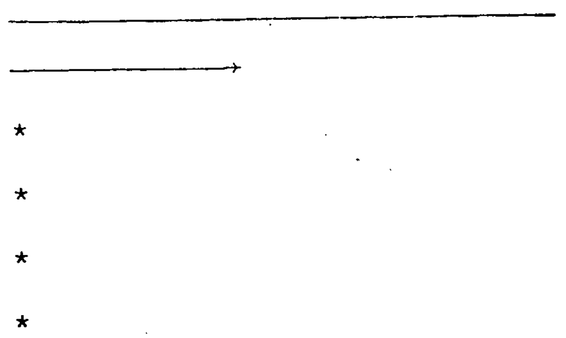

Uni-lateral rupture away from Station (*) profile.

Hypocenter depth - 8 km.

2\.

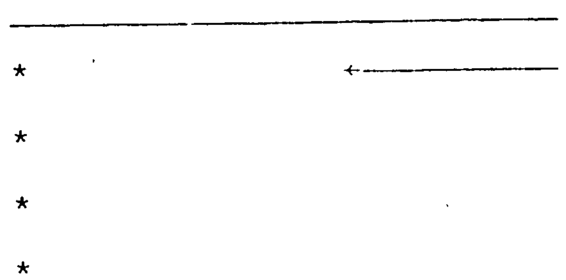

Uni-lateral rupture towards Station (*) profile.

Hypocenter depth - 8 km.

3\.

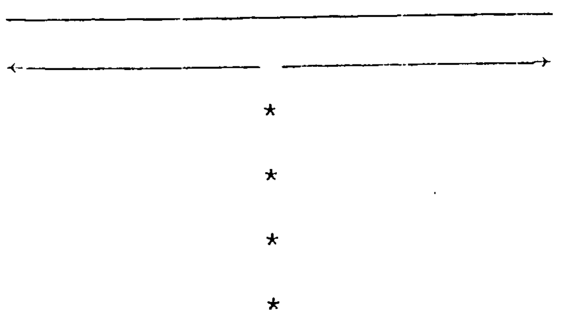

Bilateral rupture initiating at shortest epicentral distance.

Hypocentral depth - 8 km.

4\.

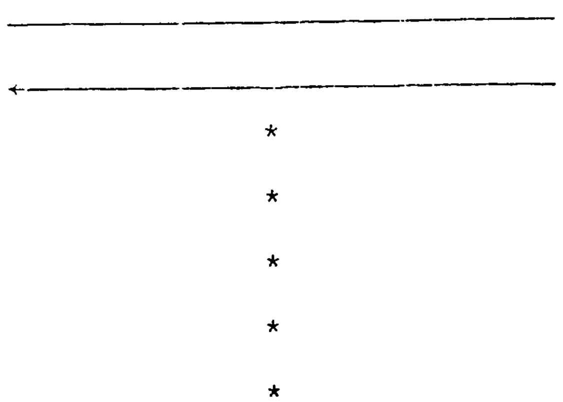

Uni-lateral rupture past Station (*) profile.

Hypocentral depth - 8 km.

Figure 361.53-1

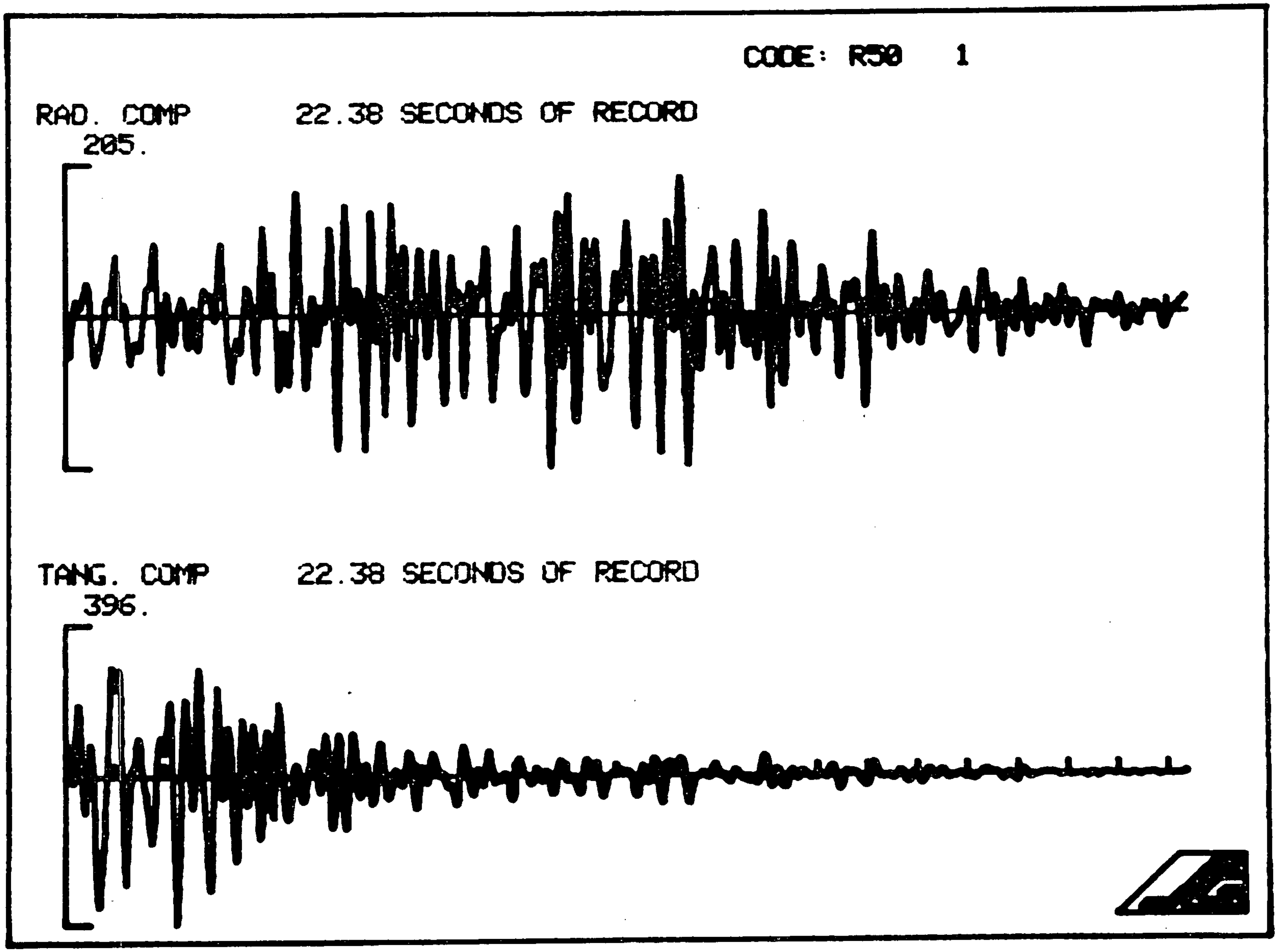

Figure 361.53-2. Example of a simulated accelerogram. The rupture direction is away from the station (geometry 1 on Figure 361.53-1) and the distance to the fault trace is 5 km.

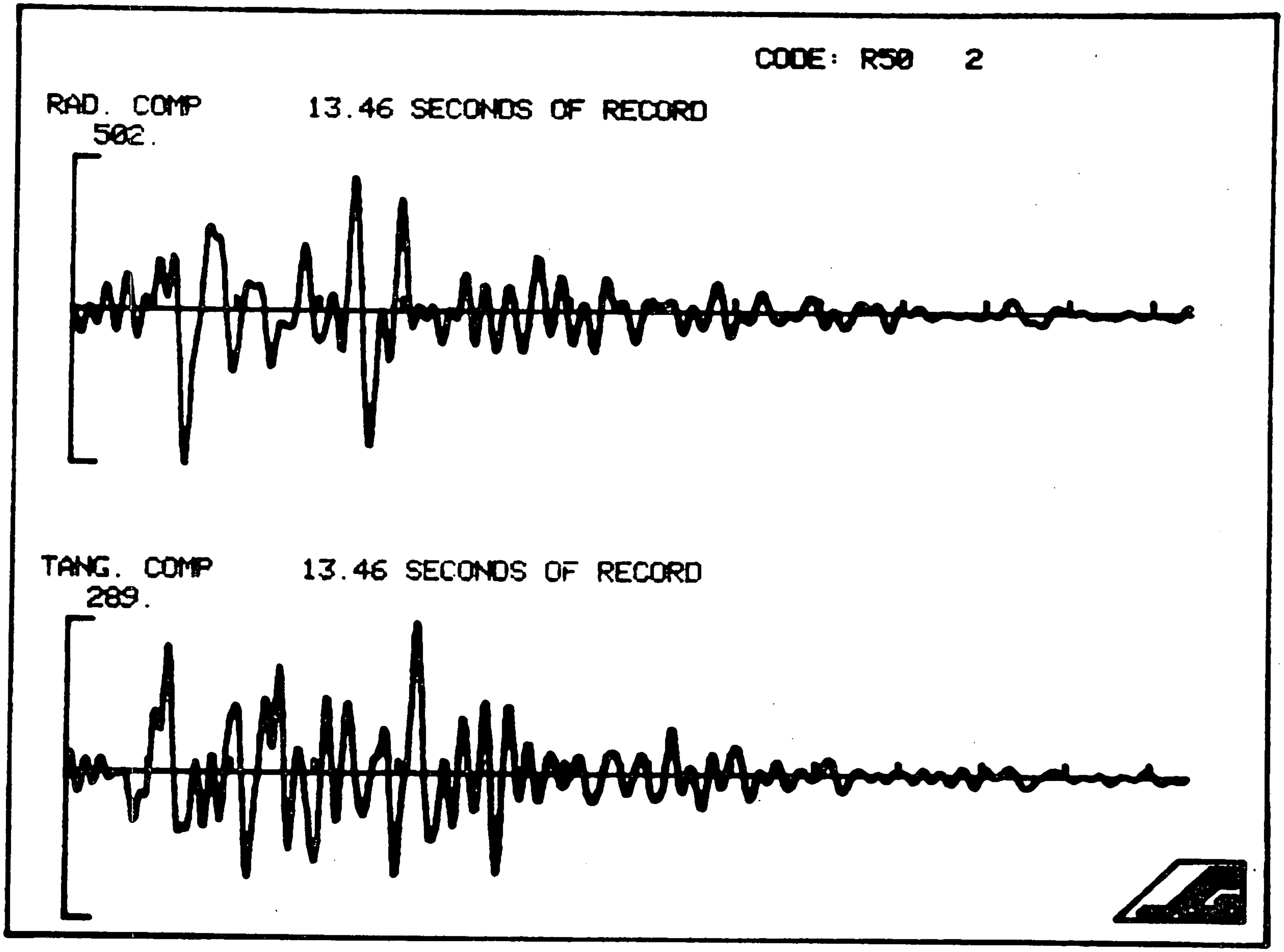

Figure 361.53-3. Example of simulated accelerogram. The rupture direction is towards the station (geometry 2 on Figure 361.53-2) and the distance to the fault trace is 5 km.

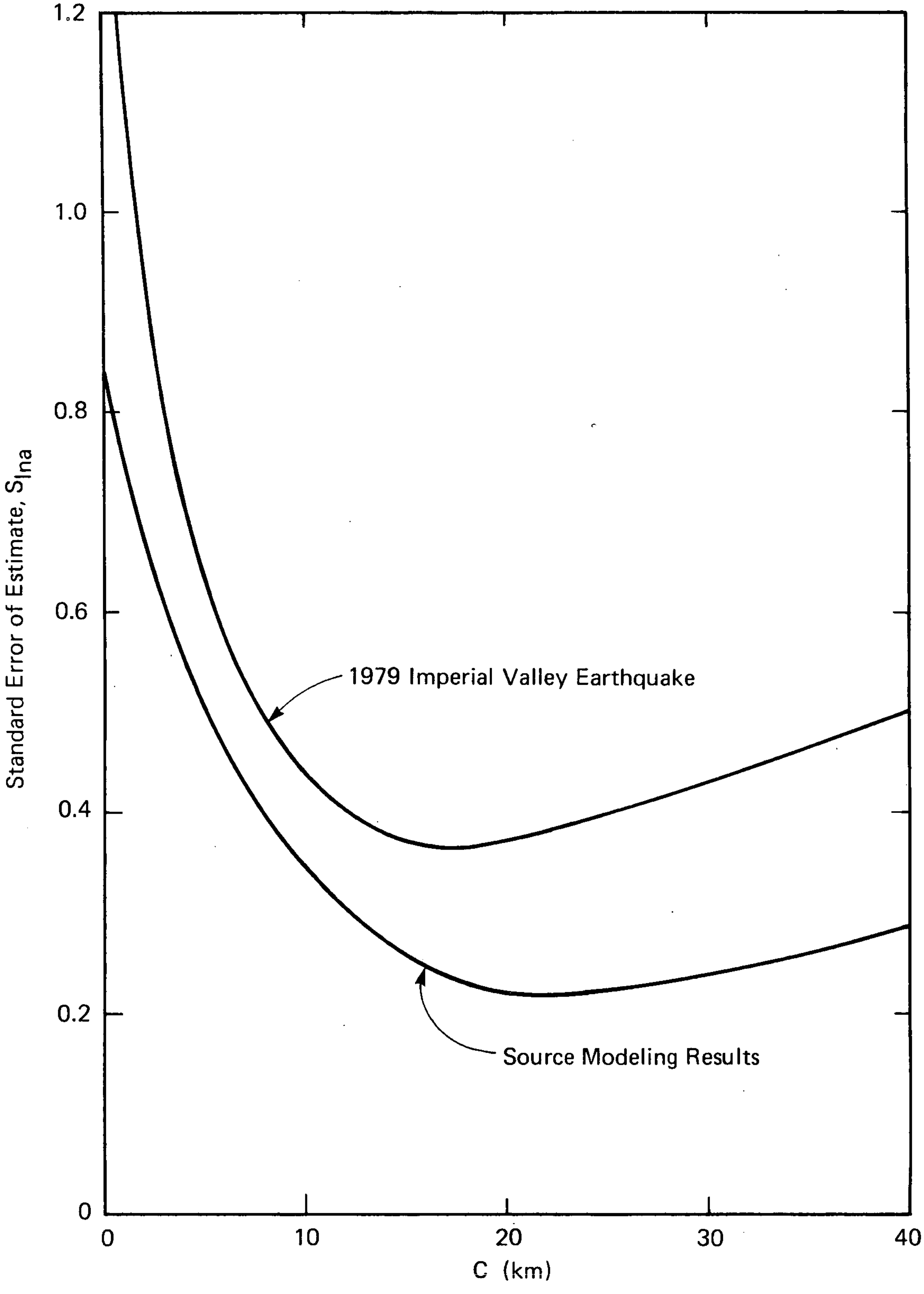

Fig. 361.53–4 – Variation in Standard Error of Estimate with Change in Parameter C

QUESTION 361.54

Using the site ground motion methodology in Chapter 5.0, extrapolate the ground motion at the site for magnitudes 7 and 7-1/2 on the OZD, given site specific spectra for magnitudes 6.5, 6.0 and 5.5 on the OZD at a distance of 10 km (See Question 361.62) from the site.

RESPONSE 361.54

The methodology used in Chapter 5.0 of the June 1979 report by Woodward-Clyde Consultants addressed only the development of ground motion parameters for earthquake magnitude 6-1/2. That methodology does not provide the means to extrapolate ground motion parameters to earthquakes with magnitudes greater than 6-1/2.

Hanks and Johnson (1976) summarized and examined most of the available near-source data; additional near-source data obtained during the 1975 Oroville earthquake aftershocks were subsequently added to these data (see Seekins and Hanks, 1978; Hanks, 1979). Based on the examination of these near-source data, Hanks (1979) restated the conclusion by Hanks and Johnson (1976) that "at least above magnitude 5, peak acceleration data at a fixed, close distance ($R \simeq 10$ km) only weakly depend on the magnitude of the earthquake. That is, peak accelerations at $R \simeq 10$ km 'saturate'."

The implication of this conclusion is that the estimated instrumental peak accelerations for SONGS due to a magnitude 6-1/2 earthquake, occurring on the hypothesized OZD at closest distance of 8 km from the site, is essentially applicable to higher magnitude earthquakes.

Alternatively, one could utilize the approach illustrated in Figure 361.54-1 to extrapolate peak accelerations at the site from magnitude 6-1/2 values to those for magnitudes greater than 6-1/2. Using the relationships provided by Idriss et al. (1980), Schanbel and Seed (1973), and Seed* (1980) the following acceleration ratios are obtained; these ratios are applicable to a closest distance of 8 km.

Relationship	a(7)/a(6-1/2)
Schnabel & Seed (1973)	1.12
Seed (1980)	1.08
Idriss and others (1980)	1.10

Using these ratios and the procedure shown in Figure 361.54-1, the extrapolated 84th percentile peak acceleration values are summarized below. Note that the 84th percentile peak acceleration estimated for SONGS is 0.57 g.

Relationship	$a(M_S = 7)$
Schnabel & Seed (1973)	0.64
Seed (1980)	0.62
Idriss et al. (1980)	0.63

The steps in extrapolating response spectra at the site from magnitude 6-1/2 values to those for larger magnitudes are shown in Figure 361.54-2. As shown in this figure, extrapolation from magnitude 6-1/2 to larger magnitudes using this procedure would require the following:

---

* Revised version of the relationships by Schnabel and Seed (1973)

1. Relationship between peak acceleration for magnitude M_s and peak acceleration for magnitude 6-1/2, i.e., $a\ (M_s)/a\ (6\text{-}1/2)$.

2. Relationship between response spectral shape for magnitude M_s and magnitude 6-1/2, i.e., $(s_v/a)_{M_s}/(S_v/a)_{6-1/2}$ as a function of period.

With regard to item 1 above, the ratio a(7)/a(6-1/2) = 1.11 is judged to be appropriate, based on the relationships by Idriss and others (1980), Schnabel and Seed (1973), and Seed (1980). Using this ratio and the 84th percentile instrumental peak acceleration of 0.57 g for M_s = 6-1/2, the extrapolated peak acceleration corresponding to M_s = 7 is 0.63 g.

As a comparison peak accelerations recorded during the 1979 Imperial Valley earthquake (M_s = 6.8) as discussed in section 3 of the response to Question 361.55 give an 84th percentile peak acceleration of 0.44 g at a closest distance of 8 km (the distance from the OZD to SONGS). Therefore, the acceleration data from the recent Imperial Valley earthquake indicate that the 84th percentile values of 0.57 g is conservative for M_s = 6-1/2. Consequently the extrapolated peak acceleration for M_s = 7 is also conservative.

With regard to item 2 (i.e., the effect of magnitude on response spectral shape), analysis of available response spectra lead to the following observations:

1. In the period range zero to approximately 0.2 seconds, the normalized spectra, S_v/a, are essentially constant and equal to unity. Therefore, the response spectral ratios, $S_v(M_s)/S_v(6\text{-}1/2)$, are essentially proportional to the ratios of the peak ground acceleration, $a(M_s)/a(6.5)$.

2. For the period range of approximately 1 to 2 seconds, the normalized spectra, S_v/a, have a value of about 1.25 for magnitude (M_s) 7.

Using the procedure illustrated in Figure 361.54-2, with the information given above, the scaling ratio, $S_v(7)/S_v(6\text{-}1/2)$, is computed to be 1.11 for periods up to 0.2 seconds and 1.4 for periods in the range 1 to 2 seconds. For periods between 0.2 and 1 seconds, scaling ratios were obtained by interpolation. The 84th percentile instrumental response spectrum for magnitude (M_s) 7 earthquake on the OZD was obtained by extrapolating the SONGS 84th percentile instrumental response spectrum for magnitude (M_s) 6-1/2 earthquake (see Figure 11 of the June 1979 WCC report). These spectra are compared with the DBE spectrum for SONGS in Figure 361.54-3. It is noted that the DBE spectrum exceeds the 84th percentile instrumental spectra for magnitudes (M_s) 6-1/2 and 7 at all periods.

REFERENCES

Hanks, T. C., 1979, Seismological aspects of strong motion seismology: 2nd U. S. National Conference on Earthquake Engineering, August 2-24, Proceedings, p. 898-912.

Hanks, T. C., and Johnson, D. A., 1976, Geophysical assessment of peak accelerations: Seismological Society of America Bulletin, v. 66, no. 3, June, p. 959-968.

Idriss, I. M., Sadigh, K., and Power, M. S. 1980, Variations of peak accelerations, velocities and displacements with magnitude at close distances to the source: Paper prepared for submission to BSSA for possible publication.

Schnabel, P. B., and Seed, H. B., 1973, Accelerations in rock for earthquakes in the western United States: Seismological Society of America Bulletin, v. 63, no. 2, p. 501-516.

Seekins, L. C., and Hanks, T. C., 1978, Strong motion accelerograms of the Oroville aftershocks and peak accelerations data: Seismological Society of America Bulletin, v. 68, p. 677-689.

Personal Communications

Seed, H. B., 1980, Professor, University of California Berkeley, California.

Results of the Empirical Study on the Effect of Magnitude on Peak Acceleration

Relationship between Peak Acceleration for Magnitude M_s and Peak Acceleration for $M_s = 6.5$

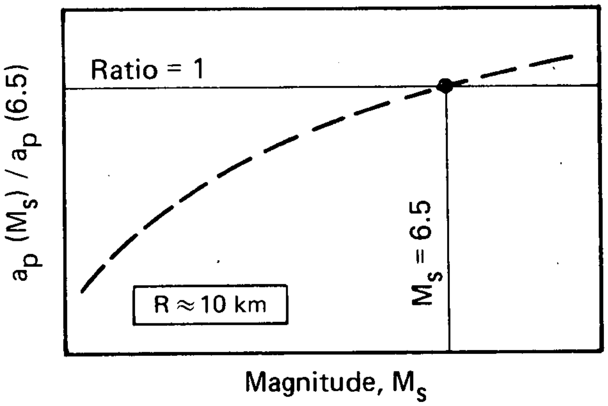

Peak Instrumental Acceleration at SONGS Site Associated with Earthquakes on the OZD for Magnitudes Greater than $M_s = 6.5$

Fig. 361.54–1 – Illustration of the Procedure to Develop Instrumental Site Acceleration Associated with Earthquakes on the OZD for Magnitudes Greater than 6.5

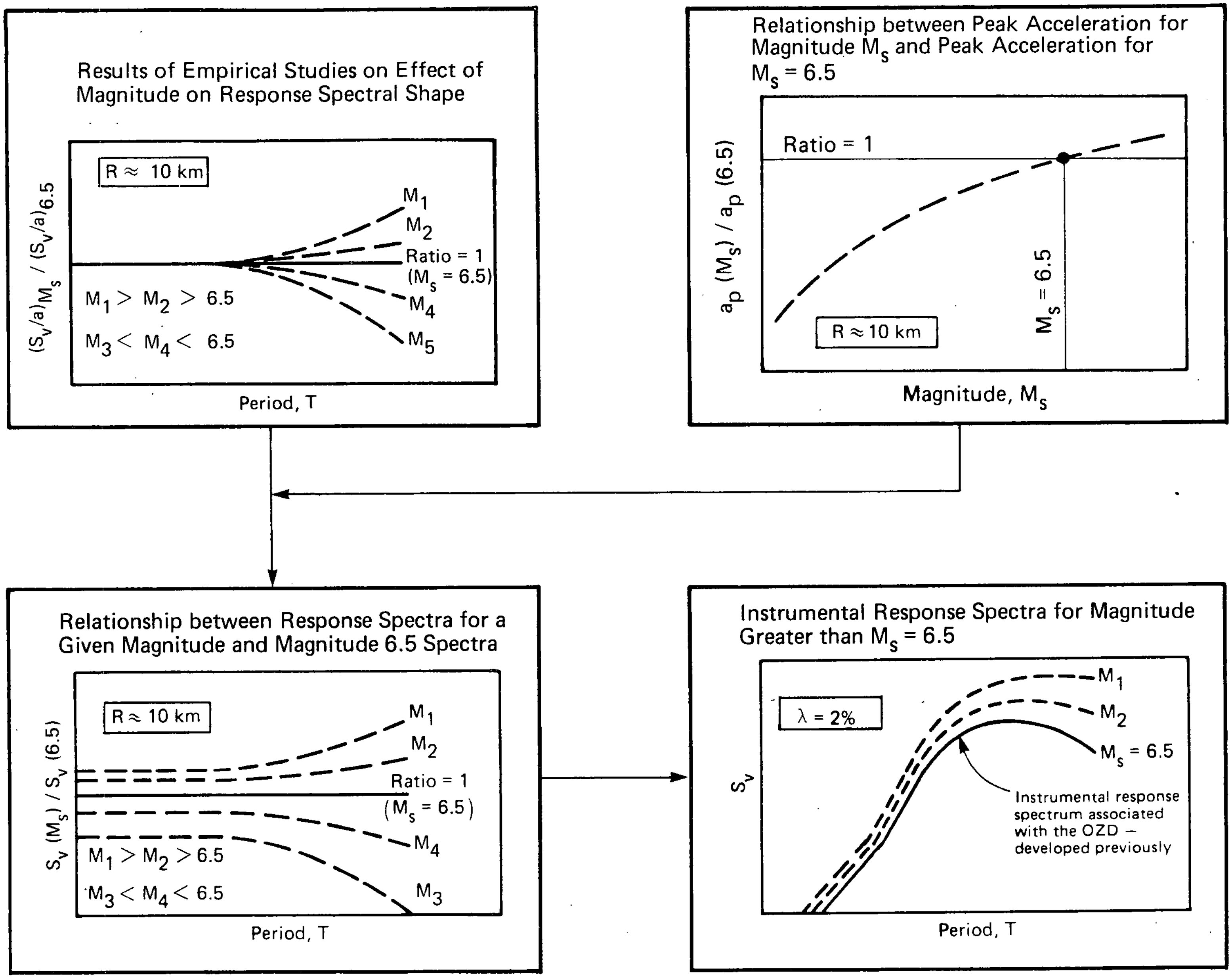

Fig. 361.54–2 — Illustration of the Procedure to Develop Instrumental Response Spectra Associated with Earthquakes on the OZD for Magnitudes Greater than 6.5

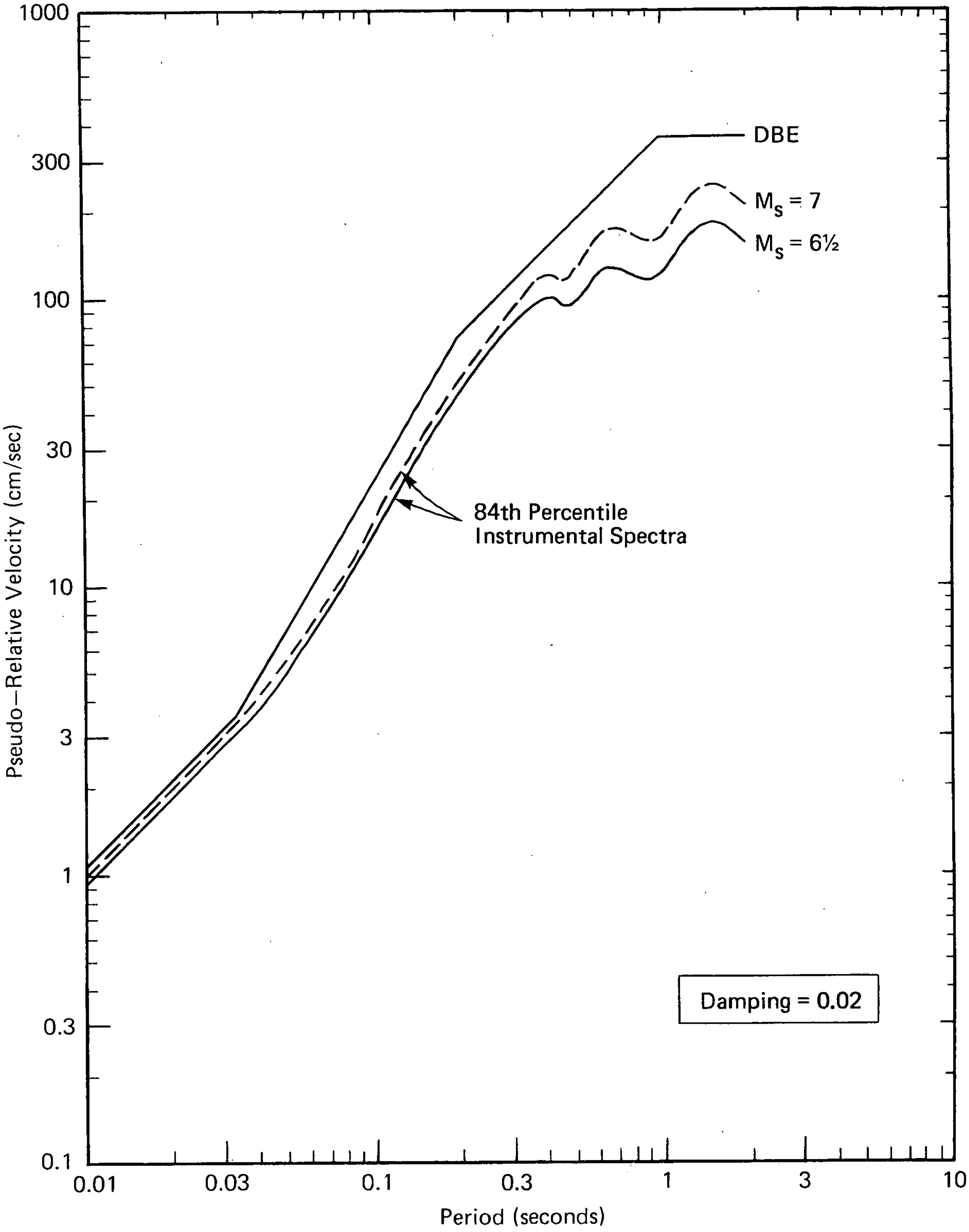

Figure 361.54 - 3 – Instrumental Response Spectra for $M_S = 7$ Extrapolated form SONGS Spectrum for $M_S = 6\frac{1}{2}$

QUESTION 361.55

Strong motion data recorded at the base of large buildings have been included in the ground motion analysis. Work by Boore and others (1978) and Crouse (1978) suggests that the peak acceleration values recorded at such sites may be biased downward from the values that would have been recorded under free-field conditions. A number of records have been included form NW California earthquakes, the locations of which are subject to notoriously large uncertainties. The weighting scheme gives these data equal weight with the San Fernando data for which the distances are much more accurately known. Also, a larger number of strong motion data points have been attained very near to the fault during the two recent California earthquakes (Coyote Lake August 6, 1979, and Imperial Valley October 15, 1979).

a. Please assess the impact of these comments and of the new data on your estimates of peak ground motion at the SONGS site.

b. Assess the impact of these comments and of the new data on the design response spectra at the SONGS site.

References

Boore, D. M. Joyner, W. B., Oliver, A. A. III, and Page, R. A., 1978, Estimation of Ground Motion Parameters: U.S. Geological Survey, Circular 795, 43 p.

Crouse, C. B., 1978, Prediction of Free-field Earthquake Ground Motions: Proceeding, ASCE Specialty Conference Earthquake Engineering and Soil Dynamics, v. 1, p. 359-379.

RESPONSE 361.55

1-a. Review of the work by Boore and others (1978) and Crouse (1978):

Through regression analyses of selected data from the 1971 San Fernando earthquake, Boore and others (1978) suggest that peak accelerations recorded at the base of large structures are less than peak accelerations recorded at the base of small structures. For their analyses, Boore and others (1978) used data from soil sites located in the distance range 15 to 100 km. Inspection of these data indicates that not for all distance ranges do the data points equally well represent both small and large structures as noted below:

	Number of Data Points from	
Distance Range (km)	Small Structures	Large Structures
15 - 20	0	4
20 - 30	3	4
30 - 50	3	4
50 - 100	6	6
	12	18

These data are plotted in Figure 32 of the report by Boore and others (1978). In the distance range 15 to 20 km, no comparison is possible of the effect of structure size on peak acceleration. In the distance range 30 to 50 km, the peak accelerations vary by an unusually large amount; thus, they may not be suitable as a basis for any statistical inferences. If the data in the distance ranges 20 to 30 km and 50 to 100 km are examined, it is difficult to discern any trend for differences in peak accelerations recorded at the base of small and large structures. Boore and others (1978) observed that "the differences between the data from the large structures and the small structures are relatively small compared with the range of either data set, and we do not believe that firm conclusions are warranted solely on the basis of formal statistical tests. The differences may be due to soil-structure interaction, but more study would be required to demonstrate this." The Applicants concur with this opinion.

The work presented by Crouse (1978) is an examination of recorded ground motions in terms of spectra rather than peak acceleration; in particular, the influence of soil-structure interaction on the recorded ground motions. Based on a comparison of free-field recordings with those from the base of nearby structures for the same earthquake, Crouse (1978) concluded that "the only significant effect of soil-structure interaction that may be present in the strong-motion records is believed to be the filtering of high frequency seismic waves by the foundation of buildings in which the motions were recorded." Crouse (1978) further states that "this phenomena is probably only significant in buildings with relatively large foundations." Crouse (1978) however, indicated that the effects of soil-structure interaction and local site conditions on spectra cannot be clearly isolated because of the types of recordings available. Most of the recordings on rock have been made in small structures, whereas most of the recordings on soil were made in larger multi-story structures and the data base for either the soil-structure interaction or local site conditions effects is not yet sufficient to draw definitive conclusions.

<u>1-b. Impact of Observations Regarding the Effect of Structure Size on Recorded Ground Motions</u>

To assess the influence of the structure size on the estimated ground motion for SONGS a review was made of the work by Boore and others (1978) and Crouse (1978). The pertinent observations from this review are described in Item 1-a. These observations indicate that it is not possible to distinguish differences in ground motions due to differences in structure size with the currently available data base.

2-a. Influence of Northwest California Earthquake Data on Regression Results

To examine the impact of including data from the Northwest California earthquakes, parametric studies were made in which records from these earthquakes were excluded from the weighted regression analyses. In the first parametric analysis, records from the 1934 Eureka earthquake, 1941 Northwest California earthquake, and 1941 Eureka earthquake records were excluded. The 1954 Eureka earthquake records were included in this first analysis because this earthquake is well located based on studies by Smith (1977). In the second parametric analysis, the records from all four Northwest California earthquakes were excluded. The results of both of these analyses gave lower peak accelerations at the 10 km energy center distance than the peak accelerations obtained from the analysis presented in Appendix J of the June 1979 WCC report.

2-b. Impact of the Northwest California Earthquake Data

The impact of including data from the Northwest California earthquakes on the estimated ground motion for SONGS is discussed in Item 2-a. Excluding these data would result in lower peak accelerations indicating no need to revise the estimated values of ground motions for SONGS due to their inclusion in the selected data base.

3-a. Examination of Recordings from the August 6, 1979 Coyote Lake and October 15, 1979 Imperial Valley Earthquakes

Recordings obtained during the August 6, 1979 Coyote Lake and the October 15, 1979 Imperial Valley earthquakes have significantly increased the available strong motion data base, particularly for recordings near the fault rupture surface. The Coyote Lake earthquake was located in the Calaveras fault zone near Gilroy, California at a focal depth of approximately 10 kilometers. The Imperial Valley earthquake was located on the Imperial fault in southern California and northern Mexico and had a shallow focal depth (approximately 10 km). Surface rupture occurred during the 1979 Imperial Valley earthquake and very closely followed the fault rupture trace of the 1940 Imperial Valley earthquake. Magnitudes for the two earthquakes have been assigned as follows:

	m_b	M_S	M_L
1979 Coyote Lake	5.3	5.6	5.9
1979 Imperial Valley	5.6	6.8	6.6

At the location of each of these recent earthquakes, an array of strong motion stations had been positioned across the fault zone and was in operation at the time of the earthquake. These and other nearby stations provided substantial information on ground motions close to the rupture. The majority of these recording stations are instrument shelters or small buildings.

For the 1979 Coyote Lake earthquake, eight stations within 20 kilometers recorded the ground motion. Of these stations, three were within five kilometers and two between 10 and 20 kilometers of the rupture surface. Forty-six other stations recorded the motion at distances between 20 and 120 kilometers from the rupture surface.

For the 1979 Imperial Valley earthquake, a total of 32 stations recorded the ground motion at distances up to 160 kilometers. Six of the stations were within 5 kilometers of the rupture; eight stations were between 5 and 10 kilometers; five were between 10 and 20 kilometers; and six were between 20 and 40 kilometers of the rupture. The other seven stations were at distances greater than 40 kilometers from the rupture.

Peak horizontal accelerations recorded during these recent earthquakes are illustrated in Figure 361.55-1 versus distance to the rupture surface. All of the data for the 1979 Imperial Valley earthquake have been presented. For the smaller magnitude 1979 Coyote Lake earthquake, however, only the data within 20 kilometers of the rupture surface are presented. The corresponding response spectra available from the 1979 Imperial Valley earthquake are illustrated for a subsequent question in Figures 361.57-2 and 361.57-3.

A subset of these spectra from the 1979 Imperial Valley earthquake is illustrated in Figure 361.55-2. These spectra are for the distance range of 6 to 13 km from the rupture surface. The envelope and mean and 84th percentile on these 14 spectra are illustrated in Figure 361.55-3.

3-b. Impact of the New Data from the 1979 Imperial Valley and the 1979 Coyote Lake Earthquakes

Both Imperial Valley and Coyote Lake earthquakes are well defined, well located, and produced a large number of high quality near source strong motion recordings as summarized in Item 3-a above. However, the recordings obtained during the 1979 Imperial Valley earthquake are of much greater significance. The features of this earthquake and its recordings, that make it particularly well-suited to developing ground motions parameters at SONGS from the postulated events on the hypothesized OZD, are summarized below:

1. The reported surface wave magnitude is (M_S) 6.8.

2. The earthquake was shallow (focal depth of approximately 10 km).

3. It had a vertical rupture surface and predominantly strike-slip right-lateral movement.

4. The earthquake rupture initiated near the United States-Mexican border and spread toward the network of ground motion recording stations around El Centro; consequently, the strong motion data include effects due to focusing.

5. The earthquake is well-located and occurred in the southern California tectonic environment.

6. Over twenty (20) high quality and uniformly processed recordings are available for distances up to 40 km.

7. Essentially all recording instruments were located in small structures at ground level.

The impact of the 1979 Imperial Valley data on the estimates of peak acceleration and response spectra at the SONGS sites is discussed below.

The recorded peak accelerations for the 1979 Imperial Valley earthquake are illustrated in Figure 361.55-4 with the SONGS attenuation curves (from Appendix J of the 1979 Woodward-Clyde Consultants report) plotted in terms of closest distance to the rupture surface. A comparision of these indicates that, in general, the SONGS curves exceed the Imperial Valley data and that the SONGS 84th percentile curve is essentially the upper bound of the Imperial Valley data. For a closest distance of 8 km (the distance from the OZD to SONGS), the 1979 Imperial Valley data give mean and 84th percentile peak acceleration values of 0.32 g and 0.44 g, respectively. The mean and 84th percentile values estimated for SONGS are 0.42 g and 0.57 g, respectively.

The mean and 84th percentile response spectral values for distances of 6 to 13 km, presented in Figure 361.55-3 for the 1979 Imperial Valley earthquake, are illustrated in Figure 361.55-5 with the DBE spectrum and the empirically derived instrumental mean and 84th percentile spectra for the 1979 Imperial Valley earthquake. The DBE spectrum exceeds both SONGS and 1979 Imperial Valley.

On the basis of these comparisons of the 1979 Imperial Valley earthquake data with the relationships developed for SONGS, it may be concluded that the peak accelerations and response spectra estimated for SONGS are realistic and conservative ground motion parameters for an earthquake of magnitude 6-1/2 on the hypothesized OZD.

REFERENCES

Boore, D. M. Joyner, W. B., Oliver, A. A. III, and Page, R. A., 1973, Estimation of ground motion parameters,: U.S. Geological Survey Circular 795, 43 p.

California Division of Mines and Geology, 1979, Partial film records and preliminary data, Imperial Valley earthquake of 15 October 1979, Imperial County Services Building."

Crouse, C. B., 1978, Prediction of free-field earthquake ground motions: ASCE Specialty Conference on Earthquake Engineering and Soil Dynamics, Proceedings, v. 1, p. 359-379.

Porcella, R. L. Matthiesen, R. B. McJunken, R. D., and Ragsdale, J. T., 1979, Compilation of strong-motion records from the August 6, 1979 Coyote Lake Earthquakes: U.S.Geological Survey Open-File Report 79-385, October.

Porcella, R. L. and Matthiesen, R. B., 1979, Preliminary summary of the U.S. Geological Survey strong-motion records from the October 15, 1979 Imperial Valley earthquake: U.S.Geological Survey Open-File Report 79-1654, 41 p.

Smith, S. W., 1977, Tectonic significance of large historic earthquakes in the Eureka Region: Draft Report from TERA Corporation submitted to PG and E September 9.

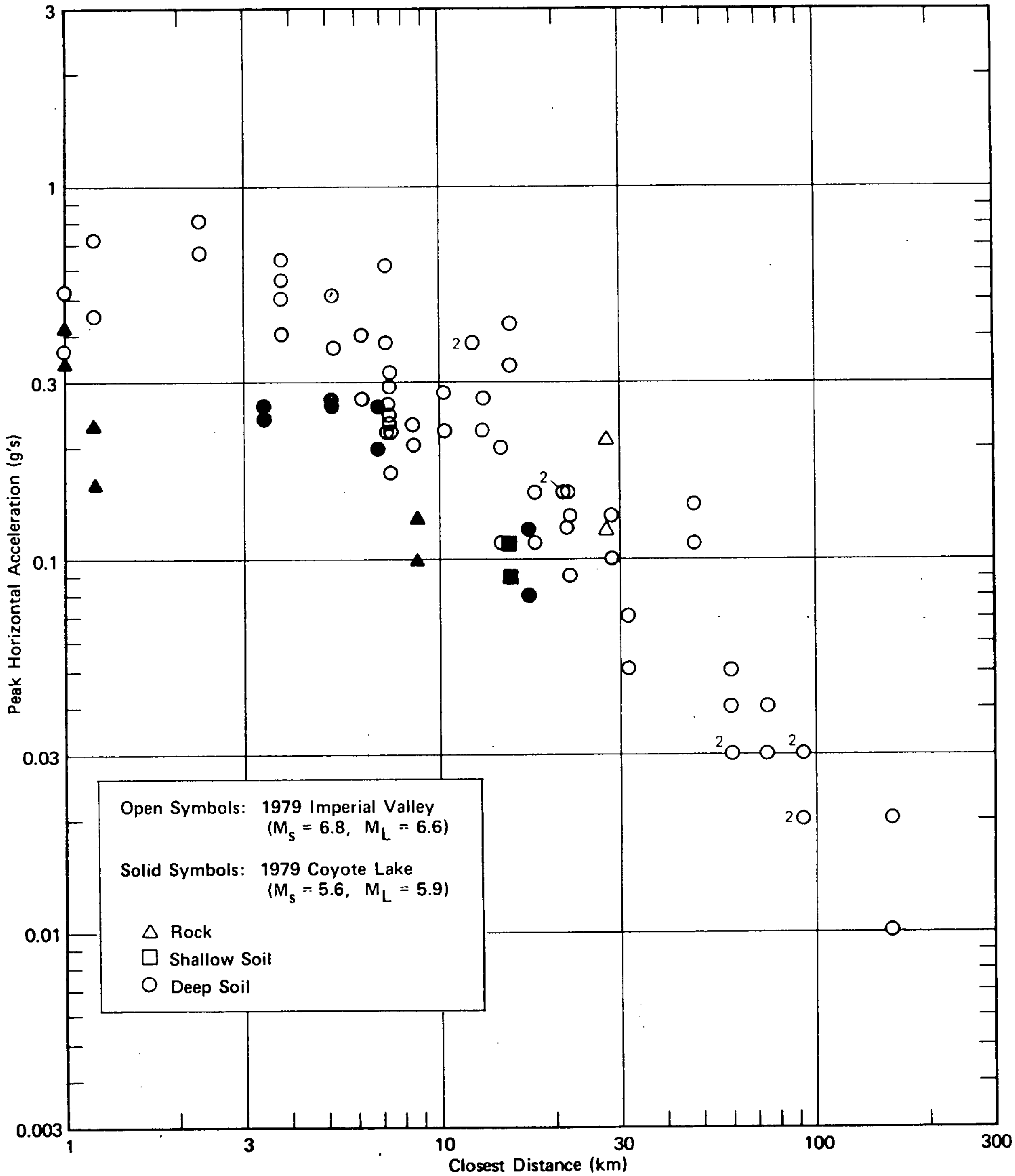

Fig. 361.55–1 – Plot of Peak Acceleration versus Closest Distance for Recordings Obtained during the 1979 Coyote Lake and 1979 Imperial Valley Earthquakes

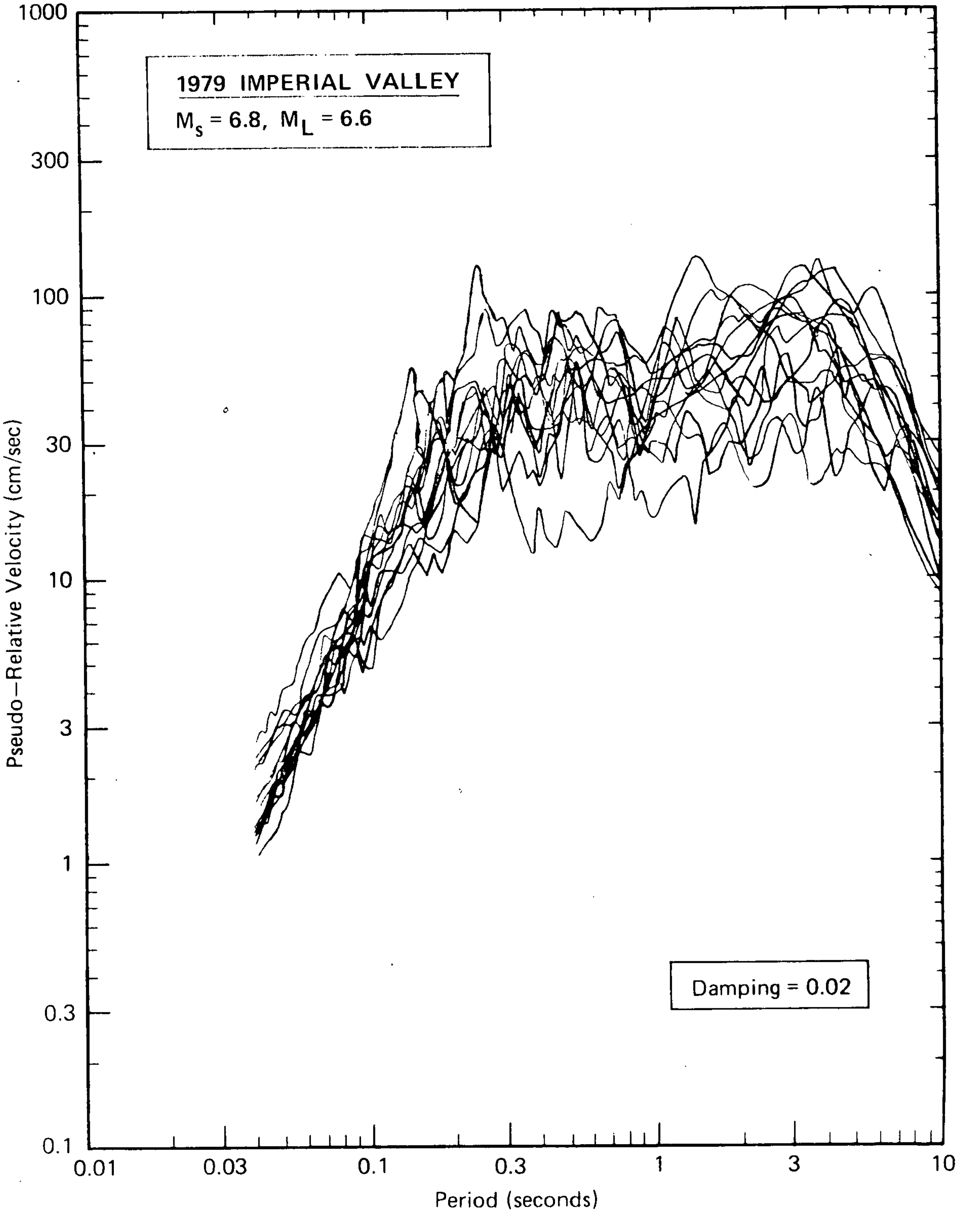

Fig. 361.55–2 – Response Spectra for the 1979 Imperial Valley Earthquake Recorded at Stations between 6 and 13 Kilometers of the Rupture Surface

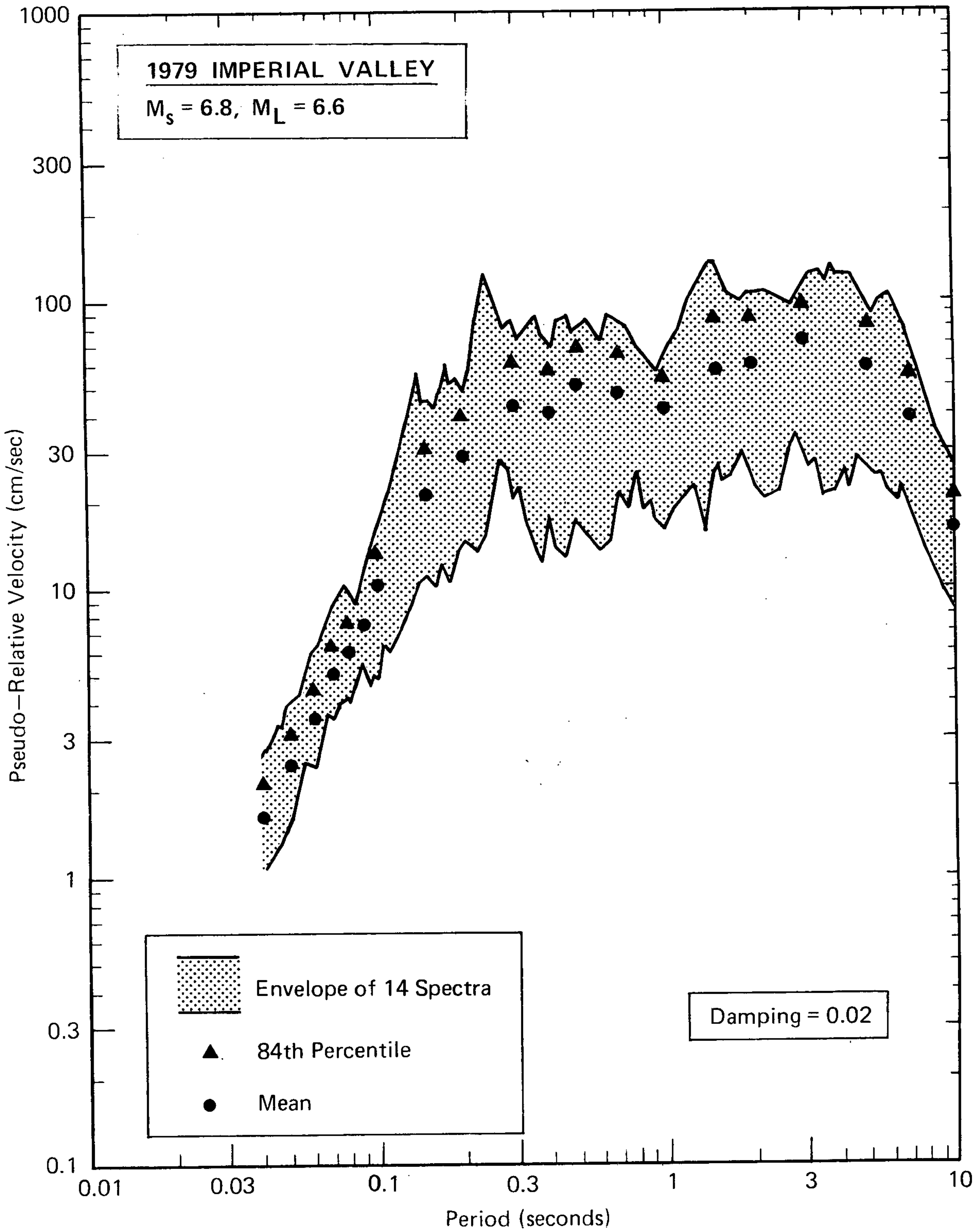

Fig. 361.55–3 – Envelope and Mean and 84th Percentile Values of the 14 Response Spectra shown in Fig. 361.55–2

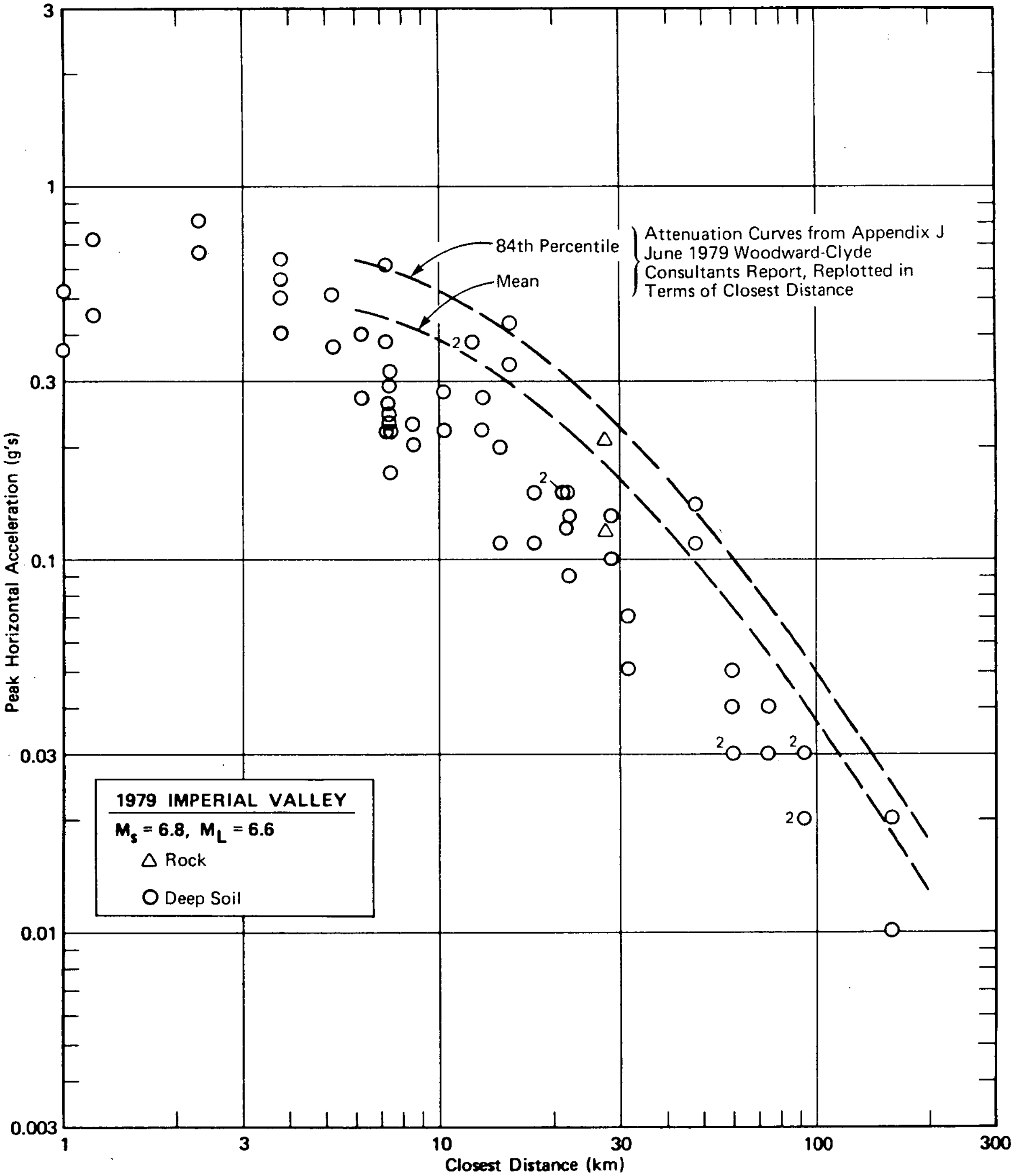

Fig. 361.55–4 – Comparison of Peak Acceleration for Recordings Obtained during the 1979 Imperial Valley Earthquake with the SONGS Attenuation Relationships Plotted in Terms of Closest Distance

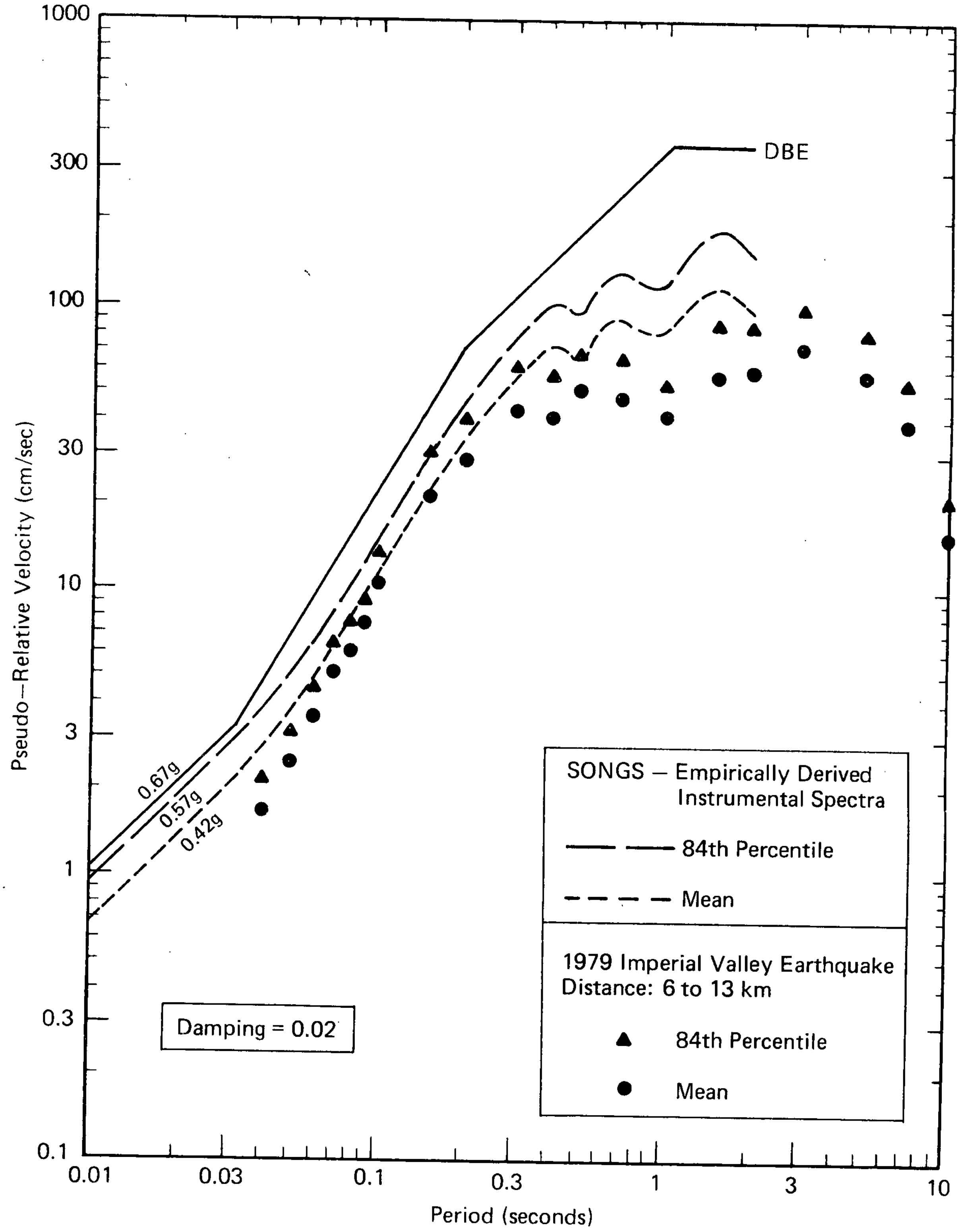

Fig. 361.55–5 – Comparison of the Mean and 84th Percentile Spectra shown in Fig. 361.55–3 for the 1979 Imperial Valley Earthquake with the SONGS Instrumental Spectra and the DBE Spectrum

QUESTION 361.56

Consider the focusing effect in developing the design spectra for San Onofre reactors 2 and 3. Explore the possible design implications of this phenomenon. If the focusing effect significantly modifies the design peak acceleration, does this materially change the selection of the appropriate design spectra which would be adopted for construction?

RESPONSE 361.56

Potential effects of focusing have been investigated using theoretical results and empirical observations. Both approaches demonstrate that the empirically derived spectra presented in the WCC report of June 1979 appropriately includes focusing effects. Furthermore, since WCC's empirically derived spectra are well below the DBE over the entire period range, the DBE accommodates any effects due to earthquake focusing, and, in fact, the DBE has a substantial degree of conservatism with respect to focusing effects.

Careful examination of the data used in the empirical study reported in the June 1979 WCC report indicates that focusing effects have been suitably included in the study. The large majority of strong motion data used in the study was recorded under conditions of above-average focusing. (See Table 361.56-1). For example, the recording of the San Francisco earthquake, located south of the San Gabriel Mountains, resulted from focused rupture within an elevated lobe of the shear-wave radiation pattern with the possibility of additional amplification due to the wedge-shaped geometry of the underlying sedimentary basin. In contrast, strike-slip faulting along the OZD cannot focus seismic energy directly at the San Onofre site due to fault-site geometry.

TABLE 361.56-1

THEORETICAL EVALUATION OF THE EFFECT OF SOURCE PARAMETERS ON STRONG MOTION DATA

EVENT	STATION (USGS No.)	DIRECT-IVITY	RADIATION PATTERN
1933 Long Beach	288	E	E
1934 Eureka	1023	I	E
1941 NW Calif.	1023	I	0
1941 N. Calif.	1023	I	D
1954 Eureka	1022	I	0
1954 Eureka	1023	0	I
1968 Borrego Mtn.	290	0	0
1971 San Fernando	241	E	E
"	157	E	E
"	110	0	E
"	137	E	E
"	288	E	E
"	190	0	E
"	1052	0	0
"	264	0	E
"	267	0	E
"	431	E	E
"	220	E	E
"	280	0	0
"	472	0	E
"	290 (C.I.T. M183)	0	0
"	290 (C.I.T. M184)	0	0

TABLE 361.56-1 (cont'd)

EVENTS	STATION (USGS No.)	DIRECT-IVITY	RADIATION PATTERN
1971 San Fernando	449	E	E
"	114	0	0
"	172	E	E
"	145	E	E
"	148	E	E
"	443	E	E

Note: The legend used in Table 361.56-1 is as follows:

SYMBOL	MEANING
D	Effect of this parameter is expected to have diminished measured ground motions;
0	No effect is expected;
E	Effect of this parameter is expected to have enhanced measured ground motions;
I	The indeterminacy of the parameter makes it impossible to provide an evaluation.

QUESTION 361.57

List the available free field strong motion records from earthquakes of magnitude (M_S) greater than 6.7 on strike slip faults recorded at distances of less than 40 km from the rupture surface. (Note the foundation conditions at the recording sites.) Plot the response spectra from these records and the SSE design spectrum for 2 percent of critical damping.

RESPONSE 361.57

The available strong motion records within 40 kilometers of the rupture surface from earthquakes of magnitude (M_S) greater than 6.7 with strike slip faulting are listed in Table 361.57-1. The information presented in Table 361.57-1 for the 1979 Imperial Valley earthquake was compiled from Porcella and Matthiesen (1979) and California Division of Mines and Geology (1979). Plots of the response spectra from these records and the SSE design spectrum for 2 percent of critical damping are illustrated in Figs. 361.57-1 through 361.57-23.

Figure 361.57-1 illustrates the response spectra obtained for the 1940 Imperial Valley earthquake (M_S = 7.1). Figures 361.57-2 through 361.57-16 illustrate the response spectra obtained for the 1979 Imperial Valley earthquake (M_S = 6.8) at stations between 0 and 16 kilometers from the rupture surface. The envelope of these 1979 Imperial Valley earthquake spectra is presented in Figure 361.57-17. Response spectra for the recordings at distances between 16 and 40 kilometers from the 1979 Imperial Valley earthquake are illustrated in Figures 361.57-18 through 361.57-22. The envelope of these 1979 Imperial Valley earthquake spectra is presented in Figure 361.57-23.

REFERENCES

California Division of Mines and Geology, 1979, Partial film records and preliminary data, Imperial Valley Earthquake of 15 October 1979, Imperial County Services Building.

Porcella, R. L., and Matthiesen, R. B., 1979, Preliminary summary of the U. S. Geological Survey strong-motion records from the October 15, 1979 Imperial Valley Earthquake: U. S. Geological Survey Open-File Report 79-1654, 41 p.

TABLE 361.57-1

AVAILABLE STRONG MOTION RECORDS WITHIN 40 KILOMETERS OF THE RUPTURE FROM EARTHQUAKES OF M_S >6.7 WITH STRIKE-SLIP FAULTING

USGS Station No.	Structure	Subsurface Conditions	Distance (km)	Acceleration Azimuth (Degree)	Acceleration Peak Value (g)
	May 18, 1940 Imperial Valley, California Earthquake M_S = 7.1				
117	2-Story Building	Alluvium, more than 300 m.	10	S00E S90W	0.35 0.22
	October 15, 1979 Imperial Valley, California Earthquake M_S = 6.8				
5028	1-Story Building	Alluvium, more than 300 m	1	230 140	0.52 0.36
942	Instrument Shelter	"	1	230 140	0.45 0.72
5054	1-Story Building	"	3	230 140	0.81 0.66
958	Instrument Shelter	"	3	230 140	0.50 0.64
952	Instrument Shelter	"	4	230 140	0.40 0.56
5165	1-Story Building	"	5	360 270	0.51 0.37
117	2-Story Building	"	6	360 090	0.40 0.27
955	Instrument Shelter	"	7	230 140	0.38 0.61
5090	6-Story Building	"	7	360 090	0.29 0.32
5090	Instrument Pad	"	7	092 002	0.24 0.24
5060	Instrument Shelter	"	7	315 225	0.22 0.17
5055	1-Story Building	"	8	315 225	0.22 0.26
412	1-Story Building	"	9	050 320	0.20 0.23
5053	1-Story Building	"	10	315 225	0.22 0.28
5058	1-Story Building	"	13	230 140	0.38 0.38
5057	1-Story Building	"	13	230 140	0.22 0.27
5051	1-Story Building	"	15	315 225	0.20 0.11
515	Instrument Shelter	"	16	230 140	0.43 0.33
931	Instrument Shelter	"	18	230 140	0.11 0.15
5061	2-Story Building	"	21	315 225	0.09 0.13
5059	1-Story Building	"	22	230 140	0.15 0.12
5056	Instrument Shelter	"	22	230 140	0.15 0.15
286	1-Story Building	Granitic Rock	26	135 045	0.21 0.12
5062	1-Story Building	Alluvium, more than 300 m	28	315 225	0.10 0.13
5052	1-Story Building	"	31	135 045	0.07 0.05

Notes:

1. Instruments located at ground level
2. Distance represents closest distance to the rupture surface
3. Response spectra presently not available for stations Nos. 117, 5061, 5062 and 5090 for the 15 Oct. 1979 Imperial Valley Earthquake.

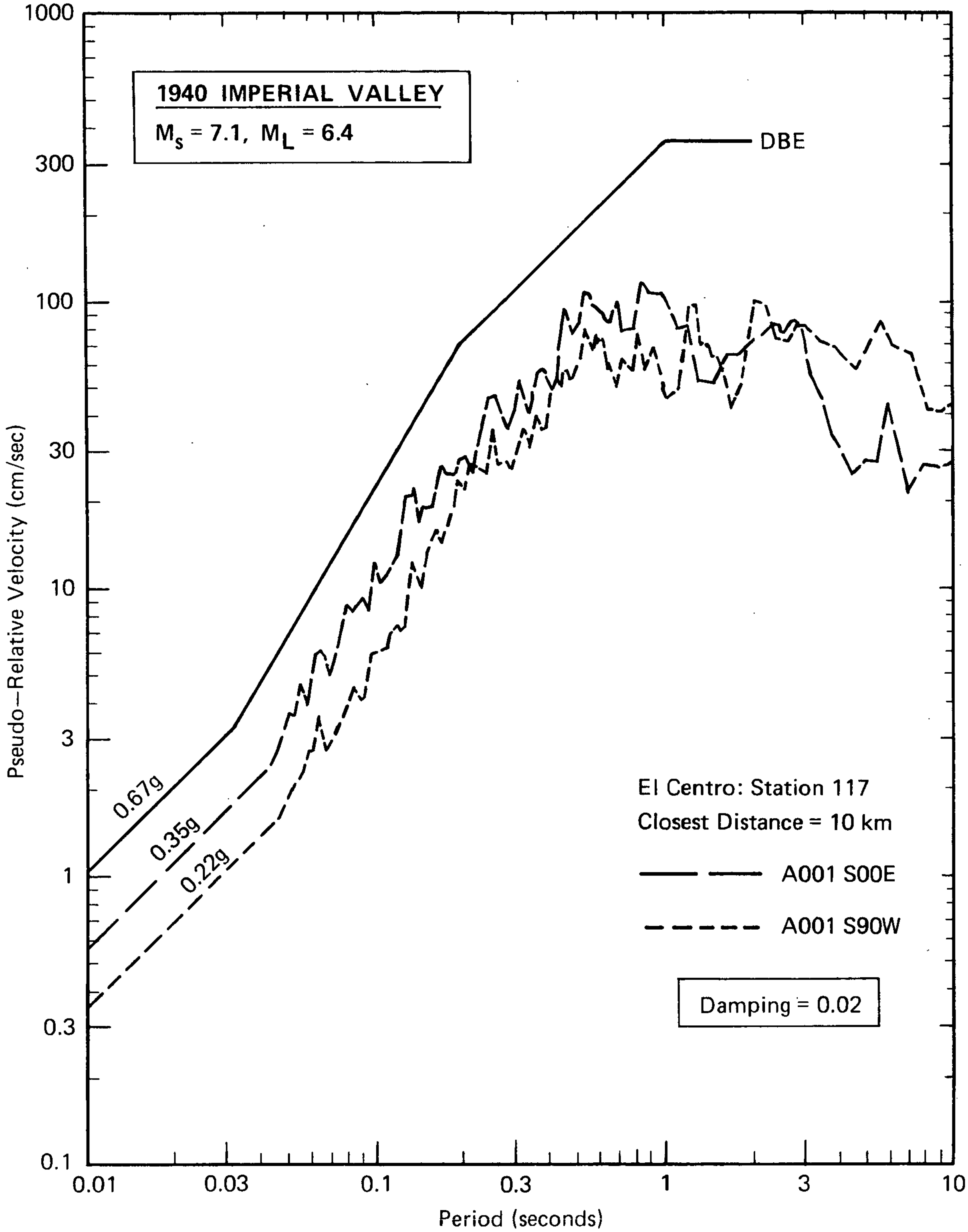

Figure 361.57–1 – Plot of the DBE Spectrum and the Response Spectra for the 1940 Imperial Valley Earthquake Recorded at USGS Station No. 117

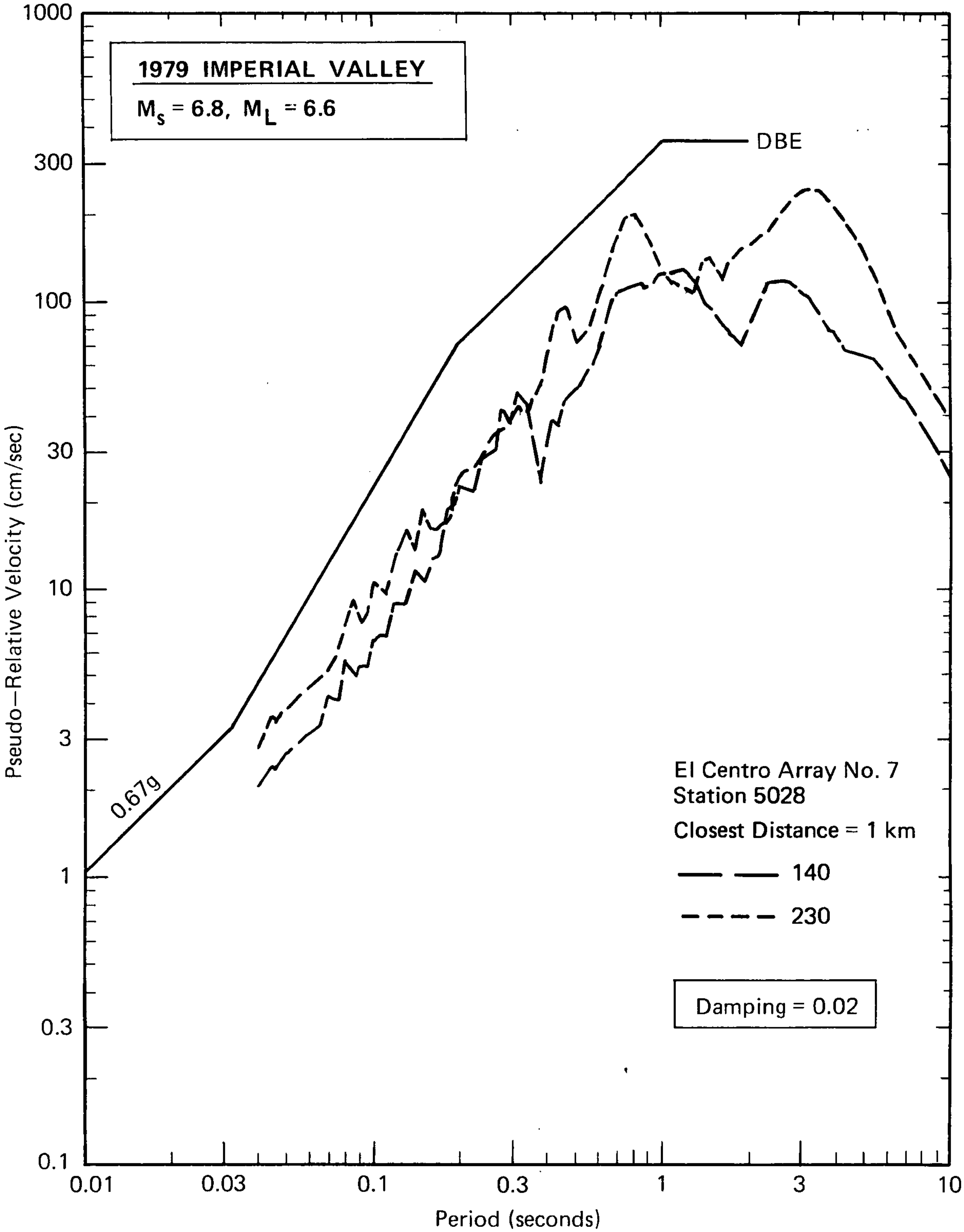

Fig. 361.57–2 – Plot of the DBE Spectrum and the Response Spectra for the 1979 Imperial Valley Earthquake Recorded at USGS Station No. 5028

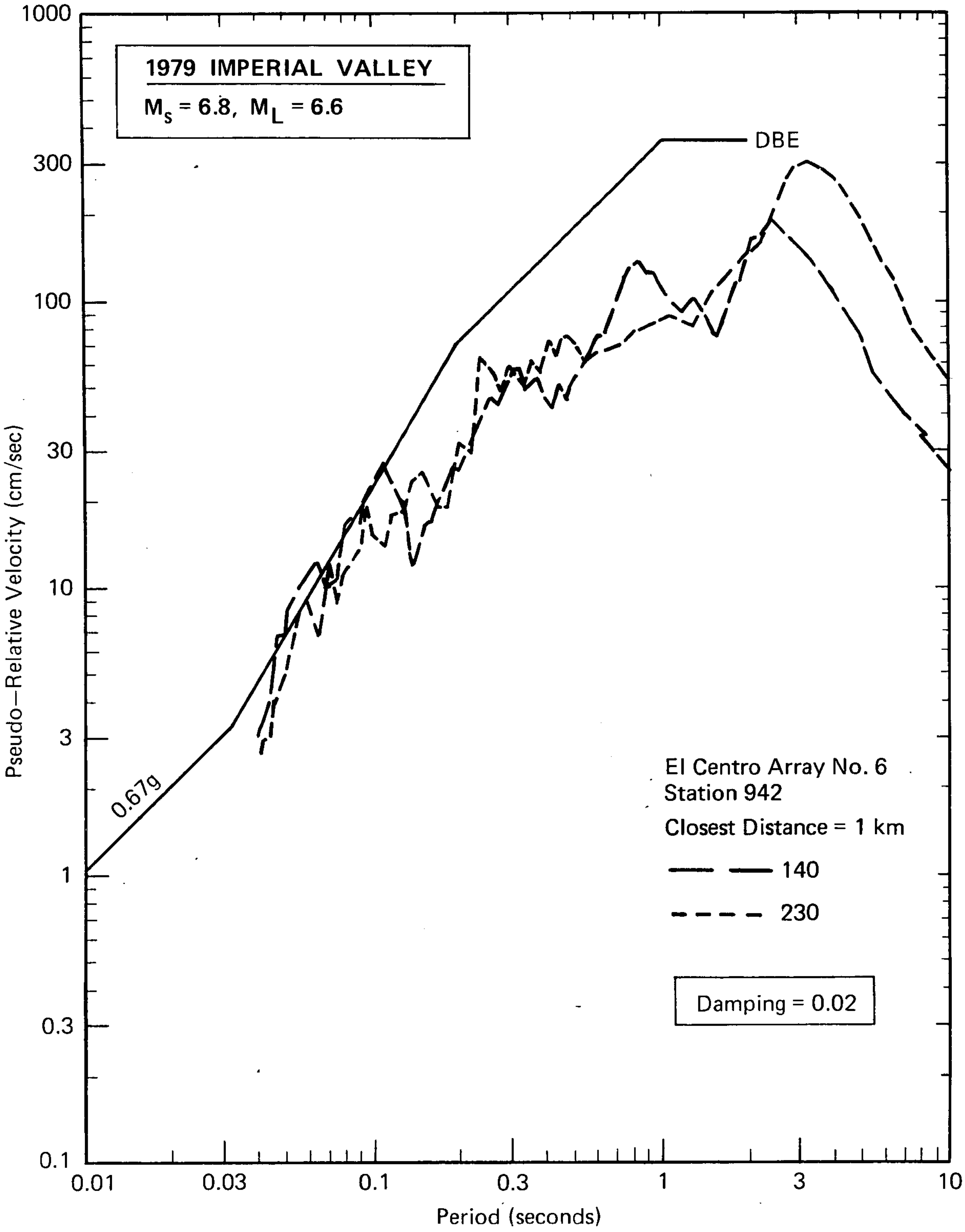

Fig. 361.57–3 – Plot of the DBE Spectrum and the Response Spectra for the 1979 Imperial Valley Earthquake Recorded at USGS Station No. 942

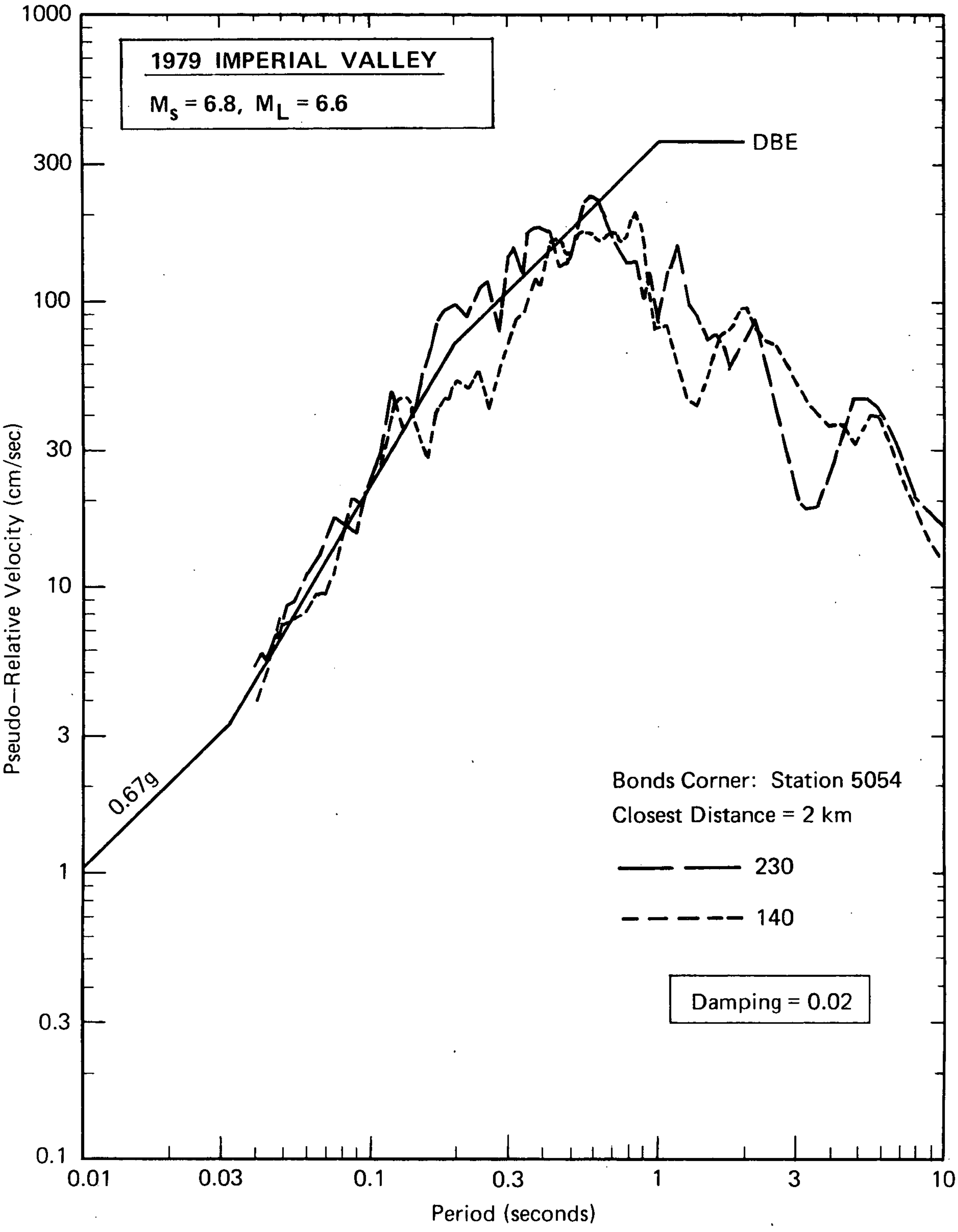

Fig. 361.57–4 – Plot of the DBE Spectrum and the Response Spectra for the 1979 Imperial Valley Earthquake Recorded at USGS Station No. 5054

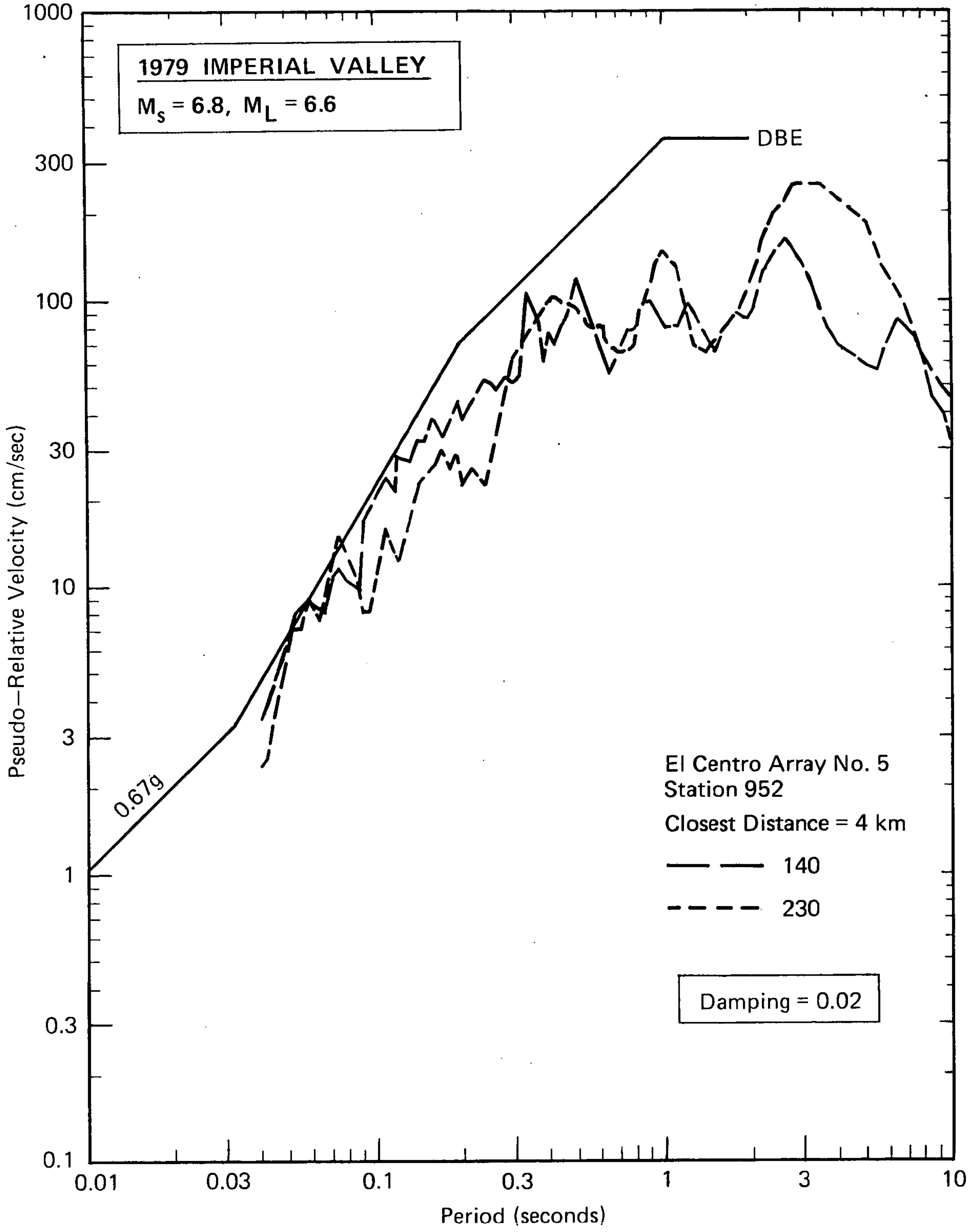

Fig. 361.57–5 – Plot of the DBE Spectrum and the Response Spectra for the 1979 Imperial Valley Earthquake Recorded at USGS Station No. 952

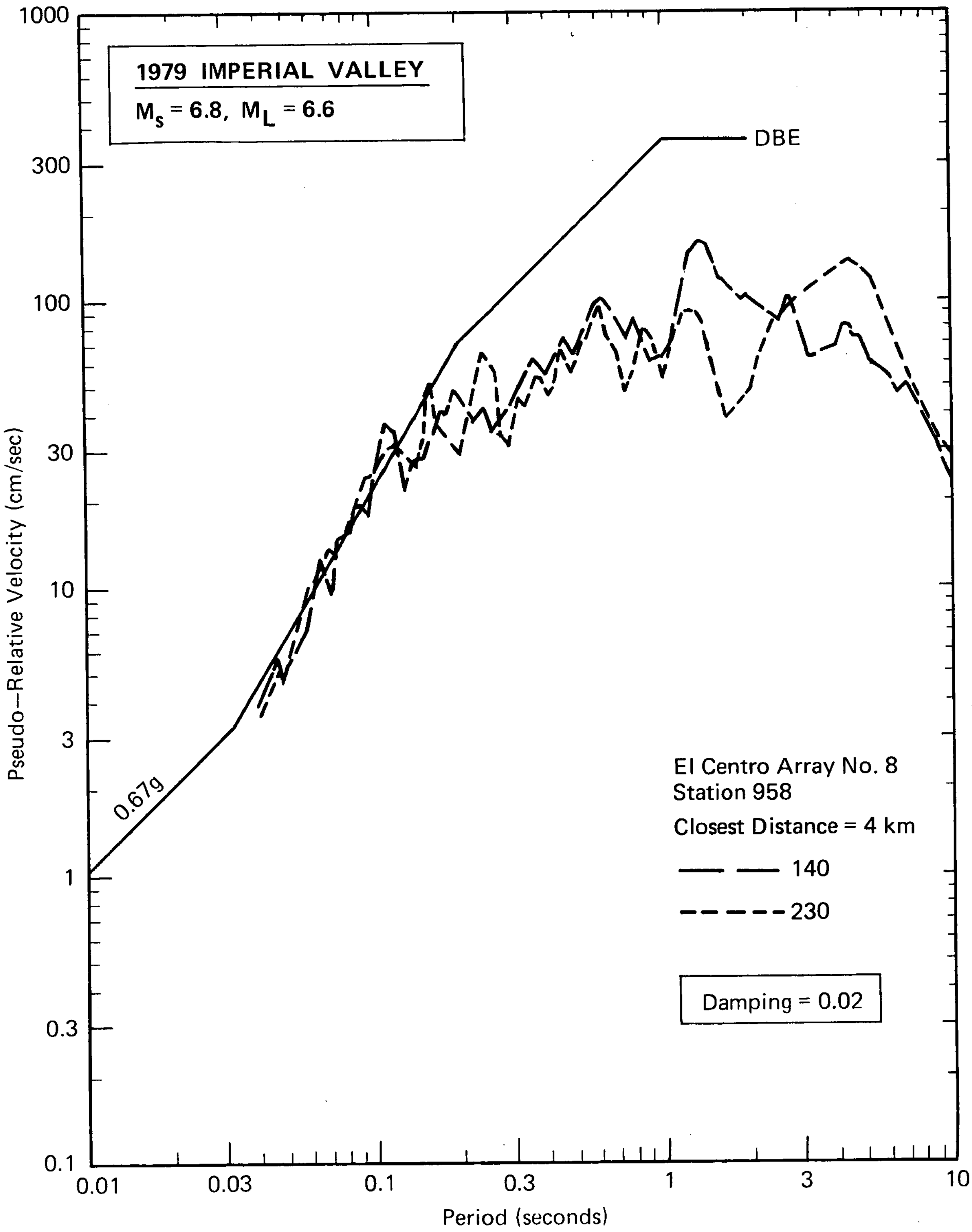

Fig. 361.57–6 – Plot of the DBE Spectrum and the Response Spectra for the 1979 Imperial Valley Earthquake Recorded at USGS Station No. 958

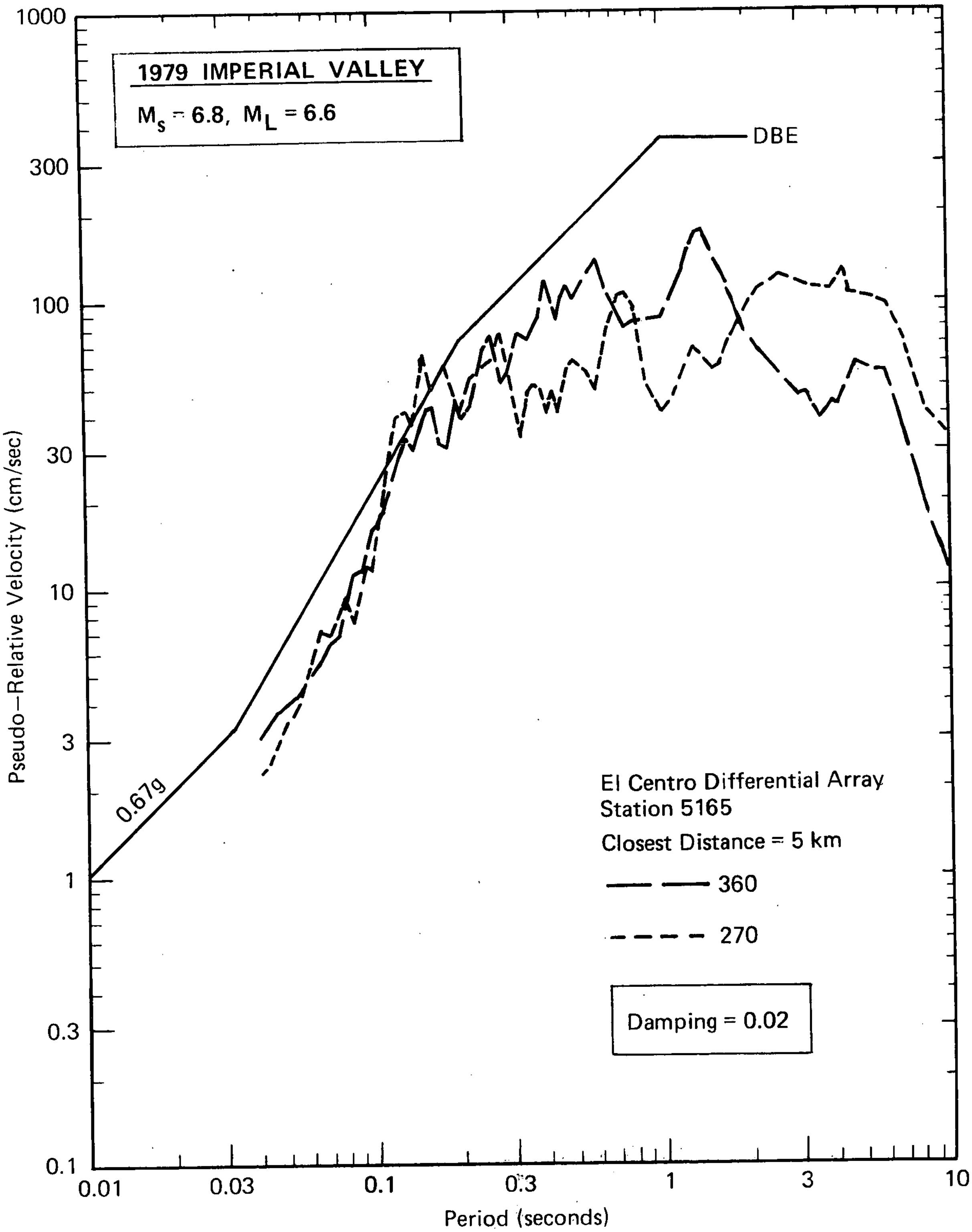

Fig. 361.57–7 – Plot of the DBE Spectrum and the Response Spectra for the 1979 Imperial Valley Earthquake Recorded at USGS Station No. 5165

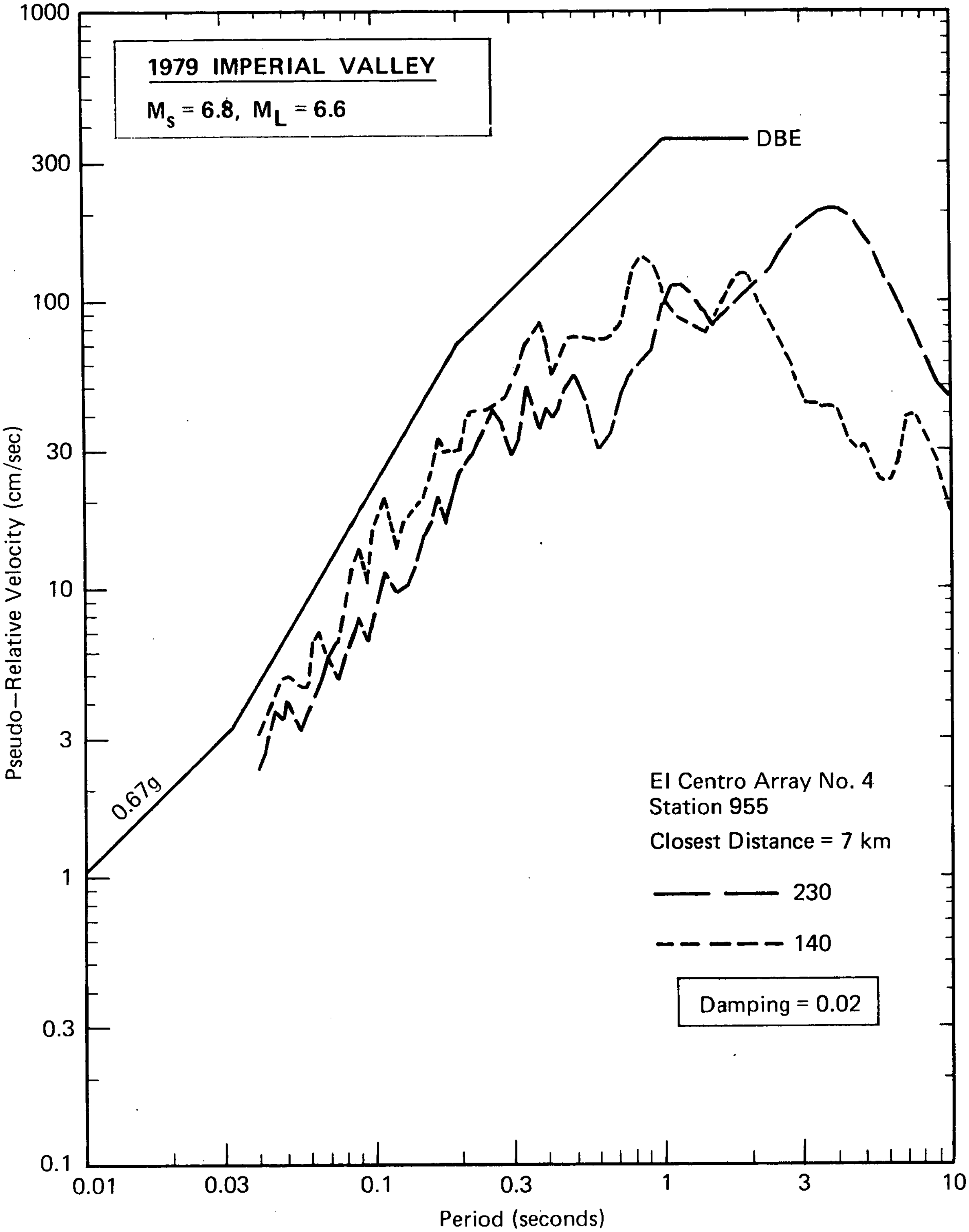

Fig. 361.57– 8 – Plot of the DBE Spectrum and the Response Spectra for the 1979 Imperial Valley Earthquake Recorded at USGS Station No. 955

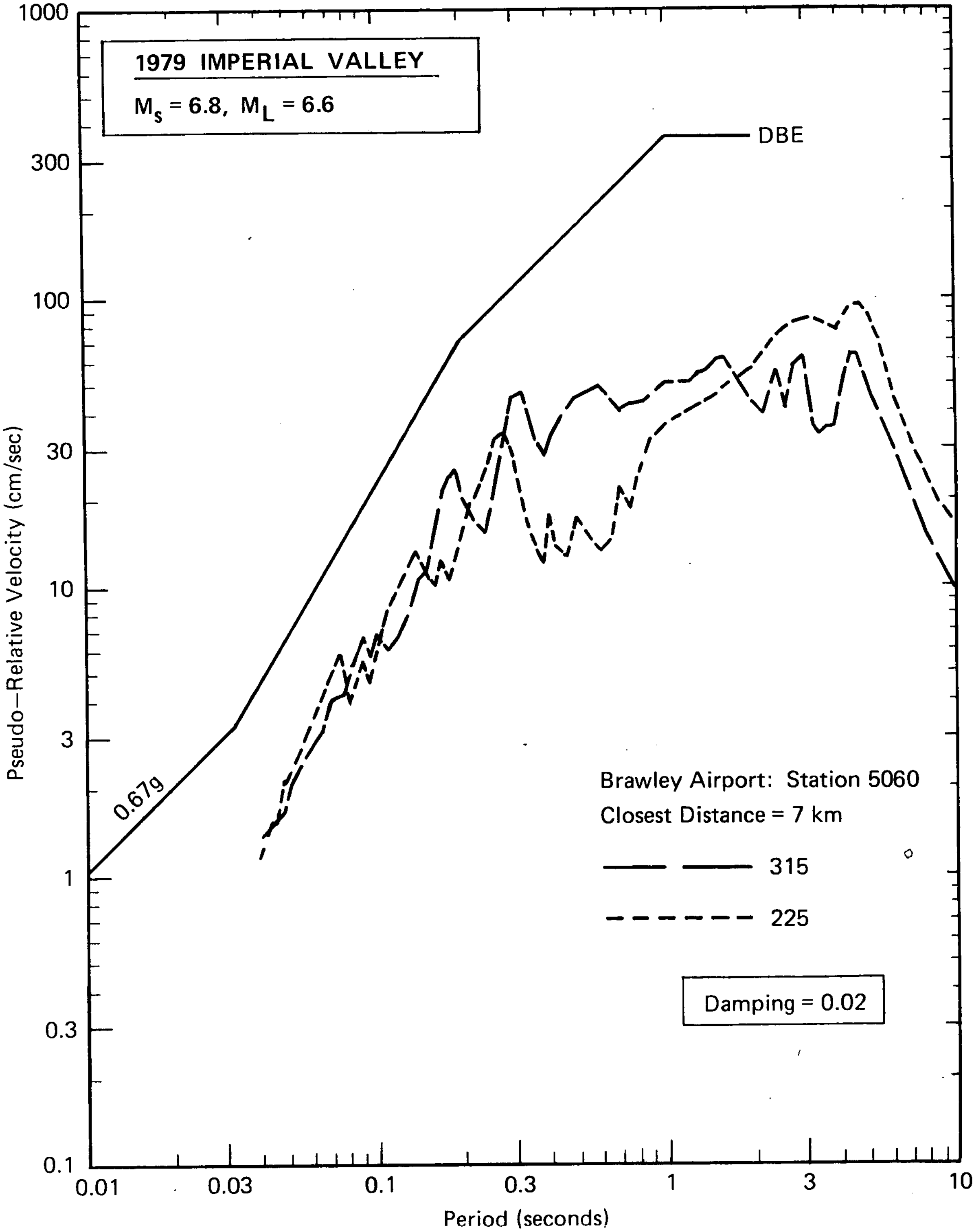

Fig. 361.57–9 – Plot of the DBE Spectrum and the Response Spectra for the 1979 Imperial Valley Earthquake Recorded at USGS Station No. 5060

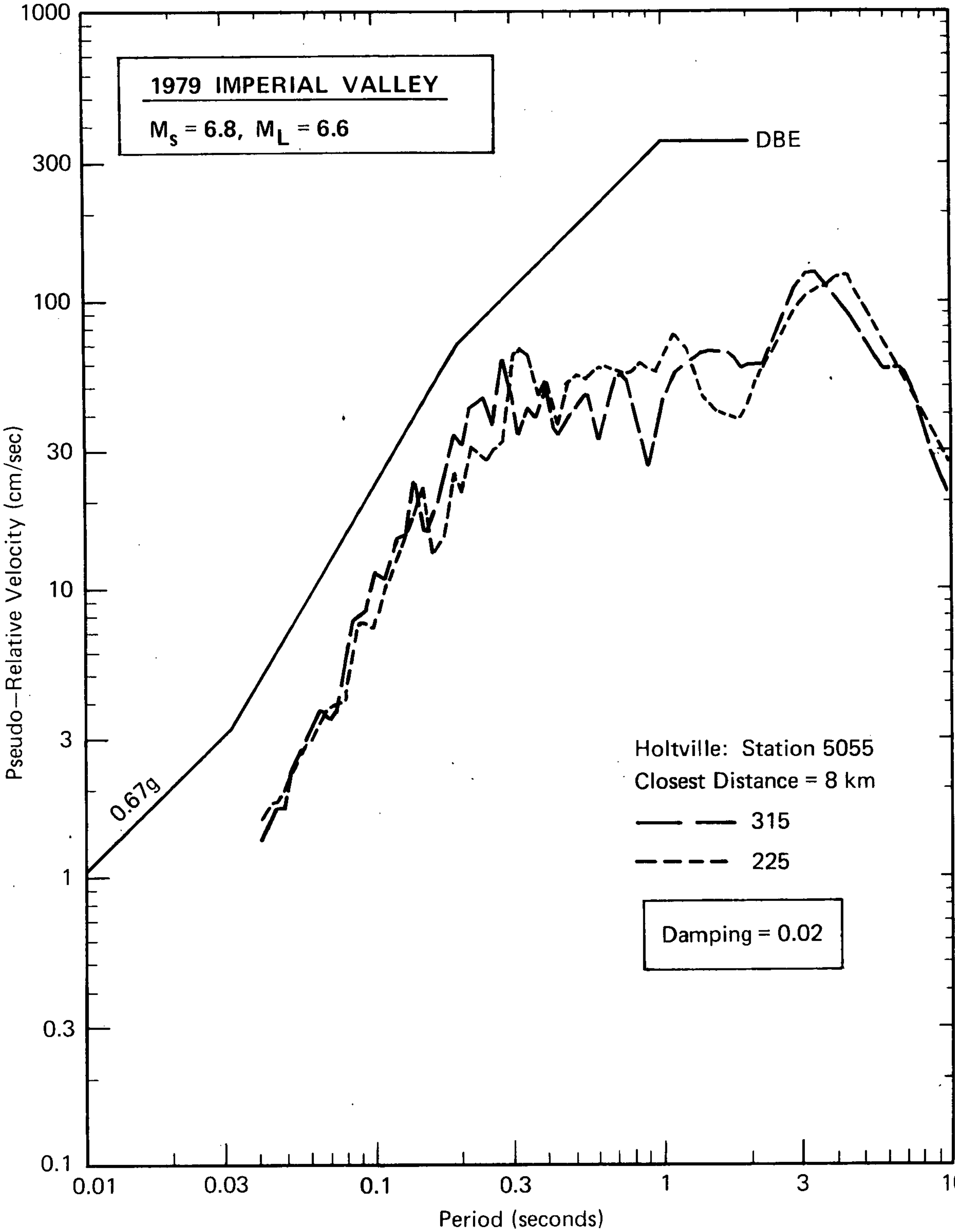

Fig. 361.57–10 – Plot of the DBE Spectrum and the Response Spectra for the 1979 Imperial Valley Earthquake Recorded at USGS Station No. 5055

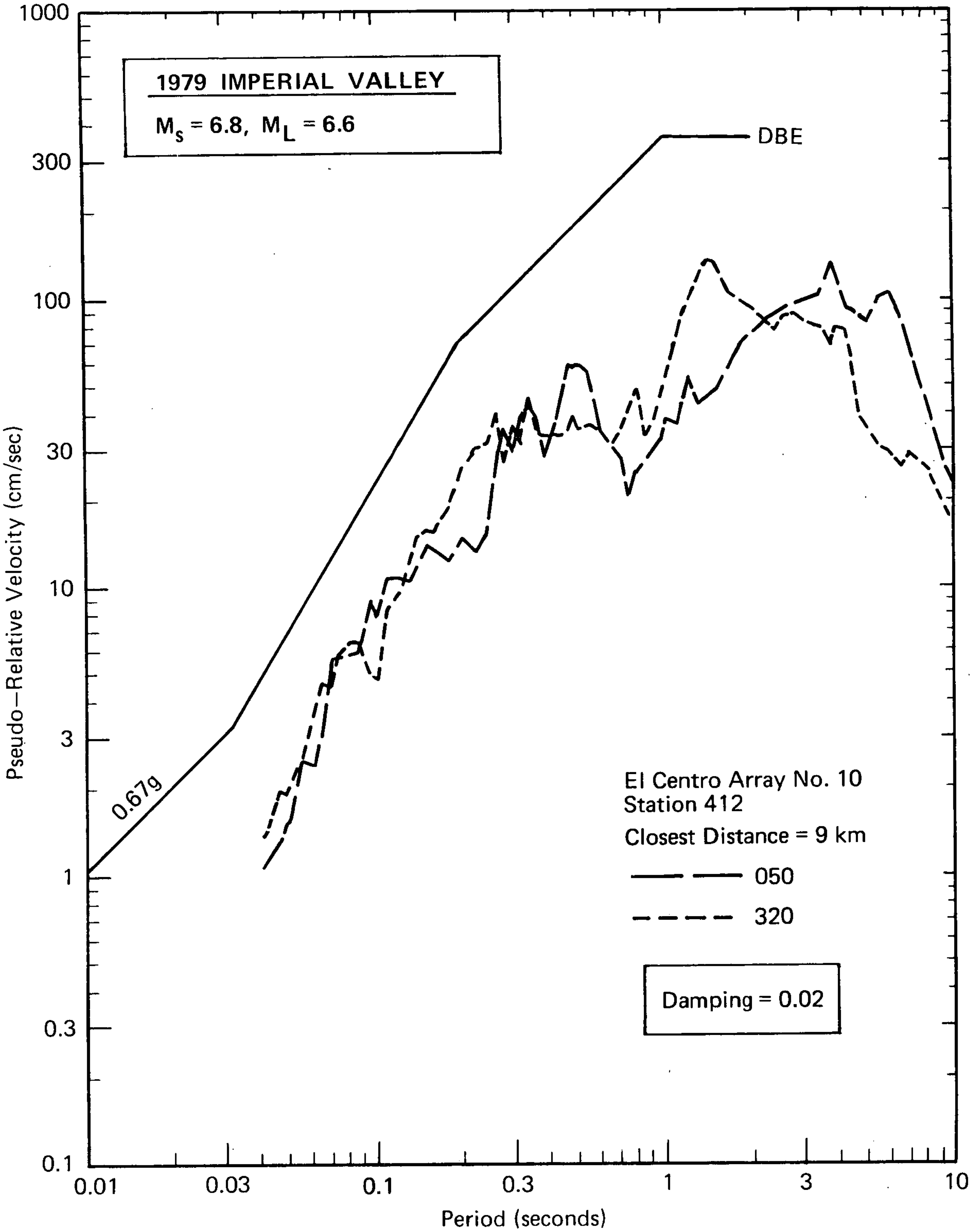

Fig. 361.57–11 – Plot of the DBE Spectrum and the Response Spectra for the 1979 Imperial Valley Earthquake Recorded at USGS Station No. 412

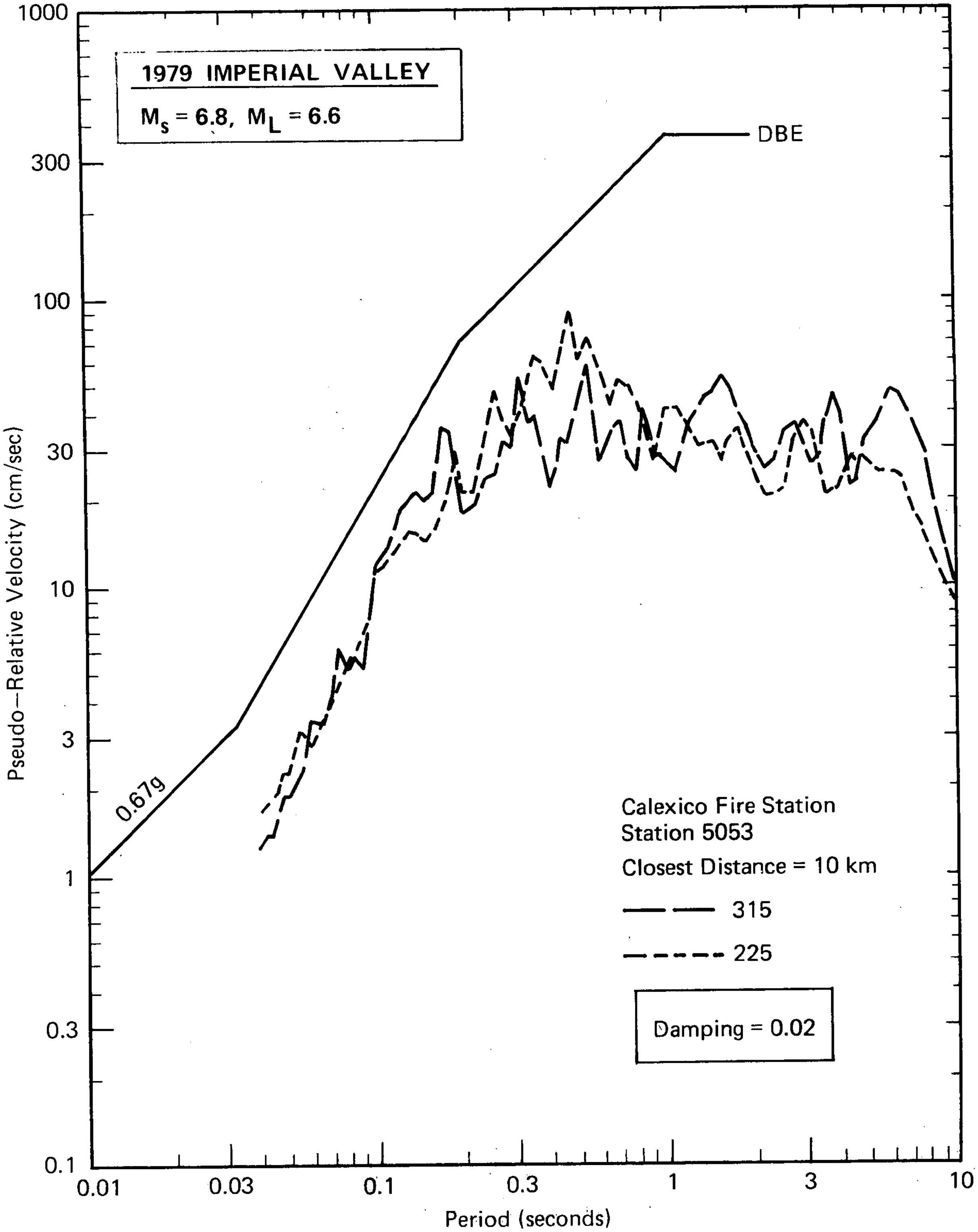

Fig. 361.57–1-2– Plot of the DBE Spectrum and the Response Spectra for the 1979 Imperial Valley Earthquake Recorded at USGS Station No. 5053

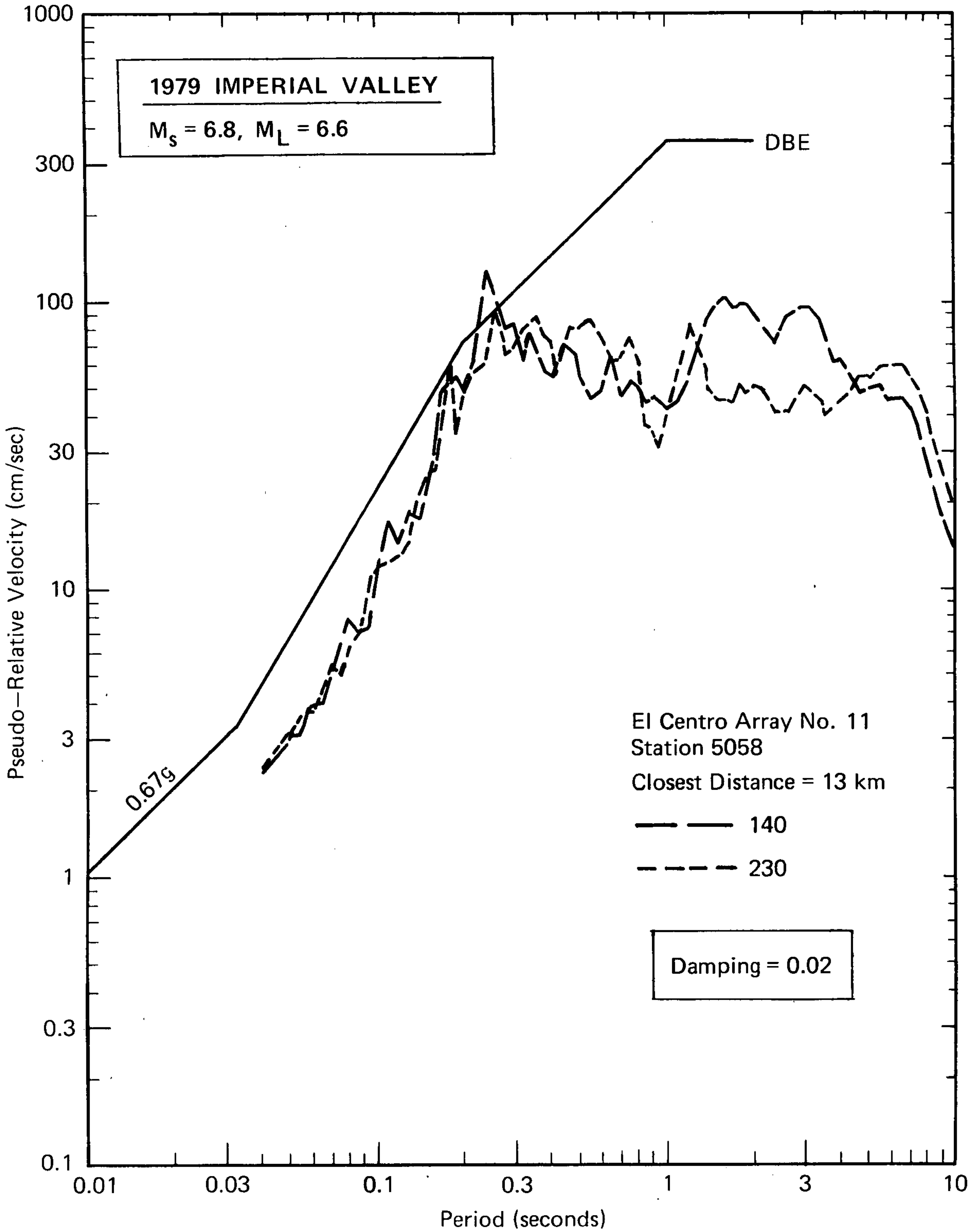

Fig. 361.57–13 – Plot of the DBE Spectrum and the Response Spectra for the 1979 Imperial Valley Earthquake Recorded at USGS Station No. 5058

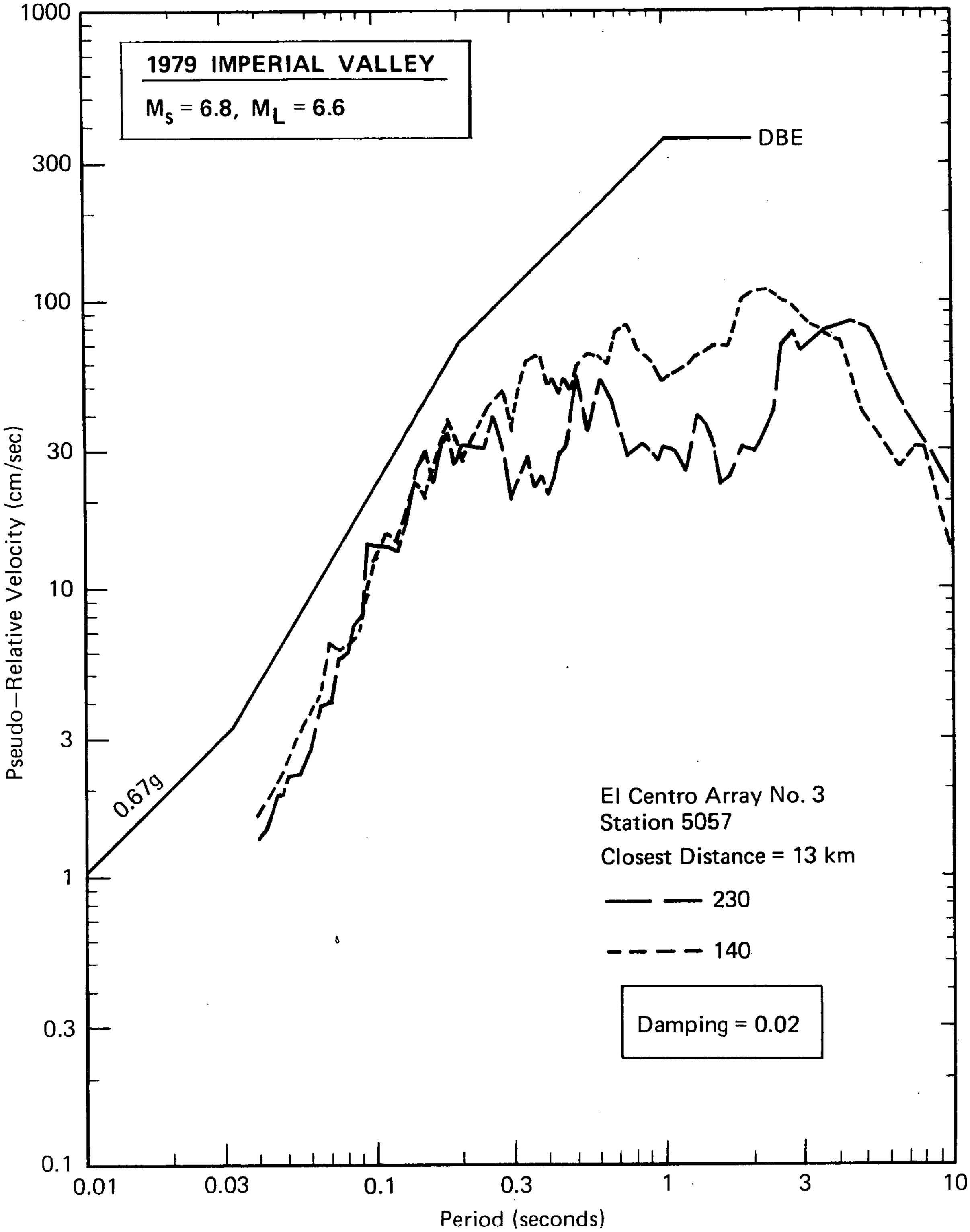

Fig. 361.57–14 – Plot of the DBE Spectrum and the Response Spectra for the 1979 Imperial Valley Earthquake Recorded at USGS Station No. 5057

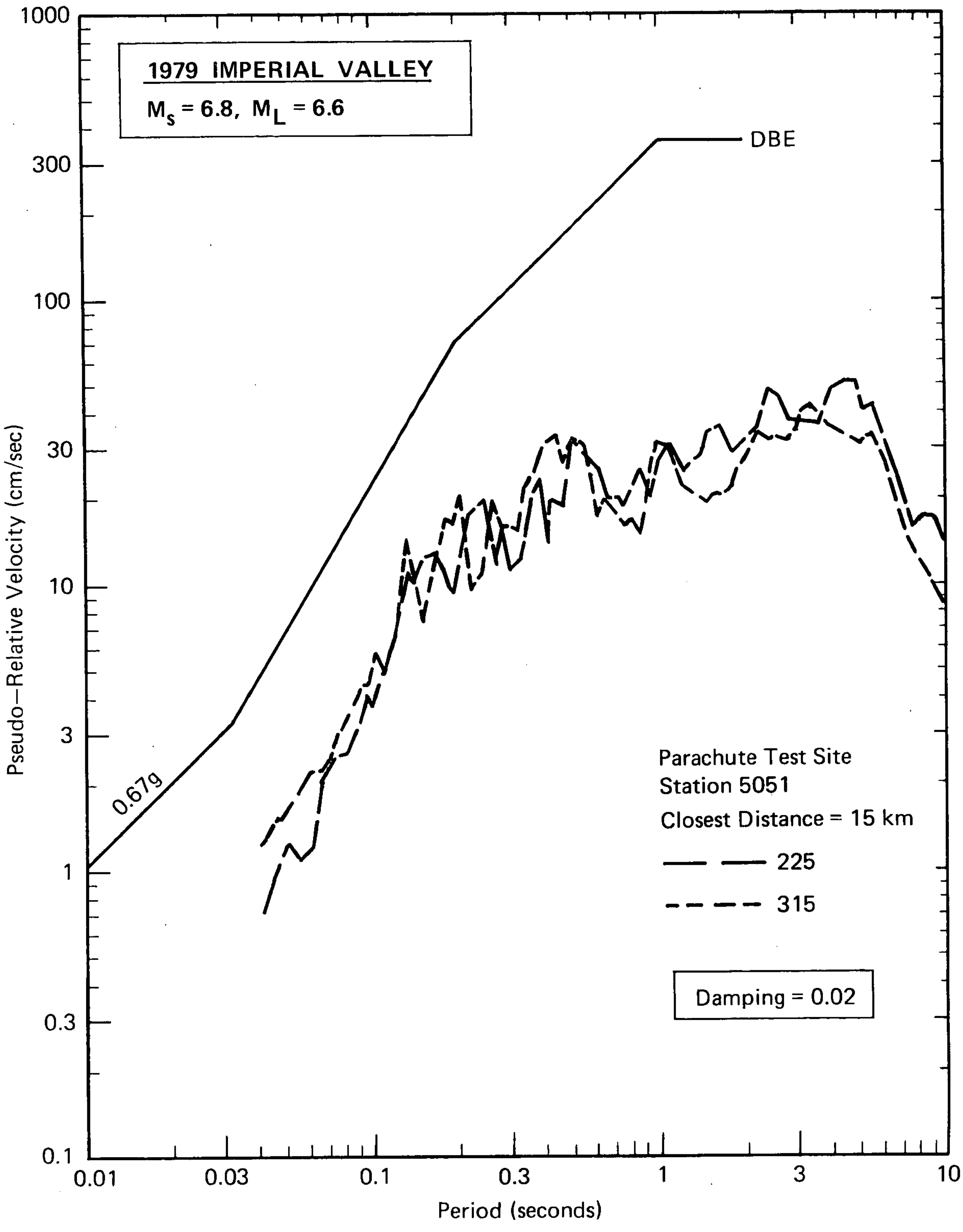

Fig. 361.57–15 – Plot of the DBE Spectrum and the Response Spectra for the 1979 Imperial Valley Earthquake Recorded at USGS Station No. 5051

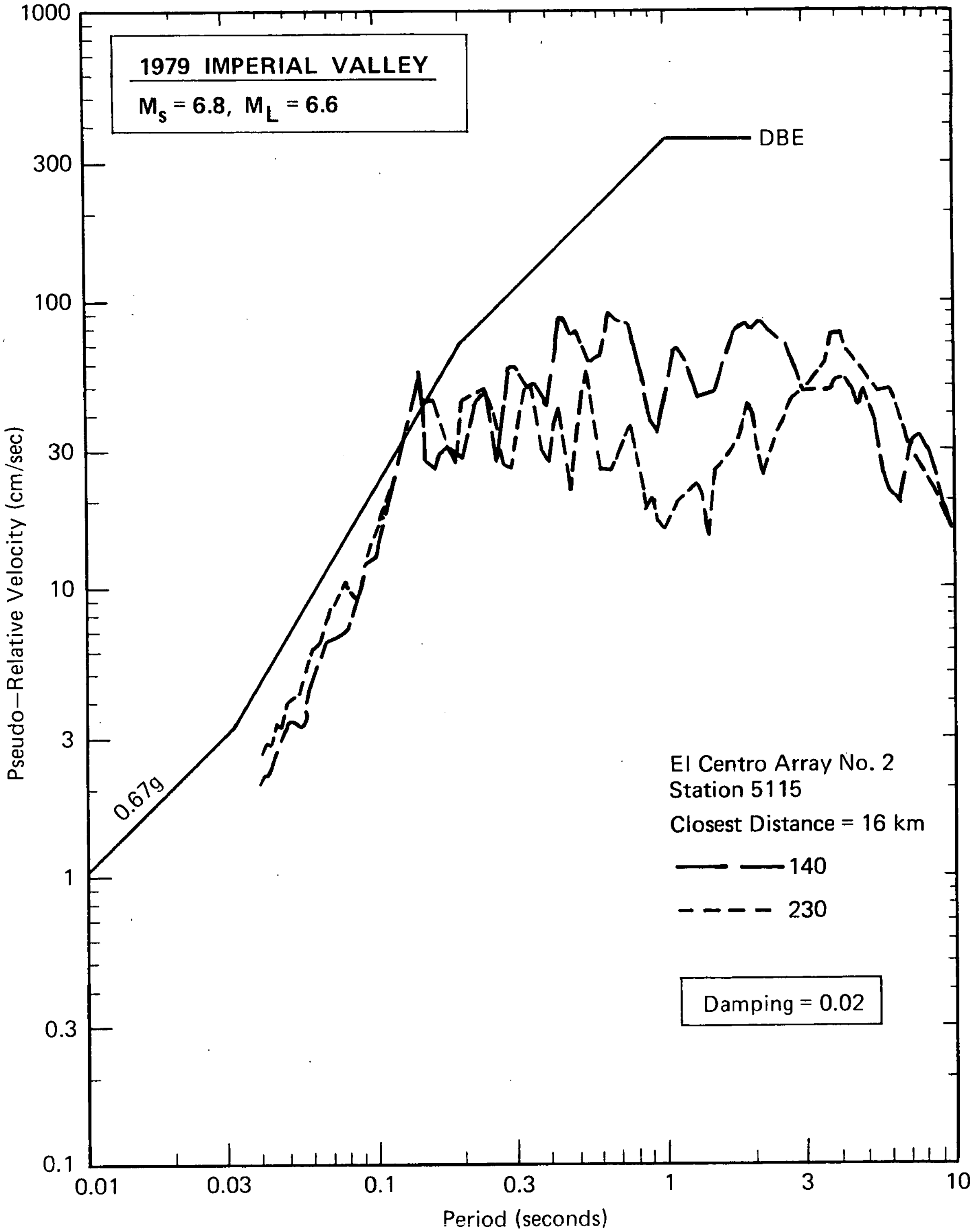

Fig. 361.57–16 – Plot of the DBE Spectrum and the Response Spectra for the 1979 Imperial Valley Earthquake Recorded at USGS Station No. 5115

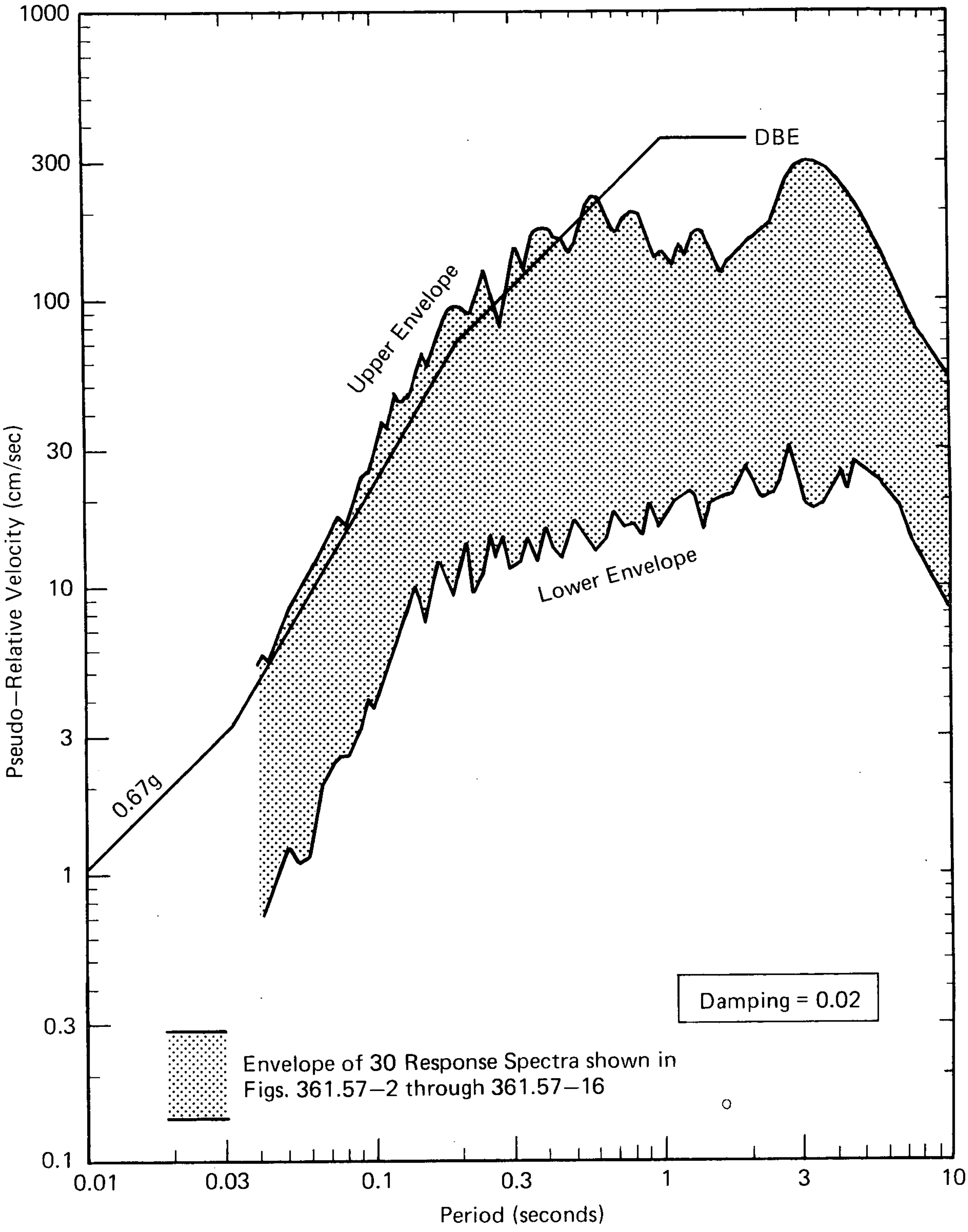

Fig. 361.57–17 – Plot of the DBE Spectrum and the Envelope of 30 Response Spectra Obtained at Distances between 0 and 16 Kilometers for the 1979 Imperial Valley Earthquake

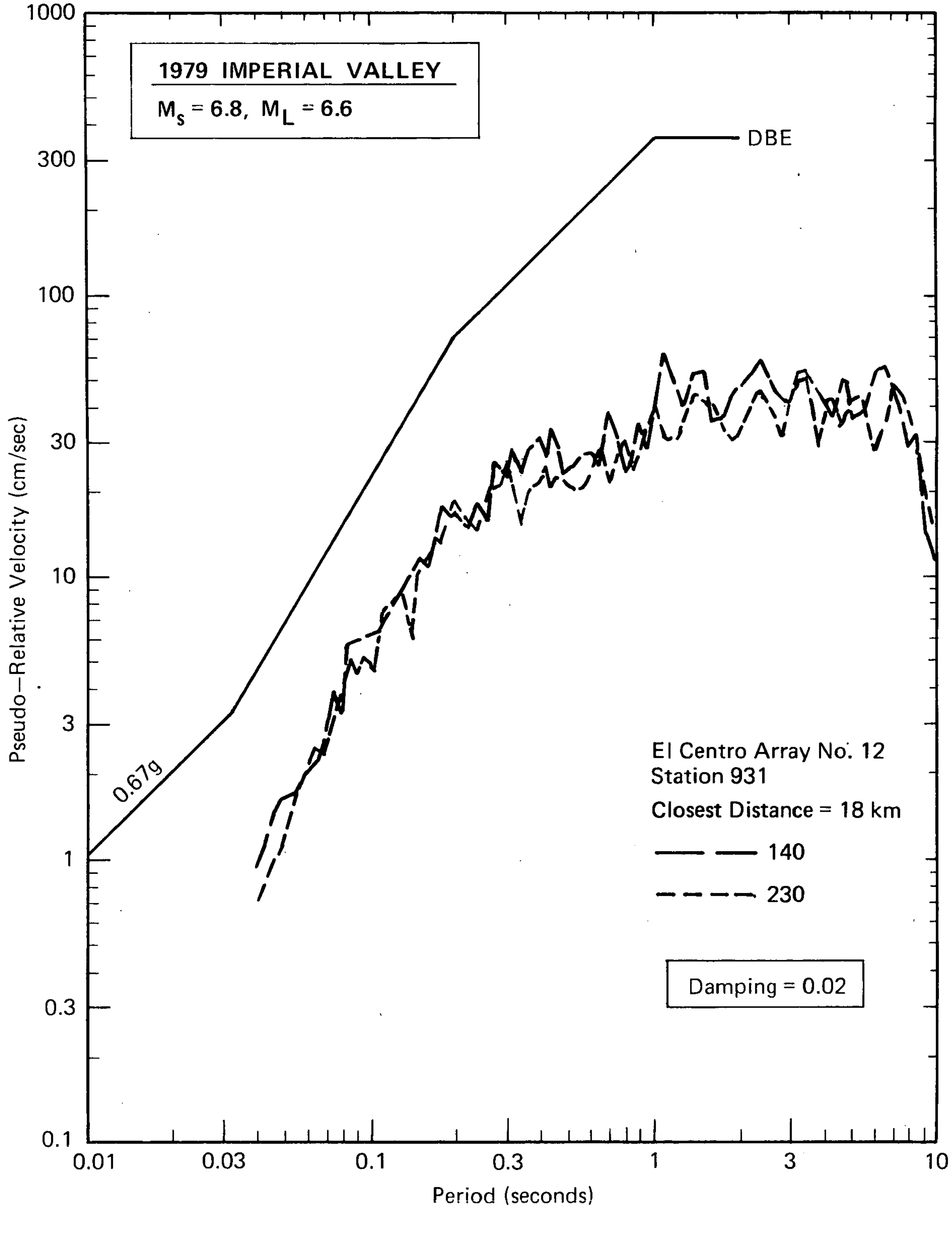

Fig. 361.57—18 — Plot of the DBE Spectrum and the Response Spectra for the 1979 Imperial Valley Earthquake Recorded at USGS Station No. 931

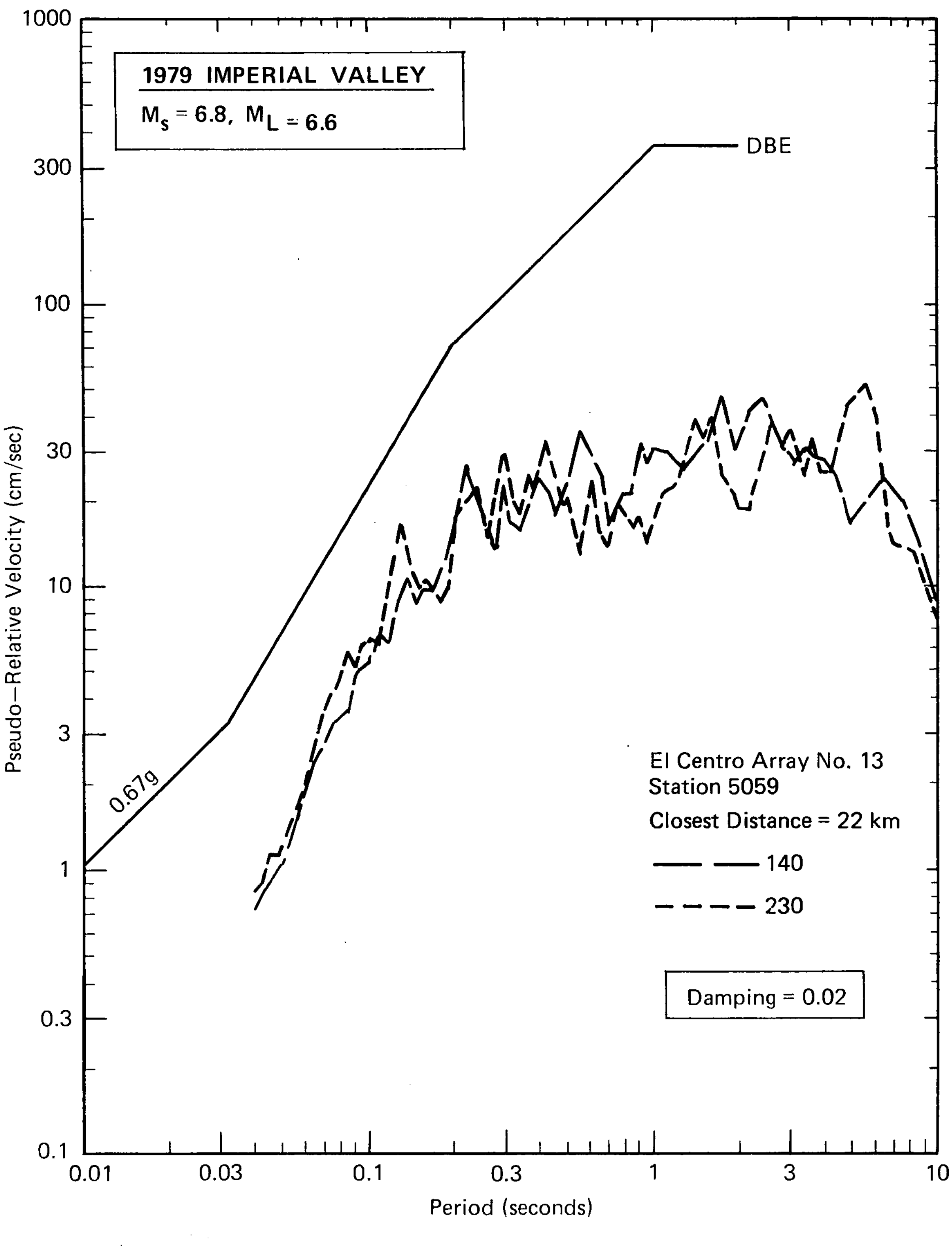

Fig. 361.57–19 – Plot of the DBE Spectrum and the Response Spectra for the 1979 Imperial Valley Earthquake Recorded at USGS Station No. 5059

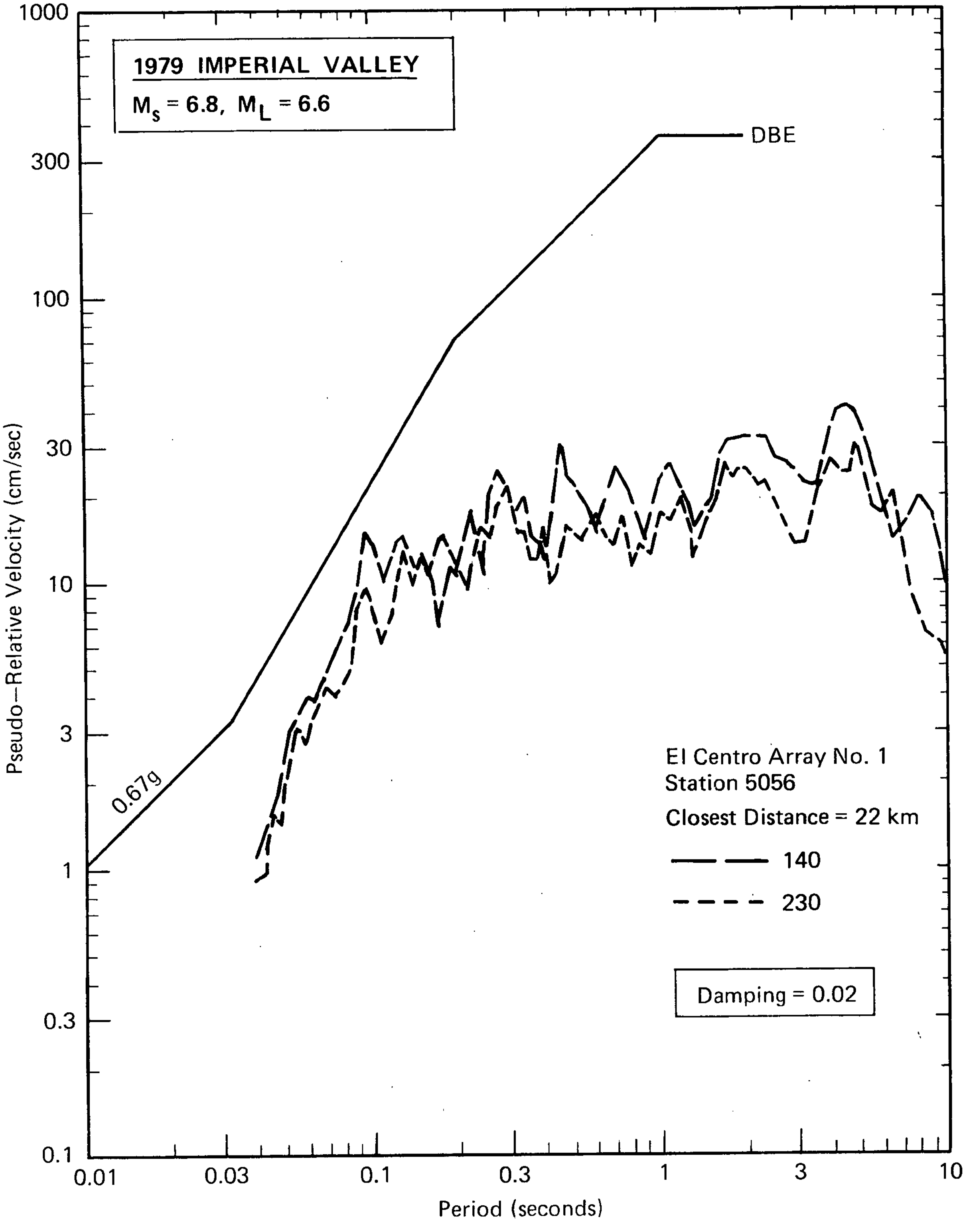

Fig. 361.57– 20 – Plot of the DBE Spectrum and the Response Spectra for the 1979 Imperial Valley Earthquake Recorded at USGS Station No. 5056

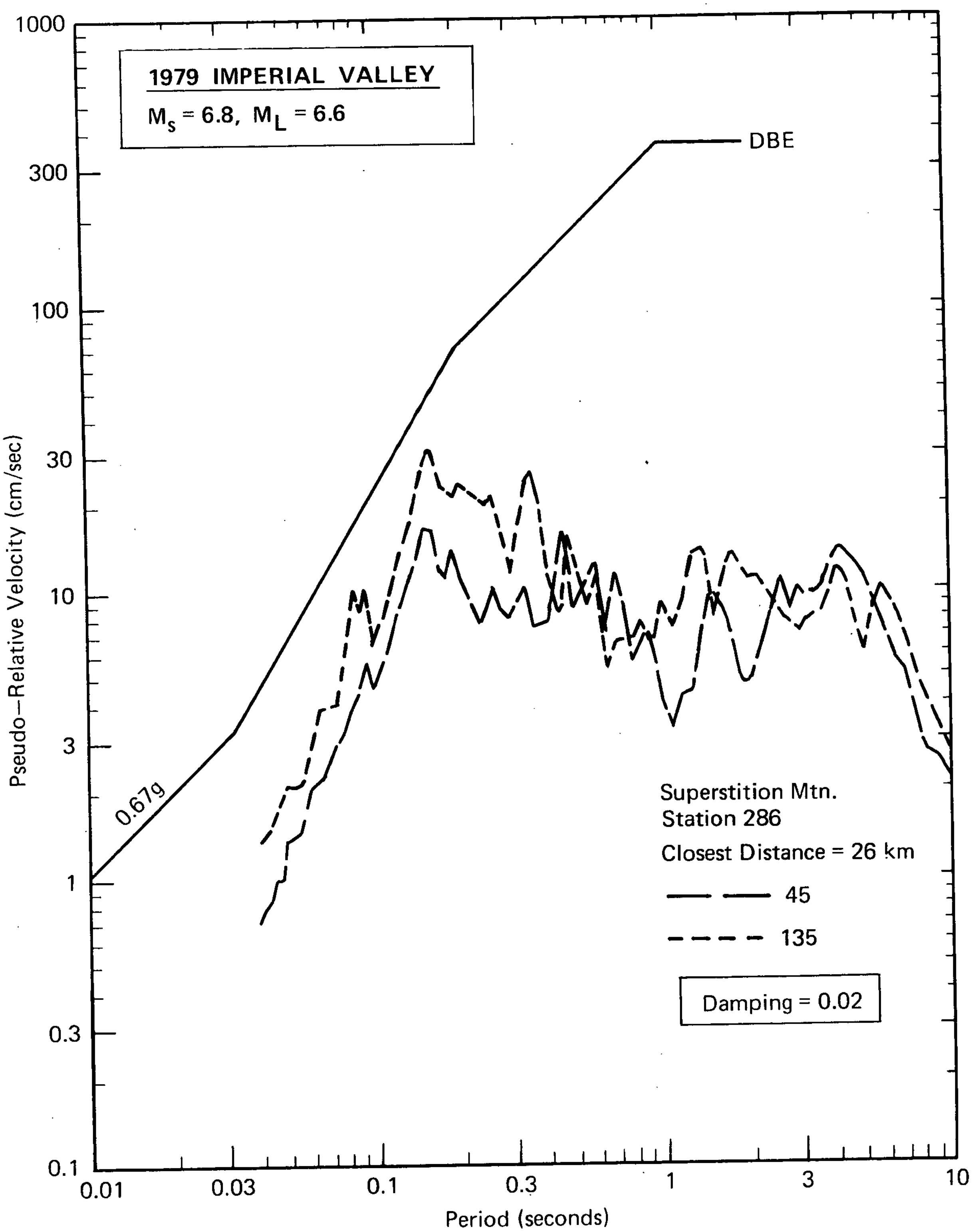

Fig. 361.57–21– Plot of the DBE Spectrum and the Response Spectra for the 1979 Imperial Valley Earthquake Recorded at USGS Station No. 286

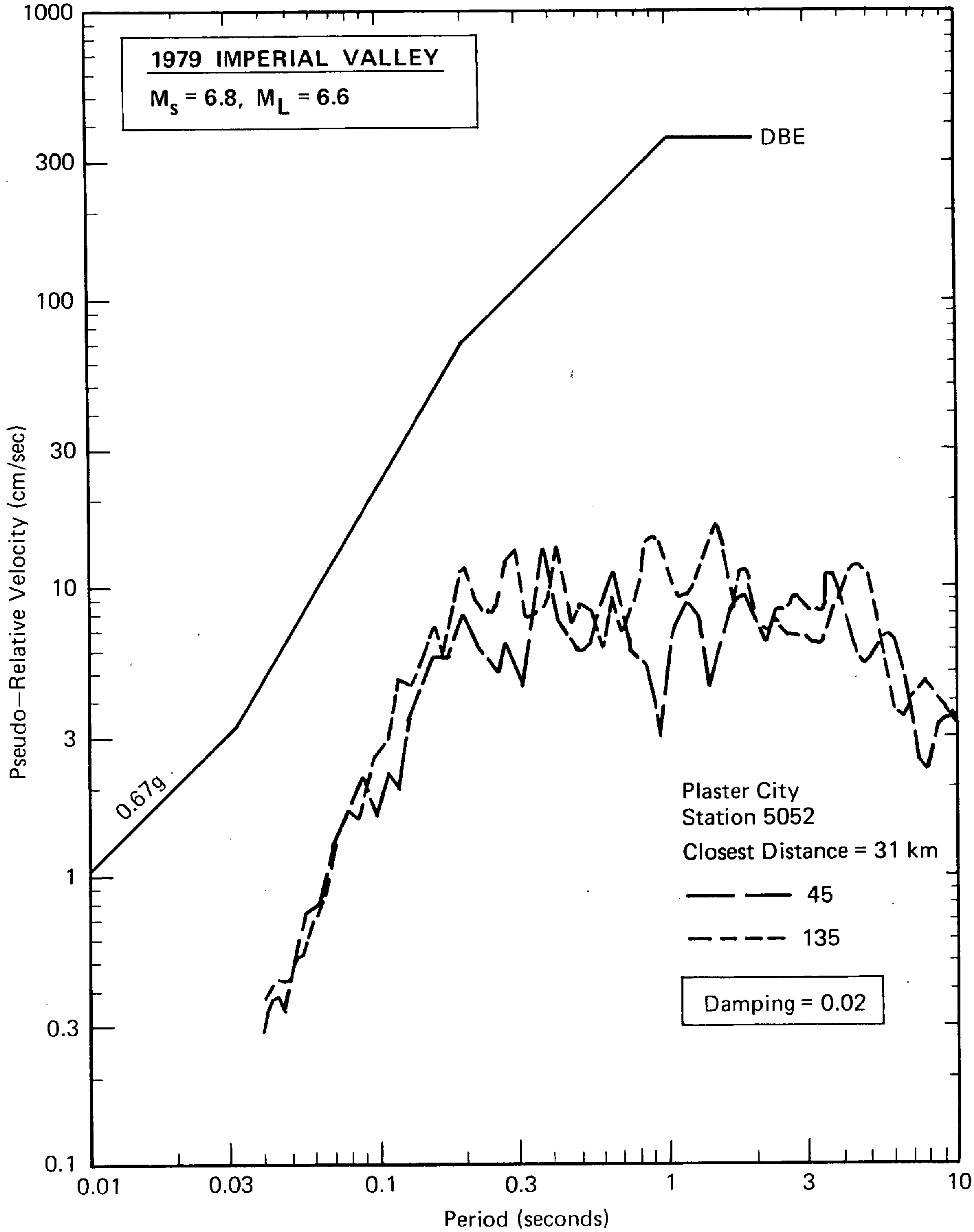

Fig. 361.57–22 – Plot of the DBE Spectrum and the Response Spectra for the 1979 Imperial Valley Earthquake Recorded at USGS Station No. 5052

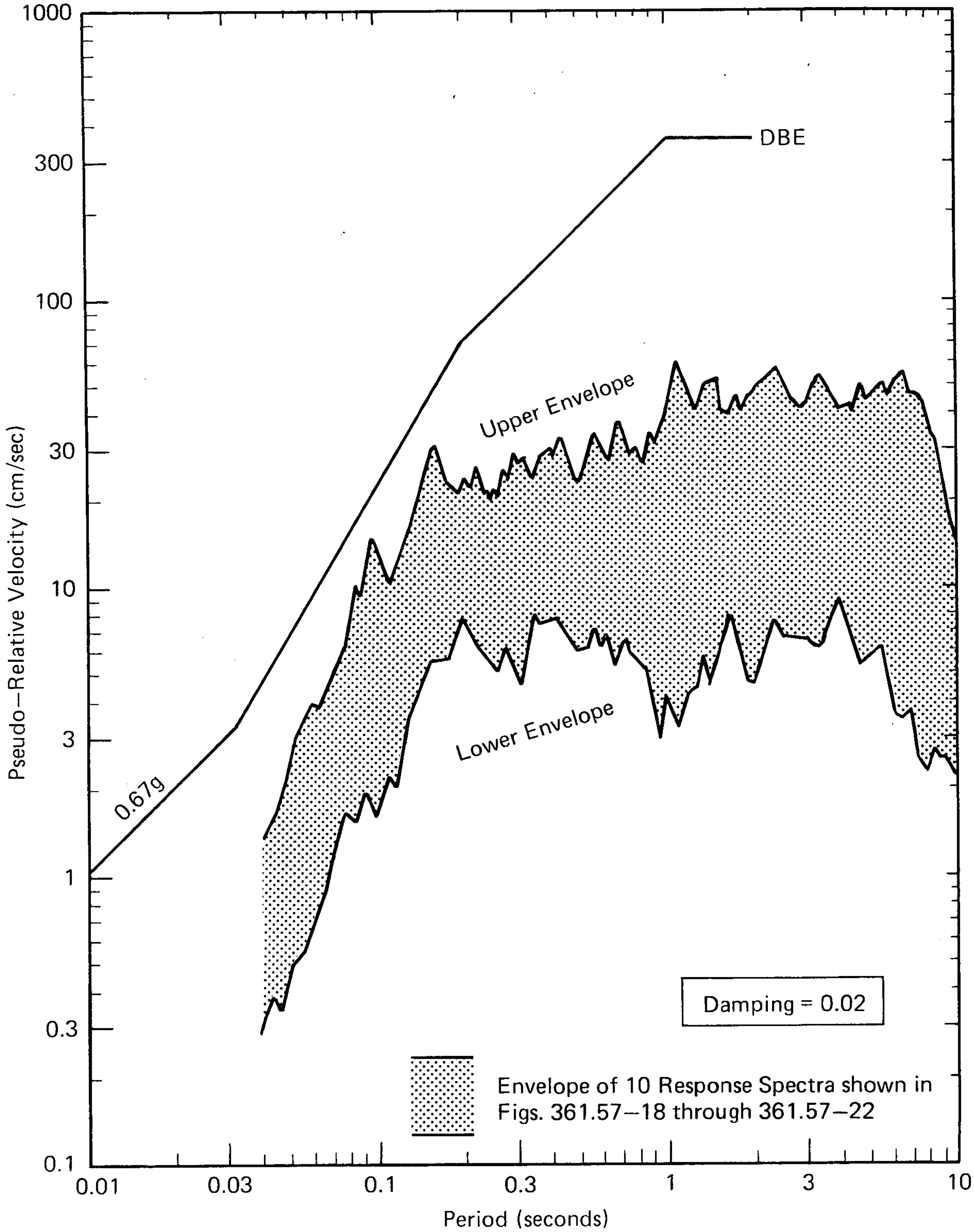

Fig. 361.57–23 – Plot of the DBE Spectrum and the Envelope of 10 Response Spectra Obtained at Distances between 16 and 40 Kilometers for the 1979 Imperial Valley Earthquake

QUESTION 361.58

Use USGS Circular 795 to determine the ground motion at the San Onofre site using earthquake magnitudes of 6-1/2, 7 and 7-1/2 on the OZD at a distance of 10 km (see Question 361.62) from the site.

RESPONSE 361.58

The authors of Circular 795 state in their report (page 25) that: "The regression lines in a preceding section of this report provide the means for estimating peak ground motion parameters at distances <u>greater than 5 km for magnitude 5.0 - 5.7 earthquakes, at distances greater than 15 km for magntiude 6.0 - 6.4 earthquakes, and at distances greater than 40 km for magnitude 7.1 - 7.6 earthquakes."</u> (Emphasis added.) Thus, the authors of Circular 795 preclude the use of their derived expressions for earthquake magnitudes of 6-1/2, 7 and 7-1/2 at a distance of 10 km.

Nevertheless, the expressions derived in Circular 795 supplemented by the statements of judgment contained in the circular, provide a means to estimate instrumental peak ground motion parameters at a distance of 8 km for magnitudes up to M = 6.5 (note that the San Onofre site is at a distance of 8 km from the OZD based on the closest distance to fault, which is the distance definition used in Circular 795). The authors of Circular 795 caution against any extrapolations for magnitudes greater than M = 6.5 at such close distances.

The following expressions and statements of judgment from Circular 795 are considered herein to estimate an instrumental peak acceleration at a closest distance of 8 km for M = 6.5.

1. Dependence of peak acceleration on magnitude: On page 26, the authors presented an evaluation of the data used by Hanks and Johnson (1976) at close distances and concluded the following: "The data set shows some dependence of peak accelerations on magnitude, but Hanks and Johnson argue that the data are consistent with the idea of magnitude-independent source properties. The data plotted as the logarithm of peak acceleration against magnitude can be fitted by a straight line with a slope equivalent to an increase by a factor of 1.4 per magnitude unit. This should not be used for extrapolation beyond magnitude 6.5...".

2. Expressions for peak horizontal accelerations for M = 5.0 to 5.7: The expression derived for peak horizontal acceleration in this magnitude range using recordings in Class I structures was based on the following data points:

Magnitude	No. of Data Points	
	Rock Sites	Soil Sites
5.2	1	4
5.3	1	-
5.4	3	2
5.5	1	4
5.6	1	-
5.7	1	-
Total	8	10

These data points were recorded at distances ranging from 6.6 to 29 km on rock sites and on soil sites. The magnitude ranges from 5.2 to 5.7, but the majority of the data points were recorded during earthquakes with magnitude 5.4 or 5.5.

The derived expression, therefore, can be considered applicable to magnitude 5.5 earthquakes and, as suggested by the authors, to distances of 5 to 30 km.

The expression for calculating peak horizontal acceleration (mean value) and the standard error given in Circular 795 are the following:

$$\ell n\ a = 0.752 - 0.93\ \ell n\ R$$

3. Influence of site conditions on peak horizontal acceleration: Circular 795 addressed the possible effects on peak horizontal acceleration using San Fernando data recorded in Class I structures on rock sites and on soil sites. The derived expressions for these two site conditions show the following trends:

Distance	mean a_r	Ratio of a_s/a_r
15 km	0.45 g	0.79
30	0.15	0.92
45	0.08	1.01

In which a_r is peak horizontal acceleration on a rock site and a_s is the corresponding value on a soil site.

Estimate of Peak Horizontal Acceleration at 8 km for M = 6.5

As noted in Consideration No. 2, the expression for peak acceleration derived in Circular 795 for the magnitude range 5.3 to 5.7 is basically applicable to M = 5.5 and is based on data from mixed site conditions of rock, stiff soil and deep soil sites. Thus, in view of Consideration No. 3

at close distances the expression probably underestimates peak acceleration on a rock site and overestimates peak acceleration on a soil site. At a distance of 8 km, the following peak accelerations may be estimated for a rock site and for a soil site for M = 5.5:

	Mean Peak Horizontal Acceleration		
Distance	Mixed Site Condition	Rock Site	Soil Site
8 km	0.31	0.33	0.29

The mean acceleration on a soil site at a distance of 8 km for M = 5.5 can be increased by a factor of 1.4 (Consideration No. 1) to obtain the mean acceleraion of 0.4 g for M = 6.5 at this distance.

Summary

Circular 795 precludes the use of the derived expressions at a closest distance of 8 km for magnitude 6-1/2, 7, or 7-1/2. Nevertheless, with the aid of the expressions together with statements of judgment given in the Circular, it was possible to estimate a mean instrumental peak horizontal acceleration of 0.4 g at a closest distance of 8 km for M = 6.5.

The authors of Circular 795 caution against any extrapolations for magnitudes greater than M = 6.5 at close distances.

REFERENCES

Boore, D. M., Joyner, W. B., Oliver, A. A., III, and Page, R. A., 1978, Estimation of ground motion parameters: U. S. Geological Survey Circular 795, 43 p.

Hanks, T. C., and Johnson, D. A., 1976, Geophysical assessment of peak accelerations: Bulletin of the Seismological Society of America, v. 66, p. 959-968.

QUESTION 361.59

Plot the results of SONGS 1 modeling study on Figure 11.

RESPONSE 361.59

Earthquake ground motions have been modeled for San Onofre Nuclear Generating Station, Unit 1, using computer methods. In Figure 361.59-1, response spectra for the computer-generated ground motions at the site are plotted on Figure 11 of the June 1979 WCC report, which contains the DBE spectrum and the 84th-percentile spectrum from empirical regression studies.

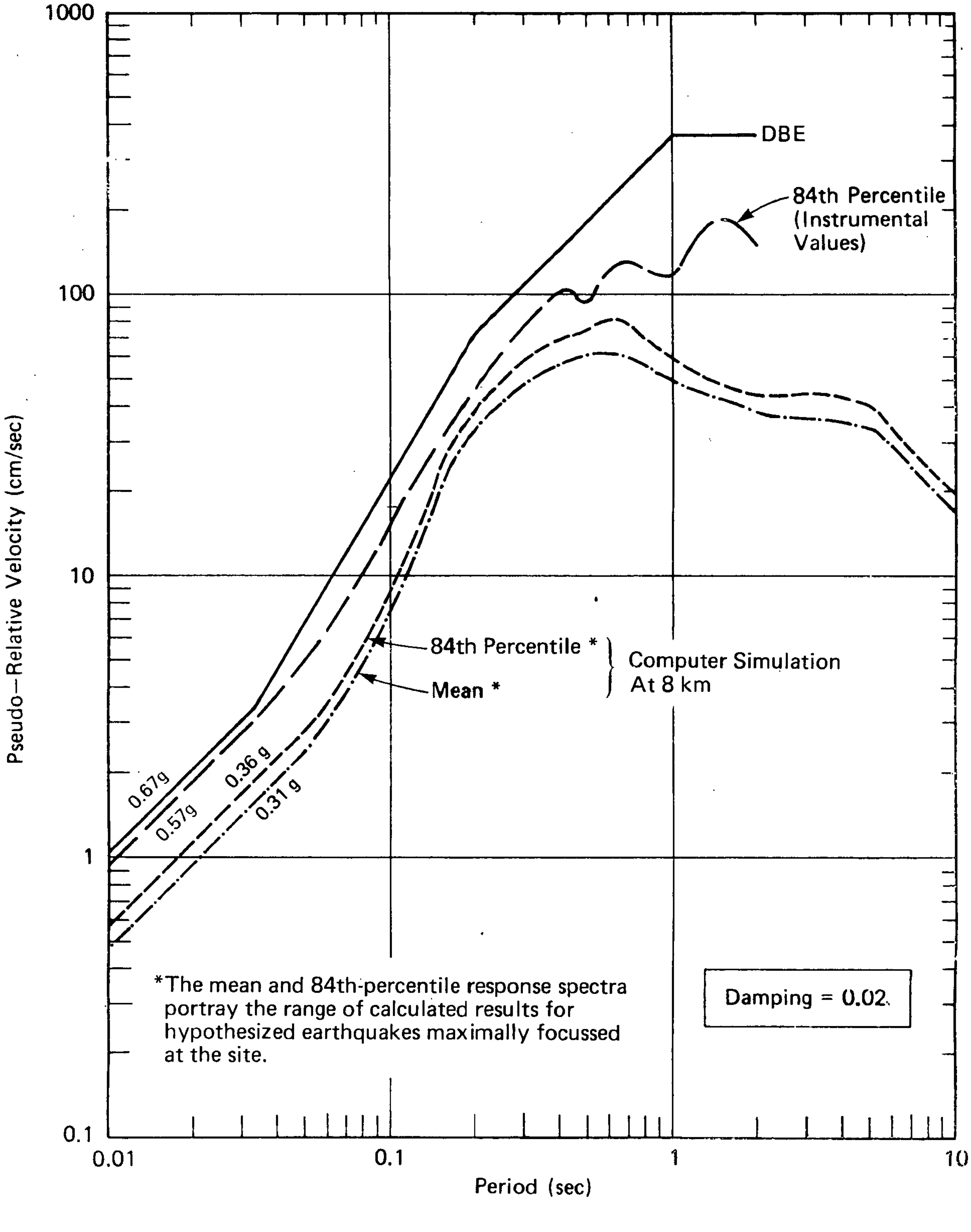

Fig. 361.59–1 — Comparison of SONGS Unit 1 Computer Simulation Spectra with the Instrumental and DBE Spectra

QUESTION 361.60

It is stated in Appendix A, page 10 of the Woodward-Clyde report "The full extent of the Rose Canyon Zone is not well known but is believed to die out toward the north in the vicinity of Oceanside and toward the south in the vicinity of San Diego Bay. However, both a northward extension to the SCOZD and southward extension to faults in Mexico have been suggested (Corey, 1954; Emery, 1960; King, 1969; Wiegand, 1970; Moore and Kennedy, 1975; Moore 1972)."

a. Discuss in detail the basis for your belief that the Rose Canyon Zone dies out toward the south in the vicinity of San Diego Bay.

b. Summarize the evidence in each of the above references given which supports or suggests a southward extension of the Rose Canyon Zone to faults in Mexico.

c. Present your rebuttal of the evidence given in item b above.

RESPONSE 361.60

361.60 a--Basis for Assumption that RCFZ Dies Out Toward the South in the Vicinity of San Diego

The Rose Canyon fault zone (RCFZ) has been studied offshore, north of Point La Jolla and southwest of the San Diego Bay (Moore, 1972; Moore and Kennedy, 1975). Faults mapped in these areas have been located on the basis of generally wide-spaced acoustic profiles and inferred correlation with bathymetric relief (for further discussion see responses 361.60 b and c). More detailed acoustic profile surveys by Kennedy (1979) and by Kennedy and others (1977 and 1978) in these offshore areas have refined the location and current understanding of this portion of the Rose Canyon fault zone. The specific information developed by Kennedy and others is summarized in Table 361.60-1.

The RCFZ in the San Diego area is characterized in general by a series of structural and topographic highs and lows that include (from north to south): the offshore faults of the Point La Jolla area (low), the Mt. Soledad area (high), Mission Bay (low), Morena-Old Town area faults (high), and the San Diego Bay area (low). The southernmost of these alternating features is underlain by the San Diego Basin that is roughly defined by the down-to-the-west faults of the La Nacion system (Artim and Pinckney, 1973) and the down-to-the-east faults offshore from San Diego Bay (Kennedy and others, 1977). This structural low, or graben, implies that the southern portion of the RCFZ is characterized by a widened zone of extensional, rather than compressional style faults, and further suggests that the sense of displacement on this portion of the RCFZ is dip-slip rather than strike-slip.

Faulting along the RCFZ in the area south of the Morena-Old Town is not well defined. Onshore evidence of fault displacement is sketchy. (For further discussion, see response 361.44 k). The bulk of evidence for faulting at the south end of the RCFZ consists of faults identified by acoustic profiling in San Diego Bay and offshore of San Diego (Moore and Kennedy, 1975 and Kennedy and others 1977). Faults identified offshore are more prominent than the faults in the southern end of San Diego Bay. The offshore faults are also expressed as fault scarps where they come onshore at Coronado (Kennedy and others, 1977). This evidence strongly suggests that a southern extension of the

RCFZ is associated with the faulting and extends offshore of San Diego and not to the south through San Diego Bay.

In summary, the character of the faulting within the RCFZ changes in the southern part of San Diego and becomes a wide zone of faulting characterized primarily by a dip-slip component. The prominent faults extend offshore to the southwest. Current data indicates that the faulting within this wide zone dies out to the south and does not connect to the Calabasas fault or the Vallecitos fault zone.

<u>361.60 b and c--Summary of Evidence for Extension of the RCFZ and Rebuttal to that Evidence</u>

The works which support the argument that the RCFZ extends northward to connect with the SCOZD and/or southward into Mexico will be discussed in chronological order (i.e., (1) Corey, 1954; (2) Emery, 1960; (3) King, 1969; (4) Wiegand, 1970; (5) Moore, 1972); (6) Moore and Kennedy, 1975). Each of these discussions will be followed by a brief rebuttal.

(1) Corey (1954) compiled paleogeographic and paleostructural maps of southern California and the adjacent continental borderland area to interpret the Tertiary history of the region. On his "pre-Pliocene fault trend" map, he inferred that several offshore faults extend from the Palos Verdes peninsula south, roughly parallel to the present coastline, to the onshore RCFZ area, then continue south in the offshore area west of Baja California.

Corey's report deals only with Tertiary sedimentary history on a regional scale and does not deal with the detailed geology of any one area. He depicted the Rose Canyon fault as being right lateral with schist basement to the west and granitic basement to the east. Exploratory borings have subsequently shown that the Santiago Peak Volcanics form the basement on both sides of the Rose Canyon fault (Gray and others, 1971). This and the presence of the same Cretaceous and Eocene formations on opposite sides of the fault indicate the Rose Canyon fault has little displacement along it; therefore, Corey's interpretation is incorrect.

(2) Emery (1960) prepared a fault map of the sea floor off southern California depicting a long "primary fault" trend similar to Corey's but along the base of the slope west of the OZD that continued on offshore and west of Baja California.

Emery, however, notes that the faults are located primarily on the basis of submarine topography. Emery assumes that such topography is for the most part of structural origin. Age determination of these structural scarps is equivocal as "some scarps on the sea floor that are believed to be late Miocene age appear sharp and clear from sounding data" (Emery, p. 77). Thus, although Emery identified a topographic lineament roughly parallel but west of the OZD, its location lies further offshore at the base of the topographic scarp and its true character and age are undocumented.

(3) King (1969), in a publication on the tectonic history of North America, described the regional tectonic setting of California and Baja California and discussed the existence of prominent high angle, northwest-trending right-lateral faults. He dealt specifically with the San Andreas fault in California and its relationship to the opening of the Gulf of California. No specific reference was made to the faulting offshore of southern California.

(4) Wiegand (1970) postulated that a fault underlying San Diego Bay was an extension of the Rose Canyon fault that "may be a segment of a longer fault system which includes . . . the San Miquel Fault in Baja California." This extended fault zone was inferred largely on the basis of the alignment of discontinuous topographic, structural, and geothermal features in the San Diego Bay-Tijuana region.

The geothermal wells used by Wiegand to support a fault in the south San Diego Bay area do not align with his proposed fault. The topographic depressions in the bay floor, used to support a proposed fault alignment, are underlain by "slump sand" of different character from the surrounding sediments, according to Wiegand (p. 112). It seems quite likely that these are disrupted sediments resulting from liquefaction rather than a sag pond depression. This area could also be a drainage channel preserved on the bay floor from a lower stand of sea level.

Weigand notes faults which are transverse to the proposed fault alignment in San Diego Bay. He suggests that the general quiesence of the Rose Canyon fault zone may be the result of these transverse faults locking off the northwest-southeast trend. It is also noteworthy that Kennedy and others (1977) surveys of the South Bay area did not identify anomalies suggestive of a southward extension of a fault through this area, but rather of a south-southwesterly trend into the offshore area west of San Diego Bay.

(5) Moore (1972) proposed an offshore extension of the Rose Canyon fault north of Point La Jolla based on generally wide spaced acoustic profiles. He acknowledged that the location of the Rose Canyon Fault" is less certain to the southeast beyond San Diego Bay" and only suggested that the Rose Canyon fault might follow the Tijuana River Valley to

connect further south with the San Miguel fault. A review of the data in the border area, as discussed in response 361.41 b, indicates that this proposed connection is incorrect.

(6) Moore and Kennedy (1975) mapped several faults within and to the southwest of San Diego Bay on the basis of acoustic reflection profiles. The indicated fault pattern suggested that the Rose Canyon fault zone broadens and becomes en echelon at the San Diego Bay area, roughly defining the west side of a structural low. This portion of the zone is characterized by normal down-to-the-east faulting. Their survey found the strongest evidence of faults extending southwestward across the north San Diego Bay area and offshore to the southwest, rather than to the southeast. Their survey also identified diminishing evidence of faulting to the southwest suggesting that the RCFZ dies out in this direction near the international border. It is the applicant's position that this interpretation represents the most probable projection of the RCFZ into the offshore area and that it further supports the lack of continuity with the Vallecitos or San Miguel fault zones.

REFERENCES

Artim, E. R., and Pinkney, C. J., 1973, La Nacion fault system, San Diego, California: Geological Society of America Bulletin, v. 84, p. 1075-1080.

Corey, W. H., 1954, Tertiary basins of southern California, in Geology of southern California: California Division of Mines and Geology Bulletin 170, Chapter 3, p. 73-83.

Emery, K. O., 1960, The sea off southern California: John Wiley and Sons, New York, 366 p., cited in Albee, A. L., and Smith, J. L., 1966, Earthquake characteristics and fault activity insouthern California, in Lung, R., and Proctor, R., eds., Enginering geology in southern California: Association of Engineering Geologists Special Publication.

Gray, C. H., Jr., Kennedy, M. P., and Morton, P. K., 1971, Petroleum potential of southern coastal and mountain area, California: American Association of Petroleum Geologists Memoir 15, p. 372-383.

Kennedy, M. P., 1979, Recency and character of faulting offshore from Metroplitan San Diego, California--U. S. Geological Survey Contract No. 14-08-001-17699: U. S. Geological Survey, National Earthquake Hazard Reduction Program, Summaries of Technical Reports, v. 8, December, p. 27-28.

Kennedy, M. P., Bailey, K. A., Greene, H. G., and Clarke, S. H., 1978, Recency and character of faulting offshore from metropolitan San Diego, California: California Division of Mines and Geology Final Technical Report.

Kennedy, M. P., Welday, E. E., Borchard, G., Chase, G. W., and Chapman, R. H., 1977, Studies of surface faulting and liquefaction as potential earthquake hazards in urban San Diego, California: California Division of Mines and Geology Final Technical Report.

King, P. B., 1969, The tectonics of North America: U. S. Geological Survey Professional Paper 68, 94 p.

Moore, G. W., 1972, Offshore extension of the Rose Canyon fault, San Diego, California: U. S. Geological Survey Professional Paper 800-C, p. 113-116.

Moore, G. W., and Kennedy, M. P., 1975, Quaternary faults at San Diego Bay, California: Journal of Research of the U. S. Geological Survey, v. 3, no. 5, p. 589-595.

Wiegand, W., 1970, Evidence of a San Diego Bay-Tijuana fault: Association of Engineering Geologists Bulletin, v. 7, no. 2, p. 107-121.

Table 361.60-1

Summary RCFZ Information, Kennedy (1979) and Kennedy and others (1977, 1978)

Area Investigated	Summary of Data
RCFZ off Point La Jolla	Kennedy and others (1978) mapped a widening zone of west to northwest-trending faults offshore to the north and west of the mapped faults of the RCFZ onshore near Mt. Soledad. The more westerly-trending faults of this zone were inferred to be principally dip-slip and generally to define a structural low underlying the La Jolla submarine canyon. Stratigraphic separations on the youngest faulted sediment (late Pleistocene to Holocene) of these dip-slip faults were on the order of 9-18 m. Further west, a subzone of north-northwest trending faults was mapped oblique to the trend of the La Jolla canyon. These faults were generally discontinuous and appeared to be overlain by about 5 m of unfaulted Quaternary sediment. The eastern edge of Kennedy and others offshore zone parallels the coast line to the 33 N latitude which is the limit of profiling. Along the eastern edge, acoustically transparent (late Pleistocene and Holocene) sediment was not faulted although near surface disruption of the Quaternary horizon was indicated. The discontinuous en echelon pattern of the eastern edge of this offshore zone is simlar to that seen within the RCFZ at San Diego Bay.
RCFZ off San Diego Bay	Detailed acoustic profiling by Kennedy and others (1977) in the offshore region west of and including San Diego Bay indicated subzones of northeast to northwest-trending down-to-the-east faults. Three of the longer faults (from north to south: the Spanish Bight fault, Coronado fault, and the Silver Strand fault) were seen to have a prominent central portion (locally expressed onshore in the North Island-Coronado vicinity) that gradually died out when traced toward the north or south. No surface displacements were identified on these offshore faults, although displacement locally extends to within 5-10 m of the seafloor. When traced in a southerly direction, these faults generally become less persistent and appear to die out in short en echelon splays. The most southerly fault, the Silver Strand fault, can be traced to the vicinity of the International Border where it also becomes less persistent and dies out in several en echelon branches.
RCFZ in San Diego Bay	Kennedy and others (1977) also describe a series of relatively short (< 3 km long) discontinuous faults east of the Silver Strand fault in the southern San Diego Bay area. Some of these faults appear prominent on acoustic profiles, but all are short and none displace the bay floor. Some of these faults extend to within 5-10 m of the bay floor.
RCFZ South of San Diego Bay	Kennedy and others (1977) conducted gravity, ground magnetic, and refraction surveys to determine if a proposed trace of the RCFZ crossed the Otay Valley area, south of the San Diego Bay, and continued south across the International Border toward the San Miguel-Vallecitos fault zone (see response 361.41 b for further discussion). Gravity and magnetic profiles indicated several anomalies that could be accociated with faults of the La Nacion system, but they are located east of a projected RCFZ-SMVFZ alignment. However, no significant anomalies were recognized on profiles across southeast projections of presently mapped faults in the RCFZ. The refraction data collected in this survey were limited by logistic and electronic difficulties. As a result, it was not possible to determine unequivocally if the section was faulted (Kennedy and others, 1977).

QUESTION 361.61

Appendix B of the WC report discusses the methodology of determining lateral displacements along the NIZD by matching sedimentary rocks facies and stratigraphic thicknesses across the fault; however, the field data i.e., pertinent electric logs, stratigraphic and lithologic interpretations used in the correlations are not provided in Appendix B. Since in this methodology extreme care is required in matching electric log correlations, the NRC staff must review the specific logs and correlations made in support of your determination of the 0.5 mm/year slip-rate for the NIZD. Show logs for the holes that are correlated and for the adjoining holes that show greater mismatch or lack of correlation for each age bracket used to support the general slip rate. Show the error bands or spread for each determination. What are the error bands in abosolute age for the sediments that have been correlated? What procedures or assumptions have been used and what is the effect on the conservatism in the result of the analysis?

RESPONSE 361.61

Data used to calculate the horizontal displacement along the NIZD in the Long Beach, Seal Beach, and Huntington Beach oil fields (Figure 361.61-1) have been forwarded to the NRC staff for their review. The data includes: (1) well location maps for each of the three oil field studied showing the wells used for correlations; (2) annotated electric logs used for correlations in each of the three oil fields; (3) a brief discussion of the methodology used to establish the horizontal displacement and general characteristics pertaining to the correlation of the E-logs, such as the intervals used and facies relationships within the intervals, and (4) stratigraphic columns and cross sections used.

Tables 361.61-1, 361.61-2, and 361.61-3 list the wells on one side of the NIZD and the well(s) to which they correlate closest with on the opposite side for each of the correlations made in each of the three fields studied. Listed also, are the measurements of the estimated horizontal displacements and an estimate of the absolute age for the correlation intervals. Each displacement estimate and correlation interval age is assigned an error factor that represents the uncertainty associated with each displacement and time estimate. The displacement estimates and ages and their uncertainty values, are shown graphically in Figures 361.61-2 and 361.61-3.

The establishment of horizontal displacement along the NIZD is estimated by matching or correlating facies of stratigraphic intervals from wells on one side of the NIZD with matching facies from wells on the opposite side of the zone based on interpretations of E-logs. The accuracy of establishing exact displacements is constrained by several factors: 1) spacing between the wells; 2) well depths; 3) distance of wells to the zone; and 4) the possibility that the facies change can be occurring at an oblique angle to the fault. Since the correlation of an E-log on one side of the zone seldom produces an exact match with an E-log on the opposite side, the location or position of the correlation was usually judged to be at some point intermediate between two wells or group of wells. The amount of displacement, therefore, was the horizontal distance between the location of the well on one side of the NIZD to the well on the opposite side to which it correlates closest. Because there is some judgement involved in selecting the closest correlation well the amount of displacement was assigned an error factor that represents the uncertainty associated with the correlation. The error factor is calculated as one-half the distance between the two wells or where one well is believed to be closer than the other, the error factor is calculated as one-half the distance between the closest correlating well and the midpoint between the other well on the same side of the fault zone.

This method of establishing correlation and ultimately the amount of horizontal displacement along the NIZD is considered to be reasonalbe and accurate for the following reasons: 1) well spacing was held to a minimum, where permitted, 2) correlation between wells on opposite sides of the zone were established not only on the basis of similarity of the E-logs for the interval correlated, but also on the basis of lateral facies changes represented on E-logs adjacent to the correlating wells; 3) the correlation of the same interval was established for different wells located along the NIZD; 4) several zones of different depth and age were correlated and measured for two of the fields studied and average slip rates were calculated from the sum of the data; and 5) an error factor value was included with each estiamted horizontal displacement to represent uncertainties associated with the E-log correlations.

The absolute geologic age for each of the displaced intervals was established on the basis of locating the position of the displaced interval within a stratigraphic unit or formation. This stratigraphic unit was then correlated with a geologic time scale to obtain a relative geologic age (i. e., epoch, such as lower Pliocene). The relative gelogic age was then converted to an absolute geologic age (in years B. P.) by correlating the position of the relative age with its equivalent absolute geologic age. Because the establishment of absolute ages involves correlations and interpretations that are judgmental, each age determination, listed on Tables 361.61-1 through 361.61-3, includes a ±10% error factor.

The assignment of absolute ages and associated ranges to the correlation intervals is considered to be reasonable and conservative because: 1) the stratigraphic units and their relative geologic ages are well defined in the three fields studied; 2) the absolute age span of the late Cenozoic era involved, covers a relatively short period of time (i.e., eight million years); and 3) the 10% error factor added to the age of each correlated interval yields a minimum 0.4 million year error band around each age assignment which increases with increasing age.

The stratigraphic data for the three oil fields, E-log markers, horizons, and relative geologic ages of the formations, was based on data available for each field from the California Division of Oil and Gas and the Cenozoic correlation section across the Los Angeles Basin (Knapp and others, 1962) published by the American Association of Petroleum Geologist. Conversion of relative geologic ages (Epochs) to absolute geologic ages (in years B.P.) was based on the Upper Cenozoic stratigraphic column applicable to the western margin of the Los Angeles Basin (Nardin and Henyey, 1978). A discussion of the geologic time scale used is presented in response 361.45 g.

REFERENCES

California Division of Oil and Gas, 1974, California oil and gas fields--south central, coastal and offshore California, report no. TR-12, v. 2.

Hazelbush, G. C., and Allen, D. R., 1958, Huntington Beach oil field: California Division of Oil and Gas, Summary of Operations, California Oil Fields, v. 44, no. 1, p. 13-25.

Hill, M. L., 1954, Tectonics of faulting in southern California, in Jahns, R. H., ed., Geology of southern California: California Division of Mines and Geology Bulletin 170, p. 5-13.

Hill, M. L., 1971, Newport-Inglewood zone and Mesozoic subduction, California: Geological Society of America Bulletin, v. 82, p. 2957-2962.

Ingram, W. L., 1968, Long Beach oil field: California Division of Oil and Gas, Summary of Operations, California Oil Fields, v. 54, no. 1, p. 5-16.

Knapp, R. R., Traxler, J. D., Newbill, T. J., Laughlin, D. J., Steward, R. D., Heath, E. G., Stark, H. E., Wissler, S. G., and Holman, W. H., 1962, Cenozoic correlation section across Los Angeles basin from Beverly Hills to Newport, California: American Association of Petroleum Geologists, Pacific Section.

Nardin, t. R., and Henyey, T. L., 1978, Pliocene-Pleistocene diastrophism of Santa Monica and San Pedro shelves, California continental borderland: American Association of Petroleum Geologists Bulletin, v. 62, no. 2, p. 247-272.

Table 361.61-1 - Revision of TABLE B-3 - Horizontal Displacement, E-Log Data - Seal Beach Oil Field

Correlation Well		Reference Well		Correlation E-Log Horizon			Distance Between Wells (ft)	Estimated Horizontal Displacement (ft)	Comments (Basis for Correlation)
Name	Depth Interval (Thickness,ft)	Name	Depth Interval (Thickness,ft)	Horizon (Zone)	Stratigraphic Unit	Age (Million of Years)			
Hellman 49	2610-3075 (465)	Bixby A64	2620-3050 (430)	A4-A5	Pico	Upper Plio. (2.9±.3)	4300	4650±350	Correlates betwen Bixby A62 and Bixby A64. Closest with A64 based on the upper blocky sand development and lateral facies changes.
Helman 49	3990-4440 (450)	San Gabriel 52	3860-4350 (510)	B2-C	Repetto	Lower Plio. (3.75±.4)	6800	6500±300	Correlates between Bixby A62 and San Gabriel 52. Closest to San Gabriel 52 based on similar sandy horizons and location with respect to facies changes.
Helman 49	4855-5160 (305)	San Gabriel 51	4745-5065 (320)	E-G (Selover)	Repetto	Lower Plio. (4.75±.5)	8000	7400±650	Correlates between San Gabriel 51 and San Gabriel 40. Closest with 51 based on individual sandy horizons and facies changes.
Bryant LW-2	2590-3070 (480)	San Gabriel 52	2670-3100 (430)	A4-A5	Pico	Upper Plio. (2.9±.3)	4500	4200±300	Correlates between San Gabriel 52 and Bixby A62. Closest to San Gabriel 52. Based on similar E-log characteristics and relative thickness of sandy facies.
Bryant LW-2	4020-4505 (485)	San Gabriel 51	3840-4320 (480)	B2-B4	Repetto	Lower Plio. (3.75±.4)	5800	6250±500	Correlates closest with San Gabriel 51, but is probably NW of 51 based on E-log characteristics and thinning facies changes and thickness.
Hellman 45	2710-3255 (545)	Bixby A64	2620-3050 (430)	A4-A5	Pico	Upper Plio. (2.9±.3)	4600	4950±350	Correlates between Bixby A62 and Bixby A64. Closest with A64 based on similar development of the upper sandy horizons and facies changes.
Hellman 45	4235-4735 (500)	Bixby A62	3890-4315 (435)	B2-C	Repetto	Lower Plio. (3.75±.4)	6000	6350±300	Correlates between Bixby A62 and San Gabriel 52. Closest with A62 based on development of sandy horizons near the top and overall facies changes.
Hellman 45	5180-5540 (360)	San Gabriel 52	4710-5000 (290)	E-G (Selover)	Repetto	Lower Plio. (4.75±.5)	7200	7500±300	Correlates between San Gabriel 52 and San Gabriel 51. Closest to 52 based on overall E-log characteristics and facies changes near the bottom of the interval.

TABLE 361.61-2 Revision of Table B-2 - Horizontal Displacement, E-Log Data - Long Beach Oil Field

Correlation Well		Reference Well		Correlation E-Log Horizon					
Name	Depth Interval (Thickness,ft)	Name	Depth Interval (Thickness,ft)	Horizon (Zone)	Stratigraphic Unit	Age (Million of Years)	Distance Between Wells (ft)	Estimated Horizontal Displacement (ft)	Comments (Basis for Correlation)
Sudduth 7	3910-4100 (190)	Amebco 2	4325-4525 (200)	J-M (lower Alamitos)	Repetto	Lower Plio. (3.75±.4)	3600	3600±300	Correlates between Amebco 2 and Encinas 1. Closest with Amebco 2 based on similar sandy horizons and thickness.
Recknagel Carlin 1	3250-3910 (660)	Encinas 1	3850-4590 (710)	TW-J (lower Wilbur)	Repetto	Lower Plio. (3.25±.3)	3900	4000±200	Closest with Encinas 1 based on similar individual sandy horizons and thinning facies to the east.
Olsen-Oliver Wallace 1	2040-2490 (450)	Amebco 1	2350-2880 (530)	A-Top of C Sands	Pico	Upper Plio. (2.25±.2)	2000	2300±300	Correlates well with Amebco 1 based on facies change. May be to the west based on thickness of individual horizons.
Morton-Dolly Dodge 3	3680-3890 (210)	Texaco B-18	2720-2930 (210)	TW-TA (lower Wilbur Sand)	Repetto	Lower Plio. (3.25±.3)	3700	3900±250	Correlates between Texaco B-18 and Texaco B-38. Closest with B-18 based on sandy horizons at the top of interval with serrated funnel shaped sands below.
Acme Dr. Co. Farrell 2-1	4010-4380 (370)	Cresson Comm. 16	2550-2790 (240)	TW-TA (lower Wilbur Sand)	Repetto	Lower Plio. (3.25±.3)	3500	3700±500	Farrell 2-1 correlates near Cresson 8 and 16 and Texaco C-8. Closest to and may be further than Cresson 16. Based on four sandy horizons near the top of the Wilbur.
Morton-Dolly Dodge 3	5770-6230 (460)	Texaco D3	4075-4490 (415)	W-Z (lower Brown)	Repetto	Lower Plio. (4.75±.5)	6000	6600±500	Correlates between Dormax 1 and Texaco D3. Closest to D3 based on the overall development of the interval and lateral facies change of the lower sand-shale facies. Becomes shaly to the southeast.
Acme Dr. Co. Farrell 2-1	5890-6270 (380)	Dormax 1	3865-4230 (365)	W-Z (lower Brown)	Repetto	Lower Plio. (4.75±.5)	5300	6900±600	Correlates between Dormax 1 and Pala 3. Closest to Dormax 1 based on the development of the upper blocky sand and the increase in shale to the southeast in the lower part of the interval.
Alamitos 48A	5490-5840 (350)	Field 28	6440-6860 (420)	AH-AL	Puente	U. Miocene (6.0±.6)	11000	10000±1000	Alamitos 48A correlates between Field B-28 and Malcom Davis 8, which penetrate through the fault zone. Closest to Field 28 based on thickening sandy horizon.
Acme Dr. Co. Farrell 2-1	4790-5230 (440)	F.F. Richards Dormax 1	2890-3280 (360)	J to Top of Brown	Repetto	Lower Plio. (3.75±.4)	5200	4800±400	Correlates between Dormax 1 and Texaco D3. Closest with Dormax 1 based on similar development of the upper and lower blocky sands.

TABLE 361.61-2 Revision of Table B-2 - Horizontal Displacement, E-Log Data - Long Beach Oil Field Continued

Correlation Well		Reference Well		Correlation E-Log Horizon			Distance Between Wells (ft)	Estimated Horizontal Displacement (ft)	Comments (Basis for Correlation)
Name	Depth Interval (Thickness,ft)	Name	Depth Interval (Thickness,ft)	Horizon (Zone)	Stratigraphic Unit	Age (Million of Years)			
Axis Pet Co. Allied 34	3300-3550 (250)	Shell Oil Pala 3	2500-2730 (230)	TW-TA (lower Wilbur sand)	Repetto	Lower Plio (3.25±.3)	3300	3300±400	Correlates between Pala 3 and Denni 9. Closest with Pala 3 based on sandy horizons and facies changes.
Axis Pet Co. Allied 34	3550-3900 (350)	ARCO Fry 5	3210-3550 (340)	TA-J Alamitos	Repetto	Lower Plio. (3.5±.4)	6100	5800±500	Correlates between TC 1 and Fry 5. Closest to Fry 5 based on sandy-silt sequence at the top and bottom of the interval.

Table 361.61-3 - Revision of TABLE B-4 - Horizontal Displacement, E-Log Data - Huntington Beach Oil Field

Correlation Well		Reference Well		Correlation E-Log Horizon			Distance Between Wells (ft)	Estimated Horizontal Displacement (ft)	Comments (Basis for Correlation)
Name	Depth Interval (Thickness, ft)	Name	Depth Interval (Thickness, ft)	Horizon (Zone)	Stratigraphic Unit	Age (Million of Years)			
Rothschild Oil Diehl 1 and Jacober 1	3385-3940[1] (555)	Signal Oil and Gas Bolsa S31, S41, S51 & S61	2640-3260[2] (620)	Top of Jones Sand to just below AG-2 (Div. "A" & "B")	Puente	Upper Mio. (6-8)	12000	12000±2100	Correlation based on similiarity in development and thickness of the sandy facies and lateral facies changes that occurs to the interval.

1 Interval from Jacober 1
2 Interval from Bolsa 541

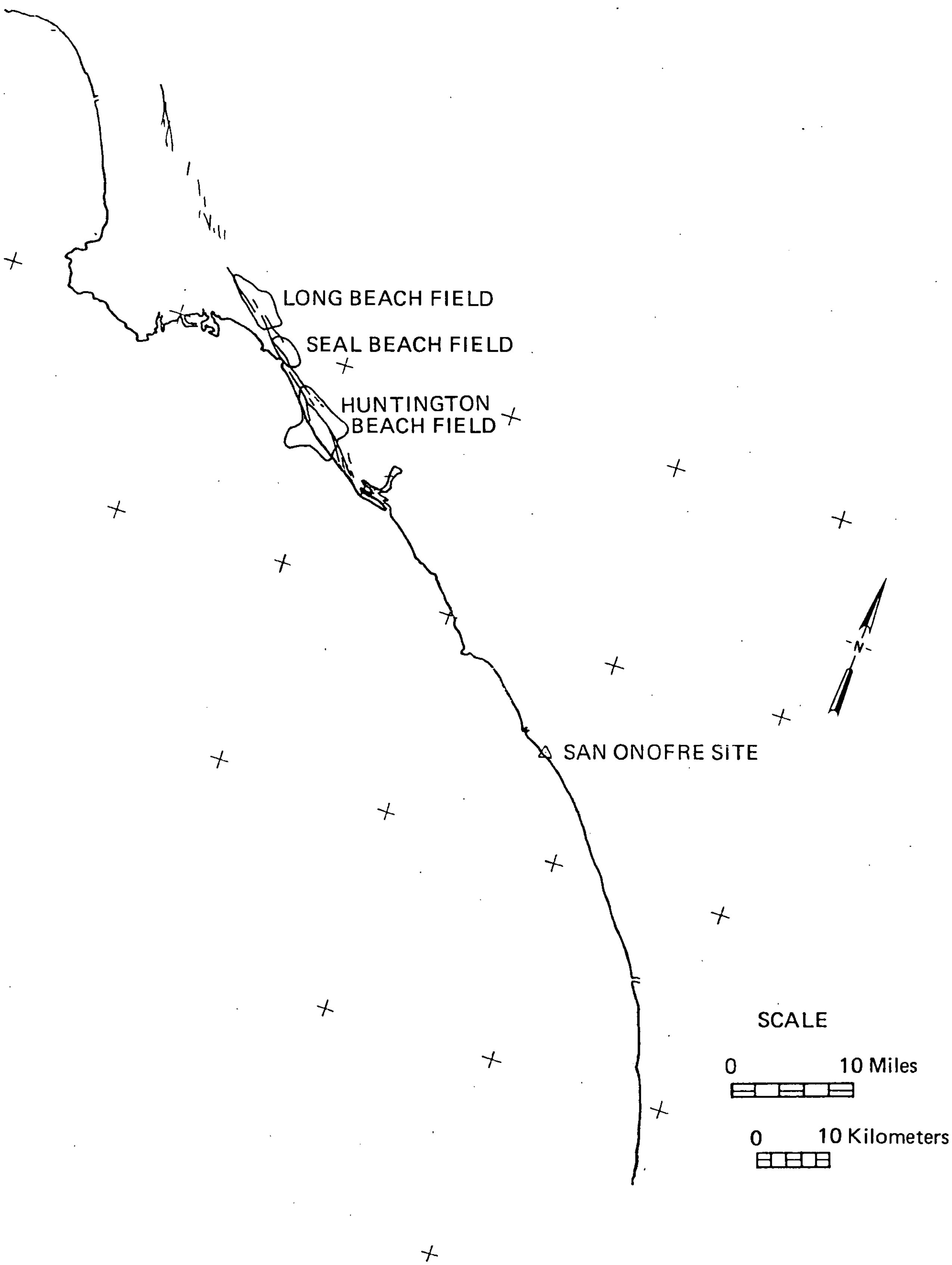

Fig. 361.61 - 1 Approximate Location of the Long Beach, Seal Beach and Huntington Beach Oil Fields Along the Newport Inglewood Zone of Deformation

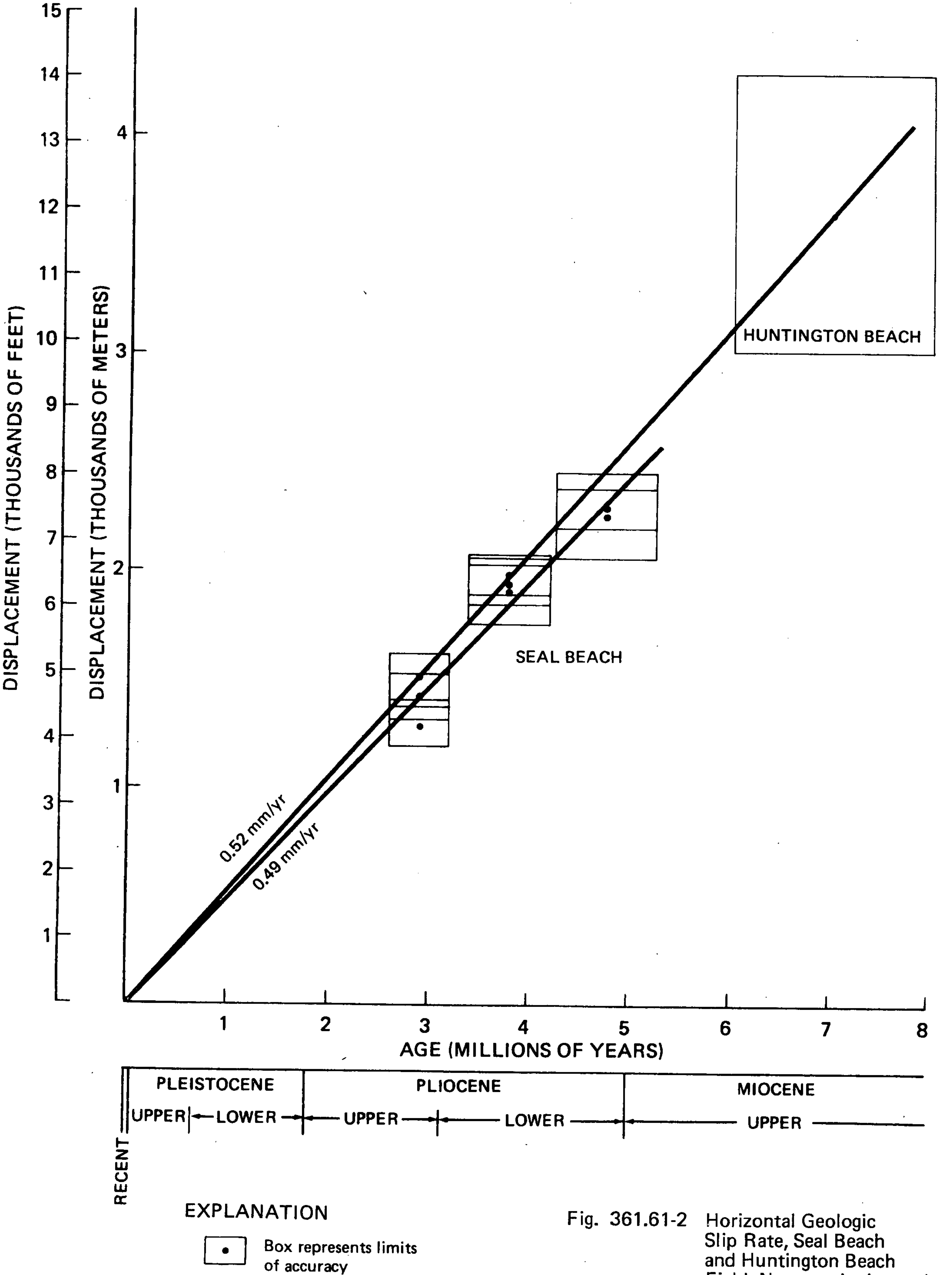

Fig. 361.61-2 Horizontal Geologic Slip Rate, Seal Beach and Huntington Beach Field, Newport Inglewood Zone of Deformation.

Revision of Figure B-7, Appendix B

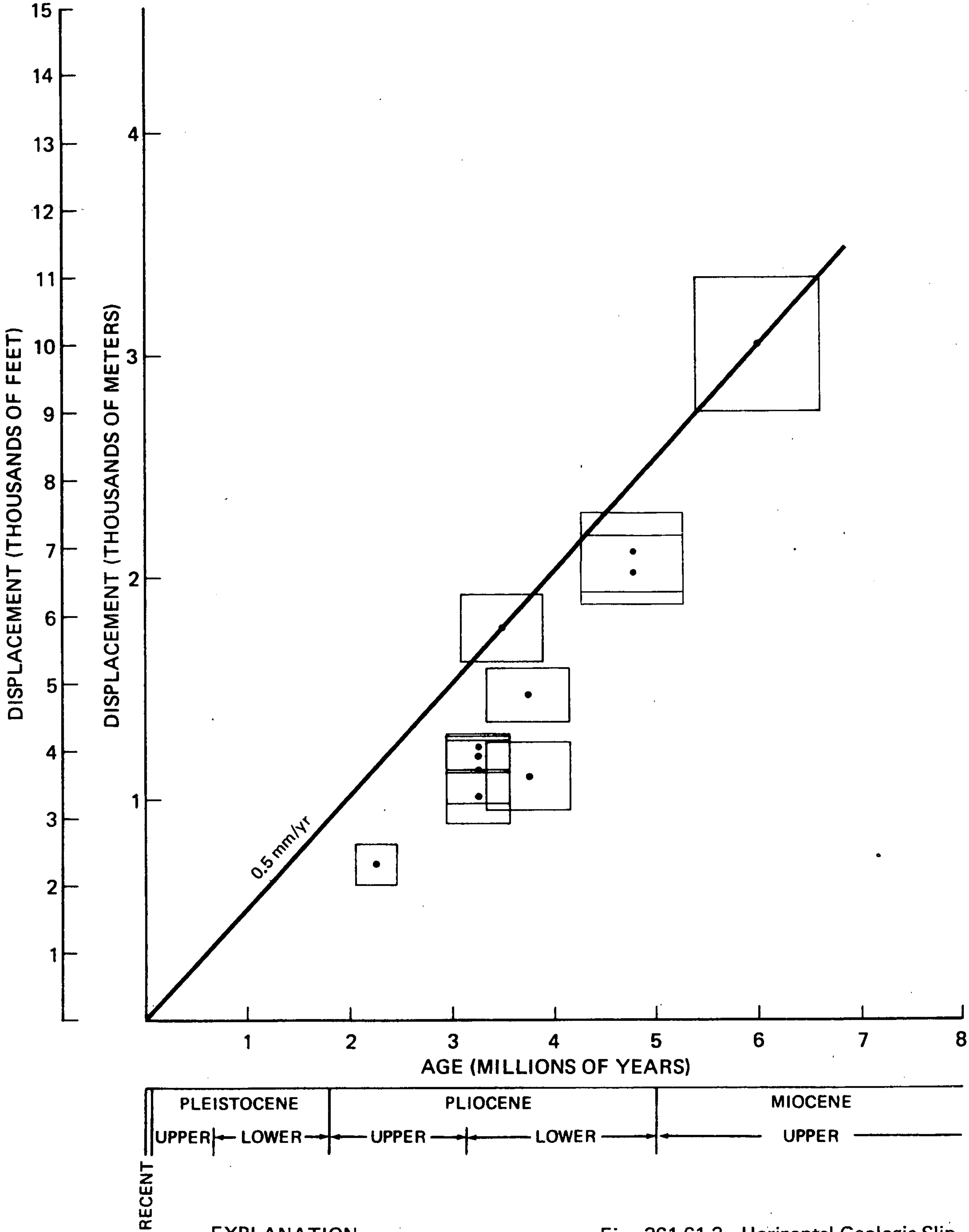

EXPLANATION

Box represents limits of accuracy

Fig. 361.61-3 Horizontal Geologic Slip Rate, Seal Beach Field, Newport Inglewood Zone of Deformation.

Revision of Figure B-8, Appendix B

QUESTION 361.62

Justify the choice of source distance used in the WC study, instead of the more conventional shortest distance in km to the surface of fault slippage as used USGS Circular 795. See also Figures 6-9 and 6-19 in Supplement 1 to the TERA Corp. study "Simulation of Earthquake Ground Motions for San Onofre Nuclear Generating Station Unit 1, July, 1979, which demonstrates the greater importance of receiver distance over hypocenter distance.

RESPONSE 361.62

Figure 361.62-1 illustrates in a general way several possible definitions of distance. Closest distance "B" was used in the USGS circular 795 analysis; distance "C" was used in the WCC study. Note that "C" is not the hypocentral distance; rather it is the closest distance from a site to a fault at the depth of the center of energy release (hereinafter referred to as energy center distance).

The objective of the analysis for SONGS was to estimate the ground motions for a magnitude 6-1/2 earthquake occurring on a vertical fault (OZD) whose surface trace is at closest distance of 8 km from SONGS. The corresponding energy center distance used in the WCC analysis (June 1979 report) is 10 km. These distances are illustrated in Figure 361.62-2.

If sufficient data were available from magnitude 6-1/2 earthquakes on vertical faults from stations with site conditions similar to SONGS, then analyses of these data using either closest distance or energy center distance should yield essentially the same results, provided that the definition of distance used to develop the attenuation curve is consistent with the definition of distance used to estimate the ground motions. However, most of the applicable data for the WCC study (June 1979 report) were from the 1971 San Fernando earthquake that occurred on a shallow-dipping thrust fault.

Furthermore, most of the San Fernando data was obtained at stations south of the rupture zone as is schematically illustrated in Figure 361.62-3. For the situation depicted in Figure 361.62-3, there is a substantial difference between closest distance, B, and distance to energy center, C. For a station at a given closest distance from the surface trace of a fault, the distance to the energy center is substantially greater for the shallow-dipping fault (Figure 361.62-3) than for the vertical fault (Figure 361.62-2). Consequently, it was felt that using the closest distance for the San Fernando data could be unconservative when applied to the vertical fault of the OZD. This motivated the choice of energy center distance.

Figure 361.62-4 illustrates the conservatism of the choice of distance definition adopted for the data set used in the WCC study. In Figure 361.62-4, the peak acceleration data used by WCC are plotted versus closest distance rather than distance to energy center. Superimposed on the data are the attenuation curves obtained from Figure J-1 of the June 1979 WCC report, but replotted in terms of closest distance rather than distance to energy center of a vertical fault. (The closest distance, B, for any distance to energy center, C, of the vertical fault is simply equal to $\sqrt{C^2-6^2}$, in which 6 is the assumed depth in km of the energy center on the fault). Figure 361.62-4 shows clearly that the attenuation curves at moderate to close distances are conservative with respect to the data.

It should be noted that another definition of distance could also have been employed in consideration of the unique geometry of the fault for the San Fernando earthquake. This distance is denoted "D" in Figure 361.62-3 and is the horizontal projection of distance C. Distance "D" could be regarded as an equivalent closest distance for the inclined fault case. The analysis for peak acceleration presented in Appendix J of the June 1979 WCC report was repeated using distance D and it was found that the accelerations predicted at a distance of 8 km were essentially the same as those presented in the WCC report for the corresponding energy center distance of 10 km.

Closest distance to the rupture surface was used to plot Figure 6-19 of the referenced Tera report. Use of distance to center of energy release would have achieved the same results shown in Figure 6-19.

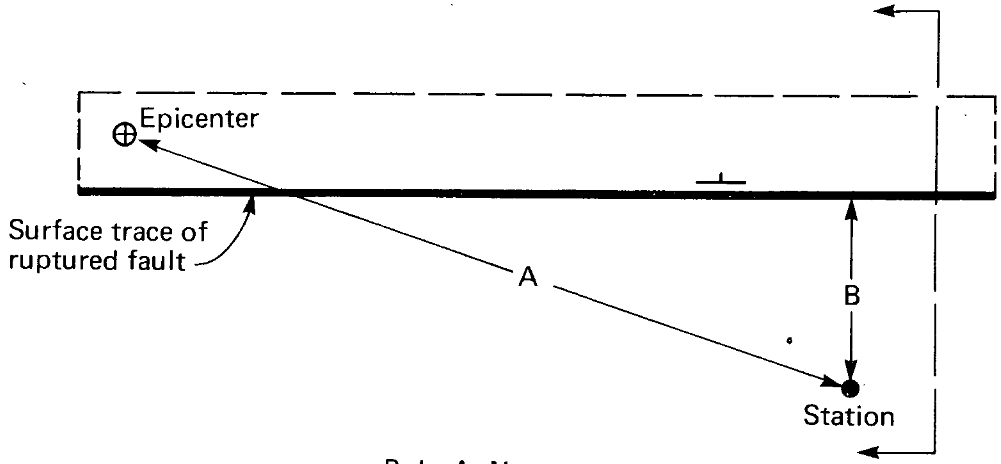

P L A N

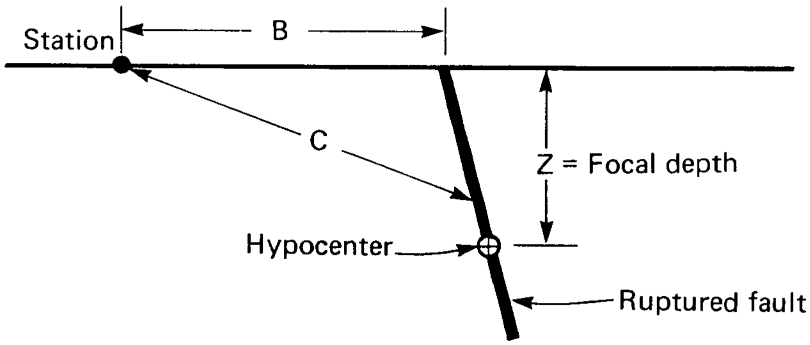

C R O S S   S E C T I O N

A = Epicentral distance

$\sqrt{A^2 + Z^2}$ = Hypocentral distance

B = Closest distance to fault

C = Closest distance to fault at mid-depth of rupture
(or at depth of center of energy release)

Fig. 361.62–1 – Illustration of Different Definitions of Distance

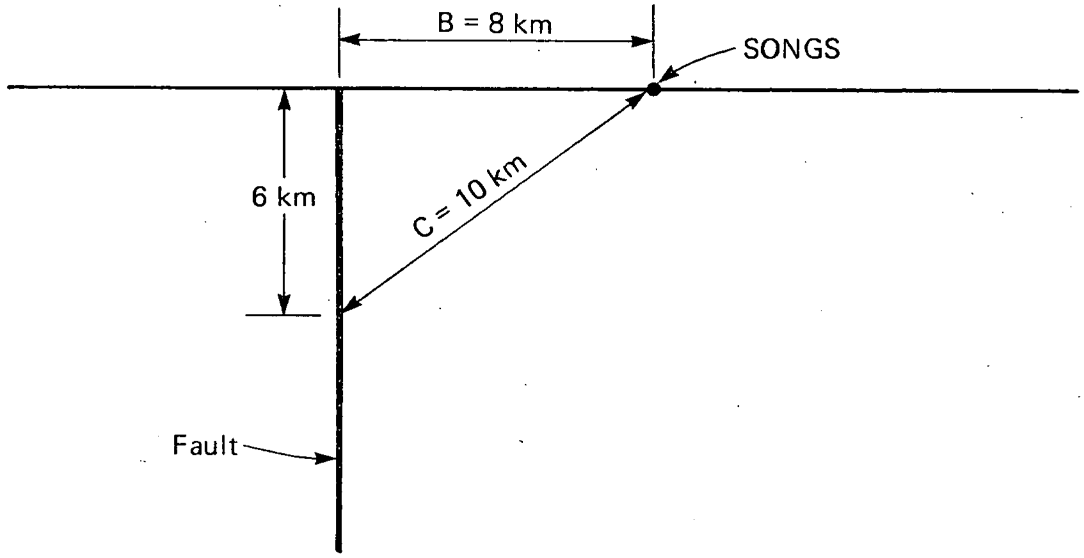

B = Closest distance

C = Closest distance to fault at depth of center of energy release

Fig. 361.62–2 – Cross Section Through Vertical Fault Representing OZD, Illustrating Definitions of Distance

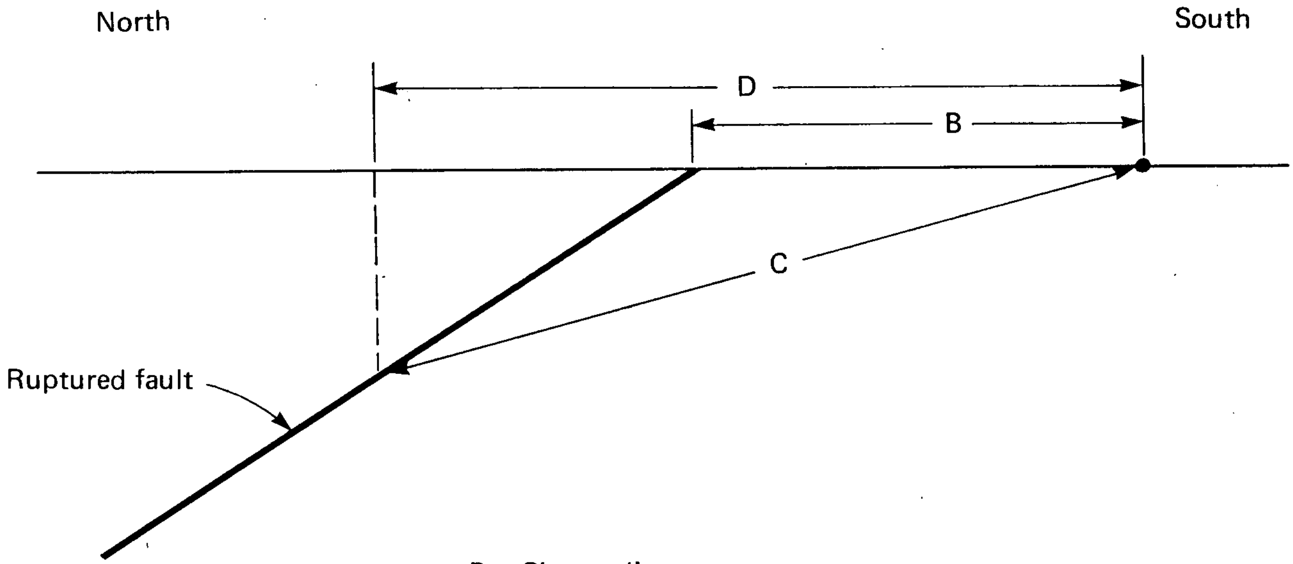

B = Closest distance

C = Closest distance to fault at depth of center of energy release

D = An "equivalent closest distance" for the inclined fault case

Fig. 361.62–3 — Cross Section Through Shallow-dipping Fault Illustrating Definitions of Distance Applicable to 1971 San Fernando Earthquake Data

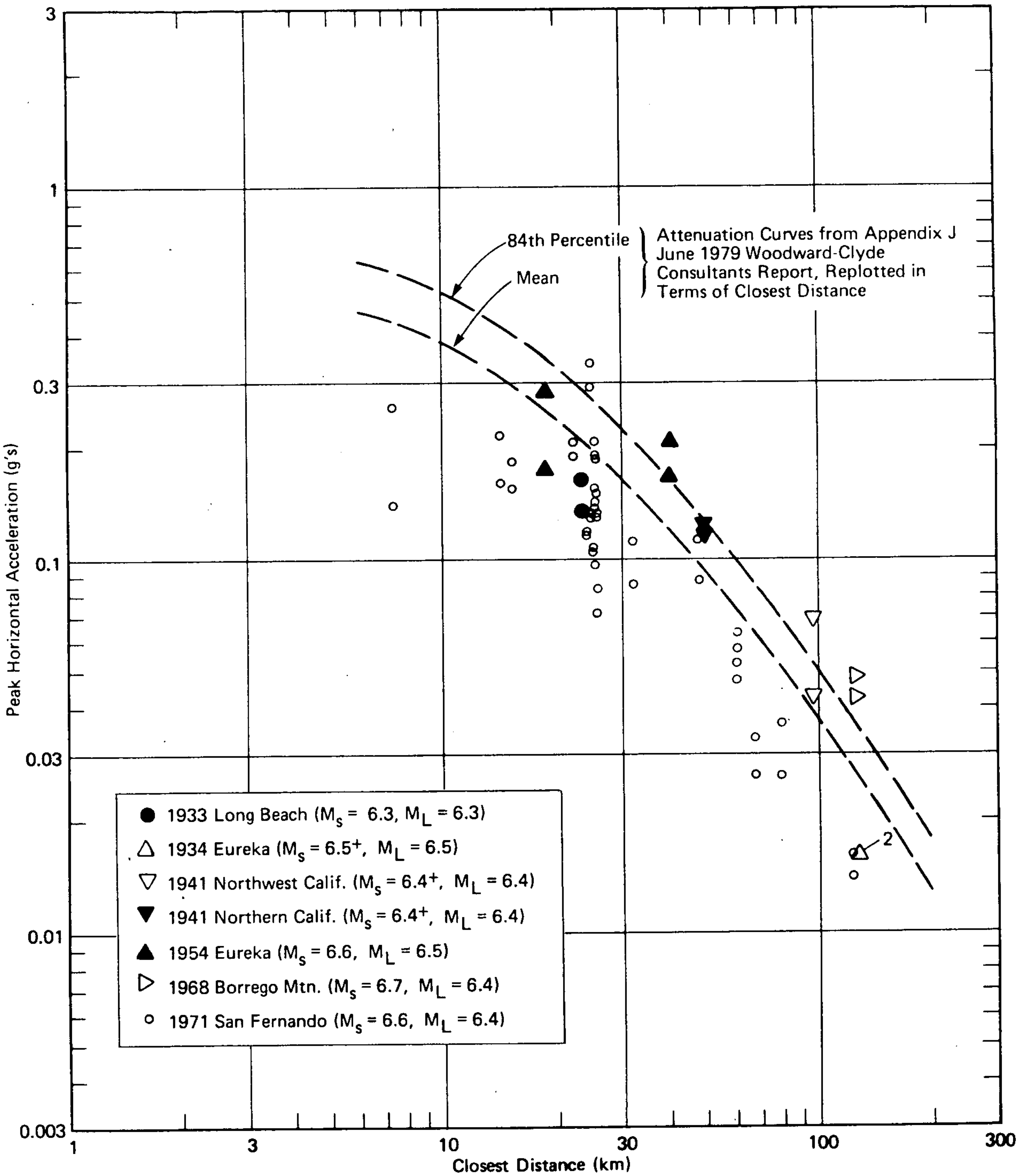

Fig. 361.62–4 – SONGS Appendix J Data Set and Regression Results Plotted in Terms of Closest Distance

REGIONAL FAULT MAP

SOUTHERN CALIFORNIA AND NORTHWESTERN BAJA CALIFORNIA AND THE CALIFORNIA CONTINENTAL BORDERLAND

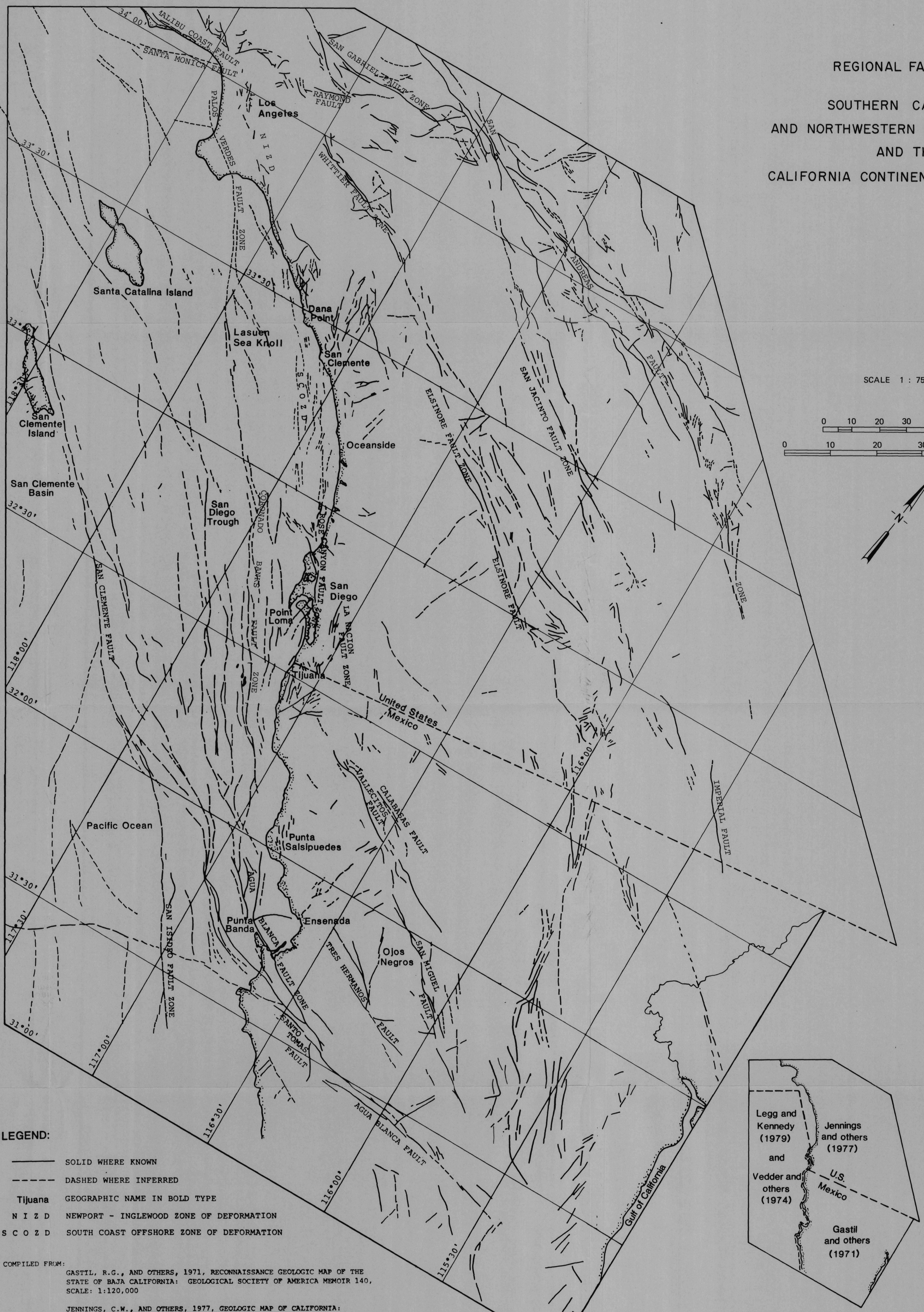

SCALE 1 : 750,000

0 10 20 30 40 50 KILOMETERS

0 10 20 30 40 50 MILES

LEGEND:

————	SOLID WHERE KNOWN
– – – –	DASHED WHERE INFERRED
Tijuana	GEOGRAPHIC NAME IN BOLD TYPE
N I Z D	NEWPORT - INGLEWOOD ZONE OF DEFORMATION
S C O Z D	SOUTH COAST OFFSHORE ZONE OF DEFORMATION

COMPILED FROM:

GASTIL, R.G., AND OTHERS, 1971, RECONNAISSANCE GEOLOGIC MAP OF THE STATE OF BAJA CALIFORNIA: GEOLOGICAL SOCIETY OF AMERICA MEMOIR 140, SCALE: 1:120,000

JENNINGS, C.W., AND OTHERS, 1977, GEOLOGIC MAP OF CALIFORNIA: CALIFORNIA DIVISION OF MINES AND GEOLOGY, SCALE: 1:250,000

LEGG, M.R., AND KENNEDY, M.P., 1979, FAULTING OFFSHORE SAN DIEGO AND NORTHERN BAJA CALIFORNIA IN EARTHQUAKE AND OTHER PERILS, SAN DIEGO REGION (ABBOTT, P.L., AND ELLIOT, W.J., EDITORS)

VEDDER, J.G., AND OTHERS, 1974, PRELIMINARY REPORT ON THE GEOLOGY OF THE CONTINENTAL BORDERLAND OF SOUTHERN CALIFORNIA, U.S.G.S. MAP MF-624

INDEX TO GEOLOGIC MAPPING